ERIC SAMSON

MODÉLISATION NUMÉRIQUE DU TRANSPORT IONIQUE DANS LES MATÉRIAUX CIMENTAIRES NON SATURÉS

Thèse présentée
à la Faculté des études supérieures de l'Université Laval
dans le cadre du programme de doctorat en génie civil
pour l'obtention du grade de Philosophiae Doctor (Ph.D.)

Département de génie civil
FACULTÉ DES SCIENCES ET DE GÉNIE
UNIVERSITÉ LAVAL
QUÉBEC

2005

Résumé court

Les travaux de recherche effectués au cours de cette thèse ont mené au développement d'un modèle numérique permettant de décrire le déplacement simultané de plusieurs ions dans le réseau poreux de matériaux cimentaires. Le modèle tient compte de la diffusion des ions, du couplage électrique entre les ions et de l'activité chimique. Lorsque le matériau n'est pas saturé, le déplacement de l'eau sous l'effet de forces capillaires et son influence sur le transport des ions apparaît dans le modèle. Plusieurs réactions chimiques sont également prises en compte: dissolution de la portlandite, décalcification des C-S-H, dissolution des monosulfoaluminates, formation d'ettringite, de gypse et de chloroaluminates. L'effet de la dissolution ou de la précipitation de ces phases solides sur les propriétés de transport du matériau est également considéré.

Résumé

Les travaux de recherche effectués au cours de cette thèse ont mené au développement d'un modèle numérique permettant de décrire le déplacement simultané de plusieurs ions dans le réseau poreux de matériaux cimentaires. L'algorithme sépare le transport des ions des réactions chimiques selon une approche SNIA (Sequential Non Iterative Approach). Dans la partie consacrée au transport, le déplacement des ions dans un milieu non saturé est basé sur la résolution de l'équation de Nernst-Planck étendue tenant compte de la diffusion, du couplage électrique entre les ions et de l'activité chimique. Un terme d'advection est ajouté à cette équation afin de considérer le transport des ions sous l'effet du mouvement du fluide dans le réseau poreux en présence de gradients de teneur en eau. Ces équations de transport sont discrétisés dans l'espace par la méthode des éléments finis. Elles sont résolues pour sept espèces ioniques de manière couplée en utilisant la méthode de Newton-Raphson. Un module d'équilibre chimique corrige ensuite les profils de concentration obtenus à l'étape de transport. Dans ce module chimique, les phases solides considérées sont la portlandite, les C-S-H, les monosulfoaluminates, l'ettringite, le gypse et les chloroaluminates. Certaines de ces phases solides sont soient dissoutes, soient précipitées afin de retrouver l'équilibre entre la pâte de ciment hydraté et la solution dans les pores du matériau. L'effet de la dissolution ou de la précipitation de ces phases solides sur les propriétés de transport du matériau est également considéré, en fonction des variations de porosité. Le modèle donne comme résultats les profils de concentrations en solution et la teneur en tout point du matériau

de chacune des phases solides. Les applications présentées à la fin du mémoire montrent l'utilisation du modèle pour des cas d'attaque aux sulfates. Une méthode permettant de déterminer le coefficient de diffusion des ions dans les matériaux cimentaires suite à une analyse des résultats de l'essai de migration a également été développée dans le cadre de ces travaux de recherche.

Avant-propos

Je tiens tout d'abord à remercier mon directeur de thèse Jacques Marchand. Au moment de commencer cette étude, je n'avais pas grand chose à offrir à Jacques, si ce n'est mes connaissances au niveau numérique. J'étais de ceux qui disent ciment en pensant béton. Il n'y a rien de mal à cela, en passant. Mais en génie civil, ça ne pardonne pas. Sa grande ouverture d'esprit du point de vue scientifique et sa confiance en mes moyens ont donné STADIUM, SIMCO, et tout le reste.

Jean-Loup Robert, mon codirecteur de recherche, a également contribué au développement du modèle. Ses explications sur la résolution couplée d'équations ont donné une grande poussée vers l'avant aux travaux.

J'ai eu la chance de collaborer, tout au long de ma thèse, avec Jim Beaudoin du NRC à Ottawa. Non seulement a-t-il été une ressource scientifique inestimable, mais il a de plus accepté de cosigner plusieurs des articles qui apparaissent dans ce document. Ses conseils m'ont toujours été très précieux.

On ne le dira jamais assez, une thèse est le fruit d'un travail en solo qu'il est impossible de réaliser seul. Je tiens donc à remercier Yannick Maltais, qui a permis au modèle d'être autre chose qu'une curiosité numérique. Ses efforts concernant la validation et sa connaissance des matériaux cimentaires ont contribué au succès de ces travaux. De plus, Yannick est l'une des rares personnes pouvant témoigner que j'ai déjà préparé un mélange de béton. Je lui dois donc beaucoup ...

Ce travail m'a également donné l'occasion de rencontré Pierre, Rémi, Annick et Guillaume. Ils ont tous contribué au développement du modèle, mais ils ont fait beaucoup plus que cela. Guillaume et Rémi peuvent en témoigner, des heures de discussion sur la porosité et Nernst-Planck, ça ressert les liens. Toutes nos discussions sur la BD, le hockey, LaTeX, la montagne et j'en passe font partie de la thèse. Et Rémi m'a permis de réduire mon stock de maté (faut dire que j'avais vu bien grand).

Quand j'y repense, Élisabeth Reid ne savait pas dans quoi elle s'embarquait lorsque l'aventure SIMCO a débuté. Elle n'avait pas côtoyé beaucoup de gens en génie physique dans sa vie et je crois qu'elle a été surprise. Mais elle a fait abstraction de nos si légères différences. Son support indéfectible dans le développement du modèle (à ce point, ce n'est plus du support, c'est de la foi), a été une grande source de motivation.

Finalement, je ne peux passer sous silence la contribution de Nathalie, qui a beaucoup sacrifié pour que STADIUM puisse voir le jour. Merci.

∞

Rémi, les meilleures idées sont destinées à être copiées. Cette thèse a vu le jour en compagnie de Pearl Jam (No Code), Daniel Bélanger (Quatre Saisons dans le Désordre), Jean Leloup (Le Dôme), The Beatles (Abbey Road), Radiohead (OK Computer), Tool (Lateralus), et le premier album de Vincent Delerm. Et pour boucler la boucle, le tout s'est terminé par l'excellent spectacle de Pearl Jam au Colisée de Québec le 22 septembre 2005.

Table des matières

Résumé court i

Résumé ii

Avant-propos iv

Table des matières vi

Liste des tableaux xi

Liste des figures xiii

Introduction 1

1 Mise en contexte 4

1.1 Revue des modèles de transport ionique 4

1.2 Objectif de la recherche 14

1.3 Description du matériau 14

1.4 Hypothèses de base 17

2 Modèle mathématique 20

2.1 Introduction 20

2.2 Describing ion diffusion mechanisms in cement-based materials using the homogeneization technique 21

2.2.1 Introduction 22

2.2.2 Description of the ionic diffusion mechanisms in the liquid phase . 23

2.2.3 Averaging over the Representative Elementary Volume (REV) . . 25
2.2.4 Concluding remarks 31
2.3 Modeling ion and fluid transport in unsaturated cement systems for isothermal conditions 31
2.3.1 Introduction 32
2.3.2 Water transport in unsaturated porous materials 33
2.3.2.1 General considerations 34
2.3.2.2 Transport of liquid water 36
2.3.2.3 Transport of water vapor 39
2.3.2.4 Total moisture transport 42
2.3.2.5 Determination of the moisture transport properties of hydrated cement systems 43
2.3.3 Ionic transport in unsaturated porous materials 43
2.3.3.1 Transport of ions in the liquid phase 44
2.3.3.2 Coupling water and ionic transport 51
2.3.3.3 Calculation of the potential 52
2.3.3.4 Evaluation of chemical activity coefficients 53
2.3.3.5 Evaluation of the ionic transport properties 53
2.3.4 Conclusion 55
2.4 Modeling chemical activity effects in strong ionic solutions 56
2.4.1 Introduction 56
2.4.2 Different models for chemical activity 58
2.4.3 Chemical activity effects on the mathematical treatment of ionic diffusion mechanisms in saturated porous media 63
2.4.4 Modification of the Davies law 65
2.4.5 Application of the modified Davies equation to a case of ionic transport 71
2.4.6 Conclusions 74
2.5 Modeling the influence of chemical reactions on the mechanisms of ionic transport in porous materials : an overview 74
2.5.1 Introduction 75
2.5.2 Types of chemical reactions 76

2.5.3 Coupling chemical reactions to ionic transport in a saturated porous medium . . . 77
2.5.4 Treatment of homogeneous chemical reactions . . . 78
2.5.5 Treatment of surface chemical reactions . . . 81
2.5.6 Treatment of dissolution/precipitation reactions . . . 84
2.5.7 Discussion and concluding remarks . . . 88

3 Modèle numérique **90**

3.1 Introduction . . . 90
3.2 Modeling ion diffusion mechanisms in porous media . . . 91
3.2.1 Introduction . . . 92
3.2.2 Mathematical model . . . 93
3.2.3 Numerical models for solving the Nernst-Planck/ Poisson system of equations . . . 95
3.2.3.1 Bibliographical review . . . 95
3.2.3.2 First algorithm: uncoupled equations . . . 98
3.2.3.3 Second algorithm: coupled equations . . . 100
3.2.4 Comparison of the two algorithms . . . 104
3.2.4.1 Results obtained with the first algorithm . . . 105
3.2.4.2 Results obtained with the second algorithm . . . 106
3.2.5 Conclusion . . . 111
3.3 Numerical solution of the extended Nernst-Planck model . . . 114
3.3.1 Introduction . . . 114
3.3.2 Mathematical model . . . 115
3.3.3 Numerical model . . . 117
3.3.4 Numerical simulations . . . 124
3.3.5 Conclusion . . . 130
3.4 Modeling the transport of ions in unsaturated cement-based materials . 130
3.4.1 Introduction . . . 131
3.4.2 Transport model . . . 132
3.4.3 Modeling the chemical reactions . . . 135
3.4.4 Numerical model . . . 142
3.4.5 Experimental validation . . . 147
3.4.6 Long-term simulation . . . 156

3.4.7 Conclusion 162

4 Application du modèle **164**

4.1 Introduction 164

4.2 Calculation of ionic diffusion coefficients on the basis of migration test results 165

4.2.1 Introduction 166

4.2.2 Description of ionic transport mechanisms in reactive porous media 168

4.2.2.1 Mathematical treatment of transport phenomena 168

4.2.2.2 Mathematical treatment of chemical reactions 171

4.2.3 Modeling of ionic transport during migration tests 172

4.2.4 A further simplication - The constant field assumption 173

4.2.4.1 Steady-state migration experiments 174

4.2.4.2 Non steady-state migration experiments 175

4.2.4.3 Discussion on the validity of the constant field hypothesis . . 176

4.2.5 An alternative approach to calculate diffusion coefficients using migration test results 181

4.2.5.1 Description of the experimental procedure 181

4.2.5.2 Description of the calculation method 182

4.2.5.3 Experimental validation of the method 183

4.2.5.4 Discussion 185

4.2.6 Conclusion 187

4.3 Theoretical analysis of the effect of weak sodium sulfate solutions on the durability of concrete 187

4.3.1 Introduction 188

4.3.2 Description of the numerical model 190

4.3.2.1 Description of the various transport processes 190

4.3.2.2 Chemical equilibrium step 192

4.3.3 Characteristics of the materials 195

4.3.4 Description of the numerical simulations 198

4.3.4.1 General information 198

4.3.4.2 Boundary conditions 201

4.3.4.3 Initial conditions 201

4.3.5 Results of the numerical simulations 202

4.3.6 Concluding remarks 209

Conclusion **210**

Bibliographie **215**

Liste des tableaux

1.1 Revue de modèles de transport ioniques dans le domaine de l'hydrogéologie. 10

1.1 (suite) Revue de modèles de transport ioniques dans le domaine de l'hydrogéologie. 11

2.1 Compositions of the electrolytic solutions 68

2.2 Activity coefficients for Na^+ 68

2.3 Activity coefficients for K^+ 69

2.4 Activity coefficients for SO_4^{2-} 69

2.5 Activity coefficients for Cl^- 70

2.6 Activity coefficients for OH^- 70

3.1 Data for the numerical simulations. 124

3.2 Analysis of the accuracy of the operator splitting scheme 137

3.3 Solid phases in hydrated cement 139

3.4 Composition of the cement. 147

3.5 Parameters for the simulation on the paste. 149

3.6 Data for the numerical simulations 157

4.1 Diffusion coefficient of various species in free water. 169

4.2 Data for the non steady-state chloride migration simulation. 178

4.3 Steady-state flux calculation for three different ionic transport model. . 181

4.4 Pore solution extraction and porosity measurement 184

4.5 Results of the migration test. 185

4.6 Recommendations for protecting concrete exposed to sulfate. 189

4.7 Equilibrium constants for solid phases in hydrated cement systems . . . 193

4.8 Characteristics of the concrete mixtures 195

4.9 Chemical and mineralogical analyses of the cements 196

4.10 Materials properties used to perform the numerical simulations - CSA Type 10 mixtures 199

4.11 Materials properties used to perform the numerical simulations - CSA Type 50 mixtures 200

Liste des figures

1.1 Proportion de pâte hydratée, de pâte anhydre, ... 17

1.2 Courbe de distribution de la porosité, d'après [194] 18

1.3 Les différentes classes de porosité selon Powers 19

2.1 The Representative Elementary Volume (REV) 26

2.2 The Representative Elementary Volume (REV) 35

2.3 Concentration and potential profile across a pore. 47

2.4 Concentration profiles of a 1-1 electrolyte near a charged surface 48

2.5 Comparison of NaOH activity coefficients for different models 60

2.6 Comparison between Pitzer and the modified Davies model 67

2.7 Concentrations across the membrane for the weak ionic strength case . 72

2.8 Potentials across the membrane for the weak ionic strength case 72

2.9 Concentrations across the membrane for the strong ionic strength case . 73

2.10 Potentials across the membrane for the strong ionic strength case . . . 73

3.1 First algorithm: solution for $\alpha^2 = 0.5$. 106

3.2 First algorithm: norm vs. number of iterations for different values of α^2. 107

3.3 Second algorithm: solution for $\alpha^2 = 0.0001$. 108

3.4 Concentration profiles for the Helfferich problem. 109

3.5 Concentration profiles at $\tilde{t} = 0.01$, $\alpha^2 = 0.01$. 110

3.6 Concentration profiles at $\tilde{t} = 0.01$, $\alpha^2 = 0.0001$. 111

3.7 Charge density for the two transient cases. 112

3.8 The axisymmetrical problem. 113

3.9 Potential profile in a pore. 113

3.10 A comparison between the chemical activity models. 117

3.11 L2 element for the two-species case. 119

3.12 Stationnary solution for the low concentration case without activity. . . 125

3.13 SO_4^{2-} profiles with different models for the low concentration case. . . . 126

3.14 Stationnary solution for the high concentration case without activity. . 127

3.15 SO_4^{2-} profiles with different models for the high concentration case. . . 128

3.16 Mg^{2+} profiles with different models for the high concentration case. . . 128

3.17 SO_4^{2-} profiles for the non-stationnary case. 129

3.18 Electrical potential profiles for the non-stationnary case. 129

3.19 The Representative Elementary Volume 133

3.20 Calcium profile for the paste exposed to water. 151

3.21 Sulfur profiles for the paste exposed to sodium sulfate. 152

3.22 Calcium profiles for the paste exposed to sodium sulfate. 154

3.23 Simulations performed without electrical coupling and chemical activity terms. 155

3.24 Desorption isotherm of a 0.5 T50 paste. 158

3.25 Solid phase distribution after 20 years. 159

3.26 Effect of time steps on the position of the ettringite front. 160

3.27 Effect of the mesh density on the position of the ettringite front. 161

3.28 Effect of the water flow on the ettringite and portlandite fronts after 20 years. 162

4.1 Typical set-up for the migration test. 167

4.2 Influence of voltage determination on diffusion coefficients. 176

4.3 Sample problem – Comparison of the chloride profiles. 179

4.4 Sample problem – Comparison of the electrical potential. 180

4.5 Chloride profile measured by Tang and Nilsson. 180

4.6 Comparison of the measured current with the numerical model. 186

4.7 Experimental set-up for the migration test 197

4.8 Distribution of the solid phases after 20 years for the 0.65 concrete. . . 202

4.9 Calcium hydroxide profiles after 20 years (Type 10) 204

4.10 Calcium hydroxide profiles after 20 years (Type 50) 205

4.11 Ettringite profiles after 20 years (Type 10) 205

4.12 Ettringite profiles after 20 years (Type 50) 206

4.13 Ettringite profiles after 20 years for the 0.65 concrete 207

4.14 Calcium hydroxide profiles after 20 years for the 0.65 concrete 208

4.15 Ettringite profiles after 20 years for the 0.65 concrete 208

4.16 Calcium hydroxide profiles after 20 years for the 0.65 concrete 209

Introduction

La dégradation des structures en béton sous l'effet d'attaques chimiques est devenue l'une des principales préoccupations des ingénieurs civils oeuvrant dans le domaine du béton. Les exemples les plus courants de dégradation chimique sont la corrosion des armatures provoquée par le contact de la structure avec du chlore, les attaques aux sulfates, la réaction alcalis-granulat, et la carbonatation. Pour le seul cas de la corrosion des armatures, on estime à 20 milliards de dollars le coût de la réfection des structures exposées à ce problème aux États-Unis.

Tous ces exemples de dégradation prématurée des structures trouvent leur origine dans les échanges ioniques entre le matériau et son environnement. La corrosion des armatures est causée principalement par la pénétration de chlore externe dans le réseau poreux du béton. Les réactions chimiques se produisant lorsque le chlore réagit avec l'acier d'armature vont causer l'apparition de produits de corrosion expansifs qui vont, à terme, faire éclater le recouvrement de béton. L'attaque aux sulfates est basée sur le même principe. Dans ce cas, ce sont les ions sulfates, souvent présent dans le sol, qui vont pénétrer dans les pores du matériau. Si les conditions chimiques dans la structure sont propices, ces ions pourront être à l'origine de la formation d'ettringite et de gypse. Si la quantité d'ettringite et de gypse formée est importante, le matériau peut se fissure et perdre ainsi une partie de son intégrité structurale.

A l'opposé, une partie des ions se trouvant dans le matériau lors de sa mise en place peut se retrouver dans le milieu extérieur en contact avec la structure. Par exemple,

une structure en contact avec de l'eau verra une partie des ses ions hydroxydes le quitter, entraînant une baisse de pH dans le béton. Cette chute de pH va entraîner la dissolution de la portlandite et la décalcification des C-S-H, deux phases minérales donnant au matériau sa résistance mécanique. Il y aura donc dans ce cas également une perte d'intégrité structurale de la structure.

Le transport des ions dans les matériaux cimentaires peut donc avoir des conséquences extrêmement importantes sur les structures et les ouvrages d'art. Ces conséquences prennent une proportion d'autant plus grande que le béton est aujourd'hui le matériau de construction le plus utilisé dans le monde.

De toute évidence, une bonne connaissance des mécanismes de transport des ions dans les matériaux cimentaires ainsi que l'implantation de ces connaissances dans un modèle numérique permettrait de mieux évaluer l'impact de ces échanges ioniques sur la durée de vie des structures en béton. L'utilisation d'un modèle fiable permettrait d'évaluer le temps à partir duquel des réparations doivent être envisagées et d'estimer la durée de vie résiduelle des ouvrages. Un tel outil pourrait aussi intervenir à l'étape du design de la structure, en permettant de sélectionner le matériau le plus approprié pour résister aux conditions environnementales locales.

L'industrie du béton prend de plus en plus au sérieux l'utilisation de modèle pour prédire la durée de vie des ouvrages. Le code de calcul *Life-365* montre bien cet enthousiasme entourant les modèles de transport ionique. Il est né d'une collaboration entre l'American Concrete Institute, la Silica Fume Association et Master Builders Technologies, qui sont tous des acteurs importants dans cette industrie. Il permet de modéliser la pénétration du chlore dans des structures en béton, afin de prédire la durée de vie d'un ouvrage en béton armé.

Malgré tout cela, très peu de nouveaux développements sont apparus récemment sur le plan scientifique dans ce domaine. La plupart des modèles sont toujours basés sur la simple loi de Fick et leur utilisation est difficilement envisageable pour en arriver à faire des prédictions à long terme. Ce travail de recherche a donc pour objectif de développer un modèle de transport des ions dans les matériaux cimentaire qui, tout en considérant les travaux de recherche les plus récents, incorpore également certains phénomènes physiques qui sont habituellement mentionnés mais négligés

faute d'algorithmes numériques appropriés, tels le couplage électrique entre les ions et l'activité chimique.

Le mémoire de thèse est le regroupement des articles qui ont été écrits au cours de ce travail de recherche. Le format de ces articles a été légèrement modifié par rapport à la version publiée afin de faciliter la lecture du document. Ainsi, les équations, les figures et les tableaux ont été renumérotés dans le but de s'enchaîner d'un article à l'autre. De plus, la bibliographie de chacun des articles a été regroupée à la fin du mémoire pour former une bibliographie globale à l'ensemble du document.

Chapitre 1

Mise en contexte

1.1 Revue des modèles de transport ionique

L'intérêt pour la modélisation du transport ionique dans les milieux poreux est né dans les années 70. La prise de conscience des problèmes environnementaux a mené au développement de modèles dont l'objectif était de prédire l'étendue de la pénétration de contaminants dans le sol. L'hydrogéologie a donc été le premier domaine scientifique à s'intéresser aux modèles de transport ionique.

Les premiers modèles consistaient en une seule équation de transport, permettant de calculer le profil de concentration d'une seule espèce ionique. Ces modèles simplifiés tenaient compte de la diffusion, de la dispersion, de l'advection et, de façon très rudimentaire, des réactions chimiques subies par l'ion. Une brève description de chacun de ces phénomènes est donnée dans les paragraphes suivants.

Le transport de particules en solution par diffusion est le résultat de leur agitation thermique. Cette agitation produit une suite de collisions aléatoires entre les particules qui a pour effet de les disperser vers des régions de la solution où la concentration est plus faible. Dans le cas des ions, leur charge électrique influence ce comportement diffusif. Celui-ci sera modifié par le couplage électrique entre les ions et également par l'activité chimique de la solution [85, 213]. Ces phénomènes sont modélisés par la loi de Nernst-Planck étendue, qui donne le flux de l'ion i selon [85]:

$$\mathbf{j}_\mathbf{i}^{\text{diff}} = \underbrace{-D_i \text{grad}(c_i)}_{\text{diffusion}} - \underbrace{\frac{D_i z_i F}{RT} c_i \text{grad}(\psi)}_{\text{couplage élect.}} - \underbrace{D_i c_i \text{grad}(\ln \gamma_i)}_{\text{activité chimique}} \tag{1.1}$$

où D_i est le coefficient de diffusion de l'ion i, c_i est la concentration, z_i est la valence de l'ion, F est la constante de Faraday, R est la constante des gaz parfaits, T est la température, ψ est le potentiel électrochimique et γ_i est l'activité chimique. Dans les premiers modèles toutefois, le couplage électrique et l'activité chimique sont négligés.

La dispersion est un phénomène lié à l'écoulement de l'eau dans le sol sous l'effet d'un gradient de pression ou de charge hydraulique. Elle est associée à des variations locales de vitesse d'écoulement à l'échelle du pore [18]. On nomme dispersion hydrodynamique la combinaison de la diffusion et de la dispersion [18]. Le phénomène de dispersion est important pour les fortes valeurs de vitesses d'écoulement [18]. Lorsque les vitesses d'écoulement sont faibles, la diffusion est dominante. Dans beaucoup de modèle de transport de contaminants, on néglige la diffusion au profit de la dispersion. Il est possible d'exprimer le flux dispersif de manière similaire au flux diffusif [18]:

$$\mathbf{j}_\mathbf{i}^{\text{disp}} = -D^D \text{grad}(c_i) \tag{1.2}$$

où D^D est le coefficient de dispersion. On peut donc définir un coefficient de dispersion hydrodynamique comme : $D_i^{DH} = D_i + D^D$.

L'advection, soit le transport des ions résultant du mouvement du milieu aqueux lui-même, peut de façon très large être divisée en deux classes. Dans un cas, le transport du fluide se fait sous l'action d'un gradient de pression ou de charge hydraulique sur le matériau poreux. C'est le cas des barrages, par exemple. Le fluide obéit alors à la loi de Darcy [58, 74]. Les matériaux soumis à ce type de comportement demeurent saturés [74]. Dans l'autre cas, le transport du fluide se fait sous l'action de forces capillaires [74, 135], qui sont présentes dans le matériau lorsqu'il n'est pas saturé. Le

niveau de saturation du matériau peut-être modifié tout au long de sa vie en fonction des différents cycles de mouillage et de séchage auxquels il sera exposé. La portion du flux ionique reliée à l'advection est donnée par:

$$\mathbf{j_i^{adv}} = c_i \mathbf{v} \tag{1.3}$$

où $\mathbf{v}$ est la vitesse du fluide.

Les réactions chimiques qui affectent les ions peuvent être divisées en deux groupes principaux [149]: les réactions homogènes et les réactions hétérogènes. Les réactions homogènes se produisent exclusivement dans la solution. Il s'agit le plus souvent de réactions de complexation, où deux ions se combinent pour en former un troisième. Les réactions hétérogènes impliquent la phase solide du matériau poreux. Il peut s'agir d'interactions avec la surface du matériau (on parle alors de sorption ou d'échange ionique) ou d'interaction avec la phase solide en entier. Cette dernière catégorie comprend les réactions de dissolution/précipitation. Les réactions chimiques impliquent généralement plusieurs ions à la fois. Cependant, dans les premiers modèles de transport ionique, elles étaient modélisées de manière très simplifiée à partir du comportement d'un seul ion.

Avec l'avènement d'ordinateurs plus puissants, les années 80 ont vu l'apparition d'une deuxième génération de modèles, plus complexes, où le transport de plusieurs ions était pris en compte. Le transport des ions s'est ainsi vu couplé à des modèles chimiques pouvant reproduire plusieurs types de réactions. Ces modèles ont d'abord consisté à résoudre de manière couplée la chimie et le transport. Cette façon de résoudre les problèmes de transport ionique en milieux réactifs se nomme DSA (Direct Substitution Approach). Un article de Miller et Benson paru en 1983 [127] est souvent cité pour illustrer ce type d'algorithme.

Mais un article de Yeh et Tripathi publié en 1989 [207] allait changer considérablement la façon d'aborder ces problèmes. Ces auteurs ont montré dans leur article qu'il est plus intéressant de découpler le transport et la chimie, afin de réduire de manière importante le temps de calcul. Cela ouvrait ainsi la porte à la résolution de problèmes encore plus complexes. Depuis, la très grande majorité des articles publiés sur le sujet dans le domaine de l'hydrogéologie sont basés sur des algorithmes où les équations de transport et de chimie sont découplées. Ces algorithmes sont connus sous le nom de

SIA (Sequential Iterative Approach). Ils consistent à résoudre séparément le transport et la chimie, en faisant des itérations entre ces deux étapes de calcul jusqu'à atteindre la convergence. A l'intérieur des algorithmes de type SIA, la méthode SNIA (Sequential Non Iterative Approach) consiste à résoudre séparément le transport et la chimie, mais sans itérer entre ces deux étapes. L'article de Yeh et Tripathi a été critiqué par Saaltink & al. [151] car les études de temps de calcul publiées dans l'article sont théoriques et ne reflètent pas, selon eux, la réalité. Ils ont de leur côté montré que dans bien des cas, l'algorithme DSA est plus économique. Par contre, pour les problèmes de très grande taille, les méthodes SIA sont avantageuses. De plus, les méthodes SIA sont beaucoup plus faciles à implanter dans un modèle numérique et permettent d'utiliser des codes d'équilibre chimique déjà existants.

Le formalisme utilisé en hydrogéologie dans les modèles de transport ionique en milieux réactifs a été résumé dans un article de Kirkner et Reeves [96]. Ils ont exprimé les équations de transport de trois manières différentes, selon le type de réaction chimique en jeu. Ces formulations (A, B et C) sont exposées brièvement dans les paragraphes qui suivent. Les N espèces chimiques réactives en solution sont divisées en N_c composants et N_x complexes, avec $N = N_c + N_x$. Les complexes sont le résultat de réactions chimiques entre les composants. Les équations gouvernant le transport des N_c composants et N_x complexes sont:

$$\frac{\partial \phi c_j}{\partial t} + \mathrm{div}(c_j \mathbf{v} - \phi \mathbf{D} \mathrm{grad} c_j) = r_j^c \qquad j = 1, \ldots, N_c \tag{1.4}$$

$$\frac{\partial \phi x_i}{\partial t} + \mathrm{div}(x_i \mathbf{v} - \phi \mathbf{D} \mathrm{grad} x_i) = r_i^x \qquad i = 1, \ldots, N_x \tag{1.5}$$

où c_j est la concentration du composant j, x_i est la concentration du complexe i, $\mathbf{v}$ est la vitesse du fluide, ϕ est la porosité, $\mathbf{D}$ est le tenseur de dispersion hydrodynamique, r_j^c est le taux de réaction du composant j, et r_i^x est le taux de réaction du complexe i. Les auteurs considèrent que $\mathbf{D}$ est le même pour toutes les espèces chimiques. Cette approximation est valide lorsque la vitesse d'écoulement du fluide est importante par rapport à la diffusion.

Les auteurs introduisent ensuite la concentration soluble totale de chaque composant:

$$u_j = c_j + \sum_{i=1}^{N_x} A_{ij} x_i \tag{1.6}$$

où A_{ij} est une matrice de coefficients stoechiométriques permettant de relier les composants aux complexes. Les taux de réactions r_j^c sont définis comme:

$$r_j^c = r_j^{c(aq)} + r_j^{c(s)} + r_j^{c(p)} \tag{1.7}$$

où:

$$r_j^{c(aq)} = -\sum_{i=1}^{N_x} A_{ij} r_i^x \qquad \text{taux de réaction de } j \text{ dû à la complexation} \tag{1.8}$$

$$r_j^{c(s)} = -\frac{\partial \phi s_j}{\partial t} \qquad \text{taux de réaction de } j \text{ dû à la sorption ou à l'échange ionique} \tag{1.9}$$

$$r_j^{c(p)} = -\sum_{i=1}^{N_p} B_{ij} \frac{\partial \phi p_i}{\partial t} \qquad \text{taux de réaction de } j \text{ dû à la précipitation/dissolution} \tag{1.10}$$

Dans les équations (1.8) à (1.10), s_j correspond au composant j sorbé, p_i est la concentration du précipité i, N_p est le nombre d'espèces immobiles (solides), et B_{ij} est une matrice de coefficients stoechiométriques. Le terme s_j peut généralement être exprimé comme une fonction (implicite ou explicite) de la concentration des composants:

$$s_j = f_j^{sc}(c_1, c_2, \ldots, c_{N_c}) \tag{1.11}$$

et peut à son tour être exprimé comme une fonction de of u_j:

$$s_j = f_j^{su}(u_1, u_2, \ldots, u_{N_c}) \tag{1.12}$$

En combinant les équations (1.4) et (1.5) avec l'aide de la relation (1.6), et en considérant les expressions (1.7) à (1.12), il est possible d'écrire:

$$\frac{\partial(\phi u_j)}{\partial t} + \frac{\partial(\phi f_j^{su})}{\partial t} + \sum_{k=1}^{N_p} B_{kj} \frac{\partial(\phi p_k)}{\partial t} + L(u_j) = 0 \qquad j = 1, \ldots, N_c \tag{1.13}$$

où $L(.)$ est l'opérateur linéaire de dispersion-convection:

$$L(.) = \text{div}[(.)\mathbf{v} - \phi \mathbf{D} \text{grad}(.)] \tag{1.14}$$

L'équation (1.13) est à la base de nombreux modèle de transport multiionique dans le domaine de l'hydrogéologie. Elle correspond à la Formulation A de Kirkner et Reeves.

Il est possible de simplifier davantage les équations de transport en introduisant la concentration totale w_j du composant j comme variable primaire:

$$w_j = u_j + s_j + \sum_{k=1}^{N_p} B_{kj} p_k \qquad j = 1, \ldots, N_c \tag{1.15}$$

De l'équation (1.15), il est possible d'écrire les expressions suivantes:

$$w_j = f_j^{uc}(c_1, \ldots, c_{N_c}) + f_j^{sc}(c_1, \ldots, c_{N_c}) + \sum_{k=1}^{N_p} B_{kj} p_k \qquad j = 1, \ldots, N_c \tag{1.16}$$

$$c_j = f_j^{cw}(w_1, \ldots, w_{N_c}) \qquad j = 1, \ldots, N_c \tag{1.17}$$

$$p_j = f_j^{pw}(w_1, \ldots, w_{N_c}) \qquad j = 1, \ldots, N_p \tag{1.18}$$

$$u_j = f_j^{uw}(w_1, \ldots, w_{N_c}) \qquad j = 1, \ldots, N_c \tag{1.19}$$

$$s_j = f_j^{sw}(w_1, \ldots, w_{N_c}) \qquad j = 1, \ldots, N_c \tag{1.20}$$

En utilisant ces relations, il est possible de transformer l'équation (1.13):

$$\frac{\partial(\phi w_j)}{\partial t} + L[f_j^{uw}(w_1, \ldots, w_{N_c})] = 0 \qquad \text{Formulation B} \tag{1.21}$$

ou

$$\frac{\partial(\phi w_j)}{\partial t} + L(w_j) = L[f_j^{sw}(w_1, \ldots, w_{N_c})] + \sum_{k=1}^{N_p} B_{kj} L[f_k^{pw}(w_1, \ldots, w_{N_c})] \qquad \text{Formulation C} \tag{1.22}$$

Tel que spécifié dans l'article de Kirkner et Reeves, le choix de la formulation dépend essentiellement du type de réactions chimiques en jeu. Avant le développement des algorithmes SIA et SNIA, La formulation A était la plus souvent utilisé lorsque les réactions de dissolution/précipitation étaient absentes. Le tableau 1.1 passe en revue des modèles de transport ionique développés pour prédire le transport d'espèces chimiques dans les eaux souterraines. Le choix de la formulation adoptée par les auteurs est indiqué. Tous les modèles présentés dans le tableau sont basés sur un opérateur de transport linéaire, ce qui permet de simplifier grandement la formulation mathématique du problème (voir l'équation 1.13). Une telle simplification ne serait pas possible avec un modèle de transport basé sur la loi de Nernst-Planck étendue (équation 1.1).

Les premiers modèles de transport ionique dans le domaine du béton sont nés à peu près à la même époque que les modèles de transport de contaminants dans les sols.

Table 1.1: Revue de modèles de transport ioniques dans le domaine de l'hydrogéologie.

Auteurs	Année	Transport	Compl.	Ech. ion., sorption	Préc., diss.	Autres	Notes
Miller, Benson [127]	1983	1D, saturé, adv., diff./disp., D const., $L(.)$ lin., DF, Euler imp.	×	×			Formulation A sans le terme de diss./préc., sorption modélisée selon un modèle d'échange ionique, CEC constant, algo DSA: résolution couplée des équations différentielles et algébriques.
Walsh et al. [197]	1984	1D, saturé, adv. seule, disp. num. pour éviter les oscillations, $L(.)$ lin., DF, Euler exp.	×		×	redox	Formulation A, algorithme SNIA, le schéma explicite permet de résoudre directement pour la concentration totale C_i^T dans le pas de transport.
Cederberg, Street, Leckie [34]	1985	1D, saturé, disp. seule, $L(.)$ lin., MEF, Crank-Nich.	×	×			Formulation A et SNIA pour les composants sans adsorption, formulation B et SIA pour les composants avec adsorption mais schéma explicite pour ces équations (solution dépend de w_t et $u_{t+\Delta t/2}$, CEC et pH constant pour le modèle d'échange ionique.
Lewis, Voss, Rubin [102]	1987	1D, saturé, adv., disp., D const., $L(.)$ lin.,	×	×			Formulation A, algo. SNIA pour les composants soumis seulement à la complexation, SIA pour les autres, CEC constant pour le modèle d'échange ionique,isotherme linéaire exprimée comme $f(u_1)$.
Liu, Narasimhan [108]	1989	2D, saturé, adv., disp., D const., $L(.)$ lin., DF intégrales., Euler exp.	×		×	redox	Formulation A, termes d'échange solide/solution éliminés, SNIA, mentionnent que 99.9% du temps CPU est dans la chimie pour les problèmes présentés.
Yeh, Tripathi [208]	1991	2D, non-sat., adv., disp., D const., $L(.)$ lin., MEF, rés. temp.: schémas θ.	×	×	×	redox,	Formulation C, algorithme SIA, donnent des exemples avec une comparaison SIA, SNIA.
Engesgaard, Kipp [61]	1992	1D, saturé, adv., disp., D const., $L(.)$ lin., DF, Euler exp.	×		×	redox	Formulation A, algo. SIA: le terme source est mis à zéro à la première itération; aux itérations suivantes $\partial c_i^s/\partial t$ est évalué en fonction de la variation du solide aux itérations précédentes.
Zysset, Stauffer, Dracos [215]	1994	1D, saturé, adv., disp., D const., $L(.)$ lin., MEF, Crank-Nich..	×		×		Formulation A à la base, modifiée pour tout exprimer en fonction de la concentration totale w_j et d'un facteur de retard ρ_j, algo. SIA: résolution des éq. de transport pour les composants conservatifs; ensuite, itérations entre le transport des éléments non-conservatifs et la chimie.

Abbréviations: adv.: advection – disp.: dispersion – const.: constant – lin.: linéaire – MEF: méthode des éléments finis – *CEC: Cation Exchange Capacity – diff.: diffusion – DF: différences finies – imp.: implicite – exp.: explicite* – Nich.: Nicholson – rés.: résolution – temp.: temporelle – redox: réactions d'oxydo-réduction.

Table 1.1: (suite) Revue de modèles de transport ioniques dans le domaine de l'hydrogéologie.

Auteurs	Année	Transport	Compl.	Ech. ion., sorption	Préc., diss.	Autres	Notes
Simunek, Suarez [169]	1994	2D, non-saturé, adv., disp., D const., $L(.)$ lin., MEF.	×	×	×	diss. de gaz, chimie du CO_2	Formulation A, algo. SIA où les termes de diss./préc. sont nuls à la première itération et mis à jour par la suite.
Walter, Frind, Blowes, Ptacek, Molson [198]	1994	2D, 3D, saturé, adv., disp., D const., $L(.)$ lin., MEF, Crank-Nich.	×	×	×	redox	Formulation A, algo. SIA et SNIA, SIA: les termes sources sont évalués au temps intermédaire à partir des résultats à l'itération précédente, SNIA: les termes sources sont éliminés, comparaison SIA-SNIA: les différences sont si faibles que l'approche SNIA est privilégiée.
Xu, Samper, Ayora, Manzano, Custodio [206]	1999	2D, non-saturé, adv., disp., D const., $L(.)$ lin., MEF, conduction.	×	×	×	redox, diss. de gaz	Formulation A, algo. SIA où les termes de diss./préc. sont nuls à la première itération et mis à jour par la suite, comparaison SIA-SNIA: SIA prend de 2 à 4 fois plus de temps CPU selon les cas testés, la différence entre les deux est faible pour les nombres de Courant faibles.
Saaltink, Carrera, Ayora [151]	2001	2D, saturé, adv., disp., D const., $L(.)$ lin., MEF, Crank-Nich.	×	×	×		Formulation A, algo. SIA, les termes de sorption et de diss./préc. sont traités comme un terme source calculé avec les données des itérations précédentes, comparaison avec l'algo DSA.

Abbréviations: adv.: advection – disp.: dispersion – const.: constant – lin.: linéaire – MEF: méthode des éléments finis – CEC: Cation Exchange Capacity – diff.: diffusion – DF: différences finies – imp.: implicite – exp.: explicite – Nich.: Nicholson – rés.: résolution – temp.: temporelle – redox: réactions d'oxydo-réduction.

Leurs caractéristiques étaient tout à fait similaires. Il s'agissait de modèles simplifiés ne tenant compte que d'un seul ion et où les réactions chimiques étaient basées sur une approche aussi très simplifiée. L'ion en question était le plus souvent le chlore, afin de déterminer le temps nécessaire pour initier la corrosion des armatures dans les structures de béton armé.

Cependant, les modèles dans ce domaine n'ont pas connu de deuxième génération similaire à ce qui s'est fait en hydrogéologie. L'augmentation de la puissance de calcul des ordinateurs n'a pas amené le développement de modèles multiioniques faisant intervenir des réactions chimiques complexes. Les raisons derrière cette absence d'évolution significative sont difficiles à expliquer. Il est vrai que le béton est un matériau fortement chargé en ion, contrairement aux sols, et par conséquent les termes de couplage électrique et d'activité chimique dans l'équation de Nernst-Planck étendue (1.1) sont plus difficilement négligeables. Un opérateur de transport non-linéaire complique grandement la résolution des problèmes de transport, ce qui peut en partie expliquer que la très grande majorité des modèles proposés encore aujourd'hui sont simplifiés.

Ainsi, les modèles de transport ionique dans les matériaux cimentaires sont encore pour la plupart basés sur la loi de diffusion de Fick. C'est le cas par exemple dans les travaux de Gospodinov et al. [72], Hansen et Saouma [76], Martín-Pérez [120], Nagesh et Bhattacharjee [130], Saetta et al. [152], et Swaddiwudhipong et al. [178]. On note cependant de plus en plus de travaux où le couplage électrique entre les ions fait partie du modèle. C'est le cas notamment des travaux de Masi et al. [122] et Truc et al. [189]. Les modèles considérant l'activité chimique sont encore plus rares. Li et Page [103] l'ont inclus dans leur modèle, en plus du couplage électrique. Leur modèle n'est cependant applicable que pour un échantillon de matériau cimentaire exposé à un courant électrique.

L'advection causée par la présence de gradients d'humidité dans une structure est considérée dans certains modèles. Dans les modèles cités précédemment, ceux de Martín-Pérez [120], Nagesh et Bhattacharjee [130], Saetta et al. [152], et Swaddiwudhipong et al. [178] considèrent l'effet des forces capillaires dans les matériaux cimentaires non saturés sur le déplacement des ions.

La diffusion et l'advection entraînent les ions à travers le réseau poreux du béton. Ils

sont alors susceptibles du subir des réactions chimiques avec la pâte de ciment hydratée. A titre d'exemples, la pénétration dans un matériau cimentaire d'ions sulfates (SO_4^{2-}) donne lieu à des réactions chimiques pouvant mener à la création d'ettringite et de gypse, alors que le chlore est à la base de la création de chloroaluminates. Des études menées sur des systèmes cimentaires simplifiés ont montré le caractère multiionique de ces réactions. Les réactions chimiques impliquant les sulfates sont couplés aux ions Ca^{2+}, OH^-, et $Al(OH)_4^-$ [49, 199]. La formation de chloroaluminates d'autre part dépend aussi du niveau de concentration des ions Ca^{2+}, OH^-, et $Al(OH)_4^-$ en plus évidemment de la concentration en chlore [1, 20]. De plus, que ce soit pour la formation d'ettringite ou de chloroaluminates, la présence d'ions Na^+ et K^+ en solution influence les réactions chimiques, même s'ils n'y prennent pas directement part [47, 48].

Tous les modèles cités précédemment incluent les réactions chimiques. Ils utilisent tous, sans exception, un modèle simplifié de réactions chimiques ne faisant appel qu'à un seul ion. Il s'agit de la méthode des isothermes d'interaction [183], dans laquelle une courbe expérimentale relie la quantité d'ions liés à la pâte de ciment, à la concentration en ion en solution. La plupart du temps, le chlore est l'ion étudié. Cette méthode est utilisée aussi bien dans les modèles à un seul ion que dans les modèles multiioniques cités auparavant. S'il permet de reproduire le comportement du chlore, par exemple, l'isotherme d'interaction ne permet pas de tenir compte des réactions chimiques qui peuvent se produire simultanément, telle que la dissolution de la portlandite et la décalcification des C-S-H. L'utilisation d'un modèle simple limite donc la possibilité de modéliser certaines réactions chimiques susceptibles d'affecter de façon importante une structure exposée à un environnement agressif.

Certains modèles multiioniques sont apparus récemment. Il s'agit entre autre des travaux de Adenot [3] et Planel [139]. Dans ces modèles, la modélisation des réactions de dissolution et de précipitation se fait selon les équations d'équilibres des différentes phases solides de la pâte de ciment hydraté. Cela constitue une grande amélioration par rapport à la méthode des isothermes qui est couramment utilisée. Cependant, les opérateurs de transport servant à décrire le déplacement des ions sont linéaires et ne considèrent ni le couplage électrique entre les ions ni les effets de l'activité chimique.

1.2 Objectif de la recherche

Comme l'a montré la brève revue bibliographique précédente, la tendance actuelle dans le domaine de la modélisation du transport ionique dans les matériaux cimentaires est toujours aux modèles à un seul ion. Cette approche simplifiée est cependant de plus en plus remise en question, comme en témoigne les rares modèles multiioniques qui commencent à apparaître.

L'objectif de la thèse est de développer un modèle numérique de transport des ions dans les matériaux cimentaires tenant compte de plusieurs ions et de l'interaction entre ces derniers. Le modèle se devra d'être multiionique autant au niveau du transport, en tenant compte du couplage électrique entre les ions et de l'activité chimique, qu'au niveau des réactions chimiques. L'effet des forces capillaires sur la solution des pores dans le cas où le matériau est non saturé sera également considéré.

Le travail fait au cours de la recherche est exposé de la façon suivante. Le chapitre 2 est consacré au développement mathématique d'un modèle de transport des ions dans un milieu poreux non saturé applicable aux matériaux cimentaires. Par la suite, les différents algorithmes développés dans le but de résoudre le système d'équations non linéaires sont décrits en détail au chapitre 3. Finalement, des exemples d'application du modèle sont donnés au chapitre 4.

1.3 Description du matériau

Les matériaux cimentaires désignent en général les matériaux faits avec du ciment et de l'eau, auxquels on ajoute des granulats de tailles diverses afin d'en augmenter les performances mécaniques. Le matériau obtenu à partir du mélange eau – ciment se nomme pâte de ciment. Si le seul type de granulat ajouté au ciment et à l'eau est du sable, on parle alors de mortier. Les bétons sont quant à eux un mélange de ciment, d'eau, de sable, et de granulats plus grossiers.

Dans les ouvrages de génie civil, le ciment le plus couramment utilisé est le ciment Portland. Il est obtenu à la suite de la cuisson à très haute température d'un mélange de chaux vive (CaO) et de divers autres oxydes tels le SiO_2, le Al_2O_3, et le Fe_2O_3. La

cuisson de ces composés donne le clinker, formé de particules ayant un diamètre de l'ordre du centimètre. Le clinker est ensuite broyé pour donner les grains de ciment. Le ciment Portland est formé de clinker broyé auquel on ajoute environ 5% de gypse.

Le clinker est composé majoritairement des quatre phases suivante[1] [185]:

- C_3S ($3CaO.SiO_2$)
- C_2S ($2CaO.SiO_2$)
- C_3A ($3CaO.Al_2O_3$)
- C_4AF ($4CaO.Al_2O_3.Fe_2O_3$)

Dans les grains de ciment, le C_3S et le C_2S forment des particules compactes reliées entre elles par une phase interstitielle composée des phases alumineuses C_3A et C_4AF.

Lorsqu'ils sont mis en contact avec de l'eau, les grains de ciment subissent une série de réactions chimiques exothermiques qui va mener à la pâte de ciment hydratée. Le C_3S et le C_2S réagissent de la façon suivante avec l'eau:

$$2C_3S + 6H_2O \rightarrow \underbrace{3CaO.2SiO_2.3H_2O}_{\text{C-S-H}} + 3\underbrace{Ca(OH)_2}_{\text{portlandite}} \tag{1.23}$$

$$2C_3S + 4H_2O \rightarrow \underbrace{3CaO.2SiO_2.3H_2O}_{\text{C-S-H}} + \underbrace{Ca(OH)_2}_{\text{portlandite}} \tag{1.24}$$

L'hydratation du C_3S et du C_2S produit les deux composés de base de la pâte hydratée, soient les C-S-H et la portlandite. La composition des C-S-H donnée aux équations (1.23) et (1.24) constitue une approximation. La formulation exacte des C-S-H est très variable et dépend entre autre du rapport calcium/silice qui entre dans leur composition [3]. Les C-S-H ainsi formés constituent un gel mal cristallisé formé d'un assemblage de particules très fines, dont la taille est de l'ordre du micron [185]. La portlandite quant à elle est formée de cristaux ayant une composition bien définie (voir les équations (1.23) et (1.24)).

L'hydratation du C_3A en présence d'eau et de gypse donne de l'ettringite selon la

[1] Selon la notation des cimentiers, C=CaO, S=SiO_2, A=Al_2O_3, F=Fe_2O_3.

réaction suivante:

$$C_3A + 3\underbrace{CaSO_4.2H_2O}_{\text{gypse}} + 26H_2O \rightarrow \underbrace{3CaO.Al_2O_3.3CaSO_4.32H_2O}_{\text{ettringite}} \quad (1.25)$$

Lorsque la source de gypse s'épuise, on rapporte que l'ettringite devient instable et se transforme en monosulfoaluminates ($3CaO.Al_2O_3.CaSO_4.12H_2O$). Cependant, l'étude de l'hydratation du système CaO - Al_2O_3 - $CaSO_4$ - H_2O a révélé que la phase sulfatique stable est l'ettringite [48, 49].

La réaction du C_3A avec le gypse n'épuise qu'une partie du C_3A. Le reste va réagir pour former divers aluminates de calcium hydratés: C_4AH_{13}, C_2AH_8, C_3AH_6. L'étude du système CaO - Al_2O_3 - $CaSO_4$ - H_2O a montré que le C_3AH_6 (hydrogrenat) est la forme stable qui apparaîtra dans une pâte parfaitement hydratée [48, 49].

L'hydratation du C_4AF a fait l'objet de beaucoup moins d'étude et est encore relativement méconnue. Des études faites sur l'hydratation de C_4AF pur en présence ou non de gypse ont révélé qu'elle est très semblable à celle du C_3A [185]. Il y a donc production, d'ettringite, de monosulfoaluminates et d'hydrogrenat, sans compter certaines phases intermédiaires comme le C_2AH_8.

La pâte hydratée forme un milieu poreux contenant une solution fortement chargée en ions OH^-, Na^+ et K^+ ayant un pH de l'ordre de 13.5 [141]. On y retrouve également en concentration plus réduite les ions SO_4^{2-}, Ca^{2+} et $Al(OH)_4^-$ [141]. En fonction du rapport eau/ciment de la pâte et des conditions d'hydratation (éprouvettes scellées, immersion dans l'eau), une partie du ciment restera anhydre. Des pores pourront également être non saturés, toujours selon le rapport eau/ciment et les conditions d'hydratation [77]. La figure 1.1 montre les proportions de pâte hydratée, de pâte anhydre, de capillaires et de capillaires vide en fonction du rapport eau/ciment pour deux conditions d'hydratation différentes, selon le modèle de Powers [77].

Une étude de porosimétrie au mercure sur des pâtes de ciment hydratées [194] révèle deux classes de porosité distinctes (voir la figure 1.2). Une partie de la porosité provient des pores capillaires, dont le rayon est de l'ordre de 0.1μm. Elle correspond au volume capillaire illustré sur la figure 1.1. L'autre classe de porosité correspond à des pores ayant un rayon beaucoup plus fin, de l'ordre de 10nm. On parle alors des pores de gel, puisqu'ils sont associés à l'espace interfeuillet du gel de C-S-H. Le modèle de Powers

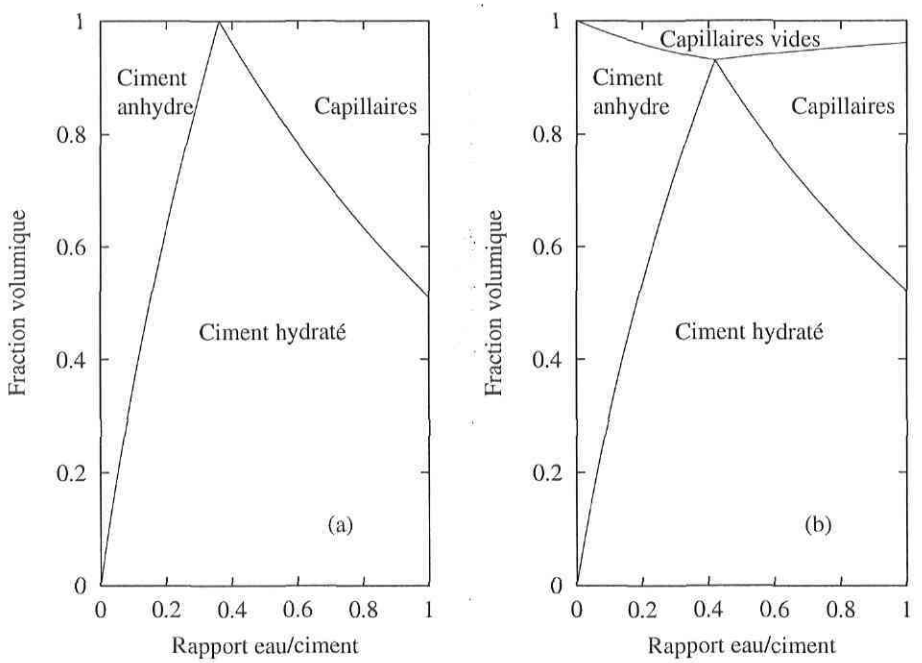

Figure 1.1: Proportion de pâte hydratée, de pâte anhydre, de capillaires et de capillaire vides dans une pâte de ciment parfaitement hydratée, selon le modèle de Powers [77]. La figure (a) correspond à une pâte de ciment hydratée en immersion continue dans l'eau. La figure (b) correspond à une pâte de ciment hydratée dans des conditions scellées.

[77] permet d'évaluer la proportion de chacune des classes de porosité dans une pâte de ciment en fonction de son degré d'hydratation et du rapport eau/ciment. La figure 1.3 montre la porosité capillaire et la porosité de gel d'une pâte de ciment ayant atteint son degré d'hydratation maximal en fonction du rapport eau/ciment.

1.4 Hypothèses de base

Le transport ionique dans les matériaux cimentaires implique une gamme très vaste de phénomènes physiques. Dans l'état actuel de la recherche dans ce domaine, tant au niveau de la compréhension de ces différents phénomènes que des algorithmes développés afin de résoudre efficacement les équations en jeu, il est impensable d'envisager un modèle global de transport. Des simplifications sont nécessaires afin de limiter le champ d'étude. Le modèle obtenu dans ces conditions pourra toujours par la suite être

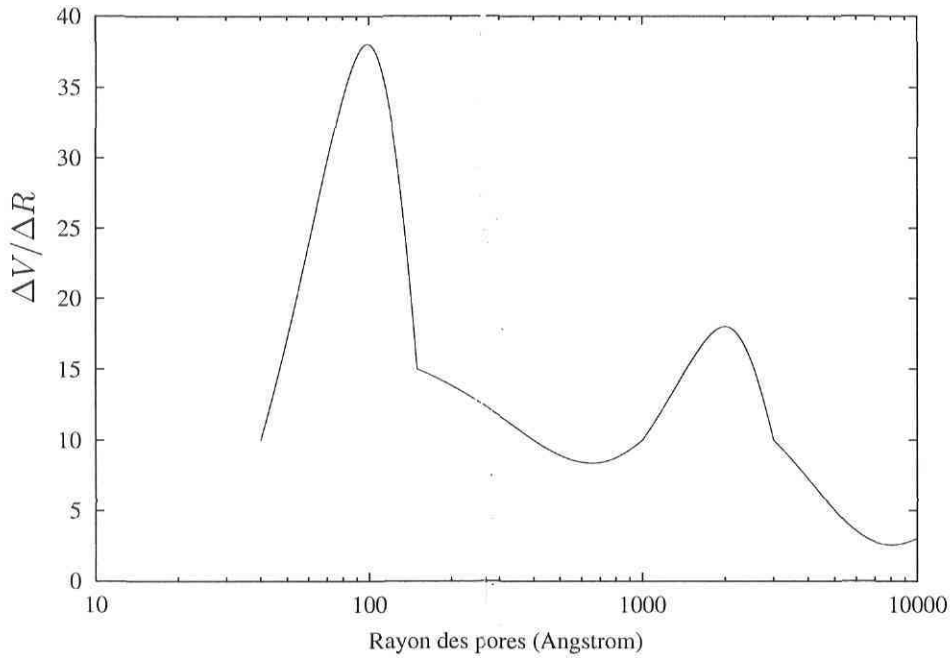

Figure 1.2: Courbe de distribution de la porosité, d'après [194]

amélioré.

La première hypothèse concerne la température. Le modèle développé dans cette thèse suppose que le transport ionique s'effectue dans des conditions isothermes. Les éventuels effets d'une variation de température aussi bien sur le transport des ions que sur la distribution d'eau et les réactions chimiques dans une matrice non saturée sont négligés.

On néglige également les effets que pourraient avoir les contraintes mécaniques sur le transport des ions. Des fissures peuvent apparaître dans les zones en traction d'une structure, ce qui facilite la progression des ions. A l'inverse, des zones en compression pourraient voir les fissures se refermer, ralentissant du même coup les ions. Les fissures peuvent aussi être une conséquence directe de la dissolution ou de la précipitation de certaines phases solides comme la portlandite ou l'ettringite. Elles sont aussi négligées. On ne tient pas compte non plus des fissures induites par le séchage de la structure. Toute ces hypothèse reviennent à considérer une pâte homogène.

L'autre hypothèse de base touche plutôt la partie numérique du projet. Même si le modèle mathématique est développé de façon générale pour des cas en trois dimensions,

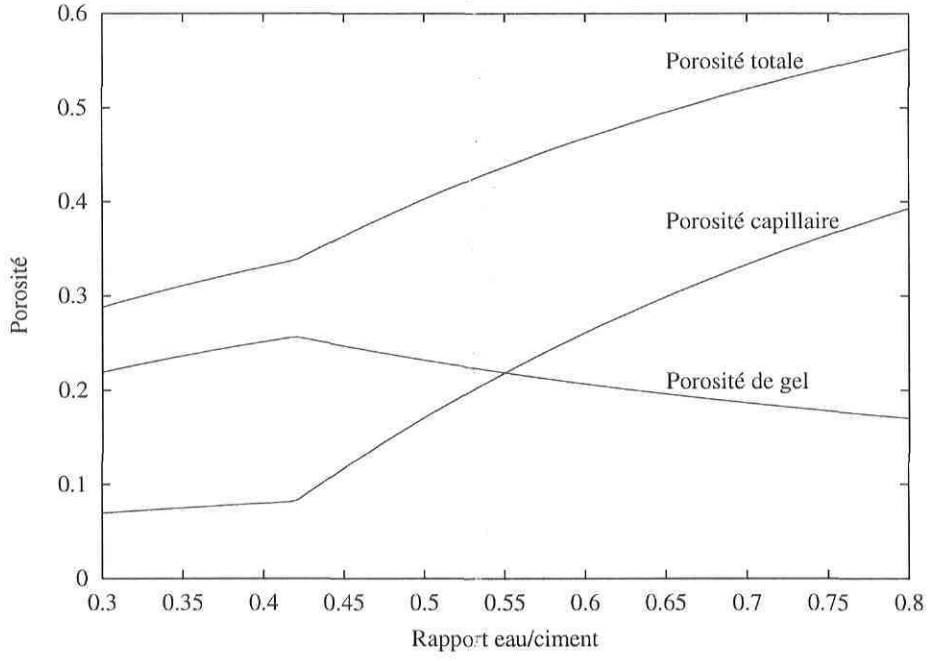

Figure 1.3: Les différentes classes de porosité selon le modèle de Powers [77]. Les calculs sont faits en supposant une pâte de ciment parfaitement hydratée.

le modèle numérique ainsi que tous les exemples présentés dans le chapitre 4 sur les applications sont unidimensionnelles.

Finalement, même si plusieurs type de réactions chimiques ont lieu dans le matériau, les travaux ont été limités aux réactions de dissolution et de précipitation. On s'attardera plus particulièrement aux cas d'attaques aux sulfates et d'exposition à l'eau pure.

Les hypothèses énoncées précédemment permettent de cerner le cadre général du travail effectué pour cette recherche. D'autres hypothèses furent utilisées pour développer certains points spécifiques du modèle mathématique ou de l'algorithme numérique. Elles seront clairement énoncées dans les chapitres suivants.

Chapitre 2

Modèle mathématique

2.1 Introduction

Ce chapitre est consacré à l'écriture mathématique du modèle de transport des ions en milieu non saturé, dans les cadre des hypothèses qui ont été évoquées au chapitre précédent, soient des conditions isothermes et une pâte homogène. La technique employée pour écrire le modèle s'appelle l'homogénéisation. Elle consiste d'abord à écrire les équations dans la phase liquide au niveau du pore dans un Volume Elémentaire Représentatif (VER). Les équations sont ensuite intégrées au niveau de ce volume élémentaire, ce qui donne les équations de tranpsort à l'échelle macroscopique.

Quatre articles sont présentés [1]. Le premier article consiste en une introduction à la technique de l'homogénéisation. La méthode est appliquée à une loi de diffusion très

[1] La référence exacte de ces articles est donnée dans la bibliographie à la fin du mémoire.

simple, la loi de Nernst-Planck, sans tenir compte des forces capillaires ou des réactions chimiques. On y jete les bases mathématiques de la méthode. Les résultats, même s'ils sont partiels compte tenu du modèle de transport simple, mettent en évidence une définition claire du coefficient de diffusion des ions.

Le modèle mathématique complet est exposé dans le deuxième article. On y développe les lois de transport des ions ainsi que l'équation de transport du fluide sous l'effet de forces capillaires.

Les matériaux cimentaires ont la particularité de porter dans leurs pores une solution très fortement concentrée. Pour des concentrations aussi fortes, les effets d'activité chimique sont susceptibles d'avoir une importance non négligeable. Toutefois, les modèles actuels pour calculer les coefficients d'activité ne sont pas adaptés à des solutions si chargées. Le troisième article présente les travaux entrepris afin de développer une loi simple d'activité permettant de combler cette lacune.

Le dernier article de ce chapitre se veut une revue bibliographique des modèles permettant de tenir compte de différents types de réactions chimiques dans les équations de transport ionique. On y discute de l'application des méthodes exposées au cas des matériaux cimentaires. Le choix de l'algorithme sera fait au chapitre suivant concernant les méthodes numériques.

2.2 Describing ion diffusion mechanisms in cement-based materials using the homogeneization technique

E. Samson[12], J. Marchand[12], J.J. Beaudoin[3]

[1]Centre de recherche interuniversitaire sur le béton,
Université Laval, Québec, Canada, G1K 7P4

[2]SIMCO Technologies inc.,
1400, boul. du Parc Technologique, Québec, Canada, G1P 4R7

[3]Materials Laboratory - Institute for Research in Construction,
National Research Council, Ottawa, Canada, K1A 0R6

Abstract

The application of the homogeneization technique to the mathematical description of the diffusion mechanisms in saturated cement-based materials is discussed. According to this approach, the transport and mass conservation equations are first written at the microscopic scale in order to describe the movement of particles in the fluid phase of the material. These equations are then averaged over the entire volume of the material. An example of the application of the homogeneization technique is given. The homogeneization technique is used to describe the diffusion of ions in cement-based systems. The various equations are written in order to consider the charged nature of the ionic particles and the coupling between the various ionic fluxes. The numerous advantages of this technique for the modeling of mass transport mechanisms in cement-based materials are discussed.

2.2.1 Introduction

Concrete structures are exposed to various types of aggression during their service life. Deterioration mechanisms generally involve the penetration of external ions into the cement system pore structure. This results in chemical and physical interaction with the binder solids including leaching of chemical species. In many cases, these phenomenons occur simultaneously. The durability of the material is therefore often directly controlled by its ability to act as an impervious barrier that can effectively impede, or at least slow down, the mass transport processes.

Although capillary absorption and permeation (i.e. the transport of a fluid under a pressure gradient) can, in certain cases, be of significant importance, numerous studies have clearly indicated that ions are mainly transported through the concrete pore structure and microcracks by a diffusion process [125, 131, 148]. This is the reason why the mechanisms of diffusion in saturated cement-based materials have received considerable attention [115].

Literature review [115] has recently indicated that despite the relative agreement on the parameters that affect the ionic diffusion mechanisms in saturated cement systems

(mixture characteristics, length and type of curing, ...), a lack of concensus on how to characterize the diffusion properties of these materials exists. Some authors choose to consider the diffusion coefficient as an intrinsic characteristic of the overall material. Others prefer to treat it as a property of the liquid phase. Unfortunately, there appears to be no definitive agreement on the mathematical procedure to convert one coefficient into another.

An attempt to clarify the mathematical treatment of diffusion mechanisms in saturated cement systems is presented. The mass transport equations are derived using the homogeneization technique. The fundamental assumptions implicit in the application of this technique lie in the theoretical treatment of the porous system. The later is considered as comprised of the sum of solid, liquid and eventually gaseous phases. Although there can be exchanges of mass between them (through chemical reactions or any physical interaction phenomena), each individual phase is treated as a distinct entity.

The first step of the homogeneization technique consists in writting the transport and mass conservation equations at the microscopic scale. These equations are then averaged over the entire volume of the material. The various aspects of the averaging technique are well described in the text. The application of this approach to the description of ionic diffusion mechanisms in cement-based materials is discussed.

2.2.2 Description of the ionic diffusion mechanisms in the liquid phase

The application of the homogeneization technique first requires writing the mass and transport equations at the microscopic scale. For the particular case of ion diffusion in saturated cement-based materials, the assumption that transport occurs predominantly in the liquid phase is required. The application of the mass conservation equation for an ionic species diffusing in the liquid phase yields:

$$\frac{\partial c_i}{\partial t} + \mathrm{div}(\boldsymbol{j_i}) = 0 \tag{2.1}$$

where c_i is the concentration of the considered species in solution and $\boldsymbol{j_i}$ is the flux of the same species in the liquid phase. It should be emphasized that equation (2.1) has

to be repeated for each and every ionic species present in solution. Also, no chemical reactions appears in this equation. At the pore scale, they are modeled by boundary conditions.

In order to reliably describe the flux of a given species, one has to account for the particularities of ionic diffusion mechanisms in liquids. Contrary to molecules, ions are charged particles. In addition to the viscous-drag force exerted by their environment, drifting ions will also be subjected to various electrical forces. For instance, the charged nature of the ionic particles is at the origin of various interactions between the drifting particles (ion/ion interactions and ion/solvent interactions). These so-called activity effects quickly become important as the concentrations of the various ions in solution increase. The electrical charge of the particles may also contribute to generate specific ion/solid interactions that can be both physical or chemical in nature. More information on these two phenomena can be found in references [115] and [117].

Despite the relative importance of activity effects and ion/solid interaction phenomena, it is emphasized that the most important feature which distinguishes ion diffusion from molecular diffusion is the electrical coupling of the various ionic flows [36, 115, 158]. In an ionic solution, the local electroneutrality shall be preserved at any point. The conservation of electroneutrality requires that the flows of all diffusing species should be coupled. During the diffusion process, all ions are not drifting at the same speed. Some ions tend to diffuse at a higher rate. However, any excess charge transferred by the faster ions builds up a local electric field (called the diffusion potential) which slows down the faster ions, and reciprocally accelerates the slower ions.

It can be shown that the mechanisms of ionic diffusion in solution can be reliably described on the basis of the following equation [85, 115, 117]:

$$\boldsymbol{j_i} = -D_i^{\mu}\mathrm{grad}(c_i) - \frac{D_i^{\mu} z_i F}{RT} c_i \mathrm{grad}(\psi) - D_i^{\mu} c_i \mathrm{grad}(\ln \gamma_i) \tag{2.2}$$

where R is the ideal gas constant (J/mol/°K), F the Faraday constant (C/mol), T the temperature (°K) and z_i the valence of the ion.

The coefficient D_i^{μ} appearing in the equation is the diffusion coefficient in the liquid phase, i.e. at the microscopic scale. It represents the diffusion coefficient in an ideal solution, i.e. in a very dilute solution. The value of D_i^{μ} for chloride ions is 2.032×10^{-9} m^2/s [43].

The variable γ_i appearing in equation (2.2) is the chemical activity coefficient of the chemical species in solution. For concentrated solutions, it can be calculated using various semi-empirical equations [115, 158].

Finally, the variable ψ in equation (2.2) stands for the diffusion potential (Volt) set up by the drifting ions. This local potential can be calculated on the basis of the Poisson equation [85, 115]:

$$\nabla^2\psi + \frac{\rho}{\epsilon} = 0 \tag{2.3}$$

Where ρ stands for the electrical charge density (C/m^3) and ϵ refers to the dielectric constant of the medium (F/m). The charge density is related to the concentration of the N ionic species through the following relationship :

$$\rho = F\sum_{i=1}^{N} z_i c_i \tag{2.4}$$

In electrochemistry, equation (2.2) is known as the extended Nernst-Planck equation. In order to keep the following mathematical derivations as simple as possible, the homogeneization technique will only be applied to a simplified version of the Nernst-Planck equation in which chemical activity effects are neglected:

$$\boldsymbol{j_i} = -D_i^{\mu}\mathrm{grad}(c_i) - \frac{D_i^{\mu} z_i F}{RT} c_i \mathrm{grad}(\psi) \tag{2.5}$$

The possible chemical reactions occuring in cement-based materials will also be neglected in this paper for simplicity.

2.2.3 Averaging over the Representative Elementary Volume (REV)

Having established the transport equations at the microscopic scale, one faces various alternatives to describe the diffusion properties of the porous material at the macroscopic scale. Numerous authors have chosen to model the pore structure of cement systems on the basis of microstructural information such as that provided by mercury intrusion porosimetry [114]. Given the intrinsic complexity of the pore structure of most cement-based systems, the effective application of these data constitutes a formidable task [18]. In most cases, these models rely on "material" parameters (determined on

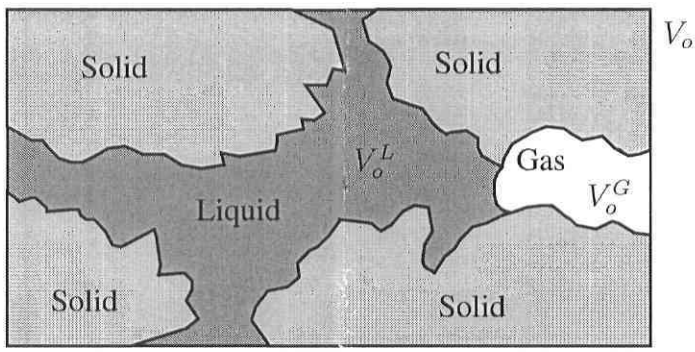

Figure 2.1: The Representative Elementary Volume (REV)

the basis of simplified assumptions which may not physically represent the system well) to fully describe the intricate nature of the microporous solid.

Another solution is to simply average the variables of interest over a representative elementary volume (REV). The main advantage of this approach (called the homogeneization technique) is that it does not require any detailed knowledge of the material inner structure. Another significant advantage is that the new averaged variables appearing in the equations can easily be measured in practice.

The notion of the REV forms the basis of the homogeneization technique. The REV should be large enough so that its physical characteristics (porosity, paste fraction, ...) are reprentative of the material. The REV can be characterized by various parameters (figure 2.1). V_o indicates the entire volume of material, V_o^L the volume occupied by the liquid phase, S_o^{LS} the boundaries between the liquid and the solid phases and S_o^{LL} is the liquid in contact with the external boundary of the REV [18].

The variable of interest for discussion of the mechanisms of ionic diffusion in porous media is the concentration. The volumetric phase average of c_i is given by:

$$\overline{c_i} \equiv \frac{1}{V_o} \int_{V_o^L} c_i \, dV \tag{2.6}$$

It is important to note that the new variable $\overline{c_i}$ is defined over the entire volume V_o.

Another useful definition is the volumetric intrinsic phase average, in which the averaging process is performed over a single specific phase, in our case the liquid phase:

$$\overline{c_i}^L \equiv \frac{1}{V_o^L} \int_{V_o^L} c_i \, dV \tag{2.7}$$

where V_o^L is the volume of liquid phase in the REV. As with $\overline{c_i}$, $\overline{c_i}^L$ is defined over the entire volume of the REV [201]. This value corresponds to the concentration that one might measure experimentally in a multi-phase system.

One should also define a quantity called the volume fraction of the liquid phase [18]:

$$\theta \equiv \frac{V_o^L}{V_o} \tag{2.8}$$

It corresponds to the water content of the material. For a fully saturated material, it is equivalent to the porosity. The two averages defined in equations (2.6) and (2.7) are related to each other through the volume fraction as :

$$\overline{c_i} = \theta\, \overline{c_i}^L \tag{2.9}$$

The fact that both averages $\overline{c_i}$ and $\overline{c_i}^L$ are defined over the REV has direct and important implications on the interpretation of the results provided by the application of the homogeneization procedure. By averaging over the REV, the different phases found in various areas of the entire volume are replaced by overlapping continua evenly distributed over the entire domain [18, 81, 201].

Having established the above definition, the averaging procedures can be applied to the mass conservation law equation (2.1) and constitutive equation equation (2.5). The average of the conservation law over all the REV (volumetric phase average) is given by:

$$\frac{1}{V_o}\int_{V_o^L}\left(\frac{\partial c_i}{\partial t} + \operatorname{div}(\boldsymbol{j_i})\right)\, dV = 0 \tag{2.10}$$

Utilizing the fact that the average of a sum equals the sum of the averages [18, 81], equation (2.10) can be developed as:

$$\frac{1}{V_o}\int_{V_o^L}\frac{\partial c_i}{\partial t}\, dV + \frac{1}{V_o}\int_{V_o^L}\operatorname{div}(\boldsymbol{j_i})\, dV = 0 \tag{2.11}$$

Using the definition of the volumetric phase average (equation 2.6), equation (2.11) can be modified as:

$$\overline{\frac{\partial c_i}{\partial t}} + \overline{\operatorname{div}(\boldsymbol{j_i})} = 0 \tag{2.12}$$

Combining equation (2.12) with equation (2.9), one finds:

$$\theta\overline{\frac{\partial c_i}{\partial t}}^L + \theta\overline{\operatorname{div}(\boldsymbol{j_i})}^L = 0 \tag{2.13}$$

It is necessary to calculate the average of a time derivative, the average of a divergence and the average of a gradient to complete the homogeneization procedure. They will be given without the appropriate demonstrations. More information on these mathematical operations can be found in references [18] and [81].

- The average of a time derivative is given by:

$$\frac{\partial(\theta\overline{c_i}^L)}{\partial t} = \theta\overline{\frac{\partial c_i}{\partial t}}^L + \frac{1}{V_o^L}\int_{S_o^{LS}} c_i\,\boldsymbol{u}\cdot\boldsymbol{n}\,dS \tag{2.14}$$

  where S^{LS} designates the surface of the solid/liquid interface (see figure 1), $\boldsymbol{n}$ is a vector normal to the surface S^{LS} and pointing outward, and $\boldsymbol{u}$ is the velocity of the surface. In the case of the diffusion of ions in concrete, $\boldsymbol{u} = 0$. One can therefore write:

$$\frac{\partial(\theta\overline{c_i}^L)}{\partial t} = \theta\overline{\frac{\partial c_i}{\partial t}}^L \tag{2.15}$$

- The average of the divergence is given by:

$$\theta\overline{\mathrm{div}(\boldsymbol{j_i})}^L = \mathrm{div}(\theta\overline{\boldsymbol{j_i}}^L) + \frac{1}{V_o^L}\int_{S_o^{LS}} \boldsymbol{j_i}\cdot\boldsymbol{n}\,dS \tag{2.16}$$

  The last term on the right-hand side of equation (2.16) describes the exchange between the liquid and the solid phase by a flux through the surface S_o^{LS}. In most practical cases, this term can be used to account for chemical reactions between the solid and the drifting ions. However, for our present simplified case, this term can be neglected, leaving:

$$\theta\overline{\mathrm{div}(\boldsymbol{j_i})}^L = \mathrm{div}(\theta\overline{\boldsymbol{j_i}}^L) \tag{2.17}$$

- The average of a gradient is given by:

$$\overline{\mathrm{grad}(c_i)}^L = \left(\frac{1}{V_o^L}\int_{S_o^{LL}} \boldsymbol{n}\otimes\mathring{\boldsymbol{x}}\,dS\right)\mathrm{grad}(\overline{c_i}^L) + \frac{1}{V_o^L}\int_{S_o^{LS}} \mathrm{grad}(c_i)\cdot\boldsymbol{n}\,dS \tag{2.18}$$

  where S^{LL} designates the surface of the liquid phase in contact with the liquid phase of the adjacent REVs (see figure 1) and $\mathring{\boldsymbol{x}}$ is the position of a point on S_o^{LL} relative to the center of the REV. The term within the first parenthesis on the right hand side of equation (2.18) corresponds to the tortuosity of the pore system, τ [18]. It is a second rank tensor and gives information on the complexity

of the shape of the porous network. It should be emphasized however that the evaluation of the tortuosity on the basis of this expression is difficult.

The last term in equation (2.18) accounts for the exchange by diffusion between the liquid and the solid phases. In the case of concrete, it can be neglected since the diffusion in the solid phase is insignificant. The exchange between the two phases, when it occurs, should be modeled using the last term in equation (2.16).

With all these considerations, the final expression for the average of a gradient is:

$$\overline{\overline{\mathrm{grad}(c_i)}}^{L} = \tau \mathrm{grad}(\overline{c_i}^{L}) \tag{2.19}$$

- The average of a product is given by:

$$\overline{\overline{c_i \mathrm{grad}(\psi)}}^{L} = \overline{c_i}^{L}\overline{\overline{\mathrm{grad}(\psi)}}^{L} + \overline{\overset{\circ}{c}_i \overset{\circ}{\mathrm{grad}}(\psi)}^{L} \tag{2.20}$$

where the terms $\overset{\circ}{c}_i$ and $\overset{\circ}{\mathrm{grad}}(\psi)$ are the deviations of the given variable around the average value. They can be neglected [18], thus leaving:

$$\overline{\overline{c_i \mathrm{grad}(\psi)}}^{L} = \overline{c_i}^{L}\overline{\overline{\mathrm{grad}(\psi)}}^{L} \tag{2.21}$$

By substituting equations (2.15) and (2.17) in equation (2.13), the average of the mass conservation equation can be expressed as:

$$\frac{\partial(\theta \overline{c_i}^{L})}{\partial t} = \mathrm{div}(\theta \overline{\boldsymbol{j_i}}^{L}) \tag{2.22}$$

As can be seen in the last equation, one should finally develop an expression for the average value of the ionic flux. Following equation (2.5), one can write:

$$\overline{\boldsymbol{j_i}}^{L} = -D^{\mu}\overline{\overline{\mathrm{grad}(c_i)}}^{L} - \frac{D_i^{\mu} z_i F}{RT}\overline{\overline{c_i \mathrm{grad}(\psi)}}^{L} \tag{2.23}$$

Combining equation (2.23) with equations (2.19) and (2.21), the final expression of the flux is given by:

$$\overline{\boldsymbol{j_i}}^{L} = -D_i^{\mu}\tau \mathrm{grad}(\overline{c_i}^{L}) - \frac{D_i^{\mu} z_i F \tau}{RT}\overline{c_i}^{L}\mathrm{grad}(\overline{\psi}^{L}) \tag{2.24}$$

A new diffusion coefficient is defined as:

$$D_i = D_i^{\mu}\tau \tag{2.25}$$

It corresponds to the diffusion coefficient at the macroscopic scale. It is important to remember that this new parameter is nothing more than the ionic diffusion coefficient

at microscopic scale (i.e. the liquid phase), modified by a purely geometrical factor accounting for the complexity of the porous system.

The variable $\overline{\psi}^L$ appearing in equation (2.24) represents the value of the electrical potential ψ in the liquid phase averaged over the REV.

Expressing equations (2.24) and (2.25) in the averaged form of the mass conservation law (equation 2.22), the diffusion model based on an averaged concentration $\overline{c_i}^L$ becomes:

$$\frac{\partial(\theta\overline{c_i}^L)}{\partial t} = \mathrm{div}(-\theta D_i \mathrm{grad}(\overline{c_i}^L) - \theta\frac{D_i z_i F}{RT}\overline{c_i}^L \mathrm{grad}(\overline{\psi}^L)) \tag{2.26}$$

This equation can be used to model the diffusion of ions in a porous media where activity effects and chemical binding are neglected.

For the particular case of a fully saturated concrete with no variation in water content θ, equation (2.26) can be written as:

$$\frac{\partial(\overline{c_i}^L)}{\partial t} = \mathrm{div}(-D_i \mathrm{grad}(\overline{c_i}^L) - \frac{D_i z_i F}{RT}\overline{c_i}^L \mathrm{grad}(\overline{\psi}^L)) \tag{2.27}$$

This is Nernst-Planck equation at the macroscopic scale. It describes an ionic species by the average concentration in the liquid phase. The diffusion is controlled by D_i, which hides the effects of the complex geometry of the porous network of the concrete. This law is often use to model ionic diffusion in concrete, but without the homogeneization technique, it is difficult to understand the meaning of each parameter in the equation.

It should be emphasized that the diffusion coefficient D_i (as defined in the last equations) is a property of the porous network and of the ionic species under consideration, while the tortuosity coefficient τ is a characteristic of the solid solely. From an engineering point of view, the determination of the tortuosity coefficient on the basis of experimental tests is quite important since it provides information on the ability of the solid to impede ion transport.

To complete the model, the averaging procedure is performed on the Poisson equation (see equations 2.3 and 2.4). It gives:

$$\mathrm{div}(\theta\tau \mathrm{grad}(\overline{\psi}^L)) + \theta\frac{F}{\epsilon}\left(\sum_{i=1}^{N} z_i \overline{c_i}^L\right) = 0 \tag{2.28}$$

It should also be underlined that neither the tortuosity coefficient nor the diffusion coefficient should be influenced by parameters such as the type and the number of

coexisting ions or the concentrations of the external solutions in contact with the solid. As previously discussed, the Nernst-Planck/Poisson set of equations already takes into account the interaction between the various ionic fluxes that may take place during the diffusion process. The system of equations can be easily modified to account for chemical activity effects or the chemical interactions of the ionic species with the solid phases.

2.2.4 Concluding remarks

Is has been demonstrated that the homogeneization technique, based on the averaging of the conservation law and constitutive equation at microscopic scale, can describe the transport of ions at the material scale. The technique was applied to the case of a very simple constitutive equation (Nernst-Planck). More complex constitutive laws, for example the extended Nernst-Planck equation, could be used in the model and averaged over the REV through the same procedure.

2.3 Modeling ion and fluid transport in unsaturated cement systems for isothermal conditions

E. Samson[12], J. Marchand[12], K.A. Snyder[3], J.J. Beaudoin[4]

[1]Centre de recherche interuniversitaire sur le béton,
Université Laval, Québec, Canada, G1K 7P4

[2]SIMCO Technologies inc.,
1400, boul. du Parc Technologique, Québec, Canada, G1P 4R7

[3]Building and Fire Research Laboratory,
National Institute of Standards and Technology, Gaithersburg, MD 20899, USA

[4]Materials Laboratory - Institute for Research in Construction,
National Research Council, Ottawa, Canada, K1A 0R6

Abstract

A description of ionic transport in unsaturated porous materials due to

gradients in the electro-chemical potential and the moisture content is developed by averaging the relevant microscopic transport equations over a representative volume element. The complete set of equations consist of a time-dependent equations for both the concentration of ionic species within the pore solution and the moisture content within the pore space. The electrostatic interactions are assumed to occur instantaneously and the resulting electrical potential satisfies Poisson's equation. Using the homogenization technique, moisture transport due to both the liquid and vapor phases is shown to obey Richards' equation, and a precise definition of the moisture content is found. The final transport equations contain transport coefficients that can be unambiguously related to experimental quantities. The approach has the advantage of making the distinction between microscopic and bulk quantities explicit.

2.3.1 Introduction

Over the past decade, a great deal of effort has been specifically devoted to the investigation of ion transport mechanisms in unsaturated cement systems. The topic is important since, in many cases, concrete structures exposed to ionic solutions are also frequently subjected to wetting and drying cycles. The coupled transport of moisture and ions often tends to accelerate physical and chemical degradation mechanisms and reduce the service life of the material [7, 62, 93].

Reports recently published on the subject have largely contributed to clarify some fundamental aspects of ion transport mechanisms in unsaturated concrete. Many investigations have also emphasized the intricate nature of these phenomena. If most of the difficulties related to the description of transport processes in concrete are linked to the intrinsic complexity of the material, it appears that part of them also lies with the fact that authors have used many different approaches to study these processes. For instance, the definition of the state variables used to describe the various transport processes tend to vary significantly from one study to another. This is most unfortunate since the lack of a unified approach often contributes to confuse the issue.

This paper is an attempt to clarify some fundamental aspects of the problem. The

transport mechanisms are described using a well established mathematical procedure, the homogenization technique. The technique has been recently used to investigate the diffusion of ions in saturated systems [156]. According to this approach, the transport equations are first written at the pore scale. They are then averaged over the scale of the material. The main advantage of the homogenization technique lies in the clear definition of the state variables.

The paper first addresses the process of moisture transport in an unsaturated porous material. For the completely coupled transport of ions in an unsaturated media, dynamical equations are required to express the moisture content as a function of time. This is achieved by averaging microscopical equations for both liquid and water vapor transport. The mathematical development yields Richard's equation, and the moisture content and the transport coefficients are well-defined.

The second part of the paper is devoted to the coupled transport of ions and moisture in the system. Here, the field quantity is the concentration of the ions within the pore solution. The homogenization technique is applied to a microscopic equation for both diffusive and convective transport. While diffusive equations already exist, reformulating the bulk equations using homogenization ensures that the transport coefficients are well defined (pore space versus microscopic quantities) and can, therefore, be unambiguously related to experimental quantities.

2.3.2 Water transport in unsaturated porous materials

The first objective is to develop an equation to characterize the mass transport of water in an unsaturated porous material. Richards [147] was among the first authors to study the mechanisms of water transport in unsaturated porous solids. In 1931, he proposed the following equation to describe the flow of water under capillary suction:

$$\frac{\partial \theta}{\partial t} - \mathrm{div}(K \mathrm{grad} \Gamma) = 0 \tag{2.29}$$

where θ is the water content, K is the permeability of the porous material, and Γ is the capillary potential.

This relationship, known as Richards' equation, was later modified to express the transport of mass solely as a function of the gradient in water content. This modification

is based on the assumption that the capillary potential Γ is a differentiable function of the moisture content θ:

$$\Gamma = f(\theta) \tag{2.30}$$

This allows to write:

$$\text{grad}\Gamma = \frac{d\Gamma}{d\theta}\text{grad}\theta \tag{2.31}$$

Substituting (2.31) into (2.29), one finds:

$$\frac{\partial\theta}{\partial t} - \text{div}(D_\theta \text{grad}\theta) \tag{2.32}$$

where $D_\theta = K(d\Gamma/d\theta)$ is the nonlinear water diffusivity coefficient. Equation (2.32) is widely used to model the evolution of water content in a porous material kept in isothermal conditions. Equation (2.32) is also known as Richards' equation.

While Richard's equation is commonly accepted among scientists, its use over the past decades has contributed to some confusion on how to describe moisture transport mechanisms in unsaturated porous materials. Richards originally wrote the equation with the water content expressed in cubic centimeters of water per gram of dry material. Over the years, some authors have preferred to define water content in kilograms of *moisture* per kilogram of dry material [53] or in kilograms of water per cubic meter of material [54, 167]. However, most authors have traditionally chosen to express the variable in cubic meter of water per cubic meter of material [32, 44, 51]. To add to the confusion, many authors tend to define the *moisture content* as the sum of liquid water and vapor while some others only consider the liquid phase.

2.3.2.1 General considerations

In an attempt to clarify these concepts, Richards' equation will be derived using the homogenization technique. In order to simplify the problem, the derivation is based on the assumptions that the isotropic porous material is an infinitely rigid solid (no significant deformations) kept under isothermal conditions (i.e. the transport of water is solely due to capillary suction). Other assumptions will arise during the development of the model.

The mathematical rules of the averaging technique can be found in textbooks [12, 18]. Only the basic definitions will be exposed in the following paragraphs. More

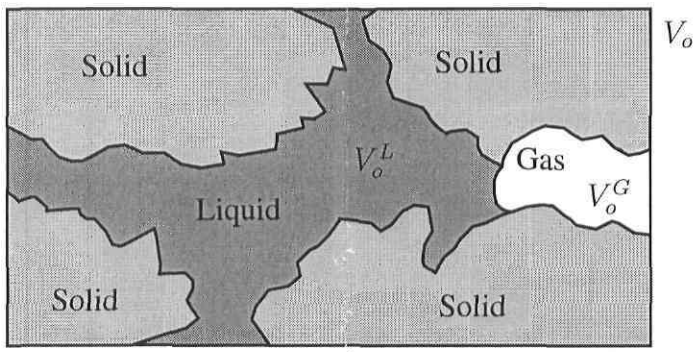

Figure 2.2: The Representative Elementary Volume (REV)

information on the technique can also be found in reference [156]. The technique is outlined here because it is at the core of development of all the transport equations.

As previously mentioned, the homogenization technique starts with a conservation and a transport equation at the microscopic level (i.e., at the scale of the pore). These equations are then integrated over a Representative Elementary Volume (REV), such as the one depicted in Figure 2.2. The size of the volume depends on the intrinsic properties of the material. For instance, for concrete and mortar mixtures, the size of the REV depends on the maximum diameter of the aggregate particles. For the hydrated cement paste, the REV is typically a few cubic centimeters.

The total volume of the REV is given by V_o. The volume occupied by the liquid phase is designated by V_o^L. The volumetric fraction of liquid θ_L is the ratio of the liquid volume to the total volume:

$$\theta_L = \frac{V_o^L}{V_o} \tag{2.33}$$

The gaseous phase occupies a volume V_o^G. It is a mixture of air and water vapor. It is assumed that both air and the water vapor fill the whole gaseous phase volume. As for the liquid phase, the volumetric fraction of gas θ_G is the ratio of the gas volume to the total volume:

$$\theta_G = \frac{V_o^G}{V_o} \tag{2.34}$$

In the remainder of the text, the subscripts L and G will designate the liquid and gaseous phases, respectively. Furthermore, the subscript V will represent the water vapor phase within the total gaseous phase.

Let a_α denote the amount per unit volume of some extensive quantity A in the phase α, either solid, liquid or gas. Concentration or mass density can serve as examples for a_α. Two averages can be defined. The *volumetric phase average* is given by:

$$\overline{a_\alpha} = \frac{1}{V_o} \int_{V_o^\alpha} a_\alpha \ dV \tag{2.35}$$

The *volumetric intrinsic phase average* is defined as:

$$\overline{a_\alpha}^\alpha = \frac{1}{V_o^\alpha} \int_{V_o^\alpha} a_\alpha \ dV \tag{2.36}$$

The two values are related by the following relationship:

$$\overline{a_\alpha} = \theta_\alpha \overline{a_\alpha}^\alpha \tag{2.37}$$

2.3.2.2 Transport of liquid water

The continuity equation for liquid water is given by [101, 202]:

$$\frac{\partial \rho_L}{\partial t} + \operatorname{div}(\rho_L \boldsymbol{v_L}) = 0 \tag{2.38}$$

where ρ_L is the mass of liquid water per unit volume of liquid phase, and $\mathbf{v}_L$ is the velocity of water. The bulk equation is obtained by averaging Equation (2.38) over the REV:

$$\frac{1}{V_o} \int_{V_o^L} \left(\frac{\partial \rho_L}{\partial t} + \operatorname{div}(\rho_L \boldsymbol{v_L}) \right) \ dV = 0 \tag{2.39}$$

This integral can be divided in two parts:

$$\frac{1}{V_o} \int_{V_o^L} \frac{\partial \rho_L}{\partial t} \ dV + \frac{1}{V_o} \int_{V_o^L} \operatorname{div}(\rho_L \boldsymbol{v_L}) \ dV = 0 \tag{2.40}$$

Using the definition of the volumetric phase average (equation 2.35), one can write:

$$\overline{\frac{\partial \rho_L}{\partial t}} + \overline{\operatorname{div}(\rho_L \boldsymbol{v_L})} = 0 \tag{2.41}$$

The average of the time derivative gives [12, 18]:

$$\frac{\partial (\theta_L \overline{\rho_L}^L)}{\partial t} = \overline{\frac{\partial \rho_L}{\partial t}} + \frac{1}{V_o} \int_{S_o^{LG}} \rho_L \boldsymbol{u} \cdot \boldsymbol{n_{LG}} \ dS + \frac{1}{V_o} \int_{S_o^{LS}} \rho_L \boldsymbol{u} \cdot \boldsymbol{n_{LS}} \ dS \tag{2.42}$$

where S_o^{LG} is the surface of the liquid/gas interface, S_o^{LS} is the surface of the liquid/solid interface, $\boldsymbol{u}$ is the velocity of the interface, $\boldsymbol{n_{LG}}$ is a unit vector pointing outward the

liquid phase at the liquid/gas interface, and $\boldsymbol{n_{LS}}$ is a unit vector pointing outward the liquid phase at the liquid/solid interface. Since it is assumed that the deformations of the solid matrix could be neglected, the last integral on the right-hand side of equation (2.42) can be dropped, which leaves:

$$\frac{\partial(\theta_L \overline{\rho_L}^L)}{\partial t} = \overline{\frac{\partial \rho_L}{\partial t}} + \frac{1}{V_o}\int_{S_o^{LG}} \rho_L \boldsymbol{u} \cdot \boldsymbol{n_{LG}}\, dS \tag{2.43}$$

The average of the divergence in equation (2.41) is given by [12, 18]:

$$\overline{\mathrm{div}(\rho_L \boldsymbol{v_L})} = \mathrm{div}\big(\theta_L(\overline{\rho_L \boldsymbol{v_L}}^L)\big) + \frac{1}{V_o}\int_{S_o^{LG}} \rho_L \boldsymbol{v_L} \cdot \boldsymbol{n_{LG}}\, dS + \frac{1}{V_o}\int_{S_o^{LS}} \rho_L \boldsymbol{v_L} \cdot \boldsymbol{n_{LS}}\, dS \tag{2.44}$$

At the solid/liquid interface, it is assumed that the liquid velocity is zero (the so-called no-slip condition of fluid mechanics [129]). Hence, the last integral on the right-hand side of equation (2.44) can be neglected, which leaves:

$$\overline{\mathrm{div}(\rho_L \boldsymbol{v_L})} = \mathrm{div}\big(\theta_L(\overline{\rho_L \boldsymbol{v_L}}^L)\big) + \frac{1}{V_o}\int_{S_o^{LG}} \rho_L \boldsymbol{v_L} \cdot \boldsymbol{n_{LG}}\, dS \tag{2.45}$$

Substituting equations (2.43) and (2.45) in equation (2.41), one finds:

$$\frac{\partial(\theta_L \overline{\rho_L}^L)}{\partial t} + \mathrm{div}\big(\theta_L(\overline{\rho_L \boldsymbol{v_L}}^L)\big) + \frac{1}{V_o}\int_{S_o^{LG}} \rho_L(\boldsymbol{v_L} - \boldsymbol{u}) \cdot \boldsymbol{n_{LG}}\, dS = 0 \tag{2.46}$$

According to Whitaker [202], the integral in equation (2.46) corresponds to the rate of vaporization per unit volume of the liquid phase at the liquid/gas interface, and is denoted by $\overline{\dot{m}}$. Also, the average value $\overline{\rho_L}^L$ corresponds to the density of the liquid ρ_L, which can be assumed constant. Equation (2.46) can thus be simplified:

$$\rho_L \frac{\partial \theta_L}{\partial t} + \rho_L \mathrm{div}(\theta_L \overline{\boldsymbol{v_L}}^L) + \overline{\dot{m}} = 0 \tag{2.47}$$

The next step consists of determining the average value of the liquid velocity. The starting point is the Darcy equation [58]:

$$\overline{\boldsymbol{v_L}} = -\frac{K}{\mu}(\mathrm{grad}P + \rho_L \boldsymbol{g}) \tag{2.48}$$

The quantity $\overline{\boldsymbol{v_L}}$ is the bulk velocity of the liquid, K is the permeability of the material, μ is the viscosity of the fluid, P is the pressure on the liquid, and $\boldsymbol{g}$ is gravitational acceleration. Darcy originally derived this equation to describe the transport of water

through the material at the macroscopic scale. Furthermore, Whitaker [202] showed that in materials having very small pores the capillary forces are dominant:

$$\overline{\boldsymbol{v_L}} = -\frac{k}{\mu}\theta_L \mathrm{grad}\overline{p_c} \tag{2.49}$$

The quantity p_c is the capillary pressure and k is the permeability of the liquid-filled pore space.

Equation (2.49) is based on the assumptions that gravity effects are negligible and that the pressure is uniform throughout the liquid and gaseous phases. It should also be emphasized that the validity of the equation also rests on the hypothesis that the liquid phase is *continuous*. The latter assumption will be further discussed in the last section of this report.

The bulk velocity of the liquid $\overline{\boldsymbol{v_L}}$ can be related to its intrinsic average counterpart through:

$$\overline{\boldsymbol{v_L}} = \theta_L \overline{\boldsymbol{v_L}}^L \tag{2.50}$$

Substituting equations (2.49) and (2.50) into equation (2.47) gives:

$$\rho_L \frac{\partial \theta_L}{\partial t} - \rho_L \mathrm{div}\left(\frac{K}{\mu}\theta_L \mathrm{grad}\overline{p_c}\right) + \overline{\dot{m}} = 0 \tag{2.51}$$

Since $\overline{p_c} = f(\theta_L)$ [202], the chain rule allows to write:

$$\mathrm{grad}\overline{p_c} = \left(\frac{d\overline{p_c}}{d\theta_L}\right)\mathrm{grad}\theta_L \tag{2.52}$$

The substitution of equation (2.52) in equation (2.51) gives:

$$\rho_L \frac{\partial \theta_L}{\partial t} - \rho_L \mathrm{div}\left(\frac{K}{\mu}\theta_L \frac{d\overline{p_c}}{d\theta_L}\mathrm{grad}\theta_L\right) + \overline{\dot{m}} = 0 \tag{2.53}$$

Let

$$D_L = \frac{K}{\mu}\theta_L \frac{d\overline{p_c}}{d\theta_L} \tag{2.54}$$

Equation (2.53) is now expressed as a function of a single field quantity θ_L to give a complete description of liquid water transport:

$$\rho_L \frac{\partial \theta_L}{\partial t} - \rho_L \mathrm{div}\left(D_L \mathrm{grad}\theta_L\right) + \overline{\dot{m}} = 0 \tag{2.55}$$

Since equation (2.55) is expressed in the form of a diffusion equation, D_L can be assimilated to a *water diffusion coefficient*. However, it should be emphasized that the

movement of liquid water considered in this section arises by capillary suction. It is not, per se, a *diffusive phenomenon.*

With the definition of D_L given in equation (2.54), combined with equation (2.52), the velocity of the liquid phase (equation 2.49) can now be written as:

$$\overline{\boldsymbol{v_L}} = -D_L \text{grad}\theta_L \tag{2.56}$$

2.3.2.3 Transport of water vapor

The treatment of the gas transport phenomenon is more complicated since two phases have to be considered: air and water vapor. However, the problem can be simplified by considering the following assumptions. As mentioned in the previous section, the development of equation (2.49) rests on the hypothesis that pressure is uniform over the gaseous phase. This implies that there is no bulk movement of air in the gaseous phase. Consequently, there will be no convective transport of water vapor within the material pore structure. Still, there can be movement of molecules in the gaseous phase as a result of their thermal agitation. The other assumption is that gravity does not have any significant effect on the behavior of the water vapor.

The continuity equation for water vapor component of a gaseous phase is the following [202]:

$$\frac{\partial \rho_V}{\partial t} + \text{div}(\rho_V \boldsymbol{v_V}) = 0 \tag{2.57}$$

The quantity ρ_V is the mass of water vapor per unit volume of gaseous phase, and $\boldsymbol{v_V}$ is the velocity of water vapor. The water vapor will be in movement as a result of its thermal agitation. It is therefore a *diffusive* process. According to Daian [44], the water vapor flux is given as:

$$\rho_V \boldsymbol{v_V} = -D \text{grad}\rho_V \tag{2.58}$$

where D is the self-diffusion coefficient of water vapor in the gaseous phase. By combining equations (2.57) and (2.58), one gets:

$$\frac{\partial \rho_V}{\partial t} - \text{div}(D \text{grad}\rho_V) = 0 \tag{2.59}$$

The bulk equation is calculated from the integration of equation (2.59) over the

REV:

$$\frac{1}{V_o}\int_{V_o^G}\left(\frac{\partial \rho_V}{\partial t} - \mathrm{div}(D\mathrm{grad}\rho_V)\right)\, dV = 0 \tag{2.60}$$

This integral can be divided in two parts, which yields:

$$\frac{1}{V_o}\int_{V_o^G}\frac{\partial \rho_V}{\partial t}\, dV - \frac{1}{V_o}\int_{V_o^G}\mathrm{div}(D\mathrm{grad}\rho_V)\, dV = 0 \tag{2.61}$$

According to the definition of the volumetric phase average (equation 2.35), equation (2.61) can be written as:

$$\overline{\frac{\partial \rho_V}{\partial t}} - \overline{\mathrm{div}(D\mathrm{grad}\rho_V)} = 0 \tag{2.62}$$

The average of the time derivative is given by:

$$\frac{\partial(\theta_G\overline{\rho_V}^G)}{\partial t} = \overline{\frac{\partial \rho_V}{\partial t}} + \frac{1}{V_o}\int_{S_o^{GL}}\rho_V \boldsymbol{u}\cdot\boldsymbol{n_{GL}}\, dS + \frac{1}{V_o}\int_{S_o^{GS}}\rho_V \boldsymbol{u}\cdot\boldsymbol{n_{GS}}\, dS \tag{2.63}$$

where S_o^{GL} is the surface of the liquid/gas interface, S_o^{GS} is the surface of the gas/solid interface, $\boldsymbol{u}$ is the velocity of the interface, $\boldsymbol{n_{GL}}$ is a unit vector pointing outward the gaseous phase at the liquid/gas interface, and $\boldsymbol{n_{GS}}$ is a unit vector pointing outward the gaseous phase at the gas/solid interface. Since it is assumed that the deformations of the solid matrix are negligible, the last integral on the right-hand side of equation (2.63) can be neglected, which leaves:

$$\frac{\partial(\theta_G\overline{\rho_V}^G)}{\partial t} = \overline{\frac{\partial \rho_V}{\partial t}} + \frac{1}{V_o}\int_{S_o^{GL}}\rho_V \boldsymbol{u}\cdot\boldsymbol{n_{GL}}\, dS \tag{2.64}$$

The average of the divergence gives:

$$\overline{\mathrm{div}(D\mathrm{grad}\rho_V)} = \mathrm{div}\big(\theta_G(\overline{D\mathrm{grad}\rho_V}^G)\big) + \frac{1}{V_o}\int_{S_o^{GS}} D\mathrm{grad}\rho_V\cdot\boldsymbol{n_{GS}}\, dS + \frac{1}{V_o}\int_{S_o^{GL}} D\mathrm{grad}\rho_V\cdot\boldsymbol{n_{GL}}\, dS \tag{2.65}$$

The first integral on the right-hand side of equation (2.65) is neglected since there is no exchange of water vapor between the solid and the gaseous phases. Accordingly, equation (2.65) can be simplified as:

$$\overline{\mathrm{div}(D\mathrm{grad}\rho_V)} = \mathrm{div}\big(\theta_G(\overline{D\mathrm{grad}\rho_V}^G)\big) + \frac{1}{V_o}\int_{S_o^{GL}} D\mathrm{grad}\rho_V\cdot\boldsymbol{n_{GL}}\, dS \tag{2.66}$$

Furthermore, by assuming that the coefficient D is constant, equation (2.66) can be written as:

$$\overline{\mathrm{div}(D\mathrm{grad}\rho_V)} = \mathrm{div}(\theta_G D\overline{\mathrm{grad}\rho_V}^G) + \frac{1}{V_o}\int_{S_o^{GL}} D\mathrm{grad}\rho_V\cdot\boldsymbol{n_{GL}}\, dS \tag{2.67}$$

The average of the gradient is given by [12, 18]:

$$\overline{\text{grad}\rho_V}^G = \tau_G \text{grad}\overline{\rho_V}^G + \frac{1}{V_o}\int_{S_o^{GS}} \overset{\circ}{\boldsymbol{x}}\,(\text{grad}\rho_V \cdot \boldsymbol{n_{GS}})\,dS + \frac{1}{V_o}\int_{S_o^{GL}} \overset{\circ}{\boldsymbol{x}}\,(\text{grad}\rho_V \cdot \boldsymbol{n_{GL}})\,dS \tag{2.68}$$

The quantity τ is referred to by Bachmat and Bear [12] as the tortuosity of the material. Conceptually, it is the ratio of the macroscopic system length to the shortest path length through the pore (liquid or gas) space. As such, it is a quantity that strictly equal to or less than one. The parameter $\overset{\circ}{\boldsymbol{x}}$ is defined as $\overset{\circ}{\boldsymbol{x}} = \boldsymbol{x} - \boldsymbol{x_o}$, where $\boldsymbol{x}$ is a position vector within the REV and $\boldsymbol{x_o}$ is the position vector of the center of the REV. The first integral on the right-hand side of equation (2.68) involves the solid/gas interface. Except for the very low water content conditions, there will be no direct contact between these two phases because water will be adsorbed on the surface of the solid. Accordingly, the integral can be neglected. It is assumed that the term $(\text{grad}\rho_V \cdot \boldsymbol{n_{GL}})$ in the second integral on the right-hand side of equation (2.68) varies very slightly over the surface S_o^{GL}. Under this assumption, it leaves an integral of a position vector times a scalar over a closed surface, which gives zero. Equation (2.68) is thus simplified as:

$$\overline{\text{grad}\rho_V}^G = \tau_G \text{grad}\overline{\rho_V}^G \tag{2.69}$$

Replacing equations (2.64), (2.67) and (2.69) into equation (2.62) gives:

$$\frac{\partial(\theta_G\overline{\rho_V}^G)}{\partial t} - \text{div}(\theta_G D\tau_G \text{grad}\overline{\rho_V}^G) + \frac{1}{V_o}\int_{S_o^{GL}} (D\text{grad}\rho_V - \rho_V \boldsymbol{u}) \cdot \boldsymbol{n_{GL}}\,dS = 0 \tag{2.70}$$

Substituting equation (2.58) in equation (2.70), one finds:

$$\frac{\partial(\theta_G\overline{\rho_V}^G)}{\partial t} - \text{div}(\theta_G D\tau_G \text{grad}\overline{\rho_V}^G) - \frac{1}{V_o}\int_{S_o^{GL}} \rho_V(\boldsymbol{v_V} - \boldsymbol{u}) \cdot \boldsymbol{n_{GL}}\,dS = 0 \tag{2.71}$$

Whitaker [202] showed that the integral in equation (2.71) has the same value as the one in equation (2.46). It represents the rate of condensation per unit volume of the water vapor phase at the liquid/gas interface. Therefore, equation (2.71) can be written as:

$$\frac{\partial(\theta_G\overline{\rho_V}^G)}{\partial t} - \text{div}(\theta_G D\tau_G \text{grad}\overline{\rho_V}^G) - \overline{\dot{m}} = 0 \tag{2.72}$$

It is possible to express the gradient in equation (2.72) as a function of θ_L since $\rho_V = f(\theta_L)$ [44]. Applying the chain rule, it gives:

$$\frac{\partial(\theta_G\overline{\rho_V}^G)}{\partial t} - \text{div}\left(\theta_G D\tau_G \frac{d\overline{\rho_V}^G}{d\theta_L}\text{grad}\theta_L\right) - \overline{\dot{m}} = 0 \tag{2.73}$$

The quantities preceding the gradient within the parenthesis can be lumped together to form a single vapor diffusion coefficient:

$$D_V = \theta_G D \tau_G \tag{2.74}$$

Equation (2.73) can be written succinctly:

$$\frac{\partial(\theta_G \overline{\rho_V}^G)}{\partial t} - \text{div}\left(D_V \frac{d\overline{\rho_V}^G}{d\theta_L} \text{grad}\theta_L\right) - \overline{\dot{m}} = 0 \tag{2.75}$$

2.3.2.4 Total moisture transport

In the previous sections, the transport equations for the liquid and the vapor phases were considered separately (equations 2.55 and 2.75). In order to get a complete description of the transport, both equations should be added together:

$$\frac{\partial}{\partial t}(\rho_L \theta_L + \theta_G \overline{\rho_V}^G) - \text{div}\left(\left(\rho_L D_L + \frac{d\overline{\rho_V}^G}{d\theta_L} D_V\right) \text{grad}\theta_L\right) = 0 \tag{2.76}$$

As the density of water vapor has a much lower value than the one of liquid water ($\overline{\rho_V}^G \ll \rho_L$) and $\theta_G \approx \theta_L$, equation (2.76) can be simplified as:

$$\rho_L \frac{\partial \theta_L}{\partial t} - \text{div}\left(\left(\rho_L D_L + \frac{d\overline{\rho_V}^G}{d\theta_L} D_V\right) \text{grad}\theta_L\right) = 0 \tag{2.77}$$

Let

$$D_\theta = \frac{\rho_L D_L + \frac{d\overline{\rho_V}^G}{d\theta_L} D_V}{\rho_L} \tag{2.78}$$

Substituting equation (2.78) into (2.77) gives:

$$\frac{\partial \theta_L}{\partial t} - \text{div}\left(D_\theta \text{grad}\theta_L\right) = 0 \tag{2.79}$$

This is Richards' equation. As can be seen, the equation fully describes the movement of both vapor and liquid water on the basis of a single variable θ_L. The influence of both phases is taken into account through the function D_θ, which contains a term associated to the vapor transport and a second one related to the transport of the liquid phase. The demonstration also indicates that the variable θ of the original equation (2.32) stands for the volumetric liquid water content, which is expressed in cubic meter of water per cubic meter of material.

2.3.2.5 Determination of the moisture transport properties of hydrated cement systems

The description of moisture transport mechanisms on the basis of equation (2.79) requires the determination of the function D_θ. An interesting discussion of the variation of this function with the water content of the material has recently been published by Martys [121]. The author clearly emphasizes the non-linear character of this function.

Measurements made on model porous material found in reference [42] show that when the humidity in the medium is higher than 4% (by weight), the contribution of the vapor phase to the overall moisture transfer is negligible. In that case, one can assume that $D_\theta = D_L$.

Over the years, numerous experimental techniques have been used to determine the moisture transport properties of hydrated cement systems. A thorough discussion of this subject is beyond the scope of this paper. Comprehensive critical reviews of this problem can be found in references [135, 100].

2.3.3 Ionic transport in unsaturated porous materials

Several mathematical models have been developed to predict the movement of ions in cement-based materials. Most of these approaches are single-ion models, considering only chloride and its detrimental effect on the durability of the material. Most of the time, such models consider the transport of ions under the effect of diffusion and advection (fluid flow). Also considered is the effect of the chemical reactions involving the considered species, although in a very simple way. For example, Saetta et al. [152], Nagesh and Bhattacharjee [130], and Gospodinov et al. [72] published such models.

However, these models oversimplify some basic physical phenomena. For instance, the electrical coupling between the ions [85] and its effect on their movements is often overlooked. This is particularly true for cement-based materials since they contain concentrated porous solution. The electrical coupling between the ions for concentrated solutions was recently put in evidence in two papers by Snyder [171, 172] that report on diffusion experiments through non reactive ceramic frits. Multiionic models taking into account electrical coupling were recently published by Masi el al. [122] and Truc

et al. [189].

Unfortunately, as it was the case with Richards' equation, there is a lack of agreement with regard to the definition and the use of some parameters in these models. For example, the diffusion coefficient is sometimes called the intrinsic diffusion coefficient, the apparent diffusion coefficient, or the effective diffusion coefficient. Once again, the averaging procedure is used to generate an ionic transport model. The method will clarify some of the basic concepts behind the modeling of ionic transport. Such a work was previously published [156] but was applied only to non-reactive saturated materials. The model presented in the following sections is more general.

2.3.3.1 Transport of ions in the liquid phase

The transport model is based on the observation that the transport of ions only occurs in the liquid phase. Hence, no equation has to be developed for the solid or gaseous phases. The conservation equation for an ionic species i in the liquid phase at pore scale is given by the following microscopic equation [18]:

$$\frac{\partial c_i}{\partial t} + \operatorname{div}(\boldsymbol{j_i}) + r_i = 0 \tag{2.80}$$

The quantity c_i is the concentration, $\boldsymbol{j_i}$ is the ionic flux and r_i is a term accounting for the chemical reactions between the ions in the solution. The bulk equation is obtained from averaging this equation over the REV, following the procedure that lead to equations (2.41) and (2.62):

$$\overline{\frac{\partial c_i}{\partial t}} + \overline{\operatorname{div}(\boldsymbol{j_i})} + \overline{r_i} = 0 \tag{2.81}$$

The average of the time derivative leads to:

$$\frac{\partial(\theta_L \overline{c_i}^L)}{\partial t} = \theta_L \overline{\frac{\partial c_i}{\partial t}}^L + \frac{1}{V_o}\int_{S_o^{LS}} c_i \boldsymbol{u}\cdot\boldsymbol{n_{LS}}\, dS + \frac{1}{V_o}\int_{S_o^{LG}} c_i \boldsymbol{u}\cdot\boldsymbol{n_{LG}}\, dS \tag{2.82}$$

The first integral on the right-hand side of equation (2.82) contains a term that accounts for the velocity of the solid/liquid interface. While this interface may possibly move as a result of some dissolution/precipitation chemical reactions, it will do so very slowly. It can thus be neglected. The other integral involves the movement of the liquid/gas interface. It is similar to the first integral in equation (2.42). While it was used in the

mathematical development of the moisture transport, it is assumed that it has only a small effect on the ionic transport, and can thus be neglected, simplifying equation (2.82):

$$\frac{\partial(\theta_L \overline{c_i}^L)}{\partial t} = \theta_L \overline{\frac{\partial c_i}{\partial t}}^L \tag{2.83}$$

The average of the divergence is given by:

$$\overline{\mathrm{div}(\boldsymbol{j_i})} = \mathrm{div}(\theta_L \overline{\boldsymbol{j_i}}^L) + \frac{1}{V_o}\int_{S_o^{LS}} \boldsymbol{j_i}\cdot\boldsymbol{n_{LS}}\, dS + \frac{1}{V_o}\int_{S_o^{LG}} \boldsymbol{j_i}\cdot\boldsymbol{n_{LG}}\, dS \tag{2.84}$$

The last integral on the right-hand side of equation (2.84) accounts for the ionic flux crossing the liquid/gaseous interface. The value of this flux is zero since ions do not go into the gaseous phase. The other integral, related to the flux of ions across the solid/liquid interface, will be used to model the various chemical reactions involving those phases. Accordingly, equation (2.84) can be reduced to:

$$\overline{\mathrm{div}(\boldsymbol{j_i})} = \mathrm{div}(\theta_L \overline{\boldsymbol{j_i}}^L) + \frac{1}{V_o}\int_{S_o^{LS}} \boldsymbol{j_i}\cdot\boldsymbol{n_{LS}}\, dS \tag{2.85}$$

Substituting equations (2.83) and (2.85) in equation (2.81) and averaging the term r_i, one finds:

$$\frac{\partial(\theta_L \overline{c_i}^L)}{\partial t} + \mathrm{div}(\theta_L \overline{\boldsymbol{j_i}}^L) + \theta_L \overline{r_i}^L + \frac{1}{V_o}\int_{S_o^{LS}} \boldsymbol{j_i}\cdot\boldsymbol{n_{LS}}\, dS = 0 \tag{2.86}$$

The next step consists of writing the proper flux expression at the microscopic level (ions in bulk electrolyte) and averaging it over the REV. Due to the charged nature of ions, this expression has to consider the electrical coupling between ionic particles. Furthermore, since the pore solution of cement-based materials is highly concentrated, it deviates from the ideal behavior of a dilute solution, requiring consideration of the chemical activity. Finally, the movement of the fluid itself will have an impact on the movement of ions. All these physical phenomena can be taken into account through the extended Nernst-Planck model to which is added an advection term [85]:

$$\boldsymbol{j_i} = -D_i^{\mu}\mathrm{grad}c_i - \frac{D_i^{\mu} z_i F}{RT} c_i \mathrm{grad}\psi - D_i^{\mu} c_i \mathrm{grad}(\ln\gamma_i) + c_i \boldsymbol{v_L} \tag{2.87}$$

The quantity D_i^{μ} is the self-diffusion coefficient [128] of species i in diluted, free water conditions, γ_i is the chemical activity coefficient, ψ is the electrical potential, z_i is the valence number of the ion, F is the Faraday constant, R is the ideal gas constant and T is the absolute temperature. The terms on the right-hand side of equation (2.87) are

associated with diffusion, electrical coupling between the ions, chemical activity effects and water transport, respectively.

The integration of the flux over the REV, similar to the procedure followed in equations (2.37) and (2.39) to (2.41), leads to:

$$\theta_L \overline{\boldsymbol{j_i}}^L = -D_i^\mu \theta_L \overline{\mathrm{grad} c_i}^L - \frac{D_i^\mu z_i F}{RT} \theta_L \overline{c_i \mathrm{grad} \psi}^L - D_i^\mu \theta_L \overline{c_i \mathrm{grad}(\ln \gamma_i)}^L + \theta_L \overline{c_i \boldsymbol{v_L}}^L \quad (2.88)$$

The next steps consist of averaging the various gradients and variables in equation (2.88).

The average of the concentration gradient is given by [12, 18]:

$$\overline{\mathrm{grad} c_i}^L = \tau_L \mathrm{grad} \overline{c_i}^L + \frac{1}{V_o} \int_{S_o^{LS}} \overset{\circ}{\boldsymbol{x}} \, (\mathrm{grad} c_i \cdot \boldsymbol{n_{LS}}) \, dS + \frac{1}{V_o} \int_{S_o^{LG}} \overset{\circ}{\boldsymbol{x}} \, (\mathrm{grad} c_i \cdot \boldsymbol{n_{LG}}) \, dS \quad (2.89)$$

For a description of the parameter $\overset{\circ}{\boldsymbol{x}}$ the readers are referred to equation (2.68). The quantity τ_L is the tortuosity of the aqueous phase. It is a purely geometrical factor accounting for the complexity of the paths the ions must travel through in liquid space. It is a function of the water content θ_L, since it is related to the volume of liquid in the pore space, and its value is less than one [12]. This definition of the tortuosity has been adopted in the following references [18, 106, 123, 169, 200]. Other authors [11, 22, 60, 154, 163, 209] are proposing the following definition for the tortuosity parameter:

$$D_i = \frac{D_i^\mu}{\tau_L} \quad (2.90)$$

To evaluate the surface integrals in equation (2.89), one has to refer to the double layer theory [26]. Figure 2.3 shows the cross-section of a pore and the schematic shape of the concentration profile along its radius. The solid bears an electrical surface charge σ_{solid}. It is neutralized by charges of the opposite sign in two different zones, the Stern and the diffuse layers, bearing respectively σ_{stern} and σ_{diff} charge per unit area. The electrical balance respects the following expression:

$$\sigma_{\mathrm{solid}} = \sigma_{\mathrm{stern}} + \sigma_{\mathrm{diff}} \quad (2.91)$$

The external limit of the Stern layer, called the outer Helmholtz plane or the shear plane, separates the solid from the aqueous phase, in which ionic diffusion occur. The aqueous phase is divided in the diffuse layer and the free water zone, where ions do

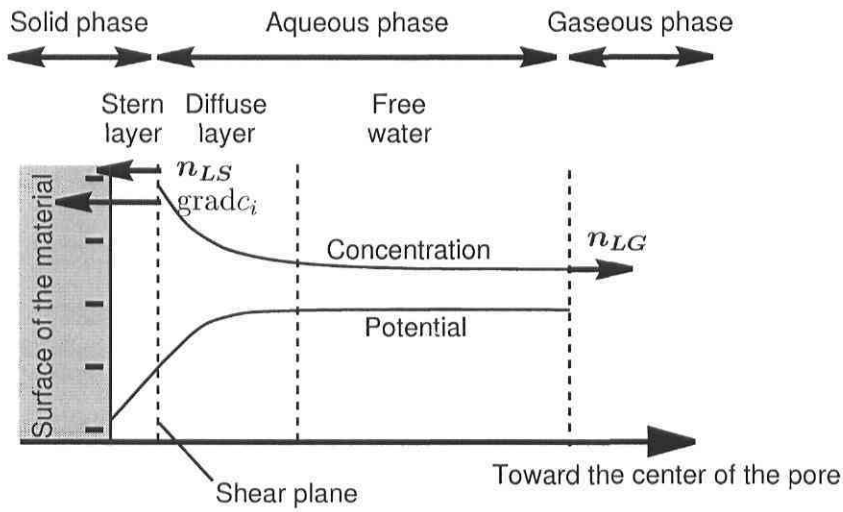

Figure 2.3: Concentration and potential profile across a pore near the solid/liquid interface according to the double layer theory.

not feel the effect of the solid/liquid interface. A recent study by Revil [146] showed that ionic transport may occur in the Stern layer. But it was also mentioned in the paper that this phenomenon is negligible *with respect to transport in the bulk pore* when the pore solution is highly concentrated, as it is the case in cement-based materials. Consequently, only the ionic transport in the aqueous phase is considered in this paper. Finally, the description of the cross-section of the pore is complete by considering a gaseous phase at the center of the pore, when the latter is not saturated [204].

Given a weak rate of evaporation of the liquid phase, it is assumed that the concentration profiles at the liquid/gas interface is flat (see figure 2.3). Consequently, the second integral in equation (2.89) is negligible since there is no concentration gradient along the radius at the liquid/gas interface. The situation is different for the first integral because of the concentration gradient along the radius at the solid/liquid interface caused by the electric charge at the surface of the solid. Simple double layer calculations made with the Gouy-Chapman model [26] are shown on figure 2.4. They emphasize that increasing the ionic strength of a solution in the vicinity of a charged surface decreases dramatically the thickness of the double layer. Since cementitious materials bear a highly charged solution, the double layer extends over a very small region. Outside this region, the concentration profile is unaffected by the surface charge.

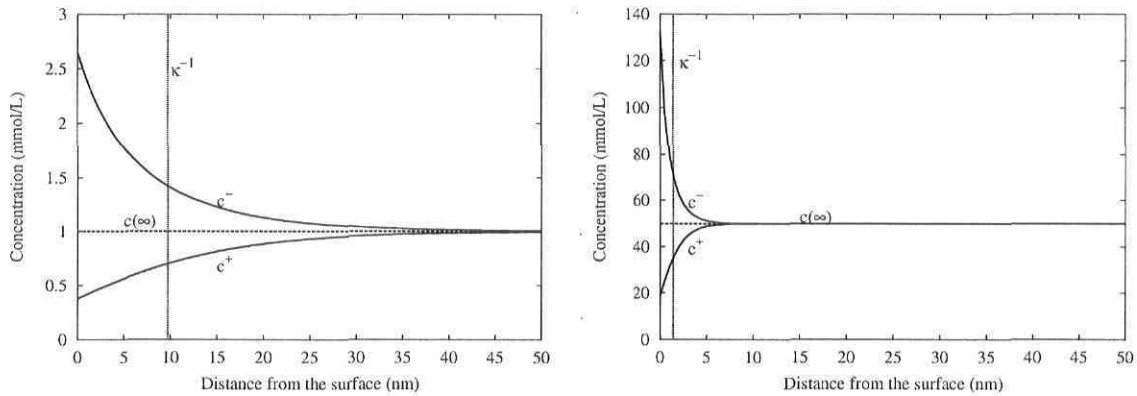

(a) $c^+(\infty) = c^-(\infty) = 1.0$ mmol/L (b) $c^+(\infty) = c^-(\infty) = 50.0$ mmol/L

Figure 2.4: Concentration profiles of a 1-1 electrolyte near a charged surface calculated with the Gouy-Chapman double layer model. The calculations were made with a surface potential of 25 mV. The Debye length κ^{-1} is indicated.

Following this, the term $\int \mathring{\boldsymbol{x}}(\mathrm{grad}c_i \cdot \boldsymbol{n_{LS}})dS$ in equation (2.89) is neglected, leaving:

$$\overline{\mathrm{grad}c_i}^L = \tau_L \mathrm{grad}\overline{c_i}^L \tag{2.92}$$

Then one needs to average the term in equation (2.88) concerned with the electrical coupling between the ions. According to the procedure for averaging a product [12, 18], one can write:

$$\overline{c_i \mathrm{grad}\psi}^L = \overline{c_i}^L \overline{\mathrm{grad}\psi}^L + \overline{\mathring{c}_i \mathring{\mathrm{grad}}\psi}^L \tag{2.93}$$

where the quantities topped by $\circ$, called deviations, are defined as:

$$\mathring{c}_i = c_i - \overline{c_i}^L \tag{2.94}$$

It is assumed that the deviations lead to small terms, which allows to neglect the deviation product in equation (2.93):

$$\overline{c_i \mathrm{grad}\psi}^L = \overline{c_i}^L \overline{\mathrm{grad}\psi}^L \tag{2.95}$$

Following the same procedure as the one used for the concentration gradient, the average of the potential gradient gives:

$$\overline{\mathrm{grad}\psi}^L = \tau_L \mathrm{grad}\overline{\psi}^L + \frac{1}{V_o}\int_{S_o^{LS}} \mathring{\boldsymbol{x}}\,(\mathrm{grad}\psi \cdot \boldsymbol{n_{LS}})\,dS + \frac{1}{V_o}\int_{S_o^{LG}} \mathring{\boldsymbol{x}}\,(\mathrm{grad}\psi \cdot \boldsymbol{n_{LG}})\,dS \tag{2.96}$$

Figure 2.3 shows a potential profile across the section of a pore. According to the double layer models [26], it has a shape similar to the concentration profile, i.e. it is disturbed

near the solid/liquid interface but tends to a flat profile toward the center of the pore. Accordingly, the integrals are neglected, assuming again that the electrical phenomena near the interface do not affect ionic movement, and, hence, equation (2.96) simplifies:

$$\overline{\mathrm{grad}\psi}^{L} = \tau_L \mathrm{grad}\overline{\psi}^{L} \tag{2.97}$$

Substituting equation (2.97) into (2.95) gives:

$$\overline{c_i \mathrm{grad}\psi}^{L} = \overline{c_i}^{L} \tau_L \mathrm{grad}\overline{\psi}^{L} \tag{2.98}$$

The same approach is used to average the chemical activity term in equation (2.88). The same assumptions concerning the deviations, as well as those concerning the effect of the electrical phenomena at the solid/liquid interface lead to:

$$\overline{c_i \mathrm{grad}(\ln \gamma_i)}^{L} = \overline{c_i}^{L} \tau_L \mathrm{grad}(\overline{\ln \gamma_i}^{L}) \tag{2.99}$$

It is assumed that the term $\overline{\ln \gamma_i}^{L}$ corresponds to the chemical activity coefficients calculated with the average concentrations $\overline{c_i}^{L}$. For simplicity, $\overline{\ln \gamma_i}^{L}$ is approximated by $\ln \overline{\gamma_i}^{L}$:

$$\overline{c_i \mathrm{grad}(\ln \gamma_i)}^{L} = \overline{c_i}^{L} \tau_L \mathrm{grad}(\ln \overline{\gamma_i}^{L}) \tag{2.100}$$

Finally, the advection term in equation (2.88) is averaged as:

$$\overline{c_i \boldsymbol{v}}^{L} = \overline{c_i}^{L} \overline{\boldsymbol{v}}^{L} + \overline{\overset{\circ}{c_i} \overset{\circ}{\boldsymbol{v}}}^{L} \tag{2.101}$$

The term in equation (2.101) containing the deviations is called the dispersive flux [18, 19]. It is shown in the previous references that it can be written under a Fickian form:

$$\overline{\overset{\circ}{c_i} \overset{\circ}{\boldsymbol{v}}}^{L} = -D^{\mathrm{disp}} \mathrm{grad}\overline{c_i}^{L} \tag{2.102}$$

where D^{disp} is called the coefficient of advective dispersion, and is due to fingering, not diffusion. Consequently, this term can be added to the ionic diffusion term that would then exhibit a new diffusion coefficient being the sum of the classical one plus the coefficient of advective dispersion. When the fluid is in movement under the effect of a water content gradient, as described in the preceding section, the velocity is relatively weak. In that case, the dispersion term can be neglected [168], leading to:

$$\overline{c_i \boldsymbol{v}}^{L} = \overline{c_i}^{L} \overline{\boldsymbol{v}}^{L} \tag{2.103}$$

Substituting equations (2.92), (2.98), (2.100), and (2.103) in equation (2.88), gives the average flux expression:

$$\theta_L \overline{\boldsymbol{j_i}}^L = -D_i^\mu \theta_L \tau_L \mathrm{grad}\overline{c_i}^L - \frac{D_i^\mu z_i F}{RT}\theta_L \tau_L \overline{c_i}^L \mathrm{grad}\overline{\psi}^L - D_i^\mu \theta_L \tau_L \overline{c_i}^L \mathrm{grad}(\ln \overline{\gamma_i}^L) + \theta_L \overline{c_i}^L \overline{\boldsymbol{v}}^L \tag{2.104}$$

The diffusion coefficient at the macroscopic level D_i is defined as:

$$D_i = \tau_L D_i^\mu \tag{2.105}$$

To simplify the expression, let:

$$C_i \equiv \overline{c_i}^L \tag{2.106}$$

$$\Psi \equiv \overline{\psi}^L \tag{2.107}$$

Substituting equations (2.105) to (2.107) in equation (2.104) gives:

$$\theta_L \overline{\boldsymbol{j_i}}^L = -D_i \theta_L \mathrm{grad}C_i - \frac{D_i z_i F}{RT}\theta_L C_i \mathrm{grad}\Psi - D_i \theta_L C_i \mathrm{grad}(\ln \overline{\gamma_i}^L) + \theta_L C_i \overline{\boldsymbol{v}}^L \tag{2.108}$$

Equation (2.108) is now inserted in the averaged mass conservation equation (2.86) to yield the macroscopic ionic transport equation:

$$\frac{\partial(\theta_L C_i)}{\partial t} - \mathrm{div}\left(D_i \theta_L \mathrm{grad}C_i + \frac{D_i z_i F}{RT}\theta_L C_i \mathrm{grad}\Psi + D_i \theta_L C_i \mathrm{grad}(\ln \overline{\gamma_i}^L) - \theta_L C_i \overline{\boldsymbol{v}}^L \right) + \theta_L \overline{r_i}^L + \frac{1}{V_o}\int_{S_o^{LS}} \boldsymbol{j_i} \cdot \boldsymbol{n_{LS}} dS = 0 \tag{2.109}$$

In order to simplify this equation, the integral must be expressed in a manner that is more friendly to a further numerical analysis. The term $(\boldsymbol{j_i} \cdot \boldsymbol{n_{LS}})$ gives the amount of ions crossing the solid/aqueous phase interface, as a result of dissolution/precipitation or ion exchange reactions. It is possible to express it differently by performing the averaging operation on the ions in the solid phase [18]. The conservation equation at the microscopic scale for the ions in solid phase is:

$$\frac{\partial c_{is}}{\partial t} + \mathrm{div}(\boldsymbol{j_{is}}) = 0 \tag{2.110}$$

where the subscript s designates the solid phase. Contrary to equation (2.80), it is assumed that no chemical reactions occur within the solid phase, since all precipitation/dissolution phenomena are taking place at the solid/aqueous phase interface. Averaging equation (2.110) over the REV leads to:

$$\frac{\partial(\theta_s C_{is})}{\partial t} + \mathrm{div}(\theta_s \overline{\boldsymbol{j_{is}}}^s) + \frac{1}{V_o}\int_{S_o^{SL}} \boldsymbol{j_{is}} \cdot \boldsymbol{n_{SL}}\, dS = 0 \tag{2.111}$$

where θ_s is the volumetric fraction of solid phase and $\boldsymbol{n_{SL}}$ is an outward (to the S-phase) unit vector on the solid/aqueous phase interface (designated as S^{SL}). The integral in equation (2.111) has the same value as the one in equation (2.109) but with an opposite sign since the ions coming out of the aqueous phase are being bound by the solid phase. Furthermore, the flux $\boldsymbol{j_{is}}$ within the solid is zero since there is no ionic movement in this phase. This allows one to write:

$$\frac{\partial(\theta_s C_{is})}{\partial t} = -\frac{1}{V_o}\int_{S_o^{SL}} \boldsymbol{j_{is}} \cdot \boldsymbol{n_{SL}}\, dS = \frac{1}{V_o}\int_{S_o^{LS}} \boldsymbol{j_i} \cdot \boldsymbol{n_{LS}}\, dS \tag{2.112}$$

Substituting equation (2.112) in equation (2.109) gives:

$$\frac{\partial(\theta_L C_i)}{\partial t} - \mathrm{div}\left(D_i\theta_L \mathrm{grad}C_i + \frac{D_i z_i F}{RT}\theta_L C_i \mathrm{grad}\Psi + D_i\theta_L C_i \mathrm{grad}(\ln\overline{\gamma_i}^L) - \theta_L C_i \overline{\boldsymbol{v}}^L\right) + \theta_L \overline{r_i}^L + \frac{\partial(\theta_s C_{is})}{\partial t} = 0 \tag{2.113}$$

This is the general expression for the ionic transport in porous materials under isothermal conditions.

2.3.3.2 Coupling water and ionic transport

To model the transport of ions under the influence of capillary suction, it would seem straightforward to substitute equation (2.56) in (2.113). However, the development of the water transport equations was made for the case of pure water in a porous material. When ions are in solution, the vapour pressure above a solution is lower than in pure water [99]. This effect is quantified through Raoult's law. Accordingly, the relationship $\overline{p_c} = f(\theta_L)$ should instead be written as:

$$\overline{p_c} = f(\theta_L, c_i) \tag{2.114}$$

since the presence of ions in solution is likely to disturb the equilibrium between the aqueous and gaseous phases in a pore. To evaluate in what extent the presence of ions will affect the vapor pressure of water, one can use Raoult's law to calculate the vapor pressure change between pure water and a 500 mmol/L NaCl solution with water as solvent. According to Raoult's law [99], the vapor pressure change is given as:

$$\Delta p_v = X_{\text{solute}}\, p_v^\circ \tag{2.115}$$

where X_{solute} is the molar fraction of solute (NaCl) in the solution and p_v° is the vapor pressure of pure water. At 25°C , the vapor pressure of bulk water is 3.17 kPa [99]. Knowing that in one liter of water there are 56 moles:

$$X_{\text{solute}} = \frac{0.5 \text{ mole NaCl}}{0.5 \text{ mole NaCl} + 56 \text{ moles water}} = 0.009 \tag{2.116}$$

This gives a change in vapor pressure of $\Delta p_v = 0.03$ kPa, which is obviously very weak. According to the result of this simple calculation, the effect of ionic concentration on the capillary pressure is neglected. It was also neglected in the models presented in references [72, 122, 130, 152].

Substituting equation (2.56) in equation (2.113) gives:

$$\frac{\partial(\theta_L C_i)}{\partial t} - \text{div}\left(D_i \theta_L \text{grad} C_i + \frac{D_i z_i F}{RT} \theta_L C_i \text{grad}\Psi + D_i \theta_L C_i \text{grad}(\ln \overline{\gamma_i}^L) + C_i D_L \text{grad}\theta_L \right) + \theta_L \overline{r_i}^L + \frac{\partial(\theta_s C_{is})}{\partial t} = 0 \tag{2.117}$$

This equation can be used to model the transport of ions in unsaturated cement-based materials when the pore fluid is in movement because of capillary suction. To complete the model, an equation must be considered to evaluate the potential Ψ, as well as an expression to calculate the chemical activity coefficients. These topics are addressed in the following sections.

2.3.3.3 Calculation of the potential

The electrical potential in equation (2.117) arises in the material to enforce the electroneutrality condition. If two species are diffusing in a material with one of the species having a greater self-diffusion coefficient. To maintain a neutral solution, the potential created slows the fastest ions and accelerates the slowest ones.

The mathematical relationship that relates electrical potential to electrical charges in a given media is given by Poisson's equation [85]

$$\nabla^2 \psi + \frac{\rho}{\epsilon} = 0 \tag{2.118}$$

where ρ is the electrical charge density and ϵ is the medium permittivity. The charge density can be related to the ionic concentration through:

$$\rho = F \sum_{i=1}^{N} z_i c_i \tag{2.119}$$

where N is the number of ionic species. Substituting equation (2.119) in (2.118) gives:

$$\nabla^2\psi + \frac{F}{\epsilon}\sum_{i=1}^{N} z_i c_i = 0 \tag{2.120}$$

It may seem awkward to have an equation from electrostatics in a model where the ions are moving through time. However, since the electromagnetic signal is moving much more rapidly than the ions, Poisson's equation is perfectly suitable.

To use equation (2.120) in the transport model, it has to be averaged over the REV. As it was done previously, it is assumed that the boundary effects at the liquid/solid and liquid/gas interfaces are negligible. Following the same average rules as in the previous sections, we get the following relationship:

$$\mathrm{div}\left(\theta_L \tau_L \mathrm{grad}\Psi\right) + \theta_L \frac{F}{\epsilon}\sum_{i=1}^{N} z_i C_i = 0 \tag{2.121}$$

2.3.3.4 Evaluation of chemical activity coefficients

The models to calculate the chemical activity coefficients are numerous. The first ones developed are the Debye-Hückel and extended Debye-Hückel models [133]. From purely electrostatic considerations, they relate the chemical activity coefficients of ionic species to the ionic strength of a solution. They are valid for ionic strengths up to 10 and 100 mmol/L respectively.

In cement-based materials, the ionic strength is much higher. To suit this particular situation, a chemical activity relationship was developed recently by Samson et al. [155] which gives good results for highly concentrated solutions:

$$\ln \gamma_i = -\frac{A z_i^2 \sqrt{I}}{1 + a_i B \sqrt{I}} + \frac{(0.2 - 4.17\times10^{-5}\, I) A z_i^2 I}{\sqrt{1000}} \tag{2.122}$$

where I is the ionic strength of the solution, and A and B are temperature dependent parameters. The parameter a_i in equation (2.122) varies with the ionic species considered.

2.3.3.5 Evaluation of the ionic transport properties

Two different transport parameters appear in equation (2.117). There is the diffusion coefficient D_i associated with the diffusion process and the liquid water diffusivity D_L

to characterize the effect of the fluid velocity on the ionic transport. A discussion of D_L was already given in section 2.3.2.5.

The diffusion coefficient is evaluated with the migration experiment test. It consists of accelerating chloride ions with an applied external potential through a disk of cement-based materials glued between two cells filled with ionic solutions. The analysis of the results yields the diffusion coefficients. Two main analysis methods are found in the literature. The first is based on steady state measurements of chloride having crossed the sample [8, 212]. The other [184] is based on measuring non-steady state chloride profiles by grinding the sample after a short exposure.

Both these methods are performed in saturated conditions. As shown in equation (2.105), the diffusion coefficient D_i depends, through τ_L, on the saturation condition. No method could be found in the literature to evaluate this parameter for unsaturated conditions. However, it is possible that D_i might not be affected by the saturation state of the material above a given saturation level, the latter being defined as $s = \theta_L/\phi$, where ϕ is the porosity. Revil [146] showed that for shaly sand, the diffusion of the ions is almost unaffected for a water saturation above 0.6. We thus infer that for concrete structures exposed to high relative humidity environment, the diffusion coefficient is independent of the water content.

In the flux equation (2.104), the recurring quantity $\tau_L\theta_L$, which could also be written $\tau_L s\phi$, is analogous to a saturation-dependent formation factor for the liquid phase of the pore system. The saturation s results from the averaging over the REV. The tortuosity τ_L is also a function of the saturation and reflects the connectedness of the moisture phase. At a critical moisture content s_c, the liquid phase is no longer connected, the tortuosity τ_L goes to zero, the transport within the liquid phase ceases.

The remaining question is the dependence of the tortuosity τ_L on the saturation. Although no precise data exist for cementitious systems, there exists qualitative data from which inferences can be made. These data typically express the relative total conduction as a function of the saturation s. The relative total conduction σ/σ_o is analogous to the product of the saturation and the relative tortuosity:

$$\frac{\sigma(s)}{\sigma(s=1)} = \frac{s\ \tau_L(s)}{\tau_L(s=1)} = \frac{s\ \tau_L}{\tau_{Lo}} \tag{2.123}$$

Therefore, dividing these results by s will yield the relative change in the tortuosity.

The work of Martys [121] suggests that for a preferentially wetting liquid being displaced by a non-wetting one, the limiting behavior of τ_L near saturation can be approximated by the dilute effective medium theory result:

$$\frac{s\ \tau_L}{\tau_{Lo}} = 1 - \frac{3}{2}(1-s) + \frac{1}{2}(1-s)^2 \qquad s \to 1 \tag{2.124}$$

(Here, the more exact coefficient of 0.558 for the quadratic term has been roughly approximated by 1/2.) The relative tortuosity can be solved for algebraically:

$$\frac{\tau_L}{\tau_{Lo}} = \frac{s}{2} + \frac{1}{2} \tag{2.125}$$

Therefore, a decrease to 80 % saturation will result in a 10 % change in the tortuosity. Given that transport coefficients can routinely change by orders of magnitude, a 10 % change in the tortuosity is relatively quite minor. Since this result is only approximate near saturation, further reductions in saturation would have a far greater effect.

2.3.4 Conclusion

The mathematical model developed in this paper is first summarized. For materials where the water transport occurs as a result of capillary suction, the water content profile can be calculated with Richards' equation (2.79). The ions will move in the material under the combined effect of diffusion (including electrical and activity effects) and water movement according to equation (2.117). The electrical potential, arising from the electrical coupling between the ions in order to maintain a neutral solution, is calculated with Poisson's equation (2.121). Finally, chemical activity coefficients, for the highly charged pore solution of cement-based materials, can be evaluated with expression (2.122).

The use of the averaging technique clearly helps to clarify the meaning of some important parameters in the model. According to this technique, the water content in Richards' model corresponds to a volumetric water content. The water diffusivity was clearly shown to be a contribution of both liquid water and vapor transport. The diffusion coefficient, the parameter that characterize the ionic diffusion process, is directly related to the geometrical properties of the material through a parameter called the tortuosity.

The averaging technique proved to be a powerful mathematical tool to lay the foundation of transport models in porous media.

2.4 Modeling chemical activity effects in strong ionic solutions

E. Samson[12], G. Lemaire[1], J. Marchand[12], J.J. Beaudoin[3]

[1]Centre de recherche interuniversitaire sur le béton,
Université Laval, Québec, Canada, G1K 7P4

[2]SIMCO Technologies inc.,
1400, boul. du Parc Technologique, Québec, Canada, G1P 4R7

[3]Materials Laboratory - Institute for Research in Construction,
National Research Council, Ottawa, Canada, K1A 0R6

Abstract

A new simple mathematical model for calculating the chemical activity coefficients of ions in electrolytic solutions is presented. The model was developed to account for the particular behavior of concentrated solutions for which short-range and long-range interactions between ions are important. The new model is essentially a modified version of the Davies equation. Given its simple mathematical form, it can be easily implemented in a numerical code aimed at modeling ionic transport phenomena in saturated porous materials. The transport equations of charged particles in concentrated solutions are also presented. Numerical results are shown and compared with experimental results. Applications of the model to ionic diffusion problems in saturated porous media are also shown.

2.4.1 Introduction

It has been clearly established that the behavior of porous materials is often directly affected by the thermodynamic characteristics of their pore solutions. It has been shown, for instance, that the swelling of clays is predominantly controlled by the presence of

certain ionic species in the interlayer spaces [41]. It is also well known that the pore solution thermodynamic properties have a significant influence on various engineering problems such as the filtration of electrolytes by ion-exchange membranes. Finally, the composition and the ionic strength of electrolytes may affect the chemical stability of numerous building materials (such as rocks and cement-based materials) and the transport of ions and pollutants through engineering barriers [85, 115, 175].

In many practical cases, the electrolytic solutions of porous solids tend to be highly concentrated. This is the case of cement-based materials and ion-exchange membranes for which the ionic strength of their pore solutions is usually over 500 mmol/L [38, 40, 85, 109, 115, 141]. The high ionic strength of the pore solution chiefly complicates the prediction of the evolution of the engineering properties of the porous materials. This is particularly the case when the overall behavior of the solid is controlled by the transport of ions through the material pore structure. Equations for ionic transport in porous media tend to be highly non-linear and their resolution often requires intricate numerical schemes [18, 157, 164].

Complications related to the high ionic concentrations of the pore solutions mainly arise from the fact that the thermodynamic properties of an electrolyte tend to vary in a non-linear fashion with its ionic strength. As the ionic strength increases, ion/ion and ion solvent interactions become more significant and the thermodynamic properties of the electrolyte gradually deviate from that of an ideal (very dilute) solution [2, 26, 38, 103].

Numerous semi-empirical models have been developed to account for the influence of ionic strength on the thermodynamic properties of electrolytic solutions. As will be seen in the following subsection, the validity of most of these models is limited to electrolytic solutions for which the ionic strength is less than 500 mmol/L, and cannot therefore be applied to many practical cases. The Pitzer model [136, 137] appears to be the only one that can reliably predict the thermodynamic behavior of concentrated electrolytic solutions. Unfortunately, its mathematical formulation is much too intricate to be implemented in a numerical model designed to predict the transport of ions in porous media.

A brief critical analysis of existing models that predict the thermodynamic properties of electrolytes and of their implication on the modeling of ionic transport in saturated porous media was conducted. A new simple mathematical model for calculating the chemical activity coefficients of ions in concentrated solutions is presented. The model was developed to account for the particular behavior of concentrated electrolytic solutions. It can be easily implemented in a numerical code used to model ionic transport phenomena in saturated porous materials.

2.4.2 Different models for chemical activity

In a solution, the electrochemical potential of an ionic species μ_i (J/mol) which can be calculated using the following equation μ_i:

$$\mu_i = \mu_i^o + RT \ln(\gamma_i c_i) + z_i F \psi \tag{2.126}$$

where μ_i^o is the standard potential, R is the ideal gas constant (8.3143 J/mol °K), T is the temperature (°K), γ_i is the chemical activity coefficient, c_i is the concentration of the ionic species i (mmol/l), z_i is the valence number, F is the Faraday constant (9.64846×10^4 C/mol), and ψ is the electrical potential (Volt). According to this equation, the electrochemical potential μ_i of an ionic species in solution is not a sole function of its ionic concentration but also depends on the activity coefficient γ_i and on the local electrical potential ψ.

The activity coefficients of ionic species in an ideal (very dilute) solution are equal to 1. However, as the concentration of the ionic solution is increased, the value of the activity coefficient will first tend to be reduced to reach a pessimum value that can be significantly different than 1 [26, 38, 141]. Once this critical value is reached, any subsequent increase in the solution ionic strength will contribute to an increase of the activity coefficient.

It should be emphasized that the activity coefficient is only a mathematical representation of the various interactions that take place in an ionic solution. Electrochemists usually distinguish two different types of interaction arising mainly from the fact that ions are, in reality, charged particles [26, 141]: ion/solvent interactions (the electrophoretic effect) and ion/ion interactions (the relaxation effect).

The first type of interaction arises from the fact that the kinetic unit of the solute in solution is an ion with several relatively firmly attached solvent (water) molecules [26, 38, 45]. As they move in solution, ions tend to drag numerous solvent molecules with them. This phenomenon may contribute to a marked decrease in the ionic mobility [38, 141].

Ion/ion interactions arise due to the electric charge carried by these particles in solution. On a time-averaged basis, an ion of a given charge is usually surrounded by ions of opposite charge. This arrangement reduces the mobility of the particles in solutions since ions cannot move independently of one another. The relaxation effect tends to increase with the solution concentration which reduces the mean distance between ions [26, 141]. Usually, electrochemists distinguish numerous types of specific interactions including short-range and long-range electrostatic forces, London's dispersion forces and the net effect of solvation.

Numerous models have been derived to calculate single ion activity coefficients. The conventional model, still at the basis of the more recent and more sophisticated equations, is the Debye-Hückel model [133]. It relates the ionic strength $I = 0.5 \sum z_i^2 c_i$ (mmol/l) of the solution to the activity coefficient through the following relationship:

$$\ln \gamma_i = -A z_i^2 \sqrt{I} \tag{2.127}$$

where the parameter A is given by:

$$A = \frac{\sqrt{2}\, F^2 e_o}{8\pi(\epsilon RT)^{3/2}} \tag{2.128}$$

In the last equation, e_o stands for the electronic charge (1.602×10^{-19} C) and $\epsilon = \epsilon_r \epsilon_o$ is the permittivity of the medium, given by the dielectric constant times the permittivity of the vacuum. For the sake of simplicity, all the calculations presented in the following paragraphs will be carried out assuming the solvent to be water at 25°C , for which $\epsilon_r = 80$. The value of ϵ_o is 8.854×10^{-12} F/m.

The basic assumption behind this model is that a cloud of ions bearing the same charge but opposite sign surrounds the central ion. Furthermore, all ions are considered as point charges, having no radii. In that respect, the model only accounts for long-range electrostatic interactions.

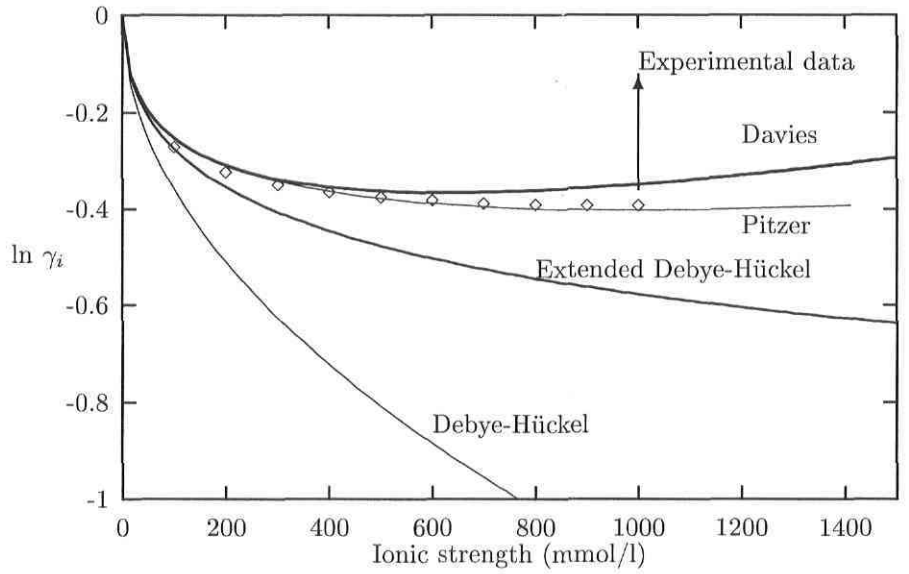

Figure 2.5: Comparison of NaOH activity coefficients for different models

It has been shown that the Debye-Hückel model can efficiently calculate the activity coefficients of a 1-1 solution with an ionic strength of 10 mmol/l or less [103]. The reliability of the model at predicting the single ion activity coefficient is illustrated in figure 2.5. In the figure, the activity coefficient of a NaOH solution measured at various ionic strengths is compared to the values yielded by the model [43]. In this specific case, the activity coefficients are the same for both species. The agreement is not satisfactory.

The Debye-Hückel model was subsequently modified to account for the radii of the central ions a_i (m). The extended Debye-Hückel model is given by the following relationship:

$$\ln \gamma_i = -\frac{Az_i^2\sqrt{I}}{1 + Ba_i\sqrt{I}} \tag{2.129}$$

where:

$$B = \sqrt{\frac{2F^2}{\epsilon RT}} \tag{2.130}$$

As can be seen in figure 2.5, this correction extends the validity of the model to an ionic strength of 100 mmol/l [2]. All values appearing in the figure were calculated assuming that the radius of all species was 3Å.

Despite this significant improvement, the extended model cannot be used in most practical cases. Furthermore, the radius a_i is a quantity that is not easily determined.

It has become a parameter with little physical meaning that is mainly used to fit the model to the experimental values. In some cases, the parameter a_i has to take a negative value in order to reliably represent the experimental data [69].

Despite the obvious advantage of the extended Debye-Hückel equation, the modification of the term a_i cannot account for the increase in the activity coefficients often observed at high concentrations. According to Bockris [26], this behavior can be explained by the fact that as the ionic concentration increases, more water molecules are used to solvate the ions in solutions, leaving less and less free water molecules. The "effective" concentrations of the various species in solution are therefore increased by the reduction in the number of free solvent molecules which yields a net increase in the activity coefficient.

Numerous models have been developed to account for this phenomenon. Most of these models possess two terms [103]. The first term is usually very similar (or derived from) to the Debye-Hückel equation. The second part of these models is a composite term (proportional to the ionic strength of the solution) which accounts for all other phenomena including the solvation and short-range interactions [103, 133].

Probably, the most well-known of these models is the Davies equation:

$$\ln \gamma_i = -\frac{Az_i^2\sqrt{I}}{1+(3\times 10^{-10})B\sqrt{I}} + \frac{CAz_i^2 I}{\sqrt{1000}} \quad \text{with} \quad C = 0.2 \tag{2.131}$$

In this model, the mean radius of all ions is fixed at 3Å. As can be seen in figure 2.5, the Davies equation can usually predict the behavior of an electrolytic solution up to a ionic strength of 500 mmol/L [133].

More recently, Li and Page [103] have proposed the following equation for the mean natural logarithm activity coefficient to account for the solvation effect:

$$\frac{1}{n}\sum_{i=1}^{n}\ln\gamma_i = \alpha I\left(\frac{2}{3}\sqrt{\frac{I}{I_{\text{cr}}}} - 1\right) \tag{2.132}$$

where n is the number of ionic species, I_{cr} is the critical ionic strength at which the value of the mean natural logarithm activity coefficient starts to increase and α is a fitting parameter.

Despite these significant improvements, most of these models cannot account for the phenomenon of ionic association [26, 69, 80]. In an electrolytic solution, ions are in

closer proximity as the ionic strength increases. At some point ions are so close that their thermal agitation is not sufficient to separate them from one another; they are trapped in each other's electrostatic field. The new pairs of ions formed according to this process have no net charge, and their presence cannot therefore by accounted for in the calculation of the activity coefficients according to the Debye-Hückel based models.

Bjerrum [26] has evaluated the proportion of ions that are likely to form pairs in a concentrated electrolytic solution, and modified the Debye-Hückel law accordingly. In Bjerrum's approach, the formation of ionic pairs is essentially the same whatever the species found in solution. Unfortunately, this assumption is not supported by experimental data.

Many recent investigations have clearly demonstrated that chemical activity effects in concentrated electrolytes can be accurately described by the semi-empirical model developed by Pitzer and his co-workers [136, 137]. As shown in figure 2.5, the model is valid for ionic strengths higher than 1 mol/L. The Pitzer equations for the single ion activity coefficients consist of a Davies core to which are added a series of terms that contain the various ion interaction parameters. These terms account for the ionic strength dependence of the short-range forces in electrolyte solutions, and the formation of pairs and even triplets and quadruplets. In order to run the model, some experimental values (specific to the type of ions and the interaction considered) are required.

According to the Pitzer model, the activity coefficient of a cation M in solution can be calculated by:

$$\begin{aligned} \ln\gamma_M \;=\; & z_M^2 F + \sum_{a=1}^{Na} m_a(2B_{Ma} + ZC_{Ma}) + \sum_{c=1}^{Nc} m_c \left(2\Phi_{Mc} + \sum_{a=1}^{Na} m_a \psi_{Mca} \right) + \\ & \sum_{a=1}^{Na-1} \sum_{a'=a+1}^{Na} m_a m_{a'} \psi_{aa'M} + |z_M| \sum_{c=1}^{Nc} \sum_{a=1}^{Na} m_c m_a C_{ca} + \sum_{n=1}^{Nn} m_n (2\lambda_{nM}) \end{aligned} \tag{2.133}$$

For an anion, the equation is:

$$\ln\gamma_X = z_X^2 F + \sum_{c=1}^{Nc} m_c(2B_{cX} + ZC_{cX}) + \sum_{a=1}^{Na} m_a \left(2\Phi_{Xa} + \sum_{c=1}^{Nc} m_c \psi_{Xac} \right) + \sum_{c=1}^{Nc-1} \sum_{c'=c+1}^{Nc} m_c m_{c'} \psi_{cc'X} + |z_X| \sum_{c=1}^{Nc} \sum_{a=1}^{Na} m_c m_a C_{ca} + \sum_{n=1}^{Nn} m_n (2\lambda_{nX}) \tag{2.134}$$

In these two equations, M and X indicate the cation and anion for which the activity coefficient calculations are carried out. The subscript c and a refer to the other cations and anions. The Davies core is hidden in the parameter F. The other parameters are used to account for the ionic association. The reliability of the Pitzer model at predicting activity coefficients can be clearly visualized in figure 2.5.

2.4.3 Chemical activity effects on the mathematical treatment of ionic diffusion mechanisms in saturated porous media

According to equation (2.126), the electrochemical potential (or the free energy) of an ionic species at a given location in solution is directly related to its concentration. Thus according to equation (2.126), if two points in a solution are at different concentrations, there exists between them a gradient of free energy. By applying the second principle of thermodynamics (the energy dissipation due to the movement of ions is always positive or equal to zero), the macroscopic diffusion flow $\boldsymbol{j_i}$ (mol/m^{2}s) of an ionic species i in a solution can be expressed by the following equation [85, 115, 157]:

$$\boldsymbol{j_i} = -B\, c_i\, \mathrm{grad}(\mu_i^o + RT \ln(\gamma_i c_i) + z_i F \psi) \tag{2.135}$$

where B is a phenomenological parameter that mainly describes the ability of the ion to move in an ideal solution. This parameter is a characteristic of the ion. B is linked to the diffusion coefficient of the species D_i (m^2/s) through the following equation :

$$B = \frac{D_i}{RT} \tag{2.136}$$

For a given ionic species, the coefficient D_i is a constant and corresponds to the diffusion coefficient of the ion in a very dilute solution. In open solutions, D_i is therefore an intrinsic property of the ionic species. In a porous media, D_i has to be corrected by

some geometrical factors that account for the tortuosity and the porosity of the pore system [18].

Substituting equation (2.136) in equation (2.135), one finds :

$$\boldsymbol{j_i} = -\frac{D_i}{RT}\, c_i\, \mathrm{grad}(\mu_i^o + RT \ln(\gamma_i c_i) + z_i F \psi) \tag{2.137}$$

Equation (2.137) includes the particular feature that accounts for the ionic diffusion mechanisms. As previously discussed, ions are, contrary to molecules, charged particles. The most important feature which distinguishes ionic diffusion from molecular diffusion is the electrical coupling of the various ionic flows [85, 115, 157]. In an ionic solution, the local electroneutrality should be preserved at any point. The conservation of electroneutrality requires that the flows of all diffusing species should be coupled. During the diffusion process, all ions are not drifting at the same speed. Some ions tend to diffuse at a higher rate. However, any excess charge transferred by the faster ions builds up a local electric field (called the diffusion potential) which slows down the faster ions, and reciprocally accelerates the slower ions. This local potential can be calculated on the basis of the Poisson equation [115, 157]:

$$\nabla^2 V + \frac{\rho}{\epsilon} = 0 \tag{2.138}$$

Where ρ stands for the electrical charge density ($\mathrm{C/m^3}$) and ϵ refers to the dielectric constant of the medium ($\mathrm{F/m}$). The charge density is related to the concentration of the various ionic species through the following relationship :

$$\rho = F \sum z_i c_i \tag{2.139}$$

Equation (2.137) can be expanded in two different ways. First, the effect of the variation of the chemical activity can be explicitly expressed in the flux equation. The resulting expression is the well known extended Nernst-Planck equation:

$$\boldsymbol{j_i} = -D_i \left(\mathrm{grad}(c_i) + \frac{z_i F}{RT} c_i \mathrm{grad}(\psi) + c_i \mathrm{grad}(\ln \gamma_i) \right) \tag{2.140}$$

As can be seen, the explicit account of the influence of the chemical activity variation simply adds a correction term to the transport equation.

Moreover, the influence of the chemical activity variation can be implicitly accounted for in the transport equation:

$$\boldsymbol{j_i} = -D_i^a(c) \mathrm{grad}(c_i) - \frac{D_i z_i F}{RT} c_i \mathrm{grad}(\psi) \tag{2.141}$$

The effect of the activity is hidden in a non-linear diffusion coefficient D_i^a and the last term of equation (2.140) is eliminated. The value of this non-linear diffusion coefficient is related to that of the diffusion coefficient D_i through the following equation :

$$D_i^a(c) = D_i \left(1 + \frac{d \ln \gamma_i}{d \ln c_i}\right) \tag{2.142}$$

The complete description of the diffusion process in saturated porous materials can be made through the extended Nernst-Planck/Poisson set of equations, i.e. on the basis of equations (2.140) or (2.141) (that should be written for each ionic species present in solution) and equation (2.138). The resolution of this system of non-linear differential equations can be quite difficult particularly for systems made of numerous polyvalent species. Over the years, numerous analytical solutions have been developed for simple cases (electrolytic solutions made of monovalent ions, ...). However, the treatment of most practical cases requires the development of numerical solutions. The inherent difficulties of the numerical integration of these equations are discussed in [157].

It should be underlined that most of the numerical solutions of the Nernst-Planck/ Poisson set of equations do not account for chemical activity effects [157]. Most of the available numerical models have been developed for ideal electrolytes and cannot therefore be applied to most practical cases. The limited number of numerical solutions specifically adapted to the treatment of ionic diffusion problems in concentrated electrolytes can be explained by the relative complexity of the semi-empirical equations devoted to the calculation of chemical activity coefficients. It can be easily understood that the implementation of the Pitzer equation in a numerical solution of the extended Nernst-Planck/Poisson set of equations presents some inherent difficulties.

2.4.4 Modification of the Davies law

Recently, a few attempts to develop simple equations to accurately calculate single activity coefficients of concentrated electrolytic solutions have been made. In that respect, the model proposed by Li and Page [103] is a good example of this new generation of equations. The model presented in the following paragraph presents another approach to the problem. This new model is essentially a modified version of the Davies equation (equation 2.131). As will be seen, the range of validity of this new model is similar

to that of the Pitzer equation (equations 2.133 and 2.134). However, its mathematical formulation is much simpler.

As previously discussed, the Davies equation (equation 2.131) can accurately predict single ion activity coefficients when the ionic strength of the electrolytic solution is below 500 mmol/L. It can be easily shown that the ability of the model at predicting the activity coefficient of ions in concentrated solutions can be significantly improved by reducing the parameter C appearing in the second term of the equation. For instance, the reduction of C from 0.2 to 0.15 tends to expand the validity of the model to solutions at ionic strengths up to 1200 mmol/L. Unfortunately, this simple operation contributes to detrimentally affect the accuracy of the model at low ionic strengths.

In order to improve the accuracy of the Davies equation over a wide range of ionic strengths, it was decided to change the constant appearing in the second term of the equation for a variable whose value would decrease as the ionic strength of the solution is increased. For an ideal solution, for which the ionic strength is near zero, the value of C is 0.2 and it decreases linearly to 0.15 for an ionic strength of 1500 mmol/L. This modifies the Davies equation as follows:

$$\ln \gamma_i = -\frac{Az_i^2\sqrt{I}}{1+(3\times 10^{-10})B\sqrt{I}} + \frac{((-4.17\times 10^{-5})I+0.2)Az_i^2 I}{\sqrt{1000}} \tag{2.143}$$

The figure 2.6 shows a comparison between the results obtained with the Pitzer equation and those yielded by the modified version of the Davies model for a sodium hydroxide solution at various ionic strengths. In all calculations made with the modified Davies equation, it was assumed that the ionic radius of all ions was equal to 3 Å. As can be seen, the slight modification made to the model significantly improves its accuracy at high concentrations without any detrimental influence on the performance of the model at low ionic strengths.

The accuracy of the modified model was also tested for various solutions containing monovalent and divalent ions such as Na^+, K^+, OH^-, SO_4^{2-} and Cl^-. The values of the activity coefficients obtained with the modified Davies equation were compared to those yielded by the Pitzer model. These comparisons showed that the predictions given by the modified equation for a few specific ions could deviate significantly from those of the Pitzer equation. To improve the reliability of the modified model, the numerical simulations were made by varying the radii of these ions as suggested by some authors

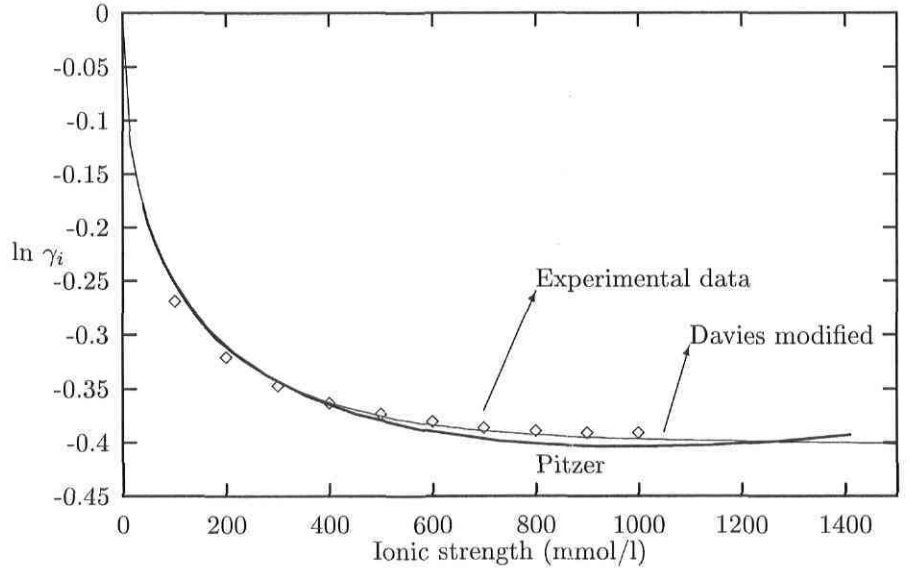

Figure 2.6: Comparison between Pitzer and the modified Davies model

[26, 69]. It was found that results yielded by the Pitzer model could be fairly well predicted by the modified Davies equation when the radii of K^+, Cl^-, SO_4^{2-} were fixed at 3.3Å, 2Å and 1Å respectively.

This last version of the modified Davies model was also tested for ten different electrolytic solutions. The compositions of these solutions are presented in table 2.1. All concentrations appearing in the table are given in (mmol/l). The results yielded by the modified model are presented in tables 2.2 to 2.6 along with those obtained with Pitzer equation.

The results presented in tables 2.2 to 2.6 clearly indicate that the modified version of the Davies equation can accurately predict single ion activity coefficients of concentrated electrolytic solutions made of monovalent and divalent ions. According to these results, the modified model appears to yield reliable values for ionic strengths ranging from 0 to 1200 mmol/L.

Table 2.1: Compositions of the electrolytic solutions

Na^+	K^+	SO_4^{2-}	Cl^-	OH^-	I
42.0	47.6	10.0	5.0	64.6	99.6
42.1	121.0	10.0	10.0	133.0	173.1
42.1	270.0	10.0	20.0	272.0	322.1
201.0	502.0	50.2	50.2	553.0	753.5
219.0	536.0	50.2	100.0	554.0	804.9
236.0	570.0	50.2	151.0	554.0	855.9
253.0	603.0	50.2	201.0	554.0	905.9
286.0	670.0	50.2	301.0	554.0	1005.9
319.0	737.0	50.2	402.0	554.0	1106.4
352.0	804.0	50.2	502.0	553.0	1205.9

Table 2.2: Activity coefficients for Na^+

I	Pitzer	Davies modified	% diff
99.6	.7730	.7764	0.4
173.1	.7380	.7411	0.4
322.1	.6973	.7060	1.2
753.5	.6482	.6763	4.3
804.9	.6458	.6752	4.5
855.9	.6437	.6743	4.8
905.9	.6419	.6736	4.9
1005.9	.6390	.6725	5.2
1106.4	.6369	.6718	5.5
1205.9	.6355	.6713	5.6

Table 2.3: Activity coefficients for K^+

I	Pitzer	Davies modified	% diff
99.6	.7831	.7813	0.2
173.1	.7346	.7482	1.9
322.1	.7290	.7162	1.8
753.5	.6992	.6924	1.0
804.9	.6932	.6918	0.2
855.9	.6877	.6914	0.5
905.9	.6826	.6912	1.3
1005.9	.6734	.6911	2.6
1106.4	.6654	.6913	3.9
1205.9	.6583	.6915	5.0

Table 2.4: Activity coefficients for SO_4^{2-}

I	Pitzer	Davies modified	% diff
99.6	.3114	.2995	3.8
173.1	.2339	.2229	4.7
322.1	.1597	.1527	4.4
753.5	.0872	.0867	0.6
804.9	.0828	.0830	0.2
855.9	.0788	.0796	1.0
905.9	.0752	.0766	1.9
1005.9	.0682	.0711	4.3
1106.4	.0636	.0665	4.6
1205.9	.0590	.0624	5.8

Table 2.5: Activity coefficients for Cl^-

I	Pitzer	Davies modified	% diff
99.6	.7581	.7584	0.04
173.1	.7137	.7149	0.2
322.1	.6579	.6674	1.4
753.5	.5795	.6138	6.4
804.9	.5767	.6105	6.3
855.9	.5741	.6075	6.2
905.9	.5719	.6048	5.8
1005.9	.5679	.5999	5.6
1106.4	.5647	.5956	5.5
1205.9	.5621	.5917	5.3

Table 2.6: Activity coefficients for OH^-

I	Pitzer	Davies modified	% diff
99.6	.7734	.7764	0.4
173.1	.7481	.7411	0.9
322.1	.7257	.7060	2.7
753.5	.6878	.6763	1.7
804.9	.6859	.6752	1.6
855.9	.6843	.6743	1.5
905.9	.6829	.6736	1.4
1005.9	.6808	.6725	1.2
1106.4	.6792	.6718	1.1
1205.9	.6783	.6713	1.0

2.4.5 Application of the modified Davies equation to a case of ionic transport

Two typical cases of ionic diffusion in a saturated porous membrane were selected to illustrate the application of the modified Davies equation. In the first case, the concentrations across the membrane were selected to comply with the limit of validity of the extended Debye-Hückel model. Concentrated electrolytic solutions were considered for the second case. In both cases, the thickness of the membrane was fixed at 1 cm, the relative permittivity in the membrane was assumed to be equal to that of water (80) and the temperature of the system was kept constant at 295°K . Furthermore, the system was assumed, in both cases, to be comprised of four different ionic species: K^+, Cl^-, SO_4^{2-} and OH^-. In both cases, the diffusion coefficient of each species is: 5.0×10^{-12} for OH^-, 1.3×10^{-12} for Na^+, 1.0×10^{-12} for SO_4^{2-}, and 1.9×10^{-12} for Cl^-.

For the weak ionic strength case, the membrane initialy contains the following species, with their respective concentrations: 80 mmol/l of OH^-, 100 mmol/l of Na^+, and 10 mmol/l of SO_4^{2-}. On the left side of the membrane, a concentration of 30 mmol/l of NaOH and 50 mmol/l of NaCl is maintained. On the right side, 30 mmol/l of NaOH are present.

For the high ionic strength case, the membrane initialy contains the following species, with their respective concentrations: 490 mmol/l of OH^-, 590 mmol/l of Na^+, and 50 mmol/l of SO_4^{2-}. On the left side of the membrane, a concentration of 300 mmol/l of NaOH and 500 mmol/l of NaCl is maintained. On the right side, 300 mmol/l of NaOH are present.

All simulations were made using a numerical solution of the extended Nernst-Planck/Poisson set of equations. More information on the numerical model can be found in references [157, 158]. The calculations were carried using 100 linear two-nodes elements. The simulations are performed over a period of 30 days and are reached after 30 steps of 86400 seconds.

The results show that for this case, the activity has little effect on the concentration profiles. It has however a stronger effect on the potential for the high ionic strength case.

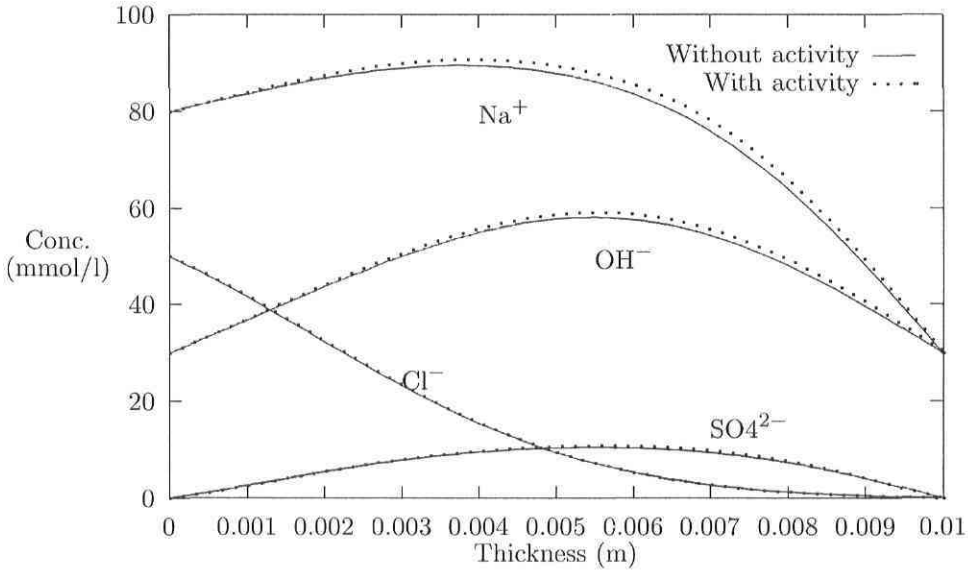

Figure 2.7: Concentrations across the membrane for the weak ionic strength case

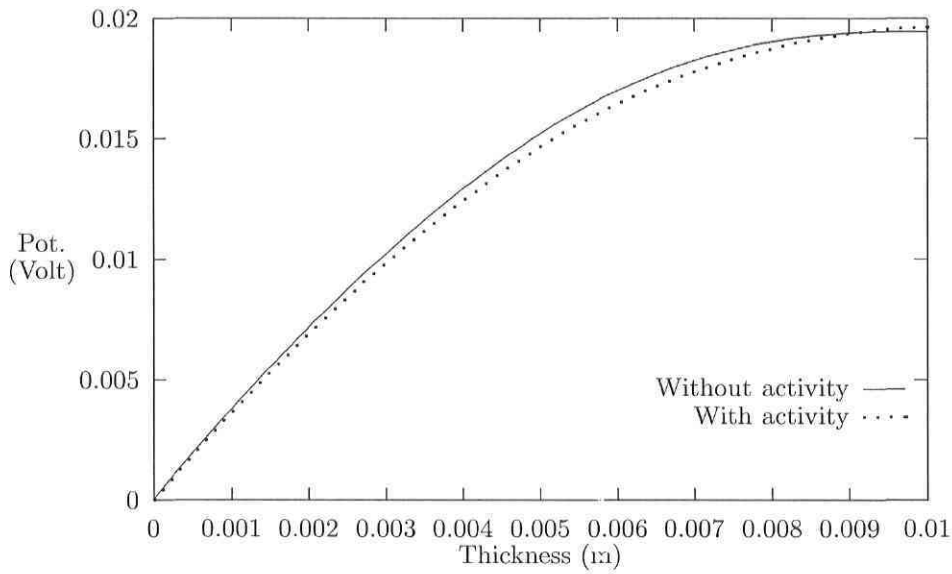

Figure 2.8: Potentials across the membrane for the weak ionic strength case

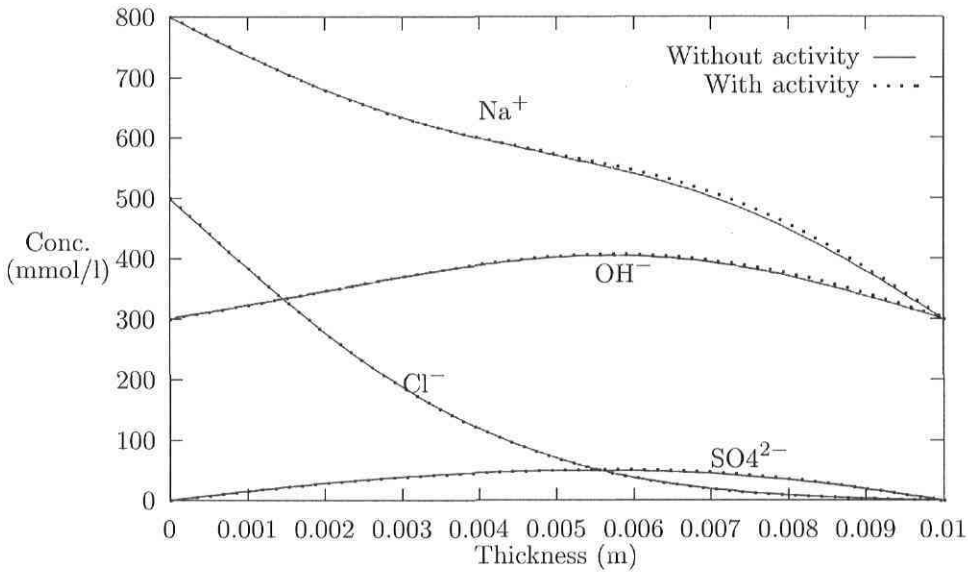

Figure 2.9: Concentrations across the membrane for the strong ionic strength case

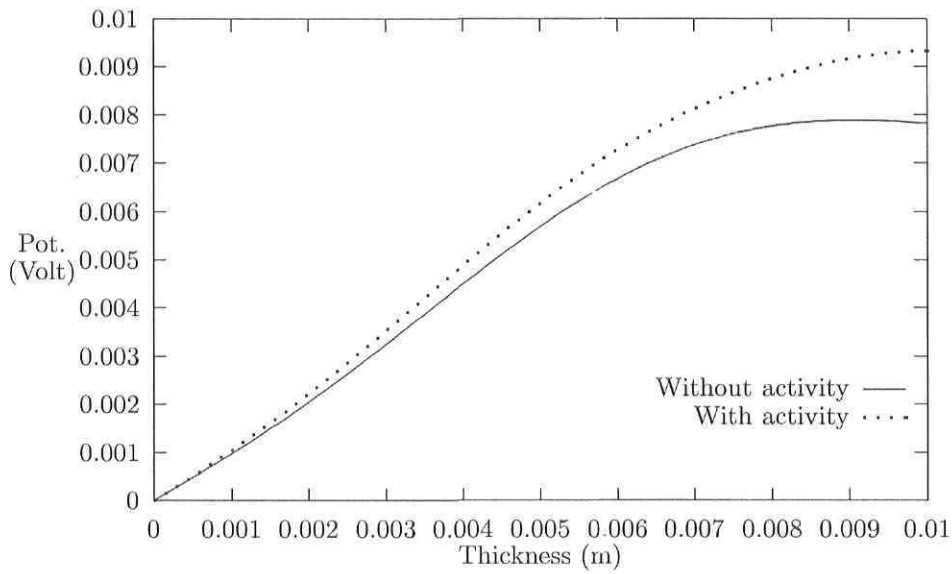

Figure 2.10: Potentials across the membrane for the strong ionic strength case

2.4.6 Conclusions

A new mathematical model for calculating the chemical activity coefficients of ions in electrolytic solutions is presented. The model was developed to account for the particular behavior of concentrated solutions for which short-range and long-range interactions between ions are important. The model is essentially a modified version of the Davies equation.

The main advantage of the new model lies in its simple mathematical formulation. Given its relative simplicity, the model can be easily implemented in a numerical code designed to model ionic transport phenomena in saturated porous materials.

2.5 Modeling the influence of chemical reactions on the mechanisms of ionic transport in porous materials : an overview

E. Samson[12], J. Marchand[12], J.J. Beaudoin[3]

[1]Centre de recherche interuniversitaire sur le béton,
Université Laval, Québec, Canada, G1K 7P4

[2]SIMCO Technologies inc.,
1400, boul. du Parc Technologique, Québec, Canada, G1P 4R7

[3]Materials Laboratory - Institute for Research in Construction,
National Research Council, Ottawa, Canada, K1A 0R6

Abstract

This paper attempts to critically review various approaches developed to model the effects of chemical reactions on the mechanisms of ionic transport in porous media. A comprehensive overview of the various types of chemical reactions that can occur in reactive porous solids is first presented. Methods to model each of these chemical reactions are then described and analyzed. The ability of each of the proposed algorithms to predict the behavior of hydrated cement systems is discussed. The implementation of these algorithms in an ionic transport numerical model is also discussed.

2.5.1 Introduction

Concrete is a porous material made of a rigid solid skeleton and a liquid (or aqueous) phase. The solid is a composite mixture of ill-crystallized hydrated calcium silicates and other more crystalline phases. The liquid phase is a highly charged ionic solution containing mainly OH^-, K^+, Na^+, SO_4^{2-} and Ca^{2+}ions. Once the initial stages of hydration are completed, the liquid phase can be considered to be in a metastable state of thermodynamic equilibrium with the various solid phases.

During the service-life of the concrete structure, the chemical composition of the material pore fluid can be modified by the penetration of external ions and/or the leaching of ions already present in the pore solution. These ionic species can be transported by simple ionic diffusion or by a coupled process of capillary suction and diffusion. The modification of the pore solution chemical composition readily perturbs the local thermodynamic equilibrium of the system. A series of dissolution/precipitation reactions can occur to restore the equilibrium state.

An example reaction is the dissolution of calcium hydroxide, $Ca(OH)_2$. The reaction is initiated when the hydrated cement paste pore solution, initially at a pH of about 13.5, is in contact with an external solution at a lower pH. Hydroxyl ions in the material pore solution will tend to be leached out of the system under the electrochemical potential gradient. In order to restore the local equilibrium, calcium hydroxide will dissolve, thus releasing OH^- and Ca^{2+} ions in solution. Numerous concrete structures are exposed to this simple form of chemical degradation.

Concrete structures, such as bridges, harbors and offshore platforms, exposed to chloride solutions are also likely to suffer from another form of degradation. As a result of the concentration gradient between the hydrated cement paste pore solution and the external solution, chloride ions will penetrate into the material pore structure. The presence of chloride readily disturbs the equilibrium conditions between the pore solution and the paste. As a result, and under certain conditions, new solid phases, eg. Friedel's salt, will precipitate to maintain equilibrium. Similar reactions can occur in hydrated cement systems exposed to sulfate and magnesium solutions. For instance, ettringite and gypsum are phases that can precipitate in hydrated cement systems exposed to sulfate solutions.

The proper modeling of these different chemical reactions is a problem of paramount importance for civil engineers and concrete technologists [37]. An adequate ionic and fluid transport model could predict the degradation of concrete structures with time. This would help engineers to properly design new structures and also allowing good planning of maintenance programs. This aspect is particularly important since contractors are increasingly required to guarantee the durability of their structures for periods often as long as 90 years.

This paper attempts to critically review various approaches developed to model chemical reactions in porous media. The ability of each of the proposed algorithms to predict the behavior of hydrated cement systems is discussed.

2.5.2 Types of chemical reactions

In a comprehensive review on the modeling of chemical reactions in porous media, Rubin [149] distinguishes two main categories: sufficiently fast and reversible, and insufficiently fast and/or irreversible. If the rate of reaction is large with respect to the ionic and fluid transport processes, then it belongs to the sufficiently fast category [149]. In this particular case, the assumption is made that the local chemical equilibrium is preserved throughout the porous system. Only this first kind of chemical reaction will be considered in the following paragraphs. As emphasized by Barbarulo and al. [14], in most practical cases involving the diffusion of ions in fluid saturated systems, the local chemical equilibrium assumption is usually valid.

All reactions falling under the sufficiently fast category are modeled through chemical equilibrium equations [149], which are algebraic, as opposed to the partial differential equations used in transport models. Since the equilibrium is, in most cases, expressed through chemical activity, algebraic relations giving the chemical activity coefficients must also be considered while modeling the chemical reactions. The resolution of a transport problem involving chemical reactions is thus called a mixed problem, because it involves algebraic and partial differential equations.

According to Rubin [149], the chemical reactions are then divided into two subcategories: homogeneous and heterogeneous. The homogeneous reactions are those involving a single phase. This sub-category includes all the complexation reactions, i.e.

the formation of products occurring in the aqueous phase. For example, the reaction:

$$Ca^{2+}{}_{(aq)} + OH^{-}{}_{(aq)} \rightleftharpoons CaOH^{+}{}_{(aq)} \tag{2.144}$$

is a homogeneous reaction since it only occurs in the aqueous phase.

As opposed to those falling in the previous category, the heterogeneous reactions involve at least two phases [149]. Rubin distinguishes two types of heterogeneous reactions: surface and classical ones [149]. Surface reactions are either adsorption, in which ions are attracted to the surface of the pore network under the influence of electrostatic forces [25], or ion exchange, in which two or more ionic species are exchanged between the surface of the solid and the aqueous phase [149]. The classical reactions are precipitation, dissolution, oxidation and reduction. The dissolution of calcium hydroxide, described in the introduction, belongs to this category since it involves the aqueous and the solid phase:

$$Ca^{2+}{}_{(aq)} + 2OH^{-}{}_{(aq)} \rightleftharpoons Ca(OH)_{2(s)} \tag{2.145}$$

2.5.3 Coupling chemical reactions to ionic transport in a saturated porous medium

In the following subsections, each of the previous sub-categories of chemical reactions will be treated in greater detail from the point of view of their implementation in an ionic transport model. In all the forthcoming examples, we will assume that the porous medium is kept in *isothermal* and *fluid saturated* conditions. For simplicity, we will assume that the ionic diffusion process can be described by Fick's law, which can be written in one dimension as:

$$\frac{\partial c_i}{\partial t} - D_i \frac{\partial^2 c_i}{\partial x^2} = 0 \tag{2.146}$$

where c_i is the concentration of the species i and D_i is the diffusion coefficient. This approximation is made to enable the reader to focus on the modeling of the chemical reactions. However, it is emphasized that Fick's law cannot accurately describe the ionic diffusion process in hydrated cement systems [179].

2.5.4 Treatment of homogeneous chemical reactions

The treatment of homogeneous chemical reactions is reviewed first. Consider the aqueous phase of a porous network in which the ions Ca^{2+}, OH^-, Na^+ and Cl^- undergo, for example, the following reactions:

$$Ca^{2+}{}_{(aq)} + OH^-{}_{(aq)} \rightleftharpoons CaOH^+{}_{(aq)} \tag{2.147}$$

$$Ca^{2+}{}_{(aq)} + Cl^-{}_{(aq)} \rightleftharpoons CaCl^+{}_{(aq)} \tag{2.148}$$

Let us define c_1 as the concentration of Ca^{2+}, c_2 as the concentration of OH^-, c_3 as the concentration of Cl^- and c_4 as the concentration of Na^+. Following that, the complexes are expressed as c_{12} for $CaOH^+$ and c_{13} as $CaCl^+$. The equilibrium relations for each of these chemical reactions are given by [149]:

$$K_1 = \frac{\gamma_1 c_1 \gamma_2 c_2}{\gamma_{12} c_{12}} \tag{2.149}$$

$$K_2 = \frac{\gamma_1 c_1 \gamma_3 c_3}{\gamma_{13} c_{13}} \tag{2.150}$$

where the γ_i's are the chemical activity coefficients. These coefficients can be calculated with various models, eg. Debye-Hückel or Davies, depending on the ionic strength of the pore solution [26]. For the specific case of cement-based materials, which contain a highly charged pore solution, the previous models are inadequate. The following expression, a modification of Davies' relationship, was found to yield good results [155]:

$$\ln \gamma_i = -\frac{A z_i^2 \sqrt{I}}{1 + a_i B \sqrt{I}} + \frac{(0.2 - 4.17 \times 10^{-5}\, I) A z_i^2 I}{\sqrt{1000}} \tag{2.151}$$

where I is the ionic strength of the solution:

$$I = 0.5 \sum_{i=1}^{N} z_i^2 c_i \tag{2.152}$$

z_i being the valence number of a given ionic species and N is the total number of ionic species in the aqueous solution. In equation (2.151), A and B are temperature dependent parameters, given by:

$$A = \frac{\sqrt{2}\, F^2 e_o}{8\pi (\epsilon RT)^{3/2}} \tag{2.153}$$

$$B = \sqrt{\frac{2F^2}{\epsilon RT}} \tag{2.154}$$

where F is the Faraday constant, e_o is the electrical charge of one electron, $\epsilon = \epsilon_r \epsilon_o$ is the permittivity of the medium, given by the dielectric constant times the permittivity of the vacuum, R is the ideal gas constant and T is the temperature. Finally, the parameter a_i in equation (2.151), often compared to an ionic radius, is specific to the ionic species. Its value (in meters) is 3×10^{-10} for OH^-, 3×10^{-10} for Na^+, 2×10^{-10} for Cl^- and 1×10^{-13} for Ca^{2+}[155].

Following this set of algebraic equations for the chemical equilibrium, mass conservation equations have to be considered for the transport of each ionic species. As previously stated, we will assume that the ionic diffusion process can be described by Fick's law (equation 2.146). Because of the complexation reactions, a reaction rate term r is added to the mass conservation equations, which yield, for each ionic species:

$$\frac{\partial c_1}{\partial t} - D_1 \frac{\partial^2 c_1}{\partial x^2} + r_{1\to 12} + r_{1\to 13} = 0 \tag{2.155}$$

$$\frac{\partial c_2}{\partial t} - D_2 \frac{\partial^2 c_2}{\partial x^2} + r_{2\to 12} = 0 \tag{2.156}$$

$$\frac{\partial c_3}{\partial t} - D_3 \frac{\partial^2 c_3}{\partial x^2} + r_{3\to 13} = 0 \tag{2.157}$$

$$\frac{\partial c_4}{\partial t} - D_4 \frac{\partial^2 c_4}{\partial x^2} = 0 \tag{2.158}$$

$$\frac{\partial c_{12}}{\partial t} - D_{12} \frac{\partial^2 c_{12}}{\partial x^2} + r_{12\to 1,2} = 0 \tag{2.159}$$

$$\frac{\partial c_{13}}{\partial t} - D_{13} \frac{\partial^2 c_{13}}{\partial x^2} + r_{13\to 1,3} = 0 \tag{2.160}$$

where for example $r_{1\to 12}$ accounts for the chemical reaction involving c_1 forming c_{12}.

The complete system of equations therefore consists of the two chemical equilibrium equations (2.149) and (2.150), five chemical activity relations corresponding to equation (2.151) (one for each species except for Na^+, which does not appear in the chemical equilibrium equations), and the six transport equations (2.155) to (2.160), a total of 13 equations. There are 17 unknowns, the six concentrations and five chemical activity coefficients (again, one for each species except Na^+) along with the different chemical reaction terms r_is.

To have a closed system, i.e. a system in which there is the same number of unknowns as there are equations, it is possible to reduce the number of equations by

noting the following relationships must hold true during the chemical reactions in order to respect mass conservation:

$$r_{1\to 12} = -r_{12\to 1,2} \tag{2.161}$$

$$r_{2\to 12} = -r_{12\to 1,2} \tag{2.162}$$

$$r_{1\to 13} = -r_{13\to 1,3} \tag{2.163}$$

$$r_{3\to 13} = -r_{13\to 1,3} \tag{2.164}$$

Adding the appropriate equations in order to eliminate the chemical reaction terms leads to:

$$\frac{\partial c_1}{\partial t} + \frac{\partial c_{12}}{\partial t} + \frac{\partial c_{13}}{\partial t} = D_1 \frac{\partial^2 c_1}{\partial x^2} + D_{12} \frac{\partial^2 c_{12}}{\partial x^2} + D_{13} \frac{\partial^2 c_{13}}{\partial x^2} \tag{2.165}$$

$$\frac{\partial c_2}{\partial t} + \frac{\partial c_{12}}{\partial t} = D_2 \frac{\partial^2 c_2}{\partial x^2} + D_{12} \frac{\partial^2 c_{12}}{\partial x^2} \tag{2.166}$$

$$\frac{\partial c_3}{\partial t} + \frac{\partial c_{13}}{\partial t} = D_3 \frac{\partial^2 c_3}{\partial x^2} + D_{13} \frac{\partial^2 c_{13}}{\partial x^2} \tag{2.167}$$

$$\frac{\partial c_4}{\partial t} = D_4 \frac{\partial^2 c_4}{\partial x^2} \tag{2.168}$$

These four transport equations, combined with the two chemical equilibrium relations and the five chemical activity relationships, form a set of 11 equations, matching the six concentrations and five chemical activity coefficients.

Two different techniques are used to solve this system of equations. In the first one, the algebraic and partial differential equations are solved altogether [92, 96, 127]. This technique is called the coupled method. The discretization of this system of equations with either the finite difference or the finite element technique will lead to very large systems of equations because of the large number of unknowns at each nodal point.

In the second technique, the partial differential equations and the algebraic ones are uncoupled [34, 96]. This is performed first by introducing a new set of variables [96, 149]:

$$u = c_1 + c_{12} + c_{13} \tag{2.169}$$

$$v = c_2 + c_{12} \tag{2.170}$$

$$w = c_3 + c_{13} \tag{2.171}$$

Since the operators $\partial(.)/\partial t$ and $\partial^2(.)/\partial x^2$ are linear, and assuming a constant diffusion coefficient D for all the species, it is possible to substitute equations (2.169,2.170,2.171)

in equations (2.165,2.166,2.167) to yield the following equations:

$$\frac{\partial u}{\partial t} = D\frac{\partial^2 u}{\partial x^2} \tag{2.172}$$

$$\frac{\partial v}{\partial t} = D\frac{\partial^2 v}{\partial x^2} \tag{2.173}$$

$$\frac{\partial w}{\partial t} = D\frac{\partial^2 w}{\partial x^2} \tag{2.174}$$

Combined with equation (2.168), this constitutes a set of independent equations, which can be solved separately [149]. Once u, v and w are known at a given time t and for any position x, a system of ten algebraic nonlinear equations, i.e. equations (2.149) and, (2.150), five equations (2.151) for chemical activity coefficients and Equations (2.169)-(2.171), is solved at given locations. These locations could be nodal points if a numerical method like finite differences or finite elements is used.

The strong argument in favor of this second technique is a reduction of the size of the system of equations to solve, a reduction which is more dramatic as the size of the problem considered is increased. However, it suffers from two important drawbacks. The operators controlling the transport of the ions have to be linear. It thus prevents the use of a more sophisticated model, like the extended Nernst-Planck equation [157], which takes into account the electrical coupling between each ion and the chemical activity effects. Furthermore, the assumption that all species must have the same diffusion coefficient may not always be valid.

2.5.5 Treatment of surface chemical reactions

The second class of chemical reactions reviewed concerns heterogeneous reactions involving surface phenomena. This means that ions are exchanged between the solution and the surface of the solid phase. Consider a solid phase $X_{(s)}$ on which a given number of sites are available for cations. Taking the same ions in aqueous phase as in the homogeneous example, OH^-, Ca^{2+}, Na^+ and Cl^-, this means that Ca^{2+} and Na^+ will compete for the available sites. The exchange between Na^+, Ca^{2+} and the solid phase can be written as [149]:

$$2Na^+_{(aq)} + CaX_{(s)} \rightleftharpoons Ca^{2+}_{(aq)} + 2NaX_{(s)} \tag{2.175}$$

where the subscript (s) stands for the solid phase. For that kind of chemical reaction, the equilibrium constant is given by [149, 192]:

$$K = \left(\frac{c_4^{(s)}}{c_4}\right)\left(\frac{c_1}{c_1^{(s)}}\right)^2 \tag{2.176}$$

The other algebraic equation required to describe the chemical reaction is given by the definition of the ion-exchange capacity $c_T^{(s)}$ [150, 192], which gives the total amount of sites available on the solid for exchanges with the aqueous phase:

$$c_T^{(s)} = \sum_{i=1}^{n} c_i^{(s)} \tag{2.177}$$

where n is the number of exchanging ions. The ion-exchange capacity is assumed to be a constant fixed value [150]. For the particular example corresponding to equation (2.176), the ion exchange capacity is given by:

$$c_T^{(s)} = c_1^{(s)} + c_4^{(s)} \tag{2.178}$$

To this set of algebraic equations, the transport equations must be added. Since ions 2 and 3 (OH^- and Cl^-) do not participate in the ion exchange described here, equations (2.156) and (2.157) can be solved independently to find concentrations c_2 and c_3. For Na^+ and Ca^{2+}, a term is added in the transport equation to account for the exchange between the aqueous and the solid phase [18]:

$$(1-\phi)\frac{\partial c_1^{(s)}}{\partial t} + \phi\frac{\partial c_1}{\partial t} = \phi D_1 \frac{\partial^2 c_1}{\partial x^2} \tag{2.179}$$

$$(1-\phi)\frac{\partial c_4^{(s)}}{\partial t} + \phi\frac{\partial c_4}{\partial t} = \phi D_4 \frac{\partial^2 c_4}{\partial x^2} \tag{2.180}$$

where ϕ is the porosity of the material, assumed constant.

The combination of the two transport equations (2.179) and (2.180) with the algebraic equation (2.176) and (2.178) give a system of four equations and four unknowns. But it is possible to reduce that number to two equations and two unknowns [150, 192] by first combining the two algebraic equations, which will give a relation of the form:

$$c_i^{(s)} = f(c_1, c_2, \ldots, c_n) \quad \text{for} \quad i = 1, 2, \ldots, n \tag{2.181}$$

This expression is called an exchange (or interaction) isotherm. It can be substituted in the proper transport equation by applying the chain rule to the time derivative of

the solid concentration:

$$\frac{\partial c_i^{(s)}}{\partial t} = \frac{\partial c_i^{(s)}}{\partial c_1}\frac{\partial c_1}{\partial t} + \frac{\partial c_i^{(s)}}{\partial c_2}\frac{\partial c_2}{\partial t} + \cdots + \frac{\partial c_i^{(s)}}{\partial c_n}\frac{\partial c_n}{\partial t} \quad \text{for} \quad i = 1, 2, \ldots, n \tag{2.182}$$

This technique, applied to the example described by equations (2.176) and (2.178) leads to:

$$c_1^{(s)} = -\frac{c_1^2}{2Kc_4} \pm \frac{1}{2}\sqrt{\frac{c_1^4}{K^2c_4^2} + \frac{4c_T^{(s)}c_1^2}{Kc_4}} \tag{2.183}$$

Depending on the values of the parameters in this relationship, only one root will have a physical meaning [192]. Equation (2.183) can be substituted into equation (2.179) through the chain rule. By finding a similar expression for $c_4^{(s)}$, the initial system of four equations is reduced to two equations and two unknowns.

Before concluding this discussion on heterogeneous surface reactions, it is worth mentioning a special case. In some specific cases, the sum of the concentrations of the various ions in the aqueous phase involved in the ion-exchange process is a constant. For the case of two monovalent ions involved in such a situation, the following expression can be written:

$$c_T = c_1 + c_2 \tag{2.184}$$

where c_T has a known constant value. For this case, the equilibrium constant and the ion exchange capacity would be:

$$K = \frac{c_1^{(s)}}{c_1}\frac{c_2}{c_2^{(s)}} \tag{2.185}$$

$$c_T^{(s)} = c_1^{(s)} + c_2^{(s)} \tag{2.186}$$

The combination of these three expressions gives the following relationship:

$$c_1^{(s)} = \frac{Ac_1}{1 + Bc_1} \quad \text{with} \quad A = \frac{Kc_T^{(s)}}{c_T} \quad \text{and} \quad B = \frac{K-1}{c_T} \tag{2.187}$$

One can recognize in this expression the familiar single-component Langmuir isotherm [18, 192]. It is sometimes used to model the chemical reactions involving chloride ions in cement-based materials [122].

It should be emphasized that the previous approach is based on the assumption that the exchange capacity of the surface remains constant. Although it might be verified in certain instances, this hypothesis is unrealistic in most practical cases that involve the

transport of OH^- ions through the material pore structure. The reduction in the pH of the pore solution is known to have a strong influence on the composition and structure of the C-S-H gel [63]. Evidence of interactions between ions and C-S-H gel reported in the literature suggest the ion-solid sorption binding coefficient depends on both the Ca:Si ratio within the C-S-H and the composition of the pore solution [30, 88, 196].

Numerous more sophisticated approaches (such surface protonation models) have been developed to describe surface exchange mechanisms [24, 175]. The main problem with these models is that the interaction mechanisms are described at the very local scale. These equations are usually difficult to homogenize over the scale of the porous solid.

2.5.6 Treatment of dissolution/precipitation reactions

The last category concerns the heterogeneous chemical reactions involving precipitation, dissolution, oxidation or reduction processes. In this paper, only dissolution and precipitation are considered. Such a reaction was already described by equation (2.145). The algebraic chemical equilibrium equation used to model these reactions is similar to those of the homogeneous or heterogeneous surface reactions, equations (2.149), (2.150) and (2.176). For the chemical reaction (2.145), the relationship is [96, 97]:

$$K = \gamma_1 c_1 \gamma_2^2 c_2^2 \tag{2.188}$$

But the similarity with the other chemical equilibrium relationships hides huge differences. For equations (2.149), (2.150) and (2.176), the relationship between the various components of the chemical reactions always applies. Furthermore, all components involved in the chemical reaction are considered in the equilibrium relationship. For the heterogeneous dissolution/precipitation process, the solid phase concentration does not appear in equation (2.188). Furthermore, when there is no solid, the product of the activity (equation 2.188) can be lower than K. So it is more precise to express it as an inequality [97]:

$$\gamma_1 c_1 \gamma_2^2 c_2^2 \quad \begin{cases} = K & \text{if the precipitate is present} \\ < K & \text{if there is no precipitate} \end{cases} \tag{2.189}$$

This inequality allows the precipitate concentration to be discontinuous in the material [96]. Suppose the usual ions (Ca^{2+}, OH^-, Na^+ and Cl^-) are initially in equilibrium

with a material containing the solid $Ca(OH)_2$ and are allowed to leach out of the porous network. Initially the concentration of Ca^{2+} and OH^- obeys the relationship (2.188) since the solid phase is present. At the surface of the material, the product $\gamma_1 c_1 \gamma_2^2 c_2^2$ will eventually be lower than its initial value. The solid will thus dissolve, putting back Ca^{2+} and OH^- ions in solution to reach equilibrium again, until there is no more solid at this location. Subsequently, the same process will occur right next to the previous location. The solid concentration will thus behave like a moving boundary [149], in this case moving in the direction opposite to the leaching of the ions.

The mass conservation equations will be affected by the discontinuous behavior of this type of chemical reaction. Ions Cl^- and Na^+, associated with concentrations c_3 and c_4, are not affected by the reaction. Hence their transport can be modeled with equations (2.157) and (2.158) at any location in the material. For ions Ca^{2+} and OH^-, the situation is different. In the zone where the precipitate concentration is zero, the transport of these species obeys the equations (2.155) and (2.156). Elsewhere, precipitate is present and Ca^{2+} follows the equation (2.179). For OH^-, the equation is similar:

$$(1-\phi)\frac{\partial c_2^{(s)}}{\partial t} + \phi\frac{\partial c_2}{\partial t} = \phi D_2 \frac{\partial^2 c_2}{\partial x^2} \tag{2.190}$$

Three techniques have been developed to solve this type of problem. The first, fully described in references [104, 105], separates the porous material into k zones of constant mineralogical properties and solves the transport equations in each zone with the proper conservation equations at the moving boundary interfaces. The mathematics of this technique is described in the following paragraphs.

First, let us define the function ζ as:

$$\zeta_k(x,t) = \begin{cases} 1 & \text{if } x \text{ is in zone } k \\ 0 & \text{elsewhere} \end{cases} \tag{2.191}$$

For unidimensional cases, k also designates one of the interfaces adjacent to a given zone. Next, the variables appearing in the transport equations, namely the concentrations in both the aqueous and the solid phase, are expressed as functions of ζ:

$$c_i = \sum_{k=1}^{N_\Xi} c_i^k \zeta_k \tag{2.192}$$

where N_Ξ is the total number of zones. The derivative of ζ introduces jumps or discontinuities in the transport equations. For the concentrations, which have to be continuous at the interfaces, these jumps are set to zero, which yields for example:

$$\frac{\partial c_i}{\partial t} = \sum_{k=1}^{N_\Xi} \frac{\partial c_i^k}{\partial t} \zeta_k \tag{2.193}$$

But certain quantities, like fluxes, are allowed to show some discontinuity at the interfaces. For example, the space derivative of a flux is given by:

$$\frac{\partial j_i}{\partial x} = \sum_{k=1}^{N_\Xi} \frac{\partial j_i^k}{\partial x} \zeta_k + \sum_{k=1}^{N_\Xi - 1} [j_i]_k \delta(x - x_k) \tag{2.194}$$

where $[\ldots]_k$ represents the jump of the function in the square brackets across a given interface, x_k is the position of the interface and $\delta(x - x_k)$ is the Dirac delta function, defined as:

$$\delta(x - x_k) = \begin{cases} 1 & \text{if} \quad x = x_k \\ 0 & \text{if} \quad x \neq x_k \end{cases} \tag{2.195}$$

The transformations applied to the transport equations in order to consider the dissolution or the precipitation reactions at various interfaces introduces a new variable: the position x_k of these interfaces.

To take into account this new variable, another equation has to be introduced in the system. It is obtained by performing mass conservation across a given interface. The resulting relationship is called the generalized Rankine-Hugoniot equation [105]:

$$\phi [j_i]_k = [c_{is}]_k \frac{dx_k}{dt} \tag{2.196}$$

presented here for a case where the porosity ϕ is considered constant.

The complete system of equations is thus made up from the proper transport equations within each zone of constant mineralogical properties, to which are added the Rankine-Hugoniot equations at the various interfaces.

Although mathematically sound, this technique creates complications from a numerical point of view. Not only does it add a new variable and the corresponding equation to the transport model, but the division of the material into zones of constant chemical properties requires the storage of a large amount of information since the

Rankine-Hugoniot equation must be solved at each interface. The transport equations are also different depending on the zone in which they are applied. This requires a very complex algorithm.

The second technique used to solve dissolution/precipitation problems combines the algebraic equations for chemical equilibrium with the partial differential transport equations to form a global system of equations [97], in a manner similar to that for the first technique involving homogeneous reactions. In such a system, there are two equations for transport (equations 2.179 and 2.190), the chemical equilibrium equation (2.188) and two equations similar to (2.151) for the chemical activity coefficients, a total of five equations. Correspondingly, there are six unknowns: two concentrations in aqueous phase c_1 and c_2, two concentrations in solid phase, $c_1^{(s)}$ and $c_2^{(s)}$, and the two chemical activity coefficients γ_1 and γ_2. One unknown is eliminated by knowing that in the solid $Ca(OH)_2$, $c_2^{(s)} = 2c_1^{(s)}$, closing the system. Finally, the chemical equilibrium relationship is presumed not to be in effect initially, and it is checked at each node every iteration and is either "turned-on" or "turned-off" appropriately [97].

The last technique consists in uncoupling the transport and the chemical reactions [73]. In the first step of calculation, the concentration profiles of the various species are calculated with a transport model, such as the Fick or the extended Nernst-Planck models. The calculation is performed without taking into account chemical reactions, i.e. the term $(1-\phi)\frac{\partial c^{(s)}}{\partial t}$ is not considered. After that step, the concentrations at a given node are checked to see if they violate the chemical equlibrium relationships of the various chemical reactions considered. If this is the case, they are brought back to equilibrium with a separate chemical code. If dissolution or precipitation occurs, the solid phases are modified appropriately. This procedure is repeated for every nodal point. After that operation, the modified concentration profiles serve as a starting point for the calculation of the next time step.

This algorithm is interesting because it allows for the use of very complex chemical equilibrium codes. The main problem of this model is that in order for the dissolution or the precipitation of the solid phases to show moving fronts, the time steps used in the calculation must be short. If they are too large, the reactions will occur on a wide area, and not on thin fronts.

2.5.7 Discussion and concluding remarks

This completes the review on the modeling of the three main types of chemical reactions that can occur in a porous material under the local equilibrium assumption. Even though they were presented separately, they occur simultaneously in most real life situations. Most of the models found in the literature consider complexation and adsorption, but overlook the dissolution/precipitation reactions [34, 92, 98, 127, 166].

This is easily understandable since the latter reactions are much more complicated to model, because of the discontinuous aspect of the chemical equilibrium equation. Nevertheless, some models consider the three types of reactions, as those in references [65, 73, 97]. But in these three cases, only one solid phase is taken into account. Finally, it is worth mentioning that all the models previously discussed were developed by geochemists and hydrogeologists.

Very little research has been specifically focused on the treatment of chemical reactions in hydrated cement systems. This is most unfortunate since these materials are quite different from other porous solids. For instance, cement-based materials are characterized by the relatively high ionic strength of their pore solution [141]. This has an important influence on the transport, since the contact with the external environment will often induce very strong concentration gradients. Ions like OH^- and Ca^{2+} which have very different diffusion coefficients, 5.273×10^{-9} m^2/s and 0.792×10^{-9} m^2/s in free water respectively, are very likely to experience an internal electrical potential that will arise to maintain electroneutrality by slowing the fast ions and accelerating the slow ones [85]. Hence, the simple Fick's law is no longer appropriate and more complex models, like the Nernst-Planck or extended Nernst-Planck equations [156, 157] should be used.

Cement-based materials are also characterized by the high reactivity of the hydrated cement paste. Aside from the dissolution of portlandite, which has already been described, other chemical reactions will occur, for example the decalcifiation of the C-S-H, the formation of ettringite under external sulfate attack or the formation of Friedel's salt upon chloride penetration in the porous network. Over the past decades, numerous reports have clearly emphasized the significant influence of these dissolution/precipitation reactions on the durability of hydrated cement systems. Although

complexation and ion adsorption phenomena can occur in a cement paste, they are likely to have a lesser influence on the ionic transport and on the degree of degradation of cement-based materials.

Over the past decade, researchers in the field of ionic transport have relied on simple models to treat chemical reactions in cement systems. Chemical reactions are usually modeled using chemical interaction isotherms. This technique is essentially an adaptation of the mathematical approach used to treat heterogeneous surface reactions (see equation 2.181).

Recently, the isotherm technique has been mainly used to model the chemical reactions on-going during the penetration of chloride in concrete. The experimental procedure, described in reference [183], shows that all types of reaction, i.e. dissolution/precipitation, complexation, and adsorption are described by one isotherm. The latter is then used in a single-ion transport model to yield chloride profiles in the material. For instance, Masi & al. [122] modeled the chloride interaction with a Langmuir isotherm (see equation 2.187), whereas Saetta & al. [152] modeled the same reaction with the linear isotherm $c^{(s)} = Ac$. The main interest in this method lies in its simplicity. However, it is also its main drawback, since it is nearly impossible to correctly model complicated reactions involving multiple ionic species while considering only one ion. This is supported by the fact that, in the two papers mentioned previously, the same chemical reaction is modeled differently.

One attempt has been made by Adenot [3] to model dissolution/precipitation reactions in cement-based materials using a technique developed by Lichtner [104, 105], where the material is divided into zones of constant mineralogical properties. While it is an important improvement over the isotherm method, the heavy mathematics of this approach usually requires a simplification of the transport model. In his work, Adenot used Fick's law as the transport model, with all ions having the same diffusion coefficient. Furthermore, the equations are solved over a 1D semi-infinite domain.

Chapitre 3

Modèle numérique

3.1 Introduction

La première phase des travaux concernant la résolution numérique des équations de transport a été consacrée au couplage électrique entre les ions, modélisé par l'équation de Nernst-Planck. Une revue bibliographique a montré que très peu de méthodes permettent de résoudre cette équation pour un nombre quelconque d'ions et pour des problèmes en une, deux ou trois dimensions. Le premier article présenté dans ce chapitre décrit les travaux effectués dans le but de résoudre cette équation de la manière la plus générale possible.

Par la suite, le niveau de complexité de la loi de comportement a été augmenté en ajoutant l'activité chimique au couplage électrique, ce qui donne l'équation de Nernst-Planck étendue. Le second article montre de quel façon cette équation a été résolue.

Le troisième article donne les détails numériques du modèle présenté dans ce mémoire de thèse. Le modèle incorpore les développements présentés dans les deux articles précédents, auxquels viennent s'ajouter l'advection et les réactions chimiques. Le modèle est validé par une comparaison de la solution numérique à des résultats expérimentaux. Ces derniers proviennent d'essais de lixiviation et de pénétration de sulfates sur des pâtes de ciment hydraté. Des simulations à long terme sont ensuite effectuées afin d'analyser la sensibilité du modèle en fonction de certains paramètres tels que la longueur du pas de temps et la densité du maillage.

3.2 Modeling ion diffusion mechanisms in porous media

E. Samson[12], J. Marchand[12], J.L. Robert[1]

[1]Centre de recherche interuniversitaire sur le béton,
Université Laval, Québec, Canada, G1K 7P4

[2]SIMCO Technologies inc.,
1400, boul. du Parc Technologique, Québec, Canada, G1P 4R7

Abstract

The main features of a numerical model aiming at predicting the drift of ions in electrolytic solutions are presented. The mechanisms of ionic diffusion are described by solving the Nernst-Planck system of equations. The electrical coupling between the various ionic fluxes is accounted for by the Poisson equation. Two algorithms using the finite element method for spatial discretization are compared for simple test cases. One is based on the Picard iteration method while the other is based on the Newton-Raphson scheme. Test results clearly indicate that the range of application is broader for the algorithm based on the Newton-Raphson method. Selected examples of the application of the algorithm to more complex 1-D and 2-D cases are given.

3.2.1 Introduction

In many engineering problems, the behavior of porous materials is directly affected by the transport of ions under a concentration gradient. For instance, it has been shown that the swelling of clays is predominantly controlled by the penetration of ions by diffusion in their interlayer spaces [56]. Given their influence on various phenomena such as the filtration by ion exchange membranes and the transport of pollutants in soils, the mechanisms of ionic diffusion in porous media has also received a great deal of attention from chemical and geological engineers [85, 216]. The process of ionic diffusion remains of primary importance in many civil engineering problems since the long-term durability of many building materials, such as concrete, is directly affected by the transport of chemical species[115].

Over the years, it has been established that the mechanisms of ionic diffusion can be adequately modeled by the Nernst-Planck/Poisson set of equations [85, 115]. These equations take into account the electrical coupling between the different ions present in an ideal solution (i.e. no chemical activity effects are considered). According to this model, the drift of an ionic species strongly influences that of all other ions dissolved in the electrolytic solution.

Although the electrical coupling between the various ionic fluxes is well known to electrochemists and engineers, most existing models aiming at describing the mechanisms of ionic diffusion tend to neglect this phenomenon [18, 216]. Furthermore, a comprehensive bibliographical review has recently shown that the proposed analytical or numerical ionic transport models are unsatisfactory, all of them being limited to unidimensional and steady-state cases. A summary of this literature survey is given in the following subsection.

In order to extent the application of the Nernst-Planck/Poisson set of equations, two algorithms were tested. The first one is based on the Picard iteration method. The second algorithm uses a Newton-Raphson scheme. Both rely on the finite element method for spatial discretization.

After this comparison, selected examples of calculations are presented to illustrate the application of the second algorithm to the treatment of steady-state and transient problems involving an important number of multivalent ionic species. An example of

application of the algorithm to the resolution of 2D cases (axisymmetrical geometries) is also given.

3.2.2 Mathematical model

The Nernst-Planck model, which describes the flux of an ionic species i in solution, is given by:

$$\boldsymbol{j_i} = -[D_i]\left(\mathrm{grad}(c_i) + \frac{z_i F}{RT} c_i \mathrm{grad}(\psi)\right) \tag{3.1}$$

where $\boldsymbol{j_i}$ stands for the flux of the species i, $[D_i]$ is the diffusion coefficient tensor of the species, c_i is the ionic concentration of the species, z_i is the valence number of the species, F is the Faraday constant, R is the perfect gas constant, T is the temperature, and ψ is the electrical potential that is locally induced in the electrolytic solution by the movement of all ionic species.

It should be emphasized that the presence of this electrical potential is probably the most important feature that distinguishes ionic diffusion from molecular diffusion. In an ionic solution, the local electroneutrality shall be preserved at any point. The conservation of electroneutrality requires that the transport of all diffusing species should be coupled. During the diffusion process, all ions are not drifting at the same speed. Some ions tend to diffuse at a higher rate. However, any excess charge transferred by the faster ions builds up a local electric field (ψ - also called the diffusion potential) which slows down the faster ions, and reciprocally accelerates the slower ionic particles. The diffusion potential has to be accounted for even in cases where an external electrical field is applied to the system. In that case, the diffusion potential is superimposed to the external field.

It should also be underlined that equation (3.1) does not consider any chemical activity effects or the transport of ions by convection of the liquid phase in the pore system. The influence of activity phenomena on the mathematical treatment of the diffusion problem is discussed elsewhere [158]. A detailed discussion on the limits of equation (3.1) is given by Helfferich [85].

For each of the ionic species present in solution, the mass conservation law is given

by:

$$\frac{\partial c_i}{\partial t} + \mathrm{div}(\boldsymbol{j_i}) = 0 \tag{3.2}$$

This equation does not account for any chemical or physical interactions that can develop between the solid and the various ionic species in solution. A comprehensive discussion of the influence of chemical reactions and physical interaction phenomena on the mathematical treatment of ionic diffusion problems is given by [96, 143].

By replacing equation (3.1) in equation (3.2), one finds the complete Nernst-Planck equation:

$$\frac{\partial c_i}{\partial t} - \mathrm{div}\left([D_i]\left(\mathrm{grad}(c_i) + \frac{z_i F}{RT} c_i \mathrm{grad}(\psi)\right)\right) = 0 \tag{3.3}$$

In order to complete this system of equations, one has to define one last relationship that will couple the transport of all ionic species to one another. Over the past decades, numerous authors have chosen to simplify the problem by assuming that the electroneutrality of the solution is preserved at any points:

$$\sum_{i=1}^{N} z_i c_i + w = 0 \tag{3.4}$$

where N is the number of species and w is a fixed charge density over the domain. For most porous materials, the fixed charge density is not a relevant parameter. It is, however, often used in the description of biological systems like thin membranes.

In many cases, it is also assumed that the global flow of all ions across the membrane yields a nil current:

$$\sum_{i=1}^{N} z_i \ \boldsymbol{j_i} = 0 \tag{3.5}$$

However, as will be discussed in the following subsection, these assumptions are not always valid. A more rigorous way to treat the problem [85] is to define the variation of the electric potential according to the spatial distribution of the electric charges. This relationship is given by the Poisson equation:

$$\nabla^2 \psi + \frac{\rho}{\epsilon} = 0 \tag{3.6}$$

where ρ is the electrical charge density and ϵ is the dielectric constant of the surrounding medium. The electrical charge density is a function of the concentration of the various ions in solution and can be calculated using the following equation:

$$\rho = F\left(\sum z_i c_i + w\right) \tag{3.7}$$

3.2.3 Numerical models for solving the Nernst-Planck/ Poisson system of equations

3.2.3.1 Bibliographical review

Over the past decades, numerous authors have tried to develop solutions for the Nernst-Planck equation. The first solution was obtained in 1890 by Planck himself [138]. He studied the case of steady-state unidimensional ionic diffusion of two monovalent species (+1 and -1) through a membrane. In the problem considered by Planck, fixed concentration and potential were imposed on both sides of the domain. The solution was obtained using the electroneutrality and nil current assumptions. The geometry and boundary conditions of this problem, although simple and very idealized, still remain about the only ones for which an analytical solution is possible.

Later on, Schlögl [165], Helfferich [85] and Teorell [186] developed other solutions for the treatment of unidimensional steady-state problem. Schlögl [165] derived an analytical solution using the same boundary conditions as Planck. Schlögl's solution was developed in such a way that it could account for any number of ions, whatever their valence number. Once again, the electroneutrality and nil current assumptions were at the basis of the development of his solution.

The application of all previous analytical solutions was limited to steady-state cases. Always using the electroneutrality and nil current assumptions Conti and Eisenman [40] proposed a different solution that could be applied to the treatment of unsteady-state problems. They developed an expression for the variation of the electrical potential through a membrane but could not obtain neither the concentration nor the electrical potential profiles. Furthermore, the validity of their solution was solely restricted to electrolytic solutions made of monovalent ions.

It should also be emphasized that all the previous analytical solutions were developed on the basis of the electroneutrality and nil current assumptions. In 1943, Goldman [70] presented a solution for the steady-state case assuming a constant electric field across the membrane(i.e. a linear variation of the electrical potential across the system). This simplification of the problem allowed the author to integrate directly the Nernst-Planck equation.

The considerable difficulty of developing analytical solutions for this system of equations has led researchers to use numerical methods. In 1965, Cohen and Cooley [39] presented an algorithm that allows solving the Nernst-Planck equation for transient cases. Their solution was obtained using a predictor-corrector scheme. But the predictor step uses Planck's analytical solution, thus limiting the application of the algorithm to very simple cases.

More recently, Hwang and Helfferich [89] developed an algorithm that can be used to solve the Nernst-Planck equation for any number of ions, for any valence number, and for transient problems, with a finite-difference discretization. The discretization is not directly performed on the equation (3.3). The system of equations first has to be transformed according to the electroneutrality and nil current hypotheses. This transformation introduces two new terms that are used as iteration coefficients in the algorithm. However, after being transformed, the equations become very complex, which makes the conversion in two or three dimensions extremely difficult. Moreover, the transformation of the equations complicates the treatment of the boundary conditions. Pátzay [134] modified the approach by using three iteration coefficients instead of two. In this case, no modification in the treatment of the boundary conditions is required.

Harden and Viovy [79], who worked on membranes subjected to a current of variable intensity, have directly discretized the conservation equation (3.3) using the finite-difference method. An explicit Euler scheme is used for time discretization. For a case with N ionic species, the concentration profiles of $N-1$ ions are calculated using the concentration and potential calculated at the preceding time step. For the remaining species, the concentration is calculated using the electroneutrality condition. The new electric field is determined knowing that the current introduced in the membrane must be equal to the internal current. The advantage of this method, compared to all those previously described, is that it can be easily transposed in two or three dimensions. This solution, however, still relies on the electroneutrality assumption.

All the previous numerical models are based on the assumption that the coupling of the Nernst-Planck equation with either the electroneutrality condition or the constant field relationship yields a reliable description of the ionic diffusion mechanisms. Even if these hypotheses may constitute a good choice in some practical cases, Helfferich [85]

mentions that the Poisson equation should be used in a more rigorous approach of the problem. MacGillivray and Hare [110, 111] have demonstrated that the electroneutrality and constant field hypotheses are, in fact, nothing but particular applications of the Poisson equation. The electroneutrality assumption is applicable only when the concentrations are high while the constant field hypothesis is rather valid for low concentrations.

Some researchers have tried to couple the Nernst-Planck equation to the Poisson equation. For instance, James et al. [91] coupled both equations to the Stokes equation to model the flow of a liquid containing charged particles in a cylinder. Their analysis was limited to steady-state cases. The conservation equations were discretized using the finite element method and a Galerkin residual weighting. The algorithm consists in solving the equations one after the other starting from an initial concentration profile (Picard iterations), the values obtained being used as starting points for the following iterations, until convergence is reached.

Kato [95] has proposed a numerical method to solve the Nernst-Planck/Poisson system of equations for unidimensional steady-state cases. Knowing that, once the steady state is reached, the fluxes are constant, a first analytical integration of the Nernst-Planck equation can be performed. The solution obtained has to be discretized afterwards by the finite-difference method. The numerical scheme used is similar to that of James et al. [91], the main difference being that the starting point is a potential profile, which is subsequently used to calculate the concentrations.

As can be seen, the development of numerical solutions clearly appears to be the most promising approach for the treatment of the Nernst-Planck/Poisson system of equations. It should however be emphasized that transient problems with any number of species for 1D or 2D cases with a finite element discretization have never been investigated. As previously discussed, all attempts to develop numerical solutions for this set of equations were limited to simpler cases. The object of this paper is to compare the ability of two numerical algorithms to treat complex ionic diffusion problems using the Nernst-Planck/Poisson equations.

3.2.3.2 First algorithm: uncoupled equations

The first algorithm proposed is based on the Picard iteration technique, also known as the successive substitution technique [142]. It is a first order method, thus having a low rate of convergence. The algorithm is similar to the numerical resolution proposed by James et al. [91] and Kato [95], in which the equations are solved one after another.

The equations are discretized separately following the standard finite element method. The results are thus presented without much detail. The weighted residual form of the Nernst-Planck equation (3.3) over the domain Ω is given by:

$$W = \int_{\Omega} \delta \left[\frac{\partial c_i}{\partial t} - \mathrm{div}\left([D_i] \left(\mathrm{grad}(c_i) + \frac{z_i F}{RT} c_i \mathrm{grad}(\psi) \right) \right) \right] \, d\Omega = 0 \tag{3.8}$$

where δ is the weighting function. From that point on, an axisymmetrical case with an orthotropic material is considered. Performing an integration by parts on W yields the following weak form:

$$W = \int_{\Omega} \delta \frac{\partial c_i}{\partial t} r \, dr \, dz + \int_{\Omega} \langle \delta_{,r} \; \delta_{,z} \rangle \left[[D_i] \begin{Bmatrix} c_{i,r} \\ c_{i,z} \end{Bmatrix} + \frac{z_i F}{RT} c_i \begin{Bmatrix} \psi_{,r} \\ \psi_{,z} \end{Bmatrix} \right] r \, dr \, dz \tag{3.9}$$

The boundary terms are omitted, since all the simulations will be performed considering Dirichlet conditions. Equation (3.9) is discretized according to the Galerkin method. The unknown c_i is interpolated at the nodes, as is δ, according to:

$$c_i = \langle N \rangle \{c_{in}\} \tag{3.10}$$

$$\delta = \langle N \rangle \{\delta_n\} \tag{3.11}$$

where $\langle N \rangle$ are the shape functions and the subscript n indicates node values. The elementary matrices are written as:

$$[K_i^e] = \int_{\Omega^e} [B]^T [D_i][B] + [B]^T [E_i][NN] \, r \, dr \, dz \tag{3.12}$$

$$[M_i^e] = \int_{\Omega^e} \{N\} \langle N \rangle \, r \, dr \, dz \tag{3.13}$$

where $[E_i]$ is the matrix coupling the concentration of each species to the electrical potential. It is written as:

$$[E_i] = \begin{bmatrix} \frac{D_{ri} z_i F}{RT} \frac{\partial \psi}{\partial r} & 0 \\ 0 & \frac{D_{zi} z_i F}{RT} \frac{\partial \psi}{\partial z} \end{bmatrix} \tag{3.14}$$

The matrices $[B]$ and $[NN]$ are defined as:

$$[B] = \begin{bmatrix} \frac{\partial}{\partial r}\langle N\rangle \\ \frac{\partial}{\partial z}\langle N\rangle \end{bmatrix} \tag{3.15}$$

$$[NN] = \begin{bmatrix} \langle N\rangle \\ \langle N\rangle \end{bmatrix} \tag{3.16}$$

The various integrals are calculated using a Gaussian quadrature method. The terms $\frac{\partial\psi}{\partial r}$ and $\frac{\partial\psi}{\partial z}$ in the matrix $[E_i]$ are evaluated at the integration points.

The Poisson equation is discretized using the same technique. The elementary matrices are:

$$[K^e] = \int_{\Omega^e} [B]^T[B]\, r\, dr\, dz \tag{3.17}$$

$$\{F^e\} = \int_{\Omega^e} \{N\}\frac{\sum z_i c_i}{\epsilon}\, r\, dr\, dz \tag{3.18}$$

$$\{F_s^e\} = \int_{\Omega^e} \{N\}\frac{w}{\epsilon}\, r\, dr\, dz \tag{3.19}$$

where $\{F_s^e\}$ is the solicitation vector coming from the fixed charge density w. The concentrations in equation (3.18) are calculated at the integration points.

The resolution steps for a steady-state problem are presented. For a transient problem, a standard θ method [142] could be used.

1. An initial concentration is assumed for each ionic species.
2. The Poisson equation is solved using the concentration of the previous iteration level.
3. A loop is performed on all the ionic species:
   (a) The gradient potential is calculated on the integration points from the numerical solution of the Poisson equation. The results are used to build the matrix $[E_i]$.
   (b) The solution of the Nernst-Planck equation is obtained for the species i using the elementary matrices (3.12) and (3.13).

4. The $L2$ norm of the vector $\Delta u = \langle c_1\ c_2 \ldots \psi \rangle^k - \langle c_1\ c_2 \ldots \psi \rangle^{k-1}$ is calculated where k stands for the iteration level.

5. If the norm is higher than a tolerance threshold ϵ, go back to step 2 by using the concentration just calculated. The loops are performed until convergence is reached.

The main advantage of this algorithm is that the same calculation code can be used, whatever the number of ionic species. Only the number of loops (step 3) is different.

3.2.3.3 Second algorithm: coupled equations

In the second algorithm, the Nernst-Planck and Poisson equations are coupled and solved simultaneously. A classical Newton-Raphson method [142, 214] is used to solve the nonlinear set of equations. As it is a second order scheme, convergence is expected to be faster than what is obtained for Picard iteration method. Once again, the discretization follows the standard finite element procedure.

The weighted residual form is written as [214]:

$$W = \int_\Omega \langle \delta_1\ \delta_2\ \ldots \rangle \begin{Bmatrix} R_1 \\ R_2 \\ \vdots \end{Bmatrix} d\Omega = 0 \tag{3.20}$$

where the R_is are the residuals associated to each of the equations and the δ_is are the corresponding weighting functions. For each of the ionic species, the residual is:

$$R_i = \frac{\partial c_i}{\partial t} - \mathrm{div}\left(-[D_i]\left(\mathrm{grad}(c_i) + \frac{z_i F}{RT} c_i \mathrm{grad}(\psi)\right)\right) \tag{3.21}$$

and for the Poisson equation:

$$R_\psi = \nabla^2 \psi + \frac{F}{\epsilon}\left(\sum z_i c_i + w\right) \tag{3.22}$$

For a case limited to ionic species, the integration by parts leads to the following weak

form:

$$
\begin{aligned}
W &= \int_\Omega \langle \delta_{c1}\ \delta_{c2}\ \delta_\psi \rangle \begin{Bmatrix} \dot{c_1} \\ \dot{c_2} \\ 0 \end{Bmatrix} r\ dr\ dz \\
&+ \int_\Omega \langle \delta_{c1,r}\ \delta_{c1,z}\ \delta_{c2,r}\ \delta_{c2,z}\ \delta_{\psi,r}\ \delta_{\psi,z} \rangle \begin{Bmatrix} D_{r1}c_{1,r} + \frac{D_{r1}z_1F}{RT}c_1\psi_{,r} \\ D_{z1}c_{1,z} + \frac{D_{z1}z_1F}{RT}c_1\psi_{,z} \\ D_{r2}c_{2,r} + \frac{D_{r2}z_2F}{RT}c_2\psi_{,r} \\ D_{z2}c_{2,z} + \frac{D_{z2}z_2F}{RT}c_2\psi_{,z} \\ \psi_{,r} \\ \psi_{,z} \end{Bmatrix} r\ dr\ dz \\
&+ \int_\Omega \langle \delta_{c1}\ \delta_{c2}\ \delta_\psi \rangle \begin{Bmatrix} -\frac{F}{\epsilon}z_1c_1 \\ -\frac{F}{\epsilon}z_2c_2 \\ 0 \end{Bmatrix} r\ dr\ dz \\
&+ \int_\Omega \langle \delta_{c1}\ \delta_{c2}\ \delta_\psi \rangle \begin{Bmatrix} 0 \\ 0 \\ -\frac{F}{\epsilon}w \end{Bmatrix} r\ dr\ dz
\end{aligned} \tag{3.23}
$$

The weak form can be discretized using a Galerkin weighting. The vector of the unknown variables is written as:

$$
\begin{Bmatrix} c_1 \\ c_2 \\ \vdots \\ \psi \end{Bmatrix} = [N]\{U_n\} \tag{3.24}
$$

$$
[N] = \begin{bmatrix}
N_1 & & & N_2 & & & \circ\circ\circ & N_G & & & \\
& N_1 & & & N_2 & & \circ\circ\circ & & N_G & & \\
& & \ddots & & & \ddots & \circ\circ\circ & & & \ddots & \\
& & & N_1 & & & N_2\ \circ\circ\circ & & & & N_G
\end{bmatrix} \tag{3.25}
$$

$$
\langle U_n \rangle = \langle c_{11}\ c_{21} \ldots \psi_1\ c_{12}\ c_{22} \ldots\ \psi_2\ \circ\circ\circ\ c_{1G}\ c_{2G} \ldots \psi_G \rangle \tag{3.26}
$$

where G is the number of nodes in the element. The small dots (...) indicate the terms to add when considering more ionic species, whereas the big dots ($\circ\circ\circ$) stand for the missing shape function terms. The subscripts i and j designate the species i and the

node j. The elementary matrices can thus be expressed as:

$$[K^e] = \int_{\Omega^e} \left(\underbrace{[B]^T[D_1][B]}_{[K_D^e]} + \underbrace{[N]^T[D_2][N]}_{[K_P^e]} + \underbrace{[B]^T[D_3][NN]}_{[K_{N-P}^e]} \right) r\, dr\, dz \quad (3.27)$$

$$[M^e] = \int_{\Omega^e} [N]^T[D_4][N]\, r\, dr\, dz \quad (3.28)$$

$$\{F^e\} = \int_{\Omega^e} [N]^T \begin{Bmatrix} 0 \\ 0 \\ \vdots \\ \frac{Fw}{\epsilon} \end{Bmatrix} r\, dr\, dz \quad (3.29)$$

The matrix $[K^e]$ is divided in three parts. The first part, $[K_D^e]$, includes all the diffusion terms. The two other parts are related to the coupling between the concentration and the electrical potential. The matrix $[K_P^e]$ comes from the discretization of the Poisson equation (the third line in equation 3.23) and $[K_{N-P}^e]$ is related to the coupling between the concentration and the electrical potential gradient in the Nernst-Planck equation. The $[NN]$ matrix is given by:

$$[NN] = \begin{bmatrix} N_1 & & N_2 & & \circ\circ\circ & N_G & & \\ N_1 & & N_2 & & \circ\circ\circ & N_G & & \\ & N_1 & & N_2 & \circ\circ\circ & & N_G & \\ & N_1 & & N_2 & \circ\circ\circ & & N_G & \\ & \ddots & & \ddots & \circ\circ\circ & & \ddots & \\ & & N_1 & & N_2 \; \circ\circ\circ & & & N_G \\ & & N_1 & & N_2 \; \circ\circ\circ & & & N_G \end{bmatrix} \quad (3.30)$$

For an axisymmetrical case, the matrix $[B]$ corresponds to:

$$[B] = \begin{bmatrix} N_{1,x} & & & \circ\circ\circ & N_{G,x} & & \\ N_{1,y} & & & \circ\circ\circ & N_{G,y} & & \\ & N_{1,x} & & \circ\circ\circ & & N_{G,x} & \\ & N_{1,y} & & \circ\circ\circ & & N_{G,y} & \\ & & \ddots & \circ\circ\circ & & \ddots & \\ & & N_{1,x} & \circ\circ\circ & & & N_{G,x} \\ & & N_{1,y} & \circ\circ\circ & & & N_{G,y} \end{bmatrix} \quad (3.31)$$

The matrices $[D_1]$ through $[D_4]$ are given by:

$$[D_1] = \begin{bmatrix} D_{r1} & & & & & \\ & D_{z1} & & & & \\ & & D_{r2} & & & \\ & & & D_{z2} & & \\ & & & & \ddots & \\ & & & & & 1 \end{bmatrix} \tag{3.32}$$

$$[D_2] = \begin{bmatrix} 0 & & & \\ 0 & & & \\ \vdots & & & \\ \frac{-Fz_1}{\epsilon} & \frac{-Fz_2}{\epsilon} & \cdots & 0 \end{bmatrix} \tag{3.33}$$

$$[D_3] = \begin{bmatrix} \frac{D_{r1}z_1F}{RT}\frac{\partial\psi}{\partial r} & & & & & & \\ & \frac{D_{z1}z_1F}{RT}\frac{\partial\psi}{\partial z} & & & & & \\ & & \frac{D_{r2}z_2F}{RT}\frac{\partial\psi}{\partial r} & & & & \\ & & & \frac{D_{z2}z_2F}{RT}\frac{\partial\psi}{\partial z} & & & \\ & & & & \ddots & & \\ & & & & & 0 & \\ & & & & & & 0 \end{bmatrix} \tag{3.34}$$

$$[D_4] = \begin{bmatrix} 1 & & & \\ & 1 & & \\ & & \ddots & \\ & & & 0 \end{bmatrix} \tag{3.35}$$

The tangent matrix is obtained by calculating the first variation of the weak form W (equation 3.20) [214]:

$$\Delta W = \int_\Omega \langle \delta_1 \ \delta_2 \ \ldots \rangle \begin{Bmatrix} \Delta R_1 \\ \Delta R_2 \\ \vdots \end{Bmatrix} d\Omega = 0 \tag{3.36}$$

For a transient case solved with an implicit Euler scheme ($\theta = 1$), the elementary tangent matrix is given by:

$$[K_T^e] = [M^e] + \Delta t[K^e] + \Delta t \int_{\Omega^e} [B^T][D_5][B] \ r \ dr \ dz \tag{3.37}$$

where:

$$[D_5] = \begin{bmatrix} 0 & 0 & 0 & 0 & \dots & \frac{D_{r1}z_1F}{RT}c_1 & 0 \\ & & & & & 0 & \frac{D_{z1}z_1F}{RT}c_1 \\ & & & & & \frac{D_{r2}z_2F}{RT}c_2 & 0 \\ & & & & & 0 & \frac{D_{z2}z_2F}{RT}c_2 \\ & & & & & \vdots & \vdots \\ & & & & & 0 & 0 \\ & & & & & 0 & 0 \end{bmatrix} \tag{3.38}$$

In contrast to the preceding numerical scheme, the characteristics of the various matrices tend to vary with the number of ionic species accounted for. Furthermore, larger matrices have to be stored.

3.2.4 Comparison of the two algorithms

In order to compare both algorithms, an example first presented by Kato [95] will be used. It is an unidimensional steady-state problem involving two ionic species. The development of the elementary matrices for 1D cases is not presented but is straightforward starting from the matrices of the axisymmetrical case. The equations are first rewritten in a non-dimensional form by stating:

$$\psi = \frac{RT}{F}\tilde{\psi} \tag{3.39}$$

$$x = L\tilde{x} \tag{3.40}$$

$$D_i = \tilde{D}_i D_o \tag{3.41}$$

$$j_i = \frac{c_o D_o}{L}\tilde{j}_i \tag{3.42}$$

$$c_i = c_o \tilde{c}_i \tag{3.43}$$

where the subscript "o" designates a reference value and L is the length of the domain. Equation (3.1) and (3.6) are rewritten as:

$$\tilde{j}_i = -\left(\frac{D_i}{D_o}\right)\frac{d\tilde{c}_i}{d\tilde{x}} - z_i\tilde{c}_i\left(\frac{D_i}{D_o}\right)\frac{d\tilde{\psi}}{d\tilde{x}} \tag{3.44}$$

$$\frac{d^2\tilde{\psi}}{d\tilde{x}^2} + \frac{\tilde{\rho}}{\alpha^2} = 0 \tag{3.45}$$

with

$$\alpha^2 = \frac{\epsilon RT}{c_o F^2 L^2} \tag{3.46}$$

$$\tilde{\rho} = \sum z_i \tilde{c}_i + (w/c_o) \tag{3.47}$$

In the domain $0 \leq \tilde{x} \leq 1$. The value of the parameter α^2 is determined mainly by the scale of the problem under consideration. For a medium kept at 25°C (298°K) and saturated with an ionic solution having a concentration of 1 mmol/l and a permittivity of 7.0832×10^{-10}C/Vm, $\alpha^2 \simeq 2 \times 10^{-16}/L^2$. For biological membranes that have thickness around 1μm, $\alpha^2 \simeq 0.0002$. For porous construction materials like concrete, the characteristic length is in the order of about 1 cm and thus $\alpha^2 \simeq 2 \times 10^{-12}$. For two problems having the same characteristic length L, a variation in α^2 corresponds to a variation in the level of concentration involved.

For this specific example, it is assumed that two monovalent species are present in solution ($z_1 = +1$ and $z_2 = -1$). For both species, $\tilde{D}_i = 1$ and $c_o = w = 1$. It is also assumed that both species have a dimensionless concentration of 1.0 at $\tilde{x} = 0$ and 1.5 at $\tilde{x} = 1$. The dimensionless potential is set at 0.0 at $\tilde{x} = 0$ and 1.0 at $\tilde{x} = 1$.

To solve this problem, both algorithms were used with a linear two-node element.

3.2.4.1 Results obtained with the first algorithm

To begin the calculations, initial concentrations were considered to vary linearly across the system. Figure 3.1 shows the solution obtained with $\alpha^2 = 0.5$ and computed with twenty elements. Twelve iterations were needed to perform the calculations. The difference with the solution obtained by Kato [95] does not exceed two per cent.

The next set of simulations consists in varying the value of α^2 while keeping the same boundary conditions. It appeared that under $\alpha^2 = 0.25$, no convergence could be obtained. Figure 3.2 clearly shows the variation of the convergence rate as a function of α^2. All simulations were made with 20 elements. In order to rectify this situation, different solutions were tested: a variation in the numbers of elements, an increase in the order of the interpolation polynomials, and a modification in the initial solution introduced to the algorithm. Results revealed that all this work was done in vain. A modification of the algorithm was also made, by updating the solution after a calculation

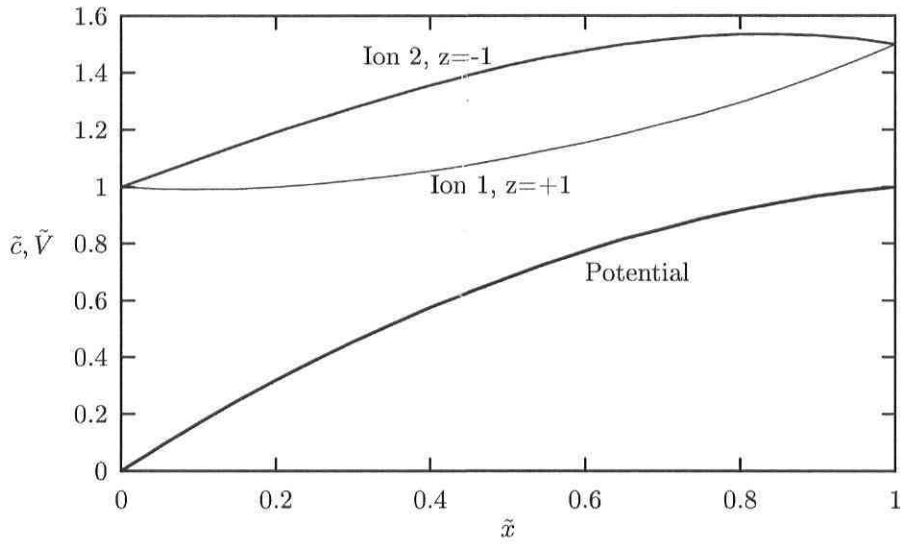

Figure 3.1: First algorithm: solution for $\alpha^2 = 0.5$.

step according to the following procedure:

$$\{u\}^{k-1} = \frac{\{u\}^{k-1} + \{u\}^{k-2}}{2} \tag{3.48}$$

This modification allowed us to break the 0.25 limit, but only to find the same problem for a value of about 0.15. For such values of α^2, only thin membranes problems can be solved. This is what justified the development of the coupled equation algorithm, in an attempt to broaden the field of application of the Nernst-Planck/Poisson set of equations.

3.2.4.2 Results obtained with the second algorithm

The same tests were carried out for the second algorithm, and proved to provide much better results. For the second algorithm, there is no evidence of a critical value of α^2 for which divergence occurs. The number of required iterations is lower and limited to approximately four. Furthermore, this number varies very little according to α^2.

To illustrate the superior behavior of the second algorithm, the same problem was solved, but this time with $\alpha^2 = 0.0001$. The results are shown on figure 3.3, and were obtained with 100 elements. More elements are needed to avoid oscillations near the

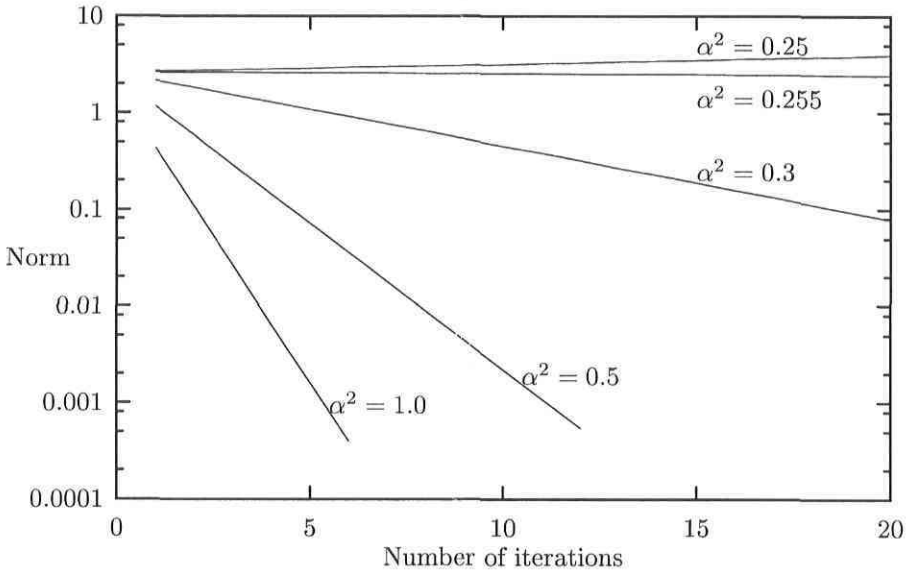

Figure 3.2: First algorithm: norm vs. number of iterations for different values of α^2.

boundaries, due to high gradient values. Comparisons with the results of Kato [95] are impossible since the author did not perform any tests for low values of α^2.

Following these results, it is clear that the second algorithm is much more robust. It was used to obtain the results that will be presented afterwards.

Various other cases were considered to test the second algorithm. The first example was inspired from Helfferich [85]. It consists in a 1D steady-state problem where four species are present: Mg^{2+}, SO_4^{2-}, Na^+ and K^+. Dimensionless variables were used in the treatment of the problem. The diffusion coefficients were 1.0 for SO_4^{2-}, Mg^{2+} and Na^+, and 1.67 for K^+. At $\tilde{x} = 0$, the boundary conditions were 1.0 for SO_4^{2-}, 0.5 for Mg^{2+} and zero for the other species. At $\tilde{x} = 1$, the conditions were 0.8345 for SO_4^{2-}, 0.0 for Mg^{2+}, 0.169 for Na^+ and 0.5 for K^+. The potential was established at 0.0 at $\tilde{x} = 0$ and 5.0 at $\tilde{x} = 1$. The fixed charge density in the membrane, w/c_o, was equal to 1.0. The only remaining unknown variable was the value of α^2.

The solution obtained analytically by Helfferich [85] for that same problem was developed on the basis of the electroneutrality hypothesis. Considering that MacGillivray and Hare [110, 111] have demonstrated that the validity of this assumption is restricted to very low values of α^2, the calculations were performed with $\alpha^2 = 1 \times 10^{-10}$.

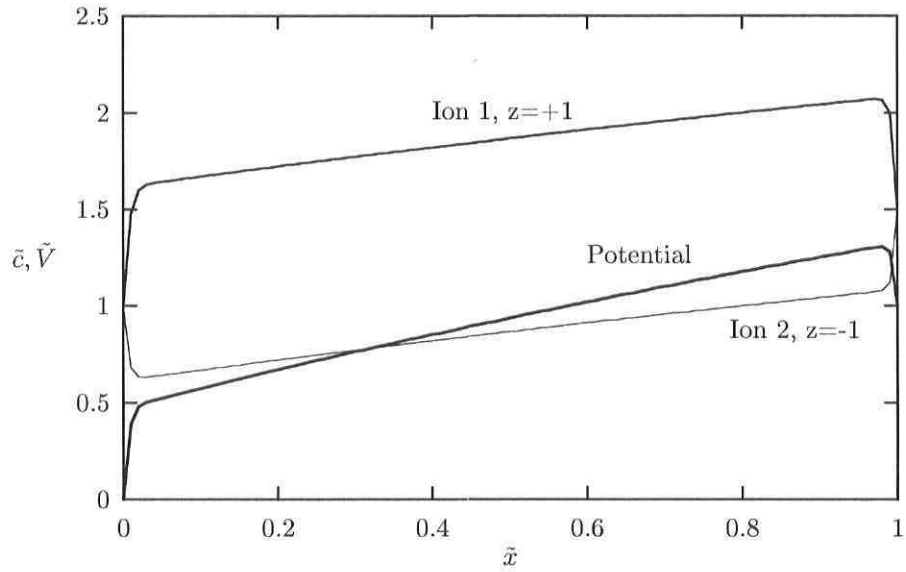

Figure 3.3: Second algorithm: solution for $\alpha^2 = 0.0001$.

The solution, computed with 50 elements, is shown on figure 3.4. The difference with the analytical solution presented by Helfferich [85] is about 3%, which confirms the results of MacGillivray and Hare [110, 111] concerning the value of α^2.

The other example concerns a transient diffusion problem. It was selected to evaluate the influence of the α^2 parameter for a fixed length domain. The calculations were performed using an implicit Euler scheme. The dimensionless variables were once again used with the addition of $\tilde{t} = D_o t/L^2$ as a time variable. Two species were considered, with $z_1 = +1$ and $\tilde{D}_1 = 3$ for the first one, and $z_2 = -1$, $\tilde{D}_2 = 1$ for the second. Initially, the concentrations were set equal to zero over the entire domain, which consisted of a bar of length 1. At $\tilde{t} = 0$, a unit concentration was imposed at $\tilde{x} = 0$ for both species. The concentrations were set at zero at $\tilde{x} = 1$.

Two simulations were performed for values of α^2 equal to 1×10^{-2} and 1×10^{-4} respectively. This implies that, for a given domain length, the concentrations involved in the second case were a hundred times higher than in the first one. Results are given in figures 3.5 and 3.6. These results were obtained at $\tilde{t} = 0.01$ and reached after 200 steps of 5×10^{-5}. All calculations were performed with 50 elements. As a comparative basis, the solutions computed without taking into account any electrostatic effect, thus derived on the sole basis of Fick's law, are also given in figures 3.5 and 3.6.

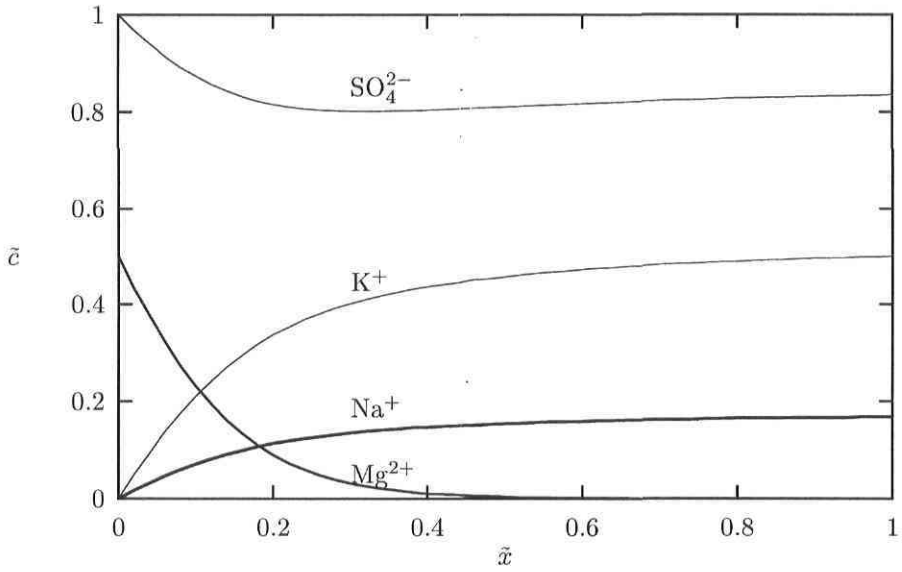

Figure 3.4: Concentration profiles for the Helfferich problem.

In figure 3.5, the influence of the electrical coupling between the species is clearly noticeable. On the one hand, results indicate that the progression of the fastest ion is slowed down by the electrical potential. On the other hand, the slowest ion, with a diffusion coefficient being three times lower, is accelerated. In the case of higher concentration (figure 3.6), this phenomenon is even more obvious. Both concentration profiles are so close that they became superposed.

These results confirm, once more, the conclusion of MacGillivray and Hare [110, 111] who suggested that the electroneutrality is gradually approached as the value of α^2 decreases. Figure 3.7 shows that the electrical charge density $\tilde{\rho}$ tends toward zero as α^2 is reduced.

The last example shows the use of this numerical scheme for a transient problem with an axisymmetrical geometry. The simulations were performed to investigate the effect of the presence of electrical charges on the inner surface of a pore. In this case, ions are diffusing in and out of the pore space. The pore, presented in figure 3.8, has a radius of 1 μm and a length of 10 μm.

Five ions were considered in the simulations: OH^-, Na^+, K^+, SO_4^{2-}, and Cl^-. Their respective diffusion coefficients (in m^2/s) are: 5.273×10^{-9}, 1.334×10^{-9}, 1.957×10^{-9},

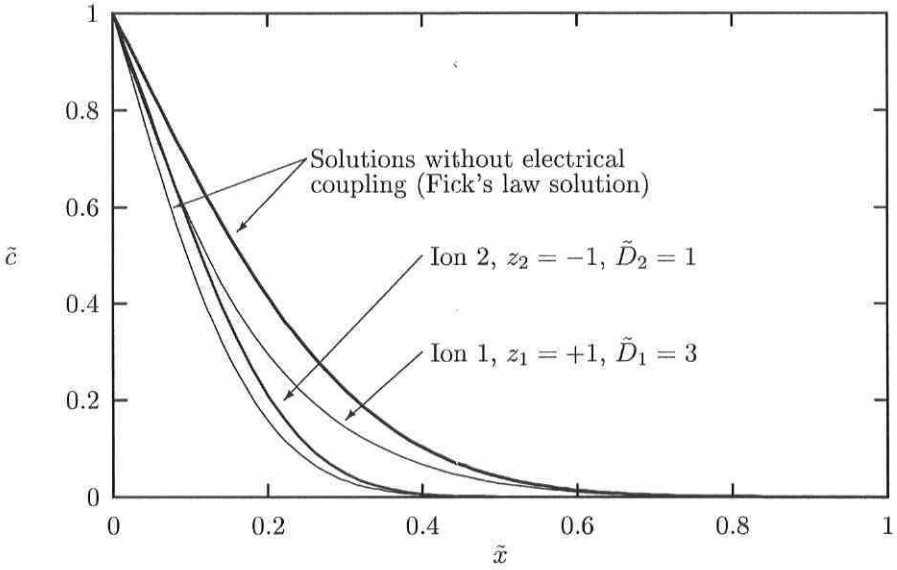

Figure 3.5: Concentration profiles at $\tilde{t} = 0.01$, $\alpha^2 = 0.01$.

1.065×10^{-9}, and 2.032×10^{-9}.

The initial concentrations in the pore were fixed at: 690 mmol/l of OH^-, 286 mmol/l of Na^+, 500 mmol/l of K^+, 48 mmol/l of SO_4^{2-}, and 0 mmol/l of Cl^-.

The boundary conditions, at the entrance of the pore, were fixed at 500 mmol/l of Cl^-, 800 mmol/l of Na^+, and 300 mmol/l of OH^-. For the electrical (diffusion) potential, the initial value was set at 0.

Two cases were investigated. In the first case, it was assumed that no electrical charges were present on the inner surface of the pore. In this case, the electrical potential was set at 0 at the entrance of the pore, since a reference value has to be fixed at some point. In the second case, the electrical potential on the inner surface of the pore was set equal to -10mV as shown on figure 3.9. The system was considered to remain in isothermal conditions (i.e. at 22°C) over the entire duration of the process. The dielectric constant of the system was fixed at 7.0823×10^{-10}C/Vm. The two simulations were performed in five time steps of 0.0002 second. For the spatial discretization, a regular mesh of 10×50 linear three-node triangles was used, as shown on figure 3.8.

According to the numerical simulations, the potential on the inner surface of the

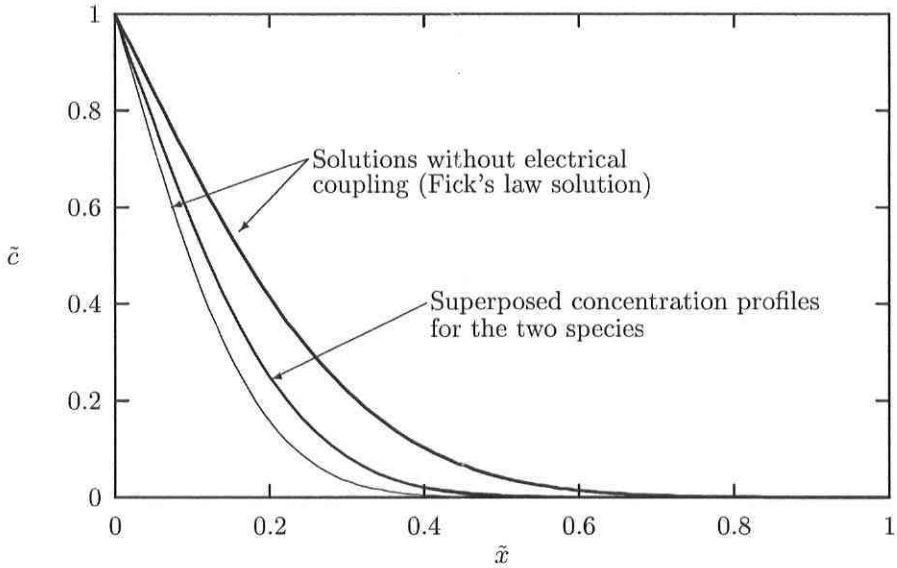

Figure 3.6: Concentration profiles at $\tilde{t} = 0.01$, $\alpha^2 = 0.0001$.

pore has no significant effect on the concentration profiles. Its influence is limited to a small region at the vicinity of the surface. Hence, the flux of ions in the pore is the same for both simulations.

For the electrical potential, the situation is however different. The potential on the inner surface tends to lower the difference of potential between both ends of the pore. For the case without any electrical charges on the pore wall, this difference has a value of 5 mV. In the other case, this value drops to 3.1 mV.

3.2.5 Conclusion

The comparison between a numerical scheme based on the Picard iteration technique and another scheme based on the Newton-Raphson method has clearly showed that the former, even tough it has already been used in some recent papers, cannot be used to solve the Nernst-Planck/Poisson system of equations for all cases.

By coupling all the equations and using the Newton-Raphson method, the Nernst-Planck/Poisson system of equations could be solved for problems with a high number of ionic species with different valence number, either for steady state or transient cases.

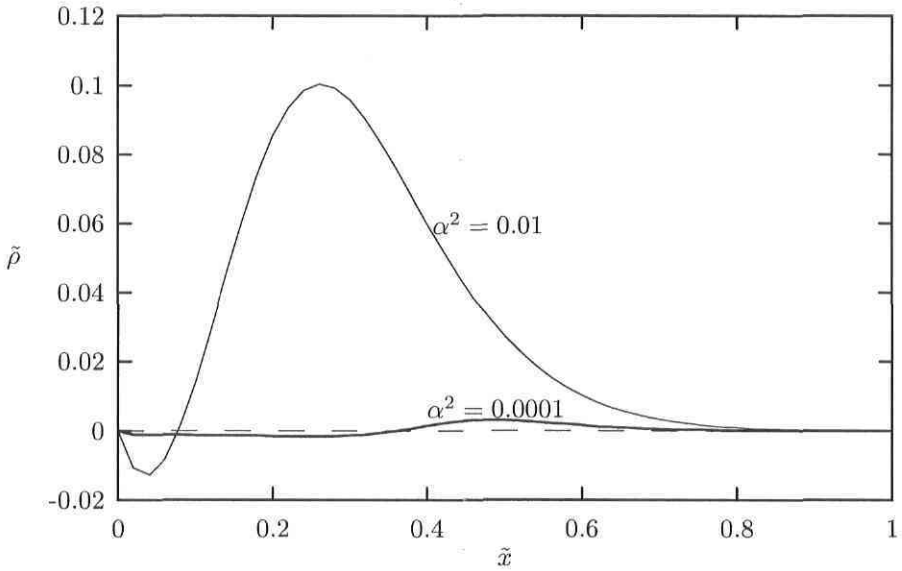

Figure 3.7: Charge density for the two transient cases.

Furthermore, the numerical scheme works for 1D geometry as well as 2D and axisymmetrical ones, and could easily be extended for 3D cases.

This work opens the way for the treatment of complex multiionic species models of transport in porous media involving chemical reactions between the species and the solid matrix, while considering the electrical coupling.

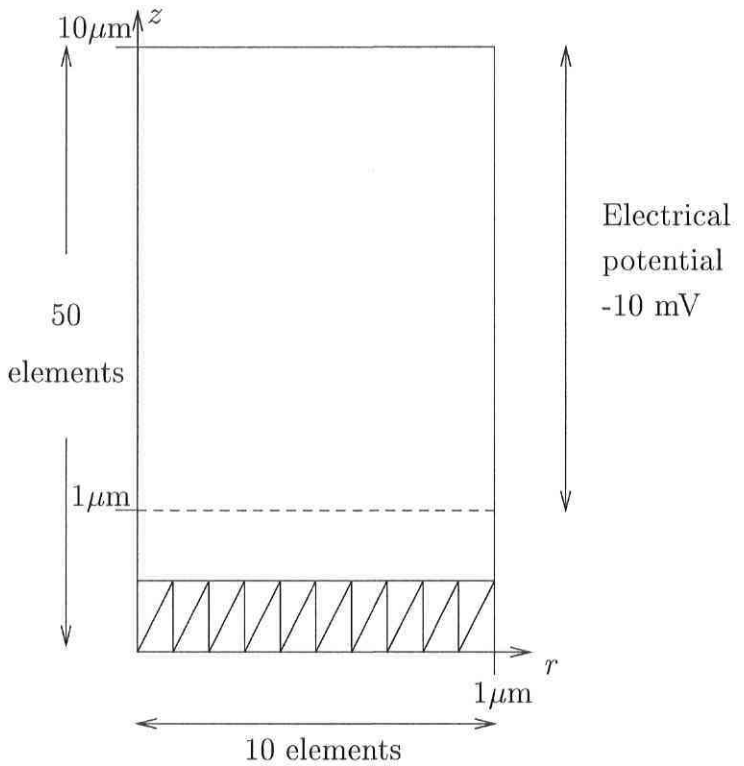

Figure 3.8: The axisymmetrical problem.

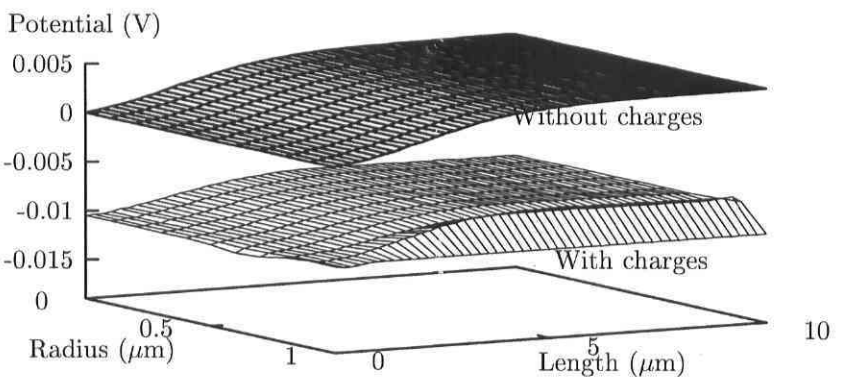

Figure 3.9: Potential profile in a pore.

3.3 Numerical solution of the extended Nernst-Planck model

E. Samson[12], J. Marchand[12]

[1]Centre de recherche interuniversitaire sur le béton,
Université Laval, Québec, Canada, G1K 7P4

[2]SIMCO Technologies inc.,
1400, boul. du Parc Technologique, Québec, Canada, G1P 4R7

Abstract

The main features of a numerical model aiming at predicting the drift of ions in an electrolytic solution upon a chemical potential gradient are presented. The mechanisms of ionic diffusion are described by solving the extended Nernst-Planck system of equations. The electrical coupling between the various ionic fluxes is accounted for by the Poisson equation. Furthermore, chemical activity effects are considered in the model. The whole system of non-linear equations is solved using the finite-element method. Results yielded by the model for simple test cases are compared to those obtained using an analytical solution. Applications of the model to more complex problems are also presented and discussed.

3.3.1 Introduction

The phenomenon of ionic diffusion in concentrated electrolytic solutions has received a great deal of attention over the past decade. The large body of research on the subject has clearly emphasized the complexity of the mechanisms involved. Ions in solution are subjected to various types of interaction that readily complicate the mathematical treatment of the problem. This is the reason why many authors have traditionally chosen to neglect chemical activity effects while predicting the transport of ions in strong electrolytes. A comprehensive overview of the mathematical treatment of the ionic diffusion process can be found in reference [157].

In the following paragraphs, a new approach to model the diffusion of ions in electrolytic solutions is presented. The main originality of this approach lies in the fact that the coupling between the various ionic fluxes is taken into account and that chemical activity effects are considered. In this model, the set of non-linear equations is solved using the finite element method. Results yielded by the model for simple test cases are compared to those obtained using an analytical solution. Applications of the model to more complex problems are also presented and discussed.

3.3.2 Mathematical model

In a non-ideal ionic solution, the extended Nernst-Planck model which describes the flux of each species is given by [85]:

$$\boldsymbol{j_i} = -[D_i]\left(\text{grad}(c_i) + \frac{z_i F}{RT} c_i \text{grad}(\psi) + c_i \text{grad}(\ln \gamma_i)\right) \tag{3.49}$$

where $\boldsymbol{j_i}$ is the flux of the ionic species i, $[D_i]$ is the diffusion coefficient tensor, c_i is the concentration of the species i, z_i is its valence number, F is the Faraday constant, R is the ideal gas constant, T is the temperature, ψ is the electrical potential and γ_i is the chemical activity coefficient.

For each ionic species, the law of mass conservation can be applied:

$$\frac{\partial c_i}{\partial t} + \text{div}(\boldsymbol{j_i}) = 0 \tag{3.50}$$

To complete the system of equations, another relation is needed to account for the electrical potential that is locally induced by the movement of all ions. Various authors [89, 134, 144] have relied on the electroneutrality (equation 3.51) and null current (equation 3.52) assumptions to determine the numerical value of the potential in the simplified Nernst-Planck model (i.e. equation 3.49 without the chemical activity term):

$$\text{electroneutrality} \quad : \quad \sum_{i=1}^{N} z_i c_i + w = 0 \tag{3.51}$$

$$\text{null current} \quad : \quad \sum_{i=1}^{N} z_i \ \boldsymbol{j_i} = 0 \tag{3.52}$$

In equation (3.51) and (3.52), N stands for the total number of ionic species and w is a fixed charge density in the domain. As emphasized by MacGillivray and Hare

[110, 111], the validity of these assumptions is limited to specific cases. In a more general model, the Poisson equation, which relates the electrical potential to the electrical charge in space, should be used [85]:

$$\nabla^2\psi + \frac{F}{\epsilon}\left(\sum_{i=1}^{N} z_i c_i + w\right) = 0 \tag{3.53}$$

This validity of this equation is based on the assumption that the electromagnetic signal travels much more rapidly than ions in solutions.

Over the past decades, numerous semi-empirical equations have been developed to calculate the chemical activity coefficients of ions in concentrated electrolytic solutions. The most well known is the Debye-Hückel model [26, 133]. According to this model, the chemical activity coefficient of a given ionic species i can be calculated by:

$$\ln \gamma_i = -Az_i^2\sqrt{I} \tag{3.54}$$

Where I is the ionic strength of the solution:

$$I = \frac{1}{2}\sum_{1}^{N}\left(z_i^2 c_i + w\right) \tag{3.55}$$

and A is a temperature-dependant parameter that can be calculated as:

$$A = \frac{\sqrt{2}\,F^2 e_o}{8\pi(\epsilon RT)^{3/2}} \tag{3.56}$$

One of the main features of the Debye-Hückel model is that ions are considered to be dimensionless (point-charge assumption). The extended Debye-Hückel equation adds a correction to the previous model by considering the radius of the various ions in solution:

$$\ln \gamma_i = -\frac{Az_i^2\sqrt{I}}{1 + Ba_i\sqrt{I}} \tag{3.57}$$

Where a_i is the radius of ion i and B is a parameter given by:

$$B = \sqrt{\frac{2F^2}{\epsilon RT}} \tag{3.58}$$

Figure 3.10 illustrates, for different valence values, the difference between the two models. Laboratory experiments have shown that the Debye-Hückel model is valid for ionic strength lower than 10 mmol/l while the extended Debye-Hückel model is valid for concentrations up to 100 mmol/l [115].

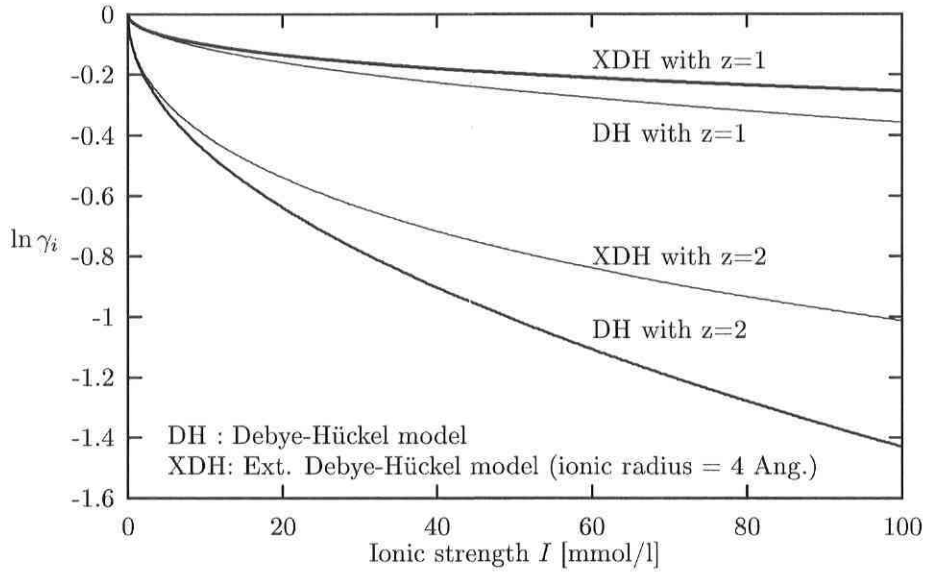

Figure 3.10: A comparison between the chemical activity models.

3.3.3 Numerical model

The numerical model used to solve the extended Debye-Hückel model is based on an algorithm tested by the authors [157]. In this model, the equations are fully coupled and discretized using the finite-element method. The application of this model to the resolution of the Nernst-Planck-Poisson system of equations (for which chemical activity effects are neglected) has been found to yield very good results.

The variational form of coupled equations is written as [214]:

$$W = \int_{\Omega} \langle \delta_1 \ \delta_2 \ \ldots \rangle \left\{ \begin{array}{c} R_1 \\ R_2 \\ \vdots \end{array} \right\} d\Omega = 0 \tag{3.59}$$

Where the R_i's are the residuals of the equations in the model, the δ_i's are the corresponding weighting functions and Ω is the domain of integration. For the sake of simplicity, the model is shown for the uni-dimensional case. However, the extension to two or three dimensions is straightforward.

Inserting the equations of the extended Debye-Hückel model (3.49) and Poisson

(3.53) in the variational form (3.59) gives:

$$W = \int_L \langle \delta c_1 \ \delta c_2 \ \ldots \delta\psi \rangle \left\{ \begin{array}{c} \frac{\partial c_1}{\partial t} - \frac{\partial}{\partial x}\left(-D_1\left(\frac{\partial c_1}{\partial x} + \frac{z_1 F}{RT} c_1 \frac{\partial \psi}{\partial x} + c_1 \frac{\partial(\ln \gamma_1)}{\partial x}\right)\right) \\ \frac{\partial c_2}{\partial t} - \frac{\partial}{\partial x}\left(-D_2\left(\frac{\partial c_2}{\partial x} + \frac{z_2 F}{RT} c_2 \frac{\partial \psi}{\partial x} + c_2 \frac{\partial(\ln \gamma_2)}{\partial x}\right)\right) \\ \vdots \\ \frac{\partial^2 \psi}{\partial x^2} + \frac{F}{\epsilon} z_1 c_1 + \frac{F}{\epsilon} z_2 c_2 + \ldots + \frac{F}{\epsilon} w \end{array} \right\} dx = 0 \tag{3.60}$$

In this equation, the dots indicate the terms that should be added in order to consider more ionic species. The weak form of this system of equations is obtained by performing an integration by parts. The contour terms are omitted since only Dirichlet-type boundary conditions will be considered in the numerical examples:

$$\begin{array}{r} W = \int_L \ \delta c_1 \frac{\partial c_1}{\partial t} + \frac{\partial \delta c_1}{\partial x}\left(D_1\left(\frac{\partial c_1}{\partial x} + \frac{z_1 F}{RT} c_1 \frac{\partial \psi}{\partial x} + c_1 \frac{\partial(\ln \gamma_1)}{\partial x}\right)\right) \\ + \delta c_2 \frac{\partial c_2}{\partial t} + \frac{\partial \delta c_2}{\partial x}\left(D_2\left(\frac{\partial c_2}{\partial x} + \frac{z_2 F}{RT} c_2 \frac{\partial \psi}{\partial x} + c_2 \frac{\partial(\ln \gamma_2)}{\partial x}\right)\right) \\ \vdots \\ + \frac{\partial \delta\psi}{\partial x}\frac{\partial \psi}{\partial x} - \delta\psi \frac{F}{\epsilon} z_1 c_1 - \delta\psi \frac{F}{\epsilon} z_2 c_2 - \ldots - \delta\psi \frac{F}{\epsilon} w \ dx = 0 \end{array} \tag{3.61}$$

Figure 3.11: L2 element for the two-species case.

This equation is organized in a matrix form, which gives:

$$
\begin{aligned}
W = & \int_L \langle \delta c_1 \ \delta c_2 \ \dots \delta\psi \rangle \begin{bmatrix} 1 & & & \\ & 1 & & \\ & & \ddots & \\ & & & 0 \end{bmatrix} \begin{Bmatrix} \dot{c_1} \\ \dot{c_2} \\ \vdots \\ \dot{\psi} \end{Bmatrix} dx \\
& + \int_L \left\langle \frac{\partial \delta c_1}{\partial x} \ \frac{\partial \delta c_2}{\partial x} \ \dots \frac{\partial \delta \psi}{\partial x} \right\rangle \begin{bmatrix} D_1 & & & \frac{D_1 z_1 F}{RT} c_1 \\ & D_2 & & \frac{D_2 z_2 F}{RT} c_2 \\ & & \ddots & \vdots \\ & & & 1 \end{bmatrix} \begin{Bmatrix} c_{1,x} \\ c_{2,x} \\ \vdots \\ \psi_{,x} \end{Bmatrix} dx \\
& + \int_L \langle \delta c_1 \ \delta c_2 \ \dots \delta\psi \rangle \begin{bmatrix} 0 & & & \\ & 0 & & \\ & & \ddots & \\ -\frac{F}{\epsilon} z_1 & -\frac{F}{\epsilon} z_2 & \dots & 0 \end{bmatrix} \begin{Bmatrix} c_1 \\ c_2 \\ \vdots \\ \psi \end{Bmatrix} dx \qquad (3.62) \\
& + \int_L \left\langle \frac{\partial \delta c_1}{\partial x} \ \frac{\partial \delta c_2}{\partial x} \ \dots \frac{\partial \delta \psi}{\partial x} \right\rangle \begin{bmatrix} D_1 \frac{\partial (\ln \gamma_1)}{\partial x} & & & \\ & D_2 \frac{\partial (\ln \gamma_2)}{\partial x} & & \\ & & \ddots & \\ & & & 0 \end{bmatrix} \begin{Bmatrix} c_1 \\ c_2 \\ \vdots \\ \psi \end{Bmatrix} dx \\
& - \int_L \langle \delta c_1 \ \delta c_2 \ \dots \delta\psi \rangle \begin{Bmatrix} 0 \\ 0 \\ \vdots \\ \frac{F}{\epsilon} w \end{Bmatrix} dx = 0
\end{aligned}
$$

The spatial discretization of this expression is performed using the finite element method with a classical Galerkin weighting [214]. As shown in figure 3.11, a simple two-nodes linear element is used. The unknown variables are described on each element

in terms of their nodal values as:

$$\{U\} = \begin{Bmatrix} c_1 \\ c_2 \\ \vdots \\ \psi \end{Bmatrix} = [N]\{U_n\} \tag{3.63}$$

$$[N] = \begin{bmatrix} N_1 & & & N_2 & & \\ & N_1 & & & N_2 & \\ & & \ddots & & & \ddots \\ & & & N_1 & & & N_2 \end{bmatrix} \tag{3.64}$$

$$\langle U_n \rangle = \langle c_{11}\ c_{21} \ldots \psi_1\ c_{12}\ c_{22} \ldots\ \psi_2 \rangle \tag{3.65}$$

Where N_1 and N_2 are the shape functions associated with the element shown in figure 3.11. The subscripts i and j in c_{ij} stand for the ion i at node j in a given element. The elementary matrices are obtained by replacing equation (3.63) in the integrals (3.63) evaluated at the elementary level:

$$[M^e] = \int_{l^e} [N]^T [H_1][N]\, dx \tag{3.66}$$

$$[K^e] = \int_{l^e} \left([B]^T [H_2][B] + [N]^T [H_3][N] + [B]^T [H_4][N] \right)\, dx \tag{3.67}$$

$$\{F^e\} = \int_{l^e} [N]^T \begin{Bmatrix} 0 \\ 0 \\ \vdots \\ \frac{F}{\epsilon} w \end{Bmatrix} dx = 0 \tag{3.68}$$

where l^e is the length of the element and

$$[B] = \begin{bmatrix} N_{1,x} & & & N_{2,x} & & \\ & N_{1,x} & & & N_{2,x} & \\ & & \ddots & & & \ddots \\ & & N_{1,x} & & & N_{2,x} \end{bmatrix} \tag{3.69}$$

$$[H_1] = \begin{bmatrix} 1 & & & \\ & 1 & & \\ & & \ddots & \\ & & & 0 \end{bmatrix} \tag{3.70}$$

$$[H_2] = \begin{bmatrix} D_1 & & & \frac{D_1 z_1 F}{RT} c_1 \\ & D_2 & & \frac{D_2 z_2 F}{RT} c_2 \\ & & \ddots & \vdots \\ & & & 1 \end{bmatrix} \tag{3.71}$$

$$[H_3] = \begin{bmatrix} 0 & & & \\ & 0 & & \\ & & \ddots & \\ -\frac{F}{\epsilon} z_1 & -\frac{F}{\epsilon} z_2 & \dots & 0 \end{bmatrix} \tag{3.72}$$

$$[H_4] = \begin{bmatrix} D_1 \frac{\partial(\ln \gamma_1)}{\partial x} & & & \\ & D_2 \frac{\partial(\ln \gamma_2)}{\partial x} & & \\ & & \ddots & \\ & & & 0 \end{bmatrix} \tag{3.73}$$

The assembly of those elementary matrices leads to the following system of equations:

$$[M]\{\dot{U}\} + [K]\{U\} = \{F\} \tag{3.74}$$

The time discretization is performed using an implicit Euler scheme:

$$[M]\left\{\frac{U_t - U_{t-\Delta t}}{\Delta t}\right\} + [K_t] = \{F_t\} \tag{3.75}$$

Where the subscript t stands for the actual time step and $t - \Delta t$ the previous one. Defining the matrices:

$$[\bar{K}] = [M] + \Delta t[K_t] \tag{3.76}$$

$$\{\bar{F}\} = [M]\{U_{t-\Delta t}\} \tag{3.77}$$

the system of equations can be written as:

$$[\bar{K}]\{U_t\} = \{\bar{F}\} \tag{3.78}$$

This non-linear system of equations is solved using the Newton-Raphson method [142, 214] which can be summarized as:

1. Calculating the variation of the solution ΔU with:

$$[K_T^{k-1}]\{\Delta U^k\} = -\{R^{k-1}\} \tag{3.79}$$

2. Updating the solution:

$$\{U^k\} = \{U^{k-1}\} + \{\Delta U^k\} \tag{3.80}$$

3. Repeating the preceeding steps until convergence is reached.

In that brief description of the algorithm, the subscript k stands for the iteration level, $\{R\}$ is the residual of the equation system, and $[K_T]$ is called the tangent matrix. It is given by the discretization of the variation of the residual $\{\Delta R\}$:

$$\{R\} = ([M] + \Delta t[K_t])\{U_t\} - [M]\{U_{t-\Delta t}\} \tag{3.81}$$

$$\{\Delta R\} = ([M] + \Delta t[K_t])\{\Delta U_t\} + \Delta t[\Delta K_t]\{U_t\} \tag{3.82}$$

The term $[\Delta K_t]\{U_t\}$ is evaluated, at the elementary level, by calculating the variation of the matrices $[H_2]$, $[H_3]$ and $[H_4]$. So, the elementary tangent matrix is given by:

$$[K_T^e] = [M^e] + \Delta t[K^e] + \Delta t \int_{l^e} \left([B]^T[H_{2nl}][N] + [B]^T[H_{4nl1}][N] + [B]^T[H_{4nl2}][B]\right) dx \tag{3.83}$$

where

$$[H_{2nl}] = \begin{bmatrix} \frac{D_1 z_1 F}{RT}\frac{\partial \psi}{\partial x} & & & \\ & \frac{D_2 z_2 F}{RT}\frac{\partial \psi}{\partial x} & & \\ & & \ddots & \\ & & & 0 \end{bmatrix} \tag{3.84}$$

The matrices $[H_{4nl1}]$ and $[H_{4nl2}]$ depend on the model used to calculate the chemical activity coefficients.

For the Debye-Hückel model, these matrices are given by:

$$[H_{4nl1}] = \frac{A}{16I^{3/2}}\left(z_1^2\frac{\partial c_1}{\partial x} + z_2^2\frac{\partial c_2}{\partial x} + \ldots\right)\begin{bmatrix} D_1z_1^4c_1 & D_1z_1^2z_2^2c_1 & \ldots & 0 \\ D_2z_1^2z_2^2c_2 & D_2z_2^4c_2 & \ldots & 0 \\ \vdots & \vdots & \ddots & 0 \\ 0 & 0 & 0 & 0 \end{bmatrix} \tag{3.85}$$

$$[H_{4nl2}] = -\frac{A}{4\sqrt{I}}\begin{bmatrix} D_1z_1^4c_1 & D_1z_1^2z_2^2c_1 & \ldots & 0 \\ D_2z_1^2z_2^2c_2 & D_2z_2^4c_2 & \ldots & 0 \\ \vdots & \vdots & \ddots & 0 \\ 0 & 0 & 0 & 0 \end{bmatrix} \tag{3.86}$$

For the extended Debye-Hückel, the matrices are:

$$[H_{4nl1}] = \frac{2A}{4\sqrt{2}}\left(z_1^2\frac{\partial c_1}{\partial x} + z_2^2\frac{\partial c_2}{\partial x} + \ldots\right)\times$$
$$\begin{bmatrix} \frac{D_1z_1^4c_1}{(1+Ba_1\sqrt{I})^2}\left(\frac{1}{2(2I)^{3/2}} + \frac{Ba_1}{\sqrt{2}(1+Ba_1\sqrt{I})}\right) & \frac{D_1z_1^2z_2^2c_1}{(1+Ba_1\sqrt{I})^2}\left(\frac{1}{2(2I)^{3/2}} + \frac{Ba_1}{\sqrt{2}(1+Ba_1\sqrt{I})}\right) & \ldots & 0 \\ \frac{D_2z_1^2z_2^2c_2}{(1+Ba_2\sqrt{I})^2}\left(\frac{1}{2(2I)^{3/2}} + \frac{Ba_2}{\sqrt{2}(1+Ba_2\sqrt{I})}\right) & \frac{D_2z_2^4c_2}{(1+Ba_2\sqrt{I})^2}\left(\frac{1}{2(2I)^{3/2}} + \frac{Ba_2}{\sqrt{2}(1+Ba_2\sqrt{I})}\right) & \ldots & 0 \\ \vdots & \vdots & \ddots & 0 \\ 0 & 0 & 0 & 0 \end{bmatrix} \tag{3.87}$$

$$[H_{4nl2}] = -\frac{A}{4\sqrt{I}}\begin{bmatrix} \frac{D_1z_1^4c_1}{(1+Ba_1\sqrt{I})^2} & \frac{D_1z_1^2z_2^2c_1}{(1+Ba_1\sqrt{I})^2} & \ldots & 0 \\ \frac{D_2z_1^2z_2^2c_2}{(1+Ba_2\sqrt{I})^2} & \frac{D_2z_2^4c_2}{(1+Ba_2\sqrt{I})^2} & \ldots & 0 \\ \vdots & \vdots & \ddots & 0 \\ 0 & 0 & 0 & 0 \end{bmatrix} \tag{3.88}$$

Obviously, the implementation of these matrices in a computer code involves a lot of calculation time. Furthermore, numerical simulations have shown that convergence is hard to reach when these matrices taken into account: it requires more nodes and smaller time steps. In order to reduce the required calculation time, these matrices are therefore not taken into account in the tangent matrix calculation, which is simplified to the following expression:

$$[K_T^e] = [M^e] + \Delta t[K^e] + \Delta t\int_{l^e}[B]^T[H_{2nl}][N]\,dx \tag{3.89}$$

Table 3.1: Data for the numerical simulations.

Ion	z_i	D_i (m^2/s)	a_i (Angstrom)	Low concentration $c(x=0)$ (mmol/L)	Low concentration $c(x=1)$ (mmol/L)	High concentration $c(x=0)$ (mmol/L)	High concentration $c(x=1)$ (mmol/L)
SO_4^{2-}	-2	3×10^{-10}	6	5.0	4.173	50.0	41.725
Mg^{2+}	2	3×10^{-10}	8	2.5	0.0	25.0	0.0
Na^+	1	3×10^{-10}	4	0.0	0.845	0.0	8.45
K^+	1	5×10^{-10}	3	0.0	2.5	0.0	25.0

3.3.4 Numerical simulations

Numerical results are presented to compare the effect of the choice of the chemical activity model on ionic profiles. The test case, inspired from Helfferich [85], is an ion transport problem across a charged membrane with an applied electric field. The simulations are performed for two cases: low and high concentration levels. In the low concentration level case, both models are expected to work properly. But for the second case (stronger concentrations), the Debye-Hückel model is out of its range of application.

Contrary to the dimensionless case considered by Helfferich [85], we chose, for practical purposes, to set the thickness of the membrane to 1 cm. Similarly to the problem treated by Helfferich [85], the simulations involve four different ionic species: SO_4^{2-}, Mg^{2+}, Na^+ and K^+. Their characteristics are given in table 3.1. The boundary conditions of the two considered cases are also defined in table 3.1.

The charge concentration of the membrane was fixed at 5 mmol/L for the low-concentration case, and at 50 mmol/L for the high concentration level. The intensity of the applied electric field was fixed at 13 V/m, directed from the left side of the system to the right. The dielectric constant in the membrane was assumed to be equal to that of water, i.e. 7.0832×10^{-10} C/Vm. Finally, the temperature was kept constant at 300°K .

The calculations were performed using a 50-element regular mesh. For the case without any activity effects, the solution is reached within 5 iterations. At the low concentration level, 12 iterations are needed for the Debye-Hückel model, compared

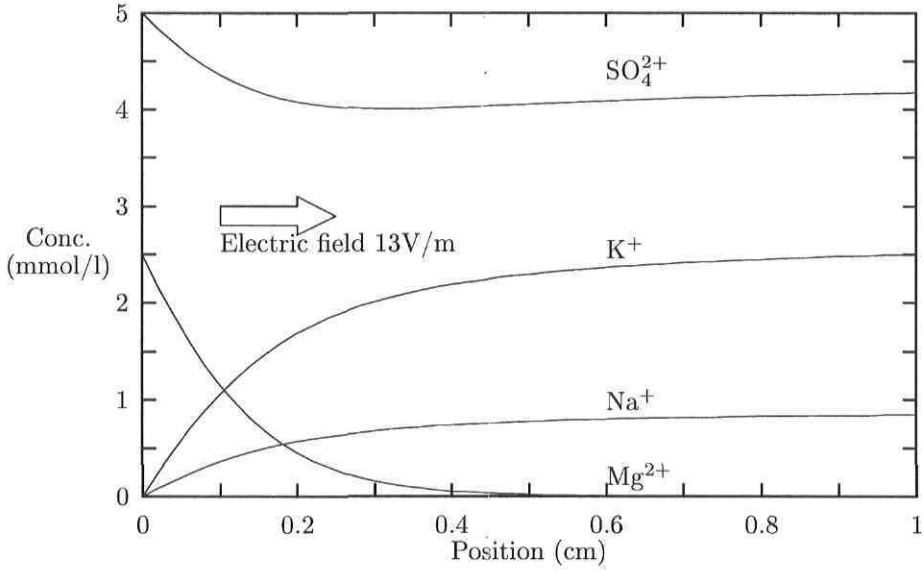

Figure 3.12: Stationnary solution for the low concentration case without activity.

to 10 with the extended Debye-Hückel. For the high concentration level, 35 and 12 iterations are required for each case respectively.

As for Helfferich [85], the results presented in the following paragraphs are limited to the steady-state case. When compared to the dimensionless data obtained using the analytical solution developed by the author, the results yielded by the numerical model for the two cases differ from less than 3%. Comparisons are solely restricted to the cases for which the activity coefficients were assumed to be equal to 1 since Helfferich [85] did not consider any activity effects in the treatment of his problem.

Figure 3.12 gives the four concentration profiles for the low concentration case without activity. Activity effects were then considered in a second series of simulations using both the Debye-Hückel and extended Debye-Hückel equations. Considering the low concentration level, the influence of the activity was found to be quite limited. Of the four ionic species, it is the SO_4^{2-} ion that experiences the strongest deviation from its ideal behavior.

The SO_4^{2-} profiles for the three cases, i.e. no activity, Debye-Hückel and extended Debye-Hückel model, are presented in figure 3.13. The strongest deviation comes from the Debye-Hückel model. This result is in good agreement with figure 3.10, that shows

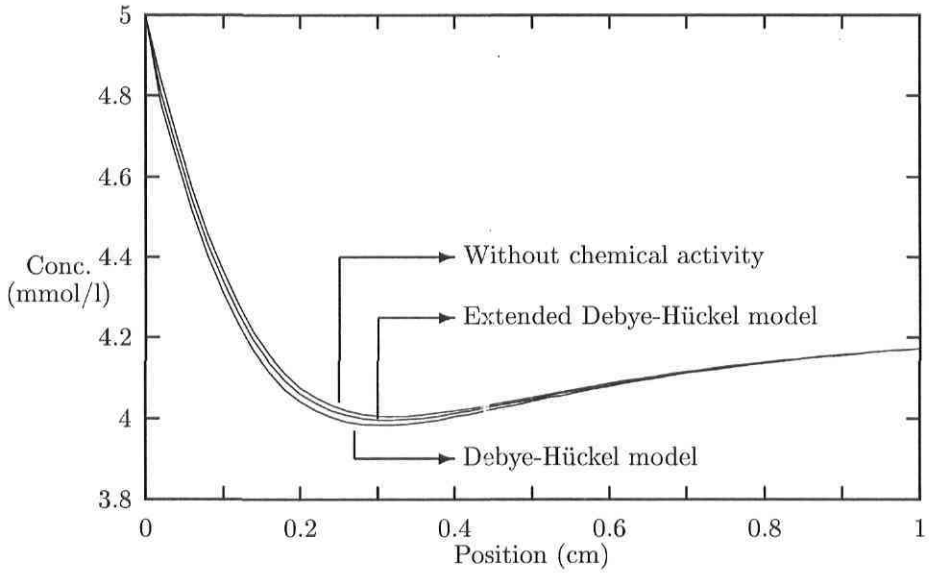

Figure 3.13: SO_4^{2-} profiles with different models for the low concentration case.

a higher value for its chemical activity coefficient.

The same simulations were performed for the high concentration case, which is well out of the range of application of the Debye-Hückel model. As for the low concentration case, the concentration profiles without considering activity are first presented (see figure 3.14). The comparison of the various models is given for the SO_4^{2-} in figure 3.15 and for Mg^{2+} in figure 3.16. As can be seen in those figures, the results obtained for the Debye-Hückel model are very far from those yielded by extended Debye-Hückel equation.

Finally, a simulation involving a non-stationary case was performed using the extended Debye-Hückel model. It corresponds to the high concentration case presented previously, except this time, no external electrical field is applied on the system. The initial solution in the membrane is formed of 25 mmol/L of SO_4^{2-} combined with the 50 mmol/L present as fixed charge. All the other conditions are the same as those presented in table 3.1. Even if there is no external electric field, at least one boundary condition is needed for the potential, to serve as a reference level. It is set equal to zero at $x = 0$. The results are presented in figures 3.17 and 3.18 for the sulfate and electrical potential profiles, at 2.5 and 5 hours.

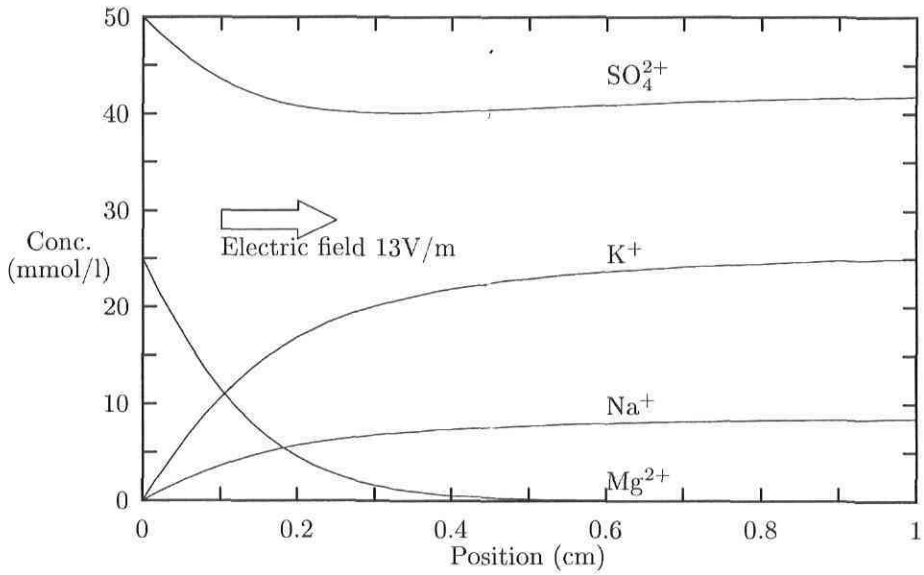

Figure 3.14: Stationnary solution for the high concentration case without activity.

The effect on the concentration profiles is not very important. So one could be tempted to neglect chemical activity and use solely the Nernst-Planck model, keeping in mind that there is just a slight error in doing so. But as shown on figure 3.18, the effect of chemical activity coefficients is very important from the potential point of view. The total membrane potential is two times larger when considering the chemical activity, so it is not to be neglected.

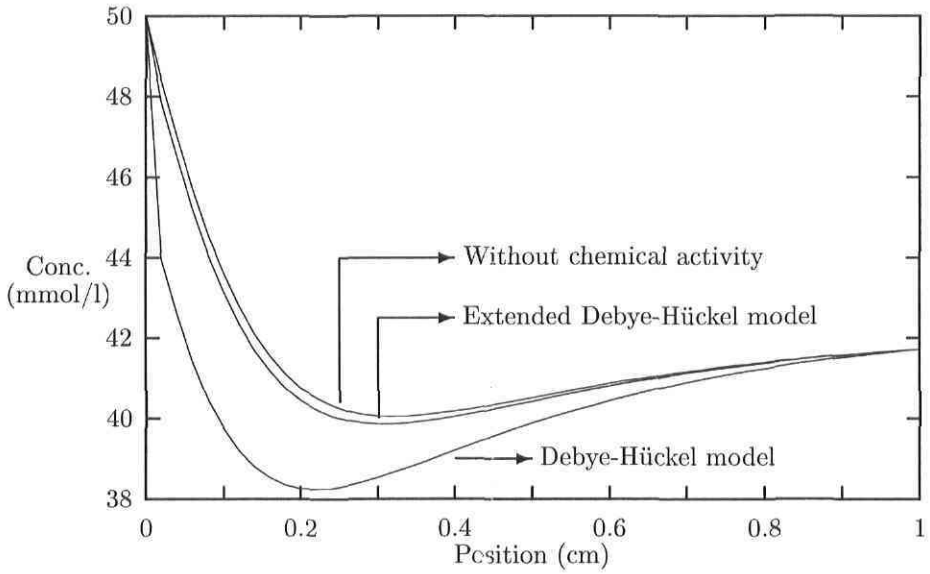

Figure 3.15: SO_4^{2-} profiles with different models for the high concentration case.

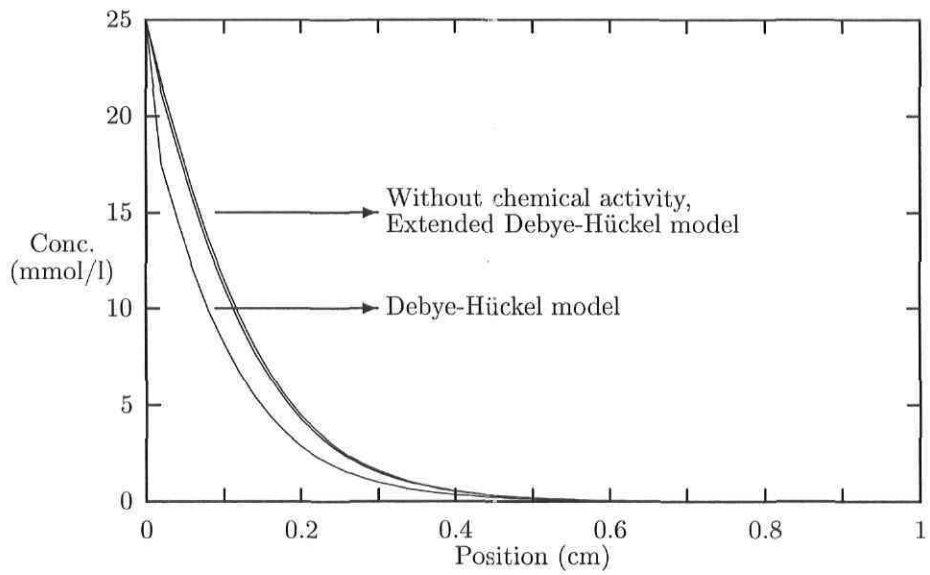

Figure 3.16: Mg^{2+} profiles with different models for the high concentration case.

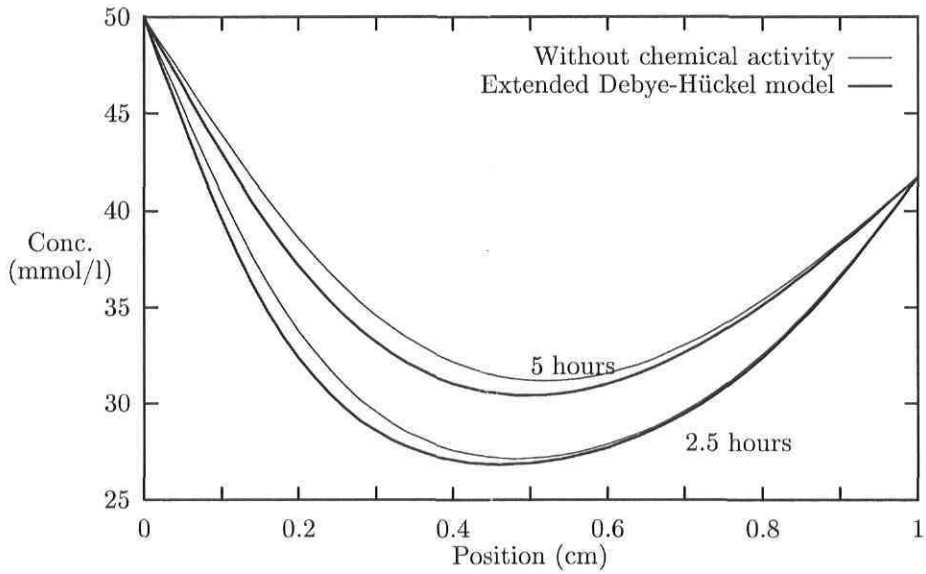

Figure 3.17: SO_4^{2-} profiles for the non-stationnary case.

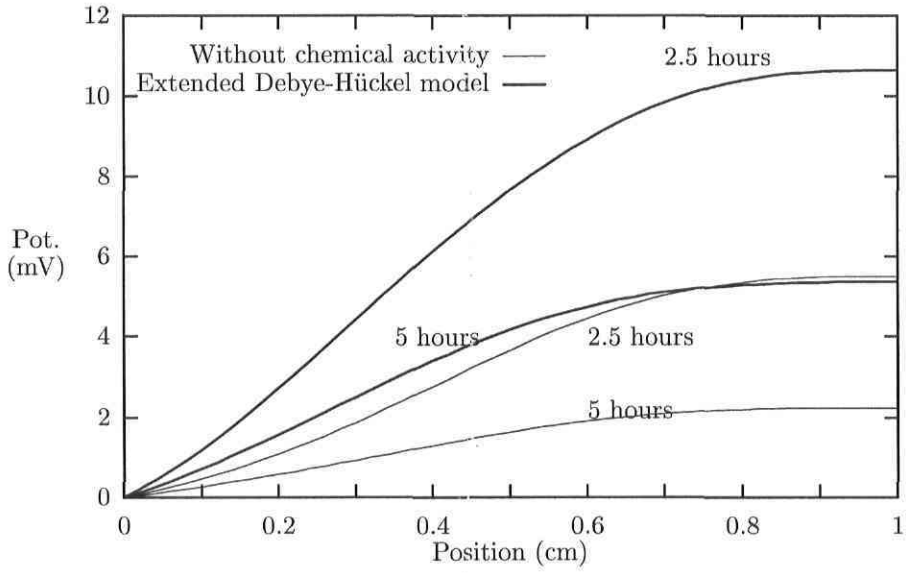

Figure 3.18: Electrical potential profiles for the non-stationnary case.

3.3.5 Conclusion

The numerical model presented in this paper is a very powerful tool. It allows to calculate the concentration and potential profiles for very complex transport cases while considering the chemical activity and without having to make *a priori* assumptions such as electroneutrality or null current. There is no limitation in the number of ions considered, nor there is a restriction on the valence number of those species. Furthermore, the 1D model presented in this paper can easily extended to 2D cases. Finally, various equations to calculate the chemical activity coefficients can be implemented in the numerical code.

3.4 Modeling the transport of ions in unsaturated cement-based materials

E. Samson[12], J. Marchand[12]

[1]Centre de recherche interuniversitaire sur le béton,
Université Laval, Québec, Canada, G1K 7P4

[2]SIMCO Technologies inc.,
1400, boul. du Parc Technologique, Québec, Canada, G1P 4R7

Abstract

This paper gives the details of a multiionic transport model intended to describe the degradation of cement-based materials exposed to aggressive environments. The main algorithm is based on an operator splitting approach. The first part of the calculations is dedicated to solving the transport equations without considering the chemical reactions. The concentration profile of each ionic species is calculated by taking into account diffusion, electrical coupling between the ions, chemical activity effects and advection caused by a capillary suction flow. In the second part, a chemical code corrects the concentration profiles to enforce the equilibrium between the pore solution and the various solid phases of an hydrated cement paste. The model is compared to experimental results of hydrated cement pastes exposed to

pure water and sodium sulfate solutions. Long term simulations were also performed to analyze the behavior of the algorithm.

3.4.1 Introduction

Concrete and other cementitious materials are very reactive media that may be significantly altered from the contact with an aggressive environment. These materials are made of three main phases in equilibrium: aqueous, solid, and gaseous. The aqueous phase, occupying a portion of the porous space, is a highly charged ionic solution containing mainly the following species: OH^-, Na^+, K^+, $SO_4^{2-}$and Ca^{2+}. The solid phase is a composite mixture of ill-crystallized hydrated calcium silicates (C-S-H) and other crystalline phases like portlandite ($Ca(OH)_2$). The aqueous and solid phases are in equilibrium; when the pore solution is disturbed, an amount of one or more solid phases will be either dissolved or precipitated in order to reach back the equilibrium state. The solid phase can also incorporate aggregates of different sizes. These aggregates are generally much less reactive than the hydrated cement paste. Consequently, their effect on the equilibrium between the paste and the aqueous solution is neglected.

The gaseous phase is a mixture of dry air and water vapor. It contains no ions. Upon drying of the materials, the pressure difference between the gaseous and the aqueous phase, called the capillary pressure, will give rise to capillary suction. The resulting movement of water will result in an advection effect on the ions of the pore solution.

The previous description could be applied to most porous materials. What distinguishes cement-based materials is first and foremost the high level of concentration of the ions in the pore solution, which means that the electrical coupling between the ions and chemical activity effects can hardly be neglected. Furthermore, it was already mentionned that the solid phase is very reactive; some phases are very soluble. Consequently, the sustained contact of a concrete structure with water can lead to a fast deterioration of the material, caused by the leaching of the ions in the pore solution. Also, the presence of aluminum in the hydrated cement paste combined with the continuous penetration of external ions like sulfate or chloride will result in the precipitation of aluminum-based solid phases that can be very detrimental to structures during their service-life.

This paper presents a multiionic transport model in unsaturated materials dedicated specifically to cementitious materials. Beside accounting for the classical Fick's diffusion mechanism, it also considers the electrical coupling between the various ions as well as chemical activity effects. Furthermore, as mentioned earlier, the advection phenomenon due to capillary suction is also considered. Finally, several chemical reactions typical to cement-based materials are taken into account.

The model was written under the hypothesis of a constant temperature. The solid phase is assumed non-deformable. External mechanical forces are thus not considered. Hydration of the cement is not considered in the calculations. It implies that the composition of the hydrated cement paste provided to the model as an input parameter will only change through time as a result of chemical reactions caused by the external environment. Finally, the hydrated products forming the solid skeleton are assumed to be uniformly distributed throughout the material. The model is presented for the 1D case. All exemples presented in the paper are related to external sulfate attack or calcium and hydroxide leaching.

3.4.2 Transport model

To model the transport of ions occuring in the liquid (aqueous) phase, the equations were first written at the microscopic scale. They were then integrated over a Representative Elementary Volume (REV, see Figure 3.19) using the homogeneization (averaging) technique, to yield the equations at the macroscopic scale. Details of this technique can be found in references [18, 156].

The macroscopic equation for the transport of ionic species i is based on the extended Nernst-Planck equation with an advection term [85]. Once integrated over the REV, it gives: [162]

$$\frac{\partial\left(\theta_s c_i^s\right)}{\partial t} + \frac{\partial(\theta c_i)}{\partial t} - \frac{\partial}{\partial x}\Bigg(\underbrace{\theta D_i \frac{\partial c_i}{\partial x}}_{\text{diffusion}} + \underbrace{\theta \frac{D_i z_i F}{RT} c_i \frac{\partial \psi}{\partial x}}_{\text{electrical coupling}} + \underbrace{\theta D_i c_i \frac{\partial \ln \gamma_i}{\partial x}}_{\text{chemical activity}} - \underbrace{c_i V_x}_{\text{advection}}\Bigg) + \theta r_i = 0 \quad (3.90)$$

where c_i is the concentration of the species i in solution, c_i^s is the concentration in solid phase, θ_s is the volumetric solid content, θ is the volumetric water content, D_i is the

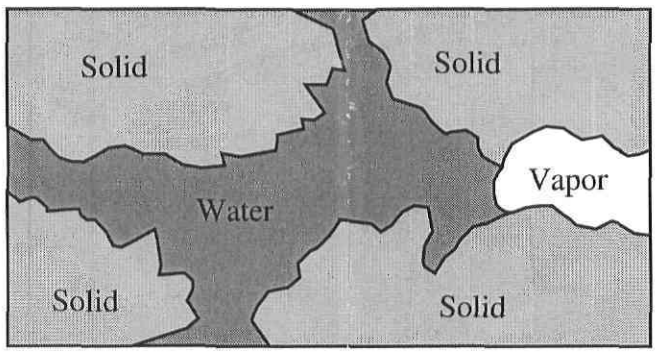

Figure 3.19: The Representative Elementary Volume

diffusion coefficient, z_i is the valence number of the species, F is the Faraday constant, R is the ideal gas constant, T is the temperature of the material, ψ is the electrical potential, γ_i is the chemical activity coefficient, V_x is the average velocity of the fluid in the pore system under the action of capillary suction, and r_i is a source/sink term accounting for the creation of the ion i in solution as a result of chemical reactions.

This equation is very different from the classical diffusion model where only the term bearing the "diffusion" label in equation (3.90) usually appears. This term models the movement of the ions as a result of their thermal agitation. It is best known as Fick's law.

But ions in solution bears electrical charges. As ions have different drifting velocities, the fastest ions tends to separate from the slower ones. However, since charges of opposite signs mutually attract each other, the faster ions are slowed down and the slowest ones are accelerated, in order to bring the system near the electroneutral state. This creates an electrical potential ψ in the material. This term is labeled "electrical coupling" in equation (3.90). Measurements of diffusion potential in cemetitious materials were performed by Zhang and Buenfeld [210]. To take this potential into account, Poisson's equation is added to the model [85]. It is given here after being averaged over the REV [156]:

$$\tau \frac{d}{dx}\left(\theta \frac{d\psi}{dx}\right) + \frac{F}{\epsilon}\,\theta\left(\sum_{i=1}^{N} z_i c_i\right) = 0 \tag{3.91}$$

where τ is the tortuosity of the porous network, ϵ is the dielectric permittivity of the solution and N is the total number of ionic species. The validity of this equation is

based on the assumption that the electromagnetic signal travels much more rapidly than ions in solutions. This allows to consider an equation from electrostatics in a transient problems. The dielectric permittivity of pure water is considered in the calculations.

The next term in equation (3.90) that differs from a classical diffusion model is related to chemical activity. To calculate the chemical activity coefficients γ_is, several models are available. However, well-known models such as Debye-Hückel or Davies [133] are not adapted to the specific case of cementitious materials, which bear a highly charged pore solution. A modification of Davies' relationship was found to yield good results [155]:

$$\ln \gamma_i = -\frac{Az_i^2\sqrt{I}}{1 + a_i B\sqrt{I}} + \frac{(0.2 - 4.17 \times 10^{-5}\, I)Az_i^2 I}{\sqrt{1000}} \tag{3.92}$$

where I is the ionic strength of the solution:

$$I = \frac{1}{2}\sum_{i=1}^{N} z_i^2 c_i \tag{3.93}$$

calculated in mmol/L. In equation (3.92), A and B are temperature dependant parameters, given by:

$$A = \frac{\sqrt{2}\, F^2 e_o}{8\pi(\epsilon RT)^{3/2}} \tag{3.94}$$

$$B = \sqrt{\frac{2F^2}{\epsilon RT}} \tag{3.95}$$

where e_o is the electrical charge of one electron, $\epsilon = \epsilon_r \epsilon_o$ is the permittivity of the medium, given by the dielectric constant times the permittivity of the vacuum. Finally, the parameter a_i in equation (3.92) depends on the ionic species. Its value is 3×10^{-10} for OH^-, 3×10^{-10} for Na^+, 3.3×10^{-10} for K^+, 1×10^{-10} for SO_4^{2-}, 2×10^{-10} for Cl^- and 1×10^{-13} for Ca^{2+}[155].

Modeling of the movement of water in the pore network under the effect of capillary suction is performed with Richard's equation [162, 44, 202]. This equation is developed under the following main assumptions: isothermal conditions, isotropic material, non-deformable solid matrix, negligible gravitational effect, and water movement slow enough to have equilibrium between the liquid and the gaseous phase. The equation is given by:

$$\frac{\partial \theta}{\partial t} - \frac{\partial}{\partial x}\left(D_\theta \frac{\partial \theta}{\partial x}\right) = 0 \tag{3.96}$$

where D_θ is the moisture diffusivity coefficient. It is the sum of the diffusivity coefficient of vapor and water. An expression is also needed for the average speed of the liquid phase, which appears in equation (3.90). It is given [44] by:

$$V_x = -D_L \frac{\partial \theta}{\partial x} \tag{3.97}$$

where D_L is the water diffusivity coefficient. Equation (3.97) allows to transform equation (3.90) as:

$$\frac{\partial(\theta_s c_i^s)}{\partial t} + \frac{\partial(\theta c_i)}{\partial t} - \frac{\partial}{\partial x}\left(\theta D_i \frac{\partial c_i}{\partial x} + \theta \frac{D_i z_i F}{RT} c_i \frac{\partial \psi}{\partial x} + \theta D_i c_i \frac{\partial \ln \gamma_i}{\partial x} + D_L c_i \frac{\partial \theta}{\partial x}\right) + \theta r_i = 0 \tag{3.98}$$

There are two terms remaining in the model that need to be discussed. The first one on the left hand side of equation (3.98) involves c_i^s, the concentration of species i in solid phase. This term is used to describe the exchange between the solid and the aqueous phase [18]. The other term is r_i, which is a source/sink term in the aqueous to model the creation or removal of ion i. They will be considered in the next section.

3.4.3 Modeling the chemical reactions

There are several types of chemical reactions (see reference [149] for a comprehensive review). The homogeneous reactions are those occuring solely in the aqueous phase, like the formation or the dissociation of acids. The heterogeneous reactions involves more than one phase, like the solid and aqueous ones, for example. They can be divided in two groups: surface and classical reactions. The surface reactions occur at the solid/liquid interface. Adsorption of ions, i.e. the capture of ions by the surface of the solid as a result of electrostatic forces, falls in this category. Finally the dissolution/precipitation reactions are part of the classical category. Dissolution and/or precipitation occur when a solid is no longer in equilibrium with the solution with which it is in contact. If the activity product of the ions in solution involved in the reaction is above the equilibrium constant, some of the ions will precipitate in order to reach equilibrium. In the inverse situation, dissolution will occur. In equation (3.98), the term $\partial(\theta_s c_i^s)/\partial t$ corresponds to heterogeneous chemical reactions whereas the term r_i corresponds to homogeneous ones.

Different techniques have been used to include chemical reactions in ionic transport problems. In early models (see for instance Miller and Benson [127]) the equations that model the chemical reactions were solved simultaneously with the transport relationships. The current trend in reactive transport modeling is to split the transport part of the process from the chemical reactions. This method gained a lot of popularity after the publication of a paper by Yeh and Tripathi in 1989 [207] which showed that important CPU times could be saved by using such an uncoupled approach. Models by Grove and Wood [73], Yeh and Tripathi [208], Walter et al. [198] and Xu et al. [206] are all based on this operator splitting approach.

The operator splitting approach is divided in two main classes. First, it is possible to iterate between the transport and chemical reaction set of equations within a time step until convergence is reached. This is called the sequential iterative approach (SIA). Another algorithm consists in solving the transport and chemical reaction part of the model without iterations between these two modules. It is called the sequential non iterative approach (SNIA). The papers cited previously [73, 208, 198, 206] are all based on the SNIA.

The operator splitting procedure introduces a numerical error in the resolution of a reactive transport problem. Systematic analyses were performed on simple models to evaluate this error. Herzer and Kinzelbach [87] studied the equation:

$$\left(\frac{\theta_s}{\phi}k_d + 1\right)\frac{\partial c}{\partial t} - D\frac{\partial^2 c}{\partial x^2} + v\frac{\partial c}{\partial x} = 0 \tag{3.99}$$

where θ_s is the solid volumetric constant, ϕ is the porosity, c is the concentration, D is the diffusion coefficient, v is the fluid velocity and k_d relates c and the concentration c_s in solid phase: $c_s = k_d c$. The difference between the exact solution and the solution calculated by separating transport and chemistry is given by:

$$\text{err} = \frac{(R-1)}{R}\frac{v\Delta t}{2} \tag{3.100}$$

where $R = 1 + k_d\theta_s/\phi$ and Δt is the time step. The error is thus proportional to Δt and tends to zero as the time step is decreased. Valocchi and Malmstead [193] studied the equation:

$$\frac{\partial c}{\partial t} - D\frac{\partial^2 c}{\partial x^2} + v\frac{\partial c}{\partial x} + kc = 0 \tag{3.101}$$

where k characterizes a radioactive decay process. The numerical error introduced in

Table 3.2: Analysis of the accuracy of the operator splitting scheme on various simple models (from reference [17]).

Case	Model	Accuracy	Notes
A	$\dot{s} = g, \quad k = 0,\ r = 0$	$O(\Delta t^2)$	
B	$\dot{s} = kc,\ r = 0,\ g = 0$	$O(\Delta t)$	
		$O(\Delta t^2)$	homog. bound. conditions
C	$\dot{s} = r\left[(R-1)c - s\right],\ g = 0,$ $k = r(R-1)$	$O(\Delta t)$	
D	$s = (R-1)c,\ r \to \infty$ in case C	$O(\Delta t)$	
		$O(\Delta t^2)$	homog. bound. conditions

the solution due to operator splitting is given by:

$$\text{err} = c_o v \left(\frac{1}{k}(1 - e^{-k\Delta t}) - \Delta t\ e^{-k\Delta t} \right) \tag{3.102}$$

where c_o is related to the flux boundary condition as: $(vc - Dc_{,x})|_{x=0} = vc_o$. Again, the error goes to zero as the time step is reduced. Kaluarachchi and Morshed [94] studied the same case as Valocchi and Malmstead but with the following boundary condition:

$$\left(-\frac{D}{vL}\frac{\partial c}{\partial x} + c \right)_{x=0} = e^{-\lambda t} \tag{3.103}$$

where $\lambda = 0$ and $\lambda \to \infty$ correspond to continuous and pulse boundary conditions, respectively. The conclusions are the same, the error being reduced as Δt is reduced. Barry et al. [17] studied the more general case:

$$\frac{\partial c}{\partial t} + \frac{\partial s}{\partial t} - D\frac{\partial^2 c}{\partial x^2} + v\frac{\partial c}{\partial x} = 0 \quad \text{with} \quad \frac{\partial s}{\partial t} = kc - rs + g \tag{3.104}$$

with both homogeneous and inhomogeneous boundary conditions. The results are summarized in Table 3.2. The results are in agreement with those presented previously. Except for the unusual homogeneous boundary condition case, the error introduced by the operator splitting procedure is of the order of the time step value.

Reducing the time step leads to an increase in calculation time. On the opposite, the SIA does not require time steps as small as in the SNIA, because the iterations between

transport and chemistry reduce the splitting error [87]. But iterations within a time step increase CPU time. Walter et al. [198] studied both approaches to determined which is the most efficient. They modeled a test-case that illustrates the controlling geochemical processes occuring in a carbonate aquifer under the impact of acidic mine tailings effluent. Simulations were performed with both SIA and SNIA algorithms. They involved complexation, dissolution/precipitation, redox and gas exchange chemical reactions. The various profiles calculated with both algorithms showed less than a 2% difference in position, calculated with regard to the position of the source of contaminant. However, the CPU load was 3.5 times more important for the SIA model. Following these results, we chose to work with the SNIA algorithm.

The transport model considered in references [73, 208, 198, 206] is a simplified version of equation (3.98). It assumes that the fluid flow is strong enough to neglect diffusion to the profit of dispersion effects (see reference [18]). Other phenomena like electrical coupling between the ions and chemical activity (see equation 3.98) are also neglected, which leaves the linear transport operator:

$$L(c_i) = -\mathbf{D}\mathrm{grad}(c_i) + c_i\mathbf{v} \tag{3.105}$$

where $\mathbf{D}$ is the dispersion tensor and $\mathbf{v}$ is the fluid velocity, both independant on the ionic species i. This allows to rewrite the transport equations in order to eliminate the terms r_i (this topic is discussed in paper [159]). Accordingly the treatment of homogeneous reactions is greatly simplified. These simplifications are common to almost all ionic transport models applied to geochemical processes.

Such simplifications are not possible for a nonlinear transport model like equation (3.98), which complicates the chemical reaction modeling. However, heterogeneous reactions are more important than homogeneous one in cementitious materials. For example the penetration of sulfate ions may lead to the formation of ettringite and gypsum in concrete in such a quantity that the materials sustains physical damage. Portlandite, which occupies more than 5% of the total volume of the material, is highly soluble; its rapid dissolution can have important effect on the overall strength of a concrete structure. Accordingly, the homogeneous reactions are neglected in the present model, which allows to eliminate the term r_i from equation (3.98). Only dissolution/precipitation reactions will be considered.

Table 3.3: Solid phases in hydrated cement

Name	Chemical formula	Expression for equilibrium	Value of equilibrium constant (*-log Ksp*)
Portlandite	$Ca(OH)_2$	$Ksp = \{Ca\}\{OH\}^2$	5.2
C-S-H	$1.65CaO.SiO_2.(2.45)H_2O$ †	$Ksp = \{Ca\}\{OH\}^2$ ‡	6.2 ‡
Ettringite	$3CaO.Al_2O_3.3CaSO_4.32H_2O$	$Ksp = \{Ca\}^6\{OH\}^4\{SO_4\}^3\{Al(OH)_4\}^2$	44.0
Monosulfates	$3CaO.Al_2O_3.CaSO_4.12H_2O$	$Ksp = \{Ca\}^4\{OH\}^4\{SO_4\}\{Al(OH)_4\}^2$	29.1
Gypsum	$CaSO_4.2H_2O$	$Ksp = \{Ca\}\{SO_4\}$	4.6
Mirabilite	$Na_2SO_4.10H_2O$	$Ksp = \{Na\}^2\{SO_4\}$	1.2

$\{\dots\}$ indicates chemical activity

† The C-S-H is considered having a C/S ratio of 1.65

‡ The C-S-H decalcification is modeled as the portlandite dissolution with a lower solubility

Within the framework of the SNIA algorithm, the term involving c_i^s is removed from equation (3.98), which leave the following equation to solve during the transport step:

$$\frac{\partial(\theta c_i)}{\partial t} - \frac{\partial}{\partial x}\left(\theta D_i \frac{\partial c_i}{\partial x} + \theta \frac{D_i z_i F}{RT} c_i \frac{\partial \psi}{\partial x} + \theta D_i c_i \frac{\partial \ln \gamma_i}{\partial x} + D_L c_i \frac{\partial \theta}{\partial x}\right) = 0 \qquad (3.106)$$

This equation still has to be coupled to equations (3.91) and (3.96). The transport part of the process is thus closed. The unknows are ψ, θ, and N times c_i, i.e. a concentration for each ionic species taken into account. There is accordingly N equations (3.106), one for each ionic species, equation (3.91) to solve the electrical potential and equation (3.96) for the water content. The other parameters are either physical constants, like T, F, R, z_i, e_o, ϵ, or material parameters that have to be determined experimentally: D_i, τ, D_θ, D_L. At the end of this calculation step, ionic profiles are known for each ionic species.

After the transport step, the concentrations may not be in equilibrium with the solids. They will be corrected in the chemical reaction step, by adjusting the solid phases properly. This is achieved by enforcing the algebraic relationship describing the equilibrium state of each solid phase present at a given location. This relationship is written in a general form as [206]:

$$K_m = \prod_{i=1}^{N} c_i^{\nu_{mi}} \gamma_j^{\nu_{mi}} \qquad \text{with} \quad m = 1, \dots, M \qquad (3.107)$$

where M is the number of solid phases, N is the number of ions, K_m is the equilibrium constant (or solubility constant) of the solid m, c_i is the concentration of the ionic species i, γ_i is its chemical activity coefficient, and ν_{mi} is the stoichiometric coefficient of the ith ionic species in the mth mineral. The right-hand side of equation (3.107) is called the ion activity product.

To illustrate the chemical modeling, we consider a problem where portlandite (CH), ettringite (AFt) and gypsum (G) are involved (see Table 3.3). The chemical equilibrium equation for each solid is:

$$K_{\mathrm{CH}} = \gamma_{\mathrm{Ca}}\gamma_{\mathrm{OH}}^{2}[\mathrm{Ca}][\mathrm{OH}]^{2} \tag{3.108}$$

$$K_{\mathrm{AFt}} = \gamma_{\mathrm{Ca}}^{6}\gamma_{\mathrm{OH}}^{4}\gamma_{\mathrm{SO4}}^{3}\gamma_{\mathrm{Al(OH)4}}^{2}[\mathrm{Ca}]^{6}[\mathrm{OH}]^{4}[\mathrm{SO_4}]^{3}[\mathrm{Al(OH)_4}]^{2} \tag{3.109}$$

$$K_{\mathrm{G}} = \gamma_{\mathrm{Ca}}\gamma_{\mathrm{SO_4}}[\mathrm{Ca}][\mathrm{SO_4}] \tag{3.110}$$

where the square brackets represent the concentrations. If the concentrations in solution do not respect the equilibrium equations (3.108) to (3.110), solids will either be dissolved or precipitated until these algebraic relationships are satisfied. Let's assume that the concentrations c_i^o (e.g. $[\mathrm{Ca}^o]$, $[\mathrm{OH}^o]$, $[\mathrm{SO}_4^o]$, $[\mathrm{Al(OH)}_4^o]$) are the output of the previous tranport calculation step and do not respect equilibrium. The equilibrium concentrations can be expressed as:

$$c_i = c_i^o + \sum_{m=1}^{M} \nu_{mi} X_m \tag{3.111}$$

where the X_ms represent the amount of a given solid that has to dissolve in order to reach the equilibrium state. Following this, the system of equations (3.108) to (3.110) is rewritten as:

$$K_{\mathrm{CH}} = \gamma_{\mathrm{Ca}}\gamma_{\mathrm{OH}}^{2}[\mathrm{Ca}^o + X_{\mathrm{CH}} + 6X_{\mathrm{AFt}} + X_{\mathrm{G}}][\mathrm{OH}^o + 2X_{\mathrm{CH}} + 4X_{\mathrm{AFt}}]^{2} \tag{3.112}$$

$$\begin{aligned} K_{\mathrm{AFt}} = {} & \gamma_{\mathrm{Ca}}^{6}\gamma_{\mathrm{OH}}^{4}\gamma_{\mathrm{SO4}}^{3}\gamma_{\mathrm{Al(OH)4}}^{2}[\mathrm{Ca}^o + X_{\mathrm{CH}} + 6X_{\mathrm{AFt}} + X_{\mathrm{G}}]^{6} \\ & \times [\mathrm{OH}^o + X_{\mathrm{CH}} + 4X_{\mathrm{AFt}}]^{4}[\mathrm{SO}_4^o + X_{\mathrm{G}} + 3X_{\mathrm{AFt}}]^{3}[\mathrm{Al(OH)}_4^o + 2X_{\mathrm{AFt}}]^{2} \end{aligned} \tag{3.113}$$

$$K_{\mathrm{G}} = \gamma_{\mathrm{Ca}}\gamma_{\mathrm{SO_4}}[\mathrm{Ca}^o + X_{\mathrm{CH}} + 6X_{\mathrm{AFt}} + X_{\mathrm{G}}][\mathrm{SO}_4^o + X_{\mathrm{G}} + 3X_{\mathrm{AFt}}] \tag{3.114}$$

This nonlinear system of equations is solved for the X_ms. Following the convention adopted previously, a positive X_m means dissolution and a negative one indicates the precipitation of solid m. At the end of the chemical equilibrium calculation, each solid phase S is adjusted according to the following relationship:

$$S_m^t = S_m^{t-1} - \theta X_m \Gamma_m / \rho \quad \text{with} \quad m = 1, \ldots, M \tag{3.115}$$

where S_m is the amount of a given solid phase (in g/kg of material), t indicates the time step, Γ_m is the molar mass of the solid m and ρ is the density of the material. The

ionic concentrations are also adjusted following the chemical equilibrium calculation, according to equation (3.111).

The solids considered in this paper are listed in Table 3.3, along with their equilibrium constant. They are portlandite, C-S-H, ettringite, monosulfates, gypsum and mirabilite. The C-S-H is treated in a particular way. This solid phase exhibits an incongruent behavior [23], which means that the dissolution rate of the ions composing this mineral does not follow the stoichiometric coefficient. As a consequence, the composition of the C-S-H varies as the dissolution progresses. According to reference [23], the calcium to silicate ratio of the C-S-H (C/S) starts at about 1.65 in the sound hydrated cement paste and decreases as calcium is lost. Berner modeled the incongruent behavior of the C-S-H by assuming that it is composed of two different solids, $Ca(OH)_2$ and CaH_2SiO_4, each having its own equilibrium constant that depends on the C/S ratio. The part associated to portlandite dissolves first. The remaining CaH_2SiO_4 dissolves very slowly [23]. Studies have shown that C-S-H exposed to pure water for a long time keeps a C/S ratio between 0.8 and one in the decalcified zone [86]. Considering this, we model the dissolution of C-S-H by considering only the $Ca(OH)_2$ part. Berner's approach is further simplified by assuming that this fraction of the C-S-H dissolves with a constant equilibrium value. Its value is an average of the solubility constant of $Ca(OH)_2$ at C/S=1.65 and C/S=1.0. It is given in Table 3.3.

The chemical reactions, beside capturing or releasing ions as solid phases are precipitated or dissolved, will have an effect on the transport properties by affecting the porosity of the material. If for example gypsum is formed at some location, the local porosity will decrease, thus reducing the area across which ions are able to diffuse. This will reflect on their diffusion coefficient. This effect can be taken into account if a relationship between the diffusion coefficient and the porosity is known. In the present paper, the following relationship is used:

$$D_{\mathrm{OH}} = 4.83\times10^{-10}\phi_{\mathrm{paste}} - 7.79\times10^{-11} \tag{3.116}$$

where ϕ_{paste} is the total porosity of the paste in the cementitious material and D_{OH} is the diffusion coefficient of the OH^- ion. Equation (3.116) was obtained from migration tests (see reference [161] for details on this test method) made on various cementitious materials made with ASTM Type 10 cement at different water to cement ratio. The total porosity of each sample was evaluated from the ASTM C642 procedure and

converted to a paste porosity by dividing by the paste volume of the mixture. Upon chemical modification to the material, the porosity of the paste is calculated as:

$$\phi_{\text{paste}} = \phi_{\text{paste}}^{\text{init}} + \sum_{m=1}^{M} (V_{\text{m}}^{\text{init}} - V_{\text{m}}) \tag{3.117}$$

where V_s is the volume of a given solid phase, per unit volume of cement paste, and M is the total number of solid phases. Based on this model, the correction factor G that multiplies the diffusion coefficients D_i of each ionic species is calculated as follow :

$$G = \frac{D_{\text{OH}}^{\text{Damaged paste}}}{D_{\text{OH}}^{\text{Initial paste}}} \tag{3.118}$$

3.4.4 Numerical model

This section is divided in two parts. First, the numerical algorithm for the transport model, i.e. equations (3.106), (3.91) and (3.96), is presented. Then, the details on the resolution of the equilibrium problem in the chemical part of the model are given.

The numerical algorithms for the Nernst-Planck/Poisson model, i.e. the diffusion of ions taking into account the electrical coupling but not the chemical activity nor the capillary suction, has already been studied [157]. The authors tested two algorithms using the finite element method. The first one, with the equations uncoupled and solved by succesive iterations, was found to converge only for very small concentrations. This algorithm is not suitable for cement-based materials since their porous network is filled with an highly charged aqueous solution. In the other algorithm, equations were solved simultaneously with the Newton-Raphson method. The results in this case were not limited to a given concentration level. The same algorithm was later used to solve the extended Nernst-Planck model [158], which takes into account chemical activity gradients. Following these results, the coupled algorithm will be used with the current model, which adds a convection term to the extended Nernst-Planck equation. Numerical tests will be performed to assess the validity of this approach.

To ease the writing, the numerical model will be shown for a two ion case in 1D. But the model can easily be extended to take into account more species. The numerical examples that will be presented later involve six ions.

The weighted residual form of the set of equations (3.106), (3.91) and (3.96), upon integration by parts, is given as:

$$
\begin{aligned}
W = \int_L \langle \delta\Psi \rangle & \begin{bmatrix} \theta & 0 & c_1 & 0 \\ 0 & \theta & c_2 & 0 \\ 0 & 0 & 1 & 0 \\ 0 & 0 & 0 & 0 \end{bmatrix} \begin{Bmatrix} \dot{c_1} \\ \dot{c_2} \\ \dot{\theta} \\ \dot{\psi} \end{Bmatrix} dx \\
& + \int_L \left\langle \frac{\partial \delta\Psi}{\partial x} \right\rangle \begin{bmatrix} G\theta D_1 & 0 & D_L c_1 & \frac{D_1 z_1 F}{RT}\theta c_1 \\ 0 & G\theta D_2 & D_L c_2 & \frac{D_2 z_2 F}{RT}\theta c_2 \\ 0 & 0 & D_\theta & 0 \\ 0 & 0 & 0 & \theta\tau \end{bmatrix} \begin{Bmatrix} c_{1,x} \\ c_{2,x} \\ \theta_{,x} \\ \psi_{,x} \end{Bmatrix} dx \\
& + \int_L \left\langle \frac{\partial \delta\Psi}{\partial x} \right\rangle \begin{bmatrix} \theta D_1 \frac{\partial(\ln \gamma_1)}{\partial x} & 0 & 0 & 0 \\ 0 & \theta D_2 \frac{\partial(\ln \gamma_2)}{\partial x} & 0 & 0 \\ 0 & 0 & 0 & 0 \\ 0 & 0 & 0 & 0 \end{bmatrix} \begin{Bmatrix} c_1 \\ c_2 \\ \theta \\ \psi \end{Bmatrix} dx \\
& + \int_L \langle \delta\Psi \rangle \begin{bmatrix} 0 & 0 & 0 & 0 \\ 0 & 0 & 0 & 0 \\ 0 & 0 & 0 & 0 \\ -\frac{F}{\epsilon} z_1 \theta & -\frac{F}{\epsilon} z_2 \theta & 0 & 0 \end{bmatrix} \begin{Bmatrix} c_1 \\ c_2 \\ \theta \\ \psi \end{Bmatrix} dx + W^{\text{ext}} = 0
\end{aligned} \tag{3.119}
$$

where W^{ext} includes the boundary integrals associated to the flux boundary conditions and $\langle \delta\Psi \rangle$ is the vector of the weighting function, defined as:

$$
\langle \delta\Psi \rangle \equiv \langle \delta_{c1} \; \delta_{c2} \; \delta\theta \; \delta\psi \rangle \tag{3.120}
$$

The correction factor G is directly included in formulation (3.119). It is calculated with the solid phases evaluated at the previous time step.

The weak form is discretized using the Galerkin method with a standard linear two-nodes element (see reference [142] for a complete text on the method). The approximation of the solution on each element is written as :

$$
\begin{Bmatrix} c_1 \\ c_2 \\ \theta \\ \psi \end{Bmatrix} = [N]\{U_n\} \tag{3.121}
$$

$$[N] = \begin{bmatrix} N_1 & 0 & 0 & 0 & N_2 & 0 & 0 & 0 \\ 0 & N_1 & 0 & 0 & 0 & N_2 & 0 & 0 \\ 0 & 0 & N_1 & 0 & 0 & 0 & N_2 & 0 \\ 0 & 0 & 0 & N_1 & 0 & 0 & 0 & N_2 \end{bmatrix} \tag{3.122}$$

$$\langle U_n \rangle = \langle c_{11}\ c_{21}\ \theta_1\ \psi_1\ c_{12}\ c_{22}\ \theta_2\ \psi_2 \rangle \tag{3.123}$$

where N_1 and N_2 are the shape functions. The subscripts i and j for the concentrations in the vector $\langle U_n \rangle$ (equation 3.123) designate the species i at the node j of one element. The elementary matrices are thus expressed as :

$$[K^e] = \int_{l^e} \Big([B]^T [D_1][B] + [B]^T [D_2][N] + [N]^T [D_3][N] \Big)\, dx \tag{3.124}$$

$$[M^e] = \int_{l^e} [N]^T [C][N]\, dx \tag{3.125}$$

with

$$[B] = \begin{bmatrix} N_{1,x} & 0 & 0 & 0 & N_{2,x} & 0 & 0 & 0 \\ 0 & N_{1,x} & 0 & 0 & 0 & N_{2,x} & 0 & 0 \\ 0 & 0 & N_{1,x} & 0 & 0 & 0 & N_{2,x} & 0 \\ 0 & 0 & 0 & N_{1,x} & 0 & 0 & 0 & N_{2,x} \end{bmatrix} \tag{3.126}$$

$$[D_1] = \begin{bmatrix} \theta D_1 & 0 & D_L c_1 & \frac{D_1 z_1 F}{RT} \theta c_1 \\ 0 & \theta D_2 & D_L c_2 & \frac{D_2 z_2 F}{RT} \theta c_2 \\ 0 & 0 & D_\theta & 0 \\ 0 & 0 & 0 & \theta \tau \end{bmatrix} \tag{3.127}$$

$$[D_2] = \begin{bmatrix} \theta D_1 \frac{\partial(\ln \gamma_1)}{\partial x} & 0 & 0 & 0 \\ 0 & \theta D_2 \frac{\partial(\ln \gamma_2)}{\partial x} & 0 & 0 \\ 0 & 0 & 0 & 0 \\ 0 & 0 & 0 & 0 \end{bmatrix} \tag{3.128}$$

$$[D_3] = \begin{bmatrix} 0 & 0 & 0 & 0 \\ 0 & 0 & 0 & 0 \\ 0 & 0 & 0 & 0 \\ -\frac{F}{\epsilon} z_1 \theta & -\frac{F}{\epsilon} z_2 \theta & 0 & 0 \end{bmatrix} \tag{3.129}$$

$$[C] = \begin{bmatrix} \theta & 0 & c_1 & 0 \\ 0 & \theta & c_2 & 0 \\ 0 & 0 & 1 & 0 \\ 0 & 0 & 0 & 0 \end{bmatrix} \tag{3.130}$$

The assembly of elementary matrices $[K^e]$ and $[M^e]$ leads to the following system of equations:

$$[M]\{\dot{U}\} + [K]\{U\} = \{F^{\text{ext}}\} \tag{3.131}$$

The time discretization is performed using the implicit Euler scheme:

$$[M_t]\left\{\frac{U_t - U_{t-\Delta t}}{\Delta t}\right\} + [K_t]\{U_t\} = \{F_t^{\text{ext}}\} \tag{3.132}$$

where Δt is the time step. The subscript t stands for the actual time step and $t - \Delta t$ the previous one. Defining the matrices

$$[\bar{K}] = [M_t] + \Delta[K_t] \tag{3.133}$$

$$\{\bar{F}\} = \{F_t^{\text{ext}}\} + [M_t]\{U_{t-\Delta t}\} \tag{3.134}$$

the system of equations can be written as:

$$[\bar{K}]\{U_t\} = \{\bar{F}\} \tag{3.135}$$

This nonlinear system of equations is solved at each time step with the modified Newton-Raphson method. Numerical simulations have shown that the convergence rate with a tangent matrix calculated without the nonlinear terms arising from the coupling between the various variables in the model is almost the same as the one with a complete tangent matrix. However, the calculation time is reduced since less terms need to be calculated. Furthermore, its wider radius of convergence makes this algorithm even more interesting. The elementary tangent matrix is thus given as:

$$[K_T^e] = [M^e] + \Delta t[K^e] \tag{3.136}$$

The elementary matrices in equations (3.124) and (3.125) are evaluated through Gauss numerical integration method. Accordingly, the variables appearing in the matrices $[D_1]$, $[D_2]$, $[D_3]$, and $[C]$ are calculated at the integration points. To calculate the terms $\partial(\ln \gamma_i)/\partial x$ in (3.128), the ionic strength (equation 3.93) is calculated at each nodes. Then the $(\ln \gamma_i)$s are calculated for each species and at each nodes with equation (3.92). The value of $\partial(\ln \gamma_i)/\partial x$ can then be evaluated at every integration points.

After solving the transport equation, the concentrations are used as input in the chemical equilibrium module. The numerical method is illustrated using the nonlinear

system of equations (3.112) to (3.114). Newton's algorithm is used to solve the system of equations:

$$[K_T^{k-1}]\{\Delta X^k\} = -\{R(X^{k-1})\} \tag{3.137}$$

$$X^k = X^{k-1} + \Delta X^k \tag{3.138}$$

where $[K_T]$ is the tangent (or Jacobian) matrix, ΔX is a variation calculated at each iteration, $\{R\}$ is the residual vector, and k indicates the iteration level. The residuals are given by:

$$R_{\mathrm{CH}} = \gamma_{\mathrm{Ca}}\gamma_{\mathrm{OH}}^2[\mathrm{Ca}^o + X_{\mathrm{CH}} + 6X_{\mathrm{AFt}} + X_{\mathrm{G}}][\mathrm{OH}^o + 2X_{\mathrm{CH}} + 4X_{\mathrm{AFt}}]^2 - K_{\mathrm{CH}} \tag{3.139}$$

$$\begin{aligned} R_{\mathrm{AFt}} &= \gamma_{\mathrm{Ca}}^6\gamma_{\mathrm{OH}}^4\gamma_{\mathrm{SO4}}^3\gamma_{\mathrm{Al(OH)4}}^2[\mathrm{Ca}^o + X_{\mathrm{CH}} + 6X_{\mathrm{AFt}} + X_{\mathrm{G}}]^6 \\ &\times [\mathrm{OH}^o + 2X_{\mathrm{CH}} + 4X_{\mathrm{AFt}}]^4[\mathrm{SO}_4^o + X_{\mathrm{G}} + 3X_{\mathrm{AFt}}]^3[\mathrm{Al(OH)}_4^o + 2X_{\mathrm{AFt}}]^2 - K_{\mathrm{AFt}} \end{aligned} \tag{3.140}$$

$$R_{\mathrm{G}} = \gamma_{\mathrm{Ca}}\gamma_{\mathrm{SO_4}}[\mathrm{Ca}^o + X_{\mathrm{CH}} + 6X_{\mathrm{AFt}} + X_{\mathrm{G}}][\mathrm{SO}_4^o + X_{\mathrm{G}} + 3X_{\mathrm{AFt}}] - K_{\mathrm{G}} \tag{3.141}$$

The jacobian matrix is given by:

$$K_T = \begin{bmatrix} \frac{\partial R_{\mathrm{CH}}}{\partial X_{\mathrm{CH}}} & \frac{\partial R_{\mathrm{CH}}}{\partial X_{\mathrm{AFt}}} & \frac{\partial R_{\mathrm{CH}}}{\partial X_{\mathrm{G}}} \\ \frac{\partial R_{\mathrm{AFt}}}{\partial X_{\mathrm{CH}}} & \frac{\partial R_{\mathrm{AFt}}}{\partial X_{\mathrm{AFt}}} & \frac{\partial R_{\mathrm{AFt}}}{\partial X_{\mathrm{G}}} \\ \frac{\partial R_{\mathrm{G}}}{\partial X_{\mathrm{CH}}} & \frac{\partial R_{\mathrm{G}}}{\partial X_{\mathrm{AFt}}} & \frac{\partial R_{\mathrm{G}}}{\partial X_{\mathrm{G}}} \end{bmatrix} \tag{3.142}$$

The calculation of each term in this matrix is made by considering the activity coefficient constant. The latter are updated after each iteration from the updated concentrations (see equation 3.111). For example the term $\frac{\partial R_{\mathrm{CH}}}{\partial X_{\mathrm{CH}}}$ in the Jacobian matrix is given by:

$$\frac{\partial R_{\mathrm{CH}}}{\partial X_{\mathrm{CH}}} = \gamma_{\mathrm{Ca}}\gamma_{\mathrm{OH}}^2\left[\frac{\partial R_{\mathrm{CH}}}{\partial[\mathrm{Ca}]}\frac{\partial[\mathrm{Ca}]}{\partial X_{\mathrm{CH}}} + \frac{\partial R_{\mathrm{CH}}}{\partial[\mathrm{OH}]}\frac{\partial[\mathrm{OH}]}{\partial X_{\mathrm{CH}}}\right] \tag{3.143}$$

where the concentrations [Ca] and [OH] are calculated according to equation (3.111). The calculation of equation (3.143) thus gives:

$$\frac{\partial R_{\mathrm{CH}}}{\partial X_{\mathrm{CH}}} = \gamma_{\mathrm{Ca}}\gamma_{\mathrm{OH}}^2\left[[\mathrm{OH}]^2 + 4[\mathrm{Ca}][\mathrm{OH}]\right] \tag{3.144}$$

All terms in the Jacobian matrix are calculated with values found at the previous iteration level.

The system of equation is solved by iterating over equations (3.137) and (3.138). This calculation procedure is repeated two times. The first time, the chemical equilibrium calculation is made only for solids that are present at a given node. During

Table 3.4: Chemical and mineralogical composition of the CSA Type 10 cement.

Oxide	%	Compound	%
SiO_2	19.78	C_3S	59.3
CaO	62.04	C_2S	12.0
Al_2O_3	4.39	C_3A	6.6
Fe_2O_3	3.00	C_4AF	9.1
SO_3	3.20		
MgO	2.84		
K_2O	0.91		
Na_2O	0.32		
LOI	2.41		

the second step, the calculation is made for solid present at the node and also for the solids for which the ion activity product is greater than the equilibrium constant. This procedure allows to avoid the impossible situation where dissolution of a non-existing solid occurs at a given location.

3.4.5 Experimental validation

Cement pastes were prepared at a water/cement ratio of 0.6 using an ordinary Portland cement (Canadian CSA Type 10). The chemical and mineralogical compositions of the cement are given in Table 3.4. The mixture proportions are listed in Table 3.5. The mixture was prepared using deionized water and without any chemical admixture. It was batched under vacuum (at 10 mbar) to prevent the formation of air void during mixing. It was then cast in plastic cylinders (diameter = 7 cm; height = 20 cm). Molds were sealed and rotated for the first 24 hours to prevent bleeding. Cylinders were then demolded and sealed with an adhesive aluminum foil for at least 12 months at room temperature.

After the hydration period, the cylinders were sawn in disks for testing, in order to determine the different parameters needed for the ionic transport simulations. Prior to testing, the disks were vacuum saturated in a 300 mmol/L NaOH solution during 24

hours.

The porosity of the paste was determined according to the ASTM C642 standard procedure. A value of 52.2% was measured. Since the ionic transport during the validation tests occurs in saturated condition, the water content is assumed constant in the material and has the same value as the porosity.

The pore solution was extracted following the experimental procedure described in reference [16]. It allows to determine the concentration of these ions: OH^-, Na^+, K^+, SO_4^{2-}, and Ca^{2+}. Because of experimental error, the solution did not respect electroneutrality. The concentration in OH^- was adjusted to make sure that the positive and negative charges are equal. The concentration of $Al(OH)_4^-$ is evaluated with the chemical equilibrium code described in the previous section in order to have a solution in equilibrium with portlandite, ettringite and monosulfates.

The ionic diffusion coefficients and tortuosity were determined from migration tests. A complete description of the testing method is given in reference [161]. The test was made on two 20 mm disks. All these measured materials parameters are listed in Table 3.5. They will be used in the numerical simulations to reproduce the tests.

The table also include the initial amount of each solid phase in the material: portlandite (CH), C-S-H, ettringite (AFt) and monosulfates (AFm). It is calculated from the cement composition (CaO, SiO_2, Al_2O_3 and SO_3) by solving the following set of equation:

$$\frac{\Gamma_{\mathrm{Ca}}}{\Gamma_{\mathrm{CH}}}S_{\mathrm{CH}} + 1.65\frac{\Gamma_{\mathrm{Ca}}}{\Gamma_{\mathrm{csh}}}S_{\mathrm{csh}} + 6\frac{\Gamma_{\mathrm{Ca}}}{\Gamma_{\mathrm{AFt}}}S_{\mathrm{AFt}} + 4\frac{\Gamma_{\mathrm{Ca}}}{\Gamma_{\mathrm{AFm}}}S_{\mathrm{AFm}} = 10\ \mathrm{CaO}\frac{\Gamma_{\mathrm{Ca}}}{\Gamma_{\mathrm{CaO}}} \tag{3.145}$$

$$\frac{\Gamma_{\mathrm{Si}}}{\Gamma_{\mathrm{csh}}}S_{\mathrm{csh}} = 10\ \mathrm{SiO_2}\frac{\Gamma_{\mathrm{Ca}}}{\Gamma_{\mathrm{SiO_2}}} \tag{3.146}$$

$$2\frac{\Gamma_{\mathrm{Al}}}{\Gamma_{\mathrm{AFt}}}S_{\mathrm{AFt}} + 2\frac{\Gamma_{\mathrm{Al}}}{\Gamma_{\mathrm{AFm}}}S_{\mathrm{AFm}} + 2\xi_{\mathrm{Al2O3}}\frac{\Gamma_{\mathrm{Al}}}{\Gamma_{\mathrm{Al2O3}}}S_{\mathrm{csh}} = 10\ \mathrm{Al_2O_3}\frac{2\Gamma_{\mathrm{Al}}}{\Gamma_{\mathrm{Al2O3}}} \tag{3.147}$$

$$3\frac{\Gamma_{\mathrm{S}}}{\Gamma_{\mathrm{AFt}}}S_{\mathrm{AFt}} + \frac{\Gamma_{\mathrm{S}}}{\Gamma_{\mathrm{AFm}}}S_{\mathrm{AFm}} = 10\ \mathrm{SO_3}\frac{\Gamma_{\mathrm{S}}}{\Gamma_{\mathrm{SO3}}} \tag{3.148}$$

where the Γ_is are the different molar masses. The term ξ_{Al2O3} is an amount of Al_2O_3 that substitutes in the C-S-H. According to reference [139], that substitution rate varies between 2% and 5%. The value of 2% is used for the calculations. To account for the hydration degree of the material, the quantity of CaO, SiO_2, Al_2O_3 and SO_3 should be multiplied by the appropriate factor, i.e. multiply each quantity by 0.9 for a 90%

Table 3.5: Parameters for the numerical simulations on the cement paste submitted to the degradation tests.

Parameter	Value	Parameter	Value
Cement type	10	Initial solid phases	(g/kg)
w/c	0.6	Portlandite	195.5
		C-S-H	89.1
Paste mixture	(kg/m^3)	Ettringite	30.7
Cement	1088.8	Monosulfates	94.3
Water	653.3		
Density	1742.1	Diffusion coefficient	(m^2/s)
		OH^-	16.1×10^{-11}
Porosity	0.522	Na^+	4.1×10^{-11}
		K^+	6.0×10^{-11}
Initial pore solution	(mmol/L)	SO_4^{2-}	3.3×10^{-11}
OH^-	429.29	Ca^{2+}	2.4×10^{-11}
Na^+	111.07	$Al(OH)_4^-$	1.7×10^{-11}
K^+	327.00		
SO_4^{2-}	5.57	T	25°C
Ca^{2+}	1.29	F	96488.46 C/mol
$Al(OH)_4^-$	0.21	R	8.3143 J/mol/°K
		ϵ (pure water)	6.94×10^{-10} C/V/m
Tortuosity	0.0305	e_o	1.602×10^{-19} C

hydration degree. This value was used for the calculations on the cement paste.

The remaining disks were submitted to a degradation test. It consists in exposing the pastes to different controlled environments. The 20 mm disks were first sealed on the side and on one face with silicon. They were then immersed in 30 L of aggressive solution for a minimum of three months. Two different solutions were used: deionized water and a 50 mmol/L Na_2SO_4 solution. In the case of the Na_2SO_4 solution, disks were also exposed during six months and one year. During the exposure period, the solution were renewed on a weekly basis in order to maintain uniform conditions.

After the test, small prisms (20 mm $\times$ 3 mm $\times$ 12 mm) were cut from the disk and immersed in isopropylic alcohol for two weeks. They were then dried under vacuum for a week. The samples were finally impregnated with an epoxy resin, polished and coated with carbon. After the conditioning was completed, the samples were analysed with a microprobe (Cameca SX-100 operating at 15 kV and 20 nA), which allows to determine their degradation state. The analysis was performed over 1000 points along the length of the sample. Profiles of calcium and sulfur were measured and compared to the numerical model. The microprobe profiles are expressed in count/sec.

The simulations were performed with the parameters listed in Table 3.5. The boundary conditions are of the Dirichlet type. For the deionized water case, all concentrations are set to zero at $x = 0$. The water content is set to the porosity value of 0.522 at $x = 0$. Finally, the potential ψ is also set to zero at $x = 0$. No boundary conditions are applied at $x = L$. The spatial discretization was performed with a uniform 100 element mesh over a 20 mm domain. Time steps of 900 second were used.

The output of the model consists in the profiles of the variables, i.e. the N concentrations along with the water content and the electrical potential, as well as the profiles of the M solid phases. The total calcium content is obtained from the addition of the calcium in each solid phase. It is then converted in grams of calcium per kg of dry material. The same procedure is followed for sulfur. The comparison between the numerical simulations and the microprobe measurements is shown in Figures 3.20 to 3.22.

Figure 3.20 shows the comparison of the model with the experiment for the case of the cement paste exposed three months to water. The experimental profile show

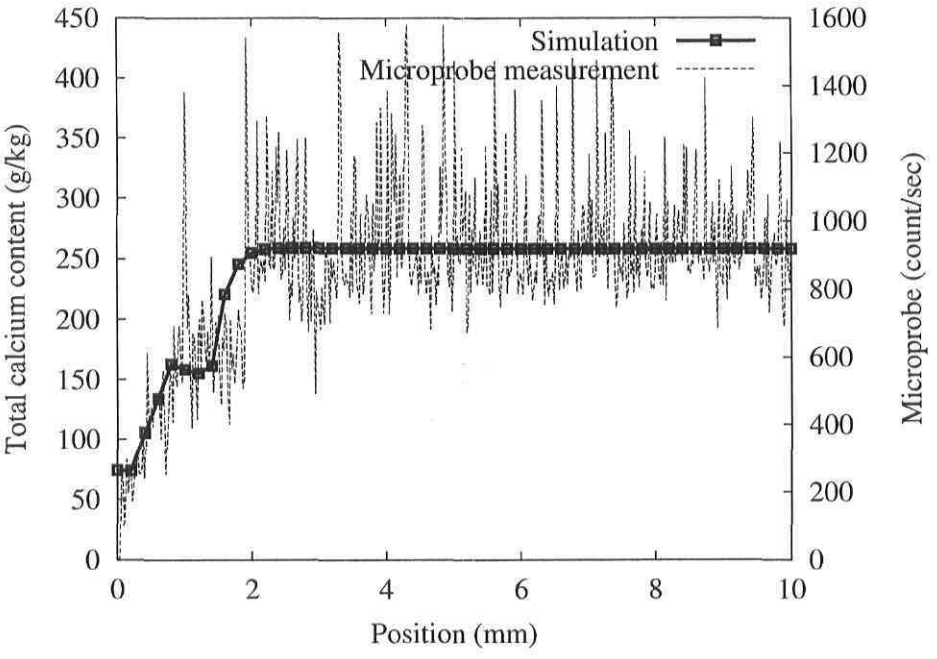

Figure 3.20: Validation test - Comparison of the model with the calcium profile for the paste exposed to water for three months. The boundary $x = 0$ corresponds to the exposed surface.

high peaks of calcium starting at about 2 mm and going deeper toward $x = L$. They correspond to portlandite. At around 2 mm, these peaks disappear, which indicates the dissolution of portlandite. A plateau is observed between 0.8 and 2 mm, followed by a drop of calcium near the surface of the material. This drop in calcium content is associated with the decalcification of C-S-H. The plateau indicates that the decalcification of C-S-H does not start immediately after the dissolution of portlandite. The model was able to reproduce with accuracy the main features of the microprobe profile. As shown in Figure 3.20, the predicted dissolution of portlandite begins at around 2 mm. The simulations shows the presence of a plateau and matches very well with the experiment for the calcium drop near the surface.

The model is then compared to the sulfur profiles measured on the paste exposed to sodium sulfate at three different time interval on Figure 3.21. Following the x axis from 10 mm to the surface, the measurements show a low level of sulfate, corresponding to the level in the sound paste. At some point, the level of sulfate increases. This increase is located roughly at 4.5 mm after 3 months, 5.5 mm after 6 months and 8 mm after a

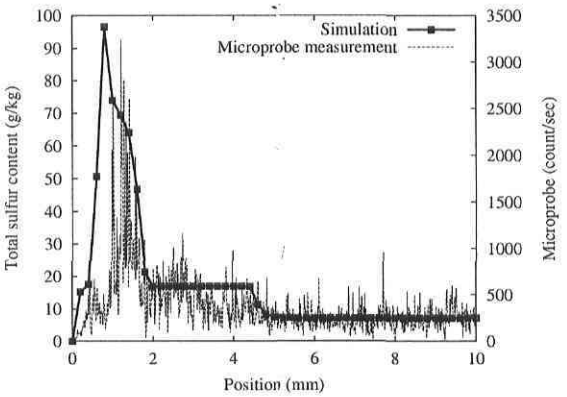

(a) Three month exposure

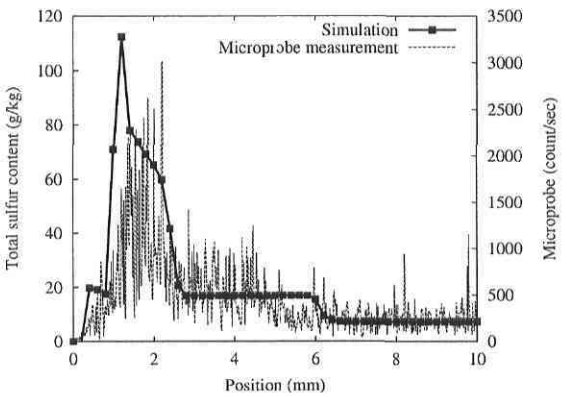

(b) Six month exposure

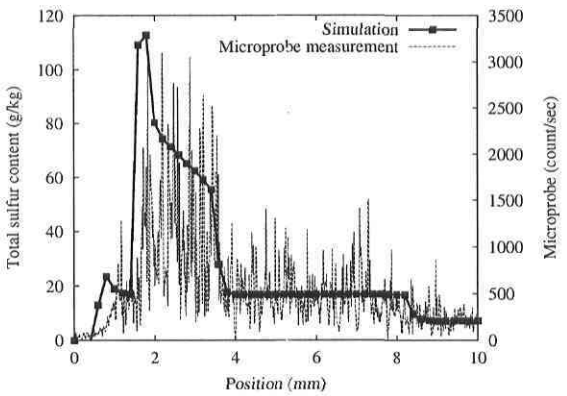

(c) Twelve month exposure

Figure 3.21: Validation test - Comparison of the model with the sulfur profiles for the paste exposed to sodium sulfate.

year. It corresponds to the penetration of an ettringite front in the material, as a result of the exposure to sodium sulfate. Finally, an important peak of sulfur is observed near the surface, corresponding to gypsum formation. Figure 3.21 shows that the model reproduces very well the experimental profiles. The penetration of the ettringite front is accurately followed, as well as the position of the gypsum peak. Furthermore, the model also predicts the widening of the gypsum peak through time.

The same analyis is done for the calcium profiles at 3, 6 and 12 months for the paste exposed to sodium sulfate. The results are shown on Figure 3.22. In all cases, the model predicts accurately the dissolution of portlandite. On Figures 3.22(b) and 3.22(c), it was observed that the plateau of calcium between the dissolution of portlandite and the decalcification of C-S-H is higher than in Figure 3.20. This can be attributed to the gypsum peak, which forms right next to the portlandite dissolution front. The model predicts this higher calcium plateau. The only discrepancy between the model and the measurements is observed in Figure 3.22(a). The model predicts the presence of a calcium plateau occuring after the dissolution of portlandite. But it can not be observed on the experimental measurement. So far, no explanation could be found for this.

Another series of simulations was performed to evaluate the impact of the electrical coupling and the chemical activity effect on the numerical results. The case of the cement paste exposed to sodium sulfate was considered. The first simulation was performed with the materials properties listed in Table 3.5, but with the electrical coupling and chemical activity terms neglected. This gives concentration profiles that do not respect the electroneutrality requirement. Another simulation was performed using the average of the diffusion coefficients in Table 3.5 for each ionic species. This allows to maintain a neutral solution throughout the calculations. Simulations made while neglecting only the chemical activity term showed very little influence of this term. However, the same can not be said about the electrical coupling term, as shown on Figure 3.23. It clearly shows that neglecting the electrical coupling leads to very different results that do not match with the experimental measurements. In the simulation made with the average D_i, the formation of a gypsum peak is not even predicted.

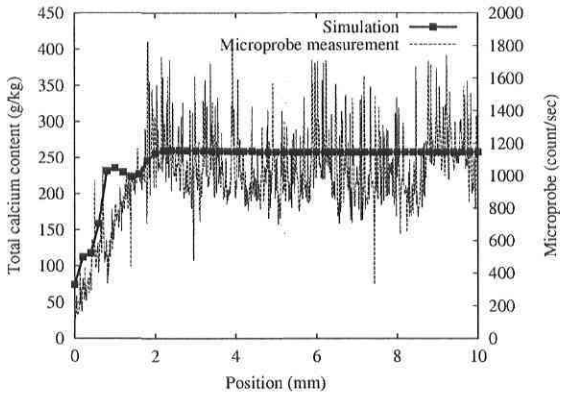

(a) Three month exposure

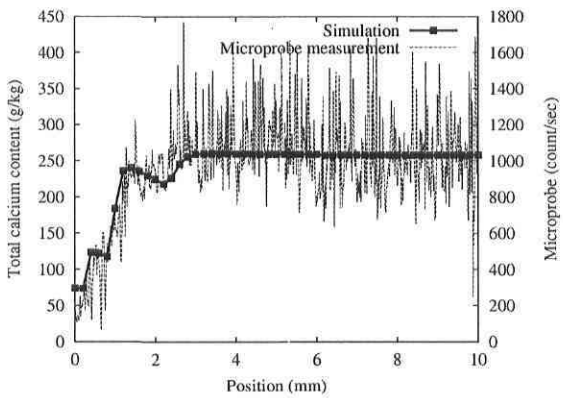

(b) Six month exposure

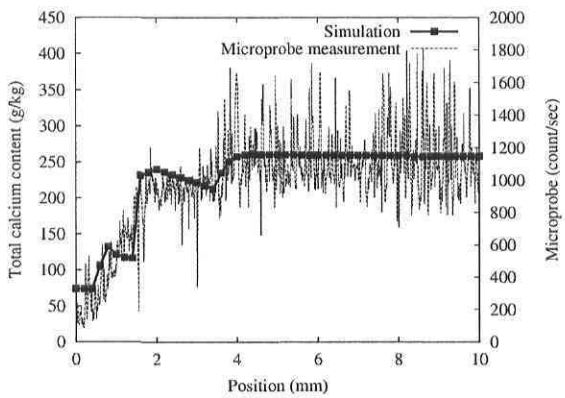

(c) Twelve month exposure

Figure 3.22: Validation test - Comparison of the model with the calcium profiles for the paste exposed to sodium sulfate.

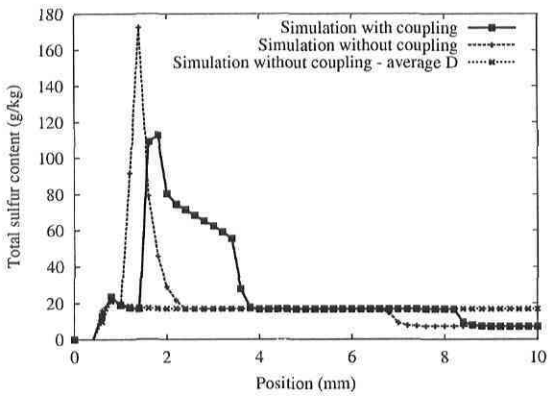

(a) Sulfur profiles

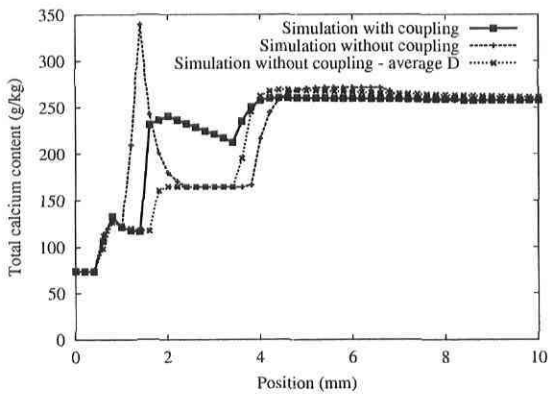

(b) Calcium profiles

Figure 3.23: Simulations performed without electrical coupling and chemical activity terms for the paste exposed to sodium sulfate for one year.

3.4.6 Long-term simulation

Other simulations are performed to investigate the behavior of the SNIA algorithm used in the model, as well as the effect of a gradient in water content on the ionic transport. The case considered consists in a 15 cm thick concrete slab lying on a soil bearing a high concentration of sodium sulfate. The concrete has a water/cement ratio of 0.5 and is made with a CSA type 50 cement. The soil is at a relative humidity of 85%. The top of the slab is exposed to air at a 70% relative humidity. This gradient in relative humidity will create a flow of water directed upward that will contribute, along with diffusion, to move the SO_4^{2-} ions into the material. The simulations were all performed at a 25°C temperature.

The material properties are listed in Table 3.6. They were obtained from tests made on several concrete samples. The evaluation of porosity, initial pore solution, diffusion coefficients, tortuosity and initial solid content was described in the previous section. The value of the parameters F, R, ϵ and e_o are given in Table 3.5.

To perform a simulation in unsaturated conditions, one needs to translate the relative humidity of the environment into water content, in order to apply the proper boundary conditions. A water desorption isotherm was determined from the climate box method [15]. It consists in exposing small hydrated paste samples to different relative humidity in tightly closed boxes. The different relative humidities are controlled with saturated salt solutions. Once equilibrium is reached, the water content of the sample is calculated from a mass measurement. The desorption isotherm is shown on Figure 3.24. The water contents for the paste are converted to concrete values by mean of the paste volume of the concrete. The water content at 70 and 85% relative humidity are given in Table 3.6.

The transport parameters D_θ (equation 3.96) and D_L (equation 3.106) are needed to model the transport of water in the concrete slab. It was shown in reference [42] that for high values of relative humidity, which approximately means 70% and above, $D_\theta \approx D_L$. This parameter is nonlinear and is generally expressed as an exponential function for construction materials [74]: $D_\theta = Ae^{B\theta}$. It was evaluated from moisture transport tests performed on materials exposed on one side to water and on the other side to different relative humidities. The tests are performed until the steady state is

Table 3.6: Data for the numerical simulations

Properties	Value	Properties	Value
Cement type	CSA 50	Cement composition	
w/c	0.50	CaO	63.5
		SiO_2	22.5
Concrete mixture	(kg/m^3)	Al_2O_3	3.0
Cement	350	SO_3	2.0
Water	175		
Agregates	1800	Initial solid phases	(g/kg)
Density	2325	C-S-H	24.4
		Portlandite	48.9
Initial pore solution	(mmol/L)	Ettringite	7.6
OH^-	215.1	Monosulfates	9.7
Na^+	98.2		
K^+	114.6	Diffusion coefficients	(m^2/s)
SO_4^{2-}	1.0	OH^-	19.4×10^{-11}
Ca^{2+}	2.2	Na^+	4.9×10^{-11}
$Al(OH)_4^-$	0.1	K^+	7.2×10^{-11}
		SO_4^{2-}	3.9×10^{-11}
Rel. humidity (%)	θ (m^3/m^3)	Ca^{2+}	2.9×10^{-11}
70	0.0597	$Al(OH)_4^-$	2.0×10^{-11}
85	0.0852		
		Water diffusivity	(m^2/s)
Porosity	0.121		$2.1\times10^{-10}e^{8.2\theta}$
Tortuosity	0.0368	Temperature	25°C

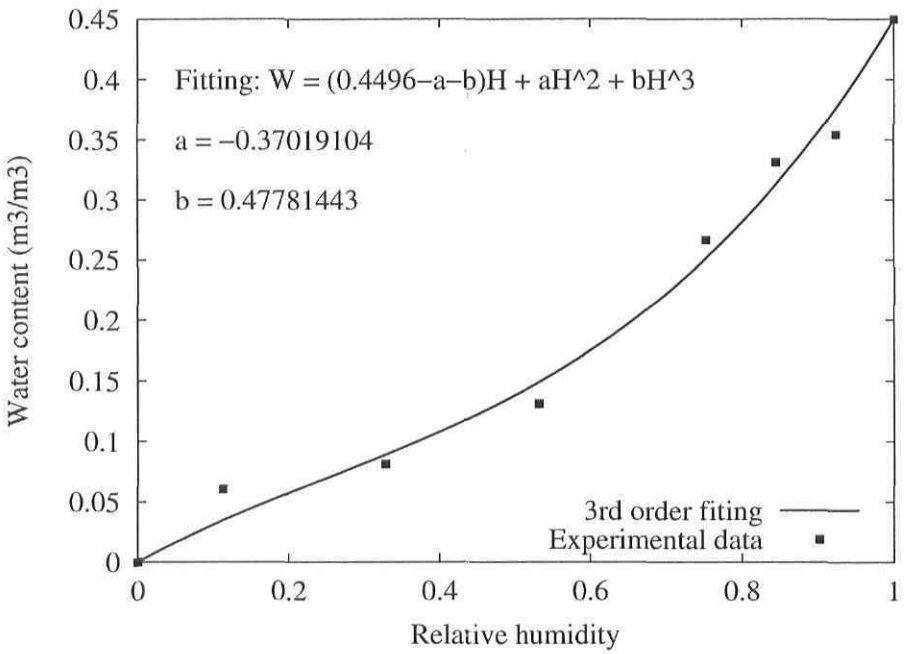

Figure 3.24: Desorption isotherm measured on a CSA Type 50 hydrated cement paste at a w/c ratio of 0.5

reached. The steady state moisture flows allow to obtain the following parameter value: $D_\theta = 2.1\times10^{-10}e^{8.2\theta}$.

The boundary conditions in $x = 0$ corresponds to the ionic concentration in the groundwater. For this particular simulation, the groundwater bears a 50 mmol/L Na_2SO_4 concentration. Accordingly, concentrations in Na^+ of 100 mmol/L and of 50 mmol/L for SO_4^{2-} are imposed through Dirichlet-type conditions. All other concentrations are set to zero. In $x = 0.15$, the material is in contact with air. A null flux is imposed for all the species at this location.

The water content on both side of the slab was discussed previously. It is applied with a convection condition:

$$q_{\text{conv}} = h(\theta - \theta_\infty) \tag{3.149}$$

where h is the convection coefficient and θ_∞ is the water content corresponding to either 70% or 85% relative humidity. The value of h for the simulations is 5×10^{-8} m/s. The slab is assumed saturated initially; the water content thus corresponds to the porosity.

For the electrical potential ψ, a value of zero is set at $x = 0$.

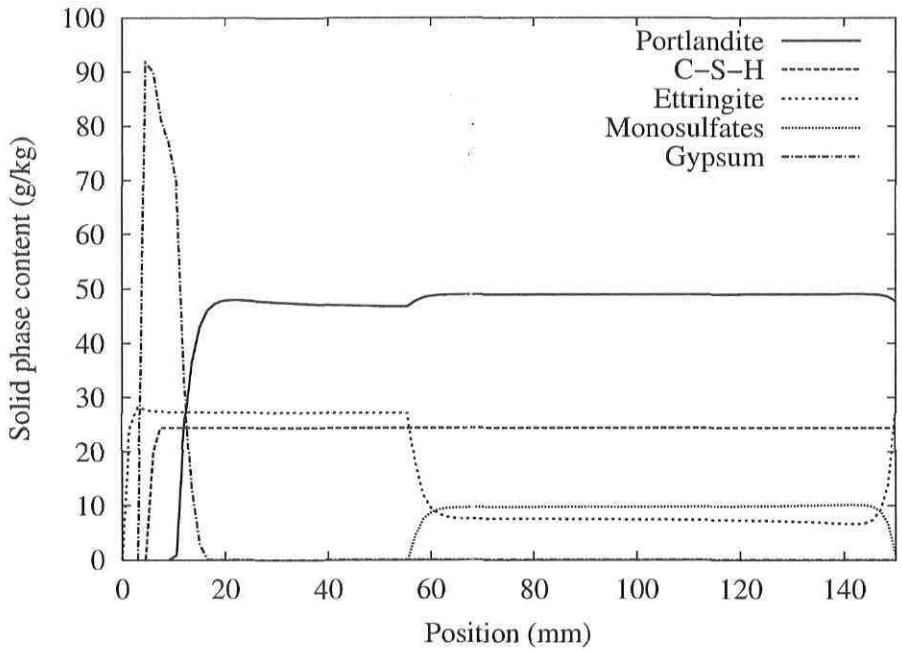

Figure 3.25: Solid phase distribution after 20 years.

Before showing any simulation results, a few words should be written on the ability of the chosen algorithm to handle the water flowing through the material as a result of capillary suction. The relative importance of the water flow compared to diffusion can be evaluated with the Peclet number (P_e). It is given by VL/D, where V is the velocity of the flow, L is the length of the domain and D is the diffusion coefficient. In the present case, V can be calculated with equation (3.97), with the gradient of water content evaluated from the analytical solution of equation (3.96) in steady-state. It gives 6.5×10^{-11} $m^3/m^2/s$. D is taken as the average diffusion coefficient, 6.7×10^{-11} m^2/s. This results in a low Peclet number of 0.15. The problems commonly associated with convection-dominated problems, like strong oscillations, are not likely to occur at such low values of P_e. Even for a very high gradient of relative humidity such as 95% – 60%, P_e is 0.36, still well below values expected to lead to numerical oscillations.

All the simulations were performed over a twenty year period. The first simulation was performed with time steps of one day over a 100 element mesh. The solid phase profiles are shown on Figure 3.25. It shows that the presence of sulfate in the groundwater leads to the penetration of an ettringite front in the concrete slab as well as the propagation of a gypsum peak toward the top of the structure. These features wera

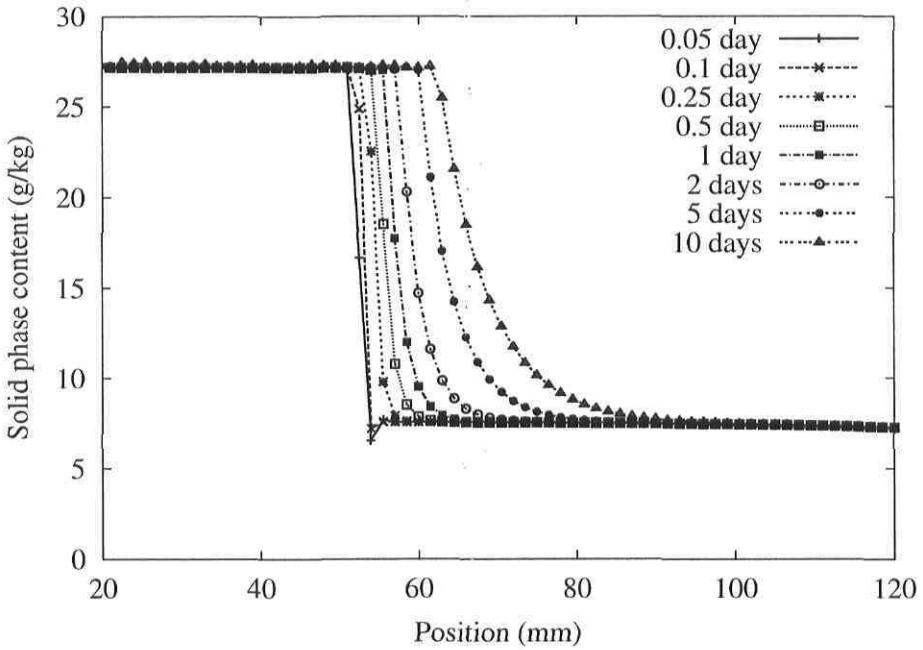

Figure 3.26: Effect of time steps on the position of the ettringite front after 20 years. The simulations were made with 100 elements.

also observed experimentally on the microprobe analyses of the previous section. The position of the ettringite front matches with the dissolution front of monosulfates. The model also predicts the dissolution of portlandite and the decalcification of C-S-H, as a result of OH^- and Ca^{2+} leaching in the groundwater. This phenomenon was also observed on the hydrated cement paste submitted to the degradation tests. Finally, it is interesting to observe the presence of ettringite formation on the top of the slab ($x = 15$ cm). This is caused by the drying process, which leads to an increase of all concentrations as the volume of liquid water is reduced.

The sensitivity of the model to time discretization was tested by doing the same simulation with different time steps: 0.01, 0.02, 0.05, 0.1, 0.25, 0.5, 1, 2, 5 and 10 days. The results are shown on Figure 3.26. All simulations were made with 100 elements. It clearly shows the influence of reducing the time steps on the solution. The ettringite front is spread over a wide area for large time steps. As the latter decreases, the front gets sharper. The figure also shows the convergence of the front as the time steps gets smaller.

A similar sensitivity analysis was performed for the spatial discretization. Figure

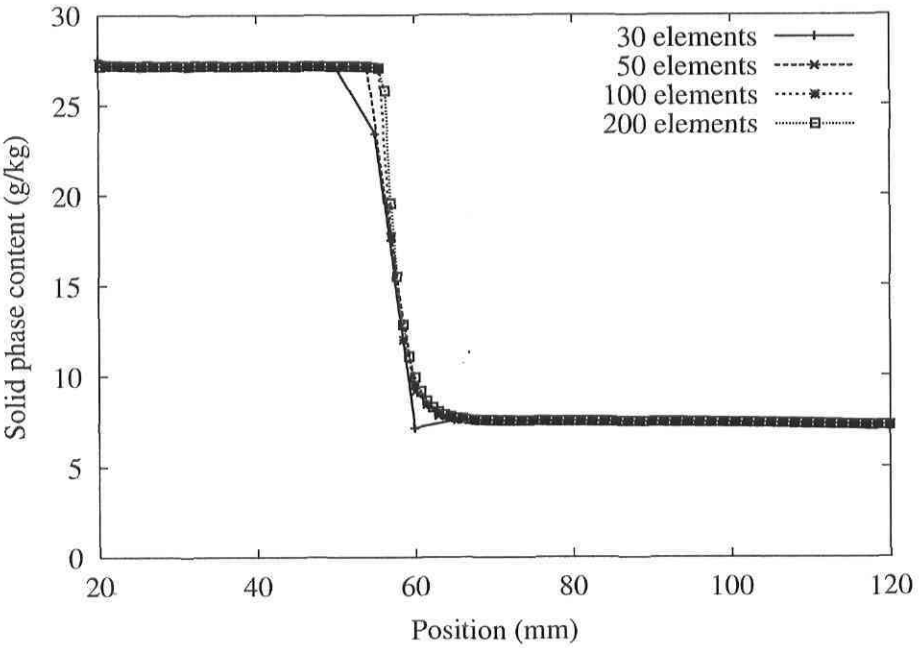

Figure 3.27: Effect of the mesh density on the position of the ettringite front after 20 years. The simulations were made with time steps of 86400 sec. (1 day).

3.27 shows the ettringite front location calculated with various mesh densities. A time step of one day (86400 sec.) was used. It clearly shows that this parameter has not a large influence on the numerical solution, contrary to the time step.

The last series of simulations was made to show the influence of the water transport on the chemical alteration of the material. The simulation made with 100 elements and a time step of one day is compared to the same simulation without any gradient of water content. In that case, the material remain saturated. The comparison for the ettringite and portlandite fronts is showed on Figure 3.28. The ettringite front penetrates faster in the material under the influence of a water content gradient. The water flow adds to the diffusion flow in the case of the SO_4^{2-} ions, which contributes to accelerating the penetration of the ettringite front. On the contrary, the dissolution of portlandite is slowed. In that case, the water flow is opposed to the diffusion flux of OH^- and Ca^{2+} ions which tend to leach out of the material. As a consequence, the outside flux for these ions is reduced, thus slowing the dissolution process of portlandite.

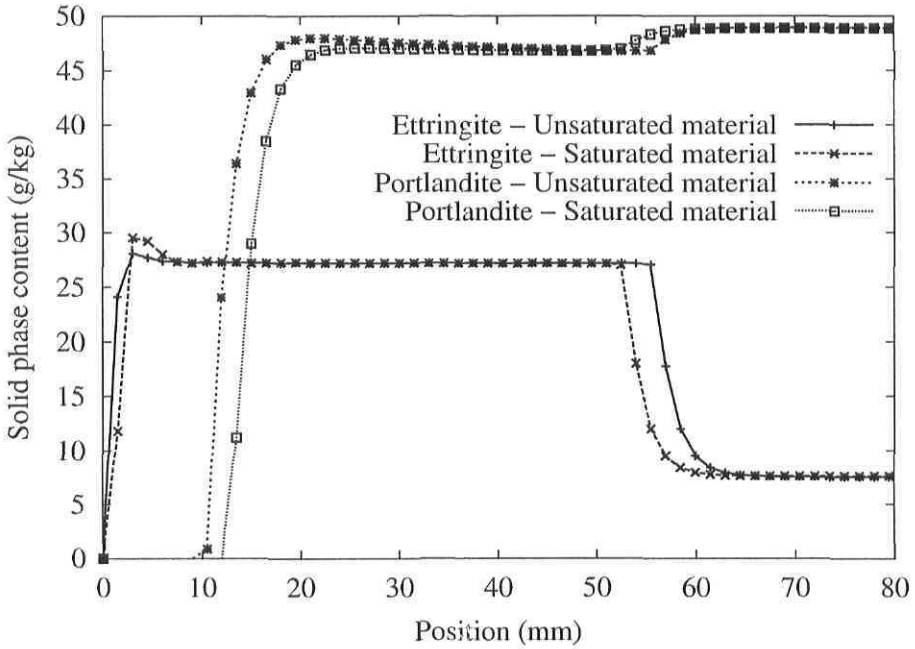

Figure 3.28: Effect of the water flow on the ettringite and portlandite fronts after 20 years.

3.4.7 Conclusion

The numerical model presented is based on the SNIA algorithm, in which the transport and chemical parts of the ionic diffusion process are solved separately without iterations between the two. Contrary to similar models existing in hydrology, the transport equations take into account the electrical coupling between the ions and the chemical activity effects. These effects are considered because cement-based materials bear a highly charged pore solution.

The model was compared to experimental results, showing a good match with the measurements. The model was able to reproduce simultaneous chemical effect like the precipitation of ettringite and gypsum, as well as the dissolution of portlandite and decalcification of C-S-H. Comparison with the experimental results emphasized the importance of electrical coupling. Simulations made without considering this term in the model showed large discrepancies with the measurements.

Another series of simulations were used to test the sensitivity of the algorithm to various numerical parameters, namely mesh density and time steps. While the mesh

density clearly showed no major influence on the numerical solution, the situation is different for the time step. The simulations showed that a small time step is needed in order to have a reliable result. Large time steps tend to produce wide, undefined fronts. As the time step gets smaller, the solution converge to a unique sharp front.

Acknowledgements

The authors would like to acknowledge the work of Mr. Yannick Maltais of SIMCO Technologies, who provided all the experimental results presented in this paper.

Chapitre 4

Application du modèle

4.1 Introduction

Ce chapitre présente différentes utilisations du modèle de transport ionique présenté au chapitre précédent. Un premier article montre l'utilisation du modèle dans le but d'analyser les résultats de l'essai de migration. Cette technique est couramment utilisée dans le domaine du béton afin déterminer les coefficients de diffusion des différentes espèces ioniques.

Le deuxième article présenté dans ce chapitre montre l'application du modèle à l'analyse d'une dalle de béton reposant sur un sol dont la solution interstitielle porte une faible teneur en sulfate. Cette analyse avait pour but de montrer qu'au-delà de la formation d'ettringite, de faibles teneurs en sulfate peuvent aussi être à l'origine de la formation de gypse. De plus, le faible pH du sol peut causer la dissolution de certaines phases de la pâte de ciment.

4.2 Calculation of ionic diffusion coefficients on the basis of migration test results

E. Samson[12], J. Marchand[12], K.A. Snyder[3]

[1]Centre de recherche interuniversitaire sur le béton,
Université Laval, Québec, Canada, G1K 7P4

[2]SIMCO Technologies inc.,
1400, boul. du Parc Technologique, Québec, Canada, G1P 4R7

[3]Building and Fire Research Laboratory
National Institute of Standards and Technology, Gaithersburg, MD 20899, USA

Abstract

Migration tests are now commonly used to estimate the diffusion coefficients of cement-based materials. Over the past decade, various approaches have been proposed to analyze migration test results. In many cases, the interpretation of test data is based on a series of simplifying assumptions. However, a thorough analysis of the various transport mechanisms that take place during a migration experiment suggests that some of them are probably not valid. Consequently, a more rigorous approach to analyze migration test results is presented. The test procedure is relatively simple and consists in measuring the evolution of the electrical current passing through the sample. Experimental results are then analyzed using the extended Nernst-Planck-Poisson set of equations. A simple algorithm is used to determine for each experiment the tortuosity factor that allows to best reproduce the current curve measured experimentally. The main advantage of this approach resides in the fact that the diffusion coefficients of all ionic species present in the system can be calculated using a single series of data. Typical examples of the application of this method are given. Results indicate that the diffusion coefficients calculated using this approach are independent of the applied voltage and depends only slightly on the concentration level and the chemical make-up of the upstream cell solution.

4.2.1 Introduction

Concrete durability is a growing concern that continues to consume an increasing amount of public funds allocated for repairing civil engineering infrastructures throughout the world. In this context, service life modeling has become a subject of focused research activity. Considerable effort has been expended in the development of service life models for predicting the long-term behavior of concrete structures. These models have been developed to improve concrete performance and to facilitate future repair planning strategies.

One approach to service life modeling of concrete structures is based on the detailed description of ionic transport mechanisms and chemical equilibrium within the hydrated cement paste fraction of the material [119, 173]. Models to predict the transport of ions in concrete pore solution and the corresponding chemical reactions are complex. Consequently, accurate transport models require a sound understanding of the various physical and chemical phenomena involved. Accordingly, research on the subject has flourished and experimental methods to properly evaluate the various parameters found in the mathematical models have been significantly improved.

For the majority of field concrete failure mechanisms, the critical chemical reaction depends upon the diffusive transport of ionic species. Therefore, one of the critical parameters characterizing the movement of ions is the diffusion coefficient. Historically, this parameter was determined using the divided cell diffusion set-up (see Figure 4.1)[64, 113]. Unfortunately, diffusion experiments tend to be very time consuming. In many instances, ions may take several months (even up to a year in certain cases) to penetrate a 1 cm thick disc of mortar [113, 131].

Over the past decades, numerous attempts to design accelerated test procedures have been made. In most cases, an experimental set-up similar to the one utilized for a diffusion experiment (see Figure 4.1) is used but the transport of ions through the samples is accelerated by the application of an electrical potential to the system. These accelerated diffusion experiments, currently called migration tests, are now commonly used to characterize the ionic diffusion properties of hydrated cement systems.

Various versions of the migration test have been developed. These different procedures can be divided into two categories. In steady-state migration experiments, the

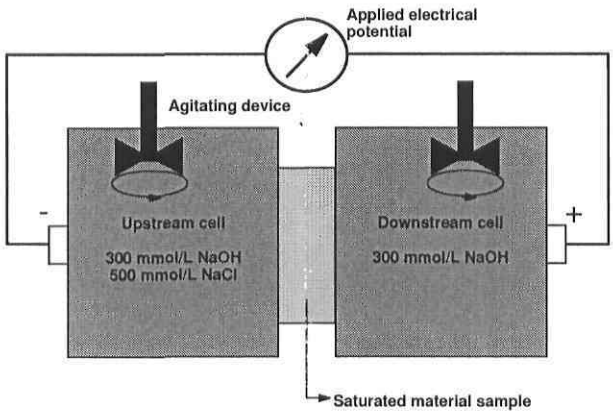

Figure 4.1: Typical set-up for the migration test.

evolution of the concentration of a given ionic species (in many cases chloride ions) in the downstream compartment of the cell is monitored for a few days [59, 190]. In non-steady state migration tests, the depth of ion penetration within the sample (or alternatively the current passing through the sample) is measured after a given period [177, 181, 184].

Despite these variations, all migration tests share some common features. Experiments are usually performed on fully saturated samples, and test solutions are typically maintained at a pH over 12.5 in order to preserve, as much as possible, the microstructure of the material during the test. In addition, the electrical potential applied on the system ranges from 400 to 1200 V/m. Comprehensive critical reviews of the various migration test procedures used to investigate the transport properties of concrete can be found in references [115, 180].

Numerous aspects of the migration tests have been investigated. For instance, it is now well established that the transport of ions (hence migration test results) is quite sensitive to temperature variations of the cell [115, 107, 174]. These investigations have clearly emphasized the importance of conducting migration experiments under isothermal conditions. Various approaches to calculate diffusion coefficients on the basis of migration test results have also been proposed [115]. Although these studies have improved knowledge on the fundamental mechanisms involved in a migration experiment, some of them have also raised questions on the relative influence of parameters such

as the nature and concentration of the test solution and the intensity of the electrical potential applied on the cell during the experiment. However, recent numerical developments have cast some doubts on the hypotheses at the basis of some of these calculation methods. This paper attempts to shed some new light on the analysis of isothermal migration test results.

4.2.2 Description of ionic transport mechanisms in reactive porous media

In (unsaturated) porous materials, the movement of ions takes place in the liquid phase that occupies a fraction of the total porous volume. It occurs as a combination of diffusion and advection (i.e. fluid movement). Since ions are charged particles, their movements in solution is affected by the presence of other ionic species through an electrical coupling. The transport of ions may also be affected by the various chemical reactions that may occur within the material. Ions can react with other species present in the pore solution to form new compounds. They can also interact with other ions found in the double layer at the surface of the pores, or eventually be bound to the various solid phases forming the skeleton of the porous material.

In hydrated cement systems, all the above phenomena are bound to occur. Electrical effects tend to be particularly significant since the pore solution is highly concentrated. The chemical reactions can also be very important since some of the solid phases of the cement paste are very reactive, particularly the ones that are alumina-based [185, 170].

4.2.2.1 Mathematical treatment of transport phenomena

Previous work has shown that it is possible to model the transport of ions by averaging the extended Nernst-Planck equation with an advection term [85] over a Representative Elementary Volume (REV). Details on the averaging technique can be found elsewhere [18, 156]. This yields the following transport equation [113] (given here for 1D cases) that should be written for each ionic species present in the system:

$$\frac{\partial(\theta_s C_{is})}{\partial t} + \frac{\partial(\theta C_i)}{\partial t} - \frac{\partial}{\partial x}\left(\theta D_i \frac{\partial C_i}{\partial x} + \theta \frac{D_i z_i F}{RT} C_i \frac{\partial \Psi}{\partial x} + \theta D_i C_i \frac{\partial \ln \gamma_i}{\partial x} - C_i V_x\right) = 0 \quad (4.1)$$

Table 4.1: Diffusion coefficient of various species in free water.

Species	D_i^μ (10^{-9} m^2/s)
OH^-	5.273
Na^+	1.334
K^+	1.957
SO_4^{2-}	1.065
Ca^{2+}	0.792
Cl^-	2.032
Mg^{2+}	0.706

The uppercase symbols represent averaged quantities: C_i is the concentration of the ionic species i, C_{is} is the concentration of the species i in solid phase, θ_s is the volumetric solid content of the material, θ is the volumetric water content in the pores, Ψ is the electrical potential, D_i is the diffusion coefficient, z_i is the valence number of the species, F is the Faraday constant, R is the ideal gas constant, T is the absolute temperature of the liquid, γ_i is the chemical activity coefficient and V_x is the bulk velocity of the fluid. The bulk ionic flux J_i is given by:

$$J_i = -\theta D_i \frac{\partial C_i}{\partial x} - \theta \frac{D_i z_i F}{RT} C_i \frac{\partial \Psi}{\partial x} - \theta D_i C_i \frac{\partial \ln \gamma_i}{\partial x} + C_i V_x \tag{4.2}$$

In equations (4.1) and (4.2), the diffusion coefficient D_i is defined as:

$$D_i = \tau D_i^\mu \tag{4.3}$$

where τ is the tortuosity of the material and D_i^μ is the diffusion coefficient of the species i in free water, which values can be found in physics handbooks (see for instance reference [43]). Values of D_i^μ for the most common species found in cement-based materials are given in Table 4.1. The values of D_i^μ appearing in Table 4.1 are constant and represent the diffusion coefficients in very dilute conditions.

The tortuosity appears in the model as a result of the averaging procedure [18, 156]. It characterizes the intricacy of the path that ions must travel in a given porous material. Equation (4.3) has very important implications. For instance, it shows that if the diffusion coefficient D_i of one ionic species is known, τ is also known and, accordingly, the diffusion coefficient of each of the other ionic species can be easily calculated. It

also shows that as long as the tortuosity of the material remains unchanged, each D_i is constant.

To evaluate the electrical potential Ψ, Poisson's equation [85, 90] must be solved simultaneously with equation (4.1). Poisson's equation relates the electrical potential Ψ to the electrical charge $\sum_i F z_i C_i$ in solution. It is given here in its averaged form [156, 113]:

$$\frac{d}{dx}\left(\theta\tau\frac{d\Psi}{dx}\right) + \theta\frac{F}{\epsilon}\sum_{i=1}^{N} z_i C_i = 0 \tag{4.4}$$

where N is the total number of ionic species and ϵ is the dielectric permittivity of the media. In this study, the permittivity is assumed to be the same as that of water.

To calculate the chemical activity coefficients, several approaches are available. Models such as those proposed by Debye-Hückel or Davies are unable to reliably describe the thermodynamic behavior of highly concentrated electrolytes such as the hydrated cement paste pore solution. A modification of the Davies equation was found to yield good results [155]:

$$\ln\gamma_i = -\frac{Az_i^2\sqrt{I}}{1+a_i B\sqrt{I}} + \frac{(0.2-4.17\times10^{-5}\ I)Az_i^2 I}{\sqrt{1000}} \tag{4.5}$$

where I is the ionic strength of the solution, and A and B are temperature dependent parameters. The parameter a_i in equation (4.5) varies with the ionic species considered.

As noted previously, the variable V_x appearing in equation (4.1) stands for the velocity of the fluid phase. In cement-based materials, the fluid will often be in movement as a result of capillary forces arising from the wetting and drying cycles to which the material is exposed. In these cases, the velocity of the fluid can be expressed as [44]:

$$V_x = -D_L\frac{\partial\theta}{\partial x} \tag{4.6}$$

where D_L is the non-linear liquid water diffusivity coefficient. The use of equation (4.6) is interesting since it involves the volumetric water content θ, a variable already used in equation (4.1). Water content profiles in the material can be evaluated on the basis of Richard's equation [44], which is given by:

$$\frac{\partial\theta}{\partial t} - \frac{\partial}{\partial x}\left(D_w\frac{\partial\theta}{\partial x}\right) = 0 \tag{4.7}$$

where D_w is the global water diffusivity coefficient, taking into account water molecules under both vapor and liquid phase.

4.2.2.2 Mathematical treatment of chemical reactions

In hydrated cement systems, chemical reactions are bound to occur during the transport of ions, whether there is an applied field or not. If there is no electrical field, the rate of transport of ions is slow compared to the kinetics of the various chemical reactions [14]. Since the evolution of the microstructure of the material is essentially controlled by the rate of transport of ions, the equilibrium of the system is considered to be *locally* maintained.

If the local equilibrium is maintained, several methods for modeling the chemical reactions can be used, as reviewed in reference [159]. A technique often used is to experimentally determine an interaction isotherm that gives a relationship between the solids concentrations C_{is} and solute concentration C_i [183]. This relationship is then directly inserted in equation (4.1). Although relatively straightforward, this method is limited by the fact that it can hardly take into account the influence of numerous ionic species on the equilibrium of a given solid phase with the surrounding pore solution. This is the reason why many authors have elected to rely on a different approach and model chemical reactions using a chemical equilibrium code [113, 159, 46, 48].

During a migration test, the situation is significantly different. A dimensional analysis of the problem indicates that the local chemical equilibrium is usually not respected during a migration experiment [13]. This can be explained by the fact that the application of a difference in potential of 400 V/m results in a rate of ionic transport that is much faster than the kinetics of chemical reaction. The dimensional analysis also demonstrates that, in most migration experiments, chemical reactions have little influence on the local ionic concentration within the test sample [1].

Since the local equilibrium is not maintained during migration experiments, the models reviewed in reference [159] are no longer appropriate. Relatively little research has been dedicated to the treatment of these non-equilibrium problems in hydrated cement systems. Rubin [149] gives a general framework to model these reactions. According to this approach, the non equilibrium reaction for a solid $\overline{M_1 M_2}$ in contact with

[1] These conclusions are valid for ordinary concrete mixtures for which the water/binder ratio is 0.40 or higher. These conclusions are probably not valid for high-performance concrete mixtures.

the ions M_1 and M_2, found in concentrations c_1 and c_2 respectively, is expressed as:

$$\overline{M_1 M_2} \underset{k_b}{\overset{k_a}{\rightleftharpoons}} M_1 + M_2 \tag{4.8}$$

where k_a and k_b are the reaction rate coefficients associated with the dissolution and precipitation, respectively. The rate of formation of ions M_1 and M_2 into solid phases can be expressed as [149]:

$$\frac{\partial c_{1s}}{\partial t} = \frac{\partial c_{2s}}{\partial t} = -k_a c_1 c_2 + k_b \tag{4.9}$$

which could be inserted directly in equation (4.1). The problem, however, is to determine k_a and k_b, which are likely to be related to the solute concentration and to the applied external voltage, since it determines the velocity of the ions. To our knowledge, no systematic data on this topic have been published. Recent work by Castellote et al. [33] has emphasized the complexity of these problems.

4.2.3 Modeling of ionic transport during migration tests

The mathematical model described previously can be used to model the transport of ions in various cases (e.g. external chemical attack, leaching problems, ...). For the specific case of the migration test, some simplifications can be made. Migration tests are performed in saturated conditions, and no pressure gradient is applied on the liquid phase. Accordingly, the advection term in equation (4.1) can be dropped, as well as Richard's equation (equation 4.7). Furthermore, the fact that the material is maintained in saturated conditions allows simplifying the expression relating porosity ϕ and volumetric water content θ:

$$\theta = \phi \tag{4.10}$$

$$\theta_s = 1 - \phi \tag{4.11}$$

These assumptions may be used to simplify equation (4.1):

$$\frac{\partial\big((1-\phi)C_{is}\big)}{\partial t} + \frac{\partial(\phi C_i)}{\partial t} - \frac{\partial}{\partial x}\left(\phi D_i \frac{\partial C_i}{\partial x} + \phi \frac{D_i z_i F}{RT} C_i \frac{\partial \Psi}{\partial x} + \phi D_i C_i \frac{\partial \ln \gamma_i}{\partial x}\right) = 0 \tag{4.12}$$

Similarly, the ionic flux of equation (4.2) can now be written as:

$$J_i = -\phi D_i \frac{\partial C_i}{\partial x} - \phi \frac{D_i z_i F}{RT} C_i \frac{\partial \Psi}{\partial x} - \phi D_i C_i \frac{\partial \ln \gamma_i}{\partial x} \tag{4.13}$$

In most papers dealing with the analysis of migration test data, it is assumed that chemical reactions can be neglected. This hypothesis is, at least partially, justified by the fact that non steady-state migration tests have a shorter duration than steady-state experiments. In addition, as previously discussed, the high velocity of the ions being transported through the pore structure of the material tends to greatly attenuate the influence of chemical reactions. Neglecting the chemical reactions also implies that there is no change to the microstructure of the paste during the duration of the test, which is equivalent to assuming that the porosity and tortuosity remain constant. Following this assumption, equation (4.12) can be simplified as:

$$\frac{\partial C_i}{\partial t} - \frac{\partial}{\partial x}\left(D_i \frac{\partial C_i}{\partial x} + \frac{D_i z_i F}{RT} C_i \frac{\partial \Psi}{\partial x} + D_i C_i \frac{\partial \ln \gamma_i}{\partial x} \right) = 0 \tag{4.14}$$

These assumptions also yields a simplified version of the averaged Poisson's equation:

$$\tau \frac{d^2 \Psi}{dx^2} + \frac{F}{\epsilon} \sum_{i=1}^{N} z_i C_i = 0 \tag{4.15}$$

The set of N equations (4.14), combined with equation (4.15) for the electrical potential and equation (4.5) for the chemical activity coefficients, has to be solved in order to model the transport of ions in saturated materials during a migration test. This coupled system of equation can be solved using the finite element method. Information on a numerical algorithm that has been specifically developed for the resolution of these problems can be found in references [157, 158].

4.2.4 A further simplication - The constant field assumption

Despite the various simplifications discussed in the previous section, solving the previous system of equations can be relatively complicated. This is the reason why numerous attempts have been made to further simplify the analysis of migration test results. The various approaches proposed in the literature can be roughly divided into two groups: those directly related to the treatment of steady-state migration test results and those

associated to the analysis of non steady-state test data [2]. Consequently, these two different families of simplifications will be reviewed separately.

4.2.4.1 Steady-state migration experiments

During a transport experiment, the steady-state regime is reached when the concentration of the species under consideration (e.g. chloride) in the downstream compartment of the cell (see Figure 4.1) varies linearly with respect to time. This indicates a constant flux, which is the basic definition of the steady-state. It implies that all chemical reactions are completed. As previously emphasized, in classical diffusion experiments performed on representative concrete samples, it usually takes a very long time to establish the steady-state. However, in migration tests, the constant flux is often reached in a few days.

From the standpoint of modeling, the treatment of steady-state problems is relatively simple since all time-dependent terms appearing in equation (4.14) are set equal to zero. This is equivalent to solving the flux equation (equation 4.13) with J_i being constant.

To further simplify the analysis, it is assumed that the external voltage is sufficiently strong to overwhelm all the other terms in the flux equation [8, 124, 188, 212]. This means that the diffusion, chemical activity effects and electrochemical coupling between the ions are neglected. This simplification allows to consider a linear variation of the electrical potential in the sample:

$$\frac{\partial \Psi}{\partial x} = \frac{\Delta \Psi_{\text{ext}}}{L} = -E_{\text{ext}} = \text{constant} \tag{4.16}$$

where $\Delta \Psi_{\text{ext}}$ is the difference in voltage applied across the sample, L is the thickness of the specimen, and E_{ext} is the corresponding constant electric field. Equation (4.16) is known as the constant field assumption. In that case, equation (4.13) reduces to:

$$J_i = -\phi \frac{D_i z_i F}{RT} C_i \frac{\Delta \Psi_{\text{ext}}}{L} \tag{4.17}$$

where J_i is a constant since steady-state is reached.

[2] This last category includes most conduction experiments for which the test period is limited to a few hours.

The knowledge of the chloride flux allows to calculate D_i from equation (4.17). This approach was used in references [8, 124, 188, 212]. In reference [212], an equation similar to (4.17) is used, but an empirical correction factor accounting for activity effects is applied.

4.2.4.2 Non steady-state migration experiments

In an attempt to determine chloride diffusion coefficient, Tang and Nilsson [184] proposed an analysis of migration test results based on non steady-state measurements. According to Tang and Nilsson's approach [184], the potential gradient across the sample is assumed to be constant and corresponds to the externally applied electrical field. Chemical activity effects are also neglected. Following these hypotheses, equation (4.12) reduces to:

$$\frac{\partial C_i}{\partial t} - \frac{\partial}{\partial x}\left(D_i \frac{\partial C_i}{\partial x} - \frac{D_i z_i F}{RT} C_i E_{\text{ext}}\right) = 0 \tag{4.18}$$

For semi-infinite media, the analytical solution of equation (4.18) with a constant D_i is:

$$C = \frac{C_o}{2}\left[\text{erfc}\left(\frac{x}{2\sqrt{D_i t}} - \frac{z_i F E_{\text{ext}}\sqrt{D_i t}}{2RT}\right) + e^{\left(\frac{z_i F E_{\text{ext}}}{RT} x\right)} \text{erfc}\left(\frac{x}{2\sqrt{D_i t}} + \frac{z_i F E_{\text{ext}}\sqrt{D_i t}}{2RT}\right)\right] \tag{4.19}$$

where C_o is the boundary condition at $x = 0$.

According to this approach, the value D_i is obtained by fitting the chloride profile calculated numerically (i.e. from equation (4.18)) to the one measured during the migration test. Experimental chloride profiles are usually obtained by milling at the end of the experiment the test sample over several depth increments[3]. The powder samples are then tested for acid-soluble chlorides in accordance with ASTM C1152. Alternatively, the test sample can be splitted into two pieces. The total depth of penetration is then estimated using a colorimetric method (see for instance reference [184]).

[3]Each increment is typically a few millimeters in depth.

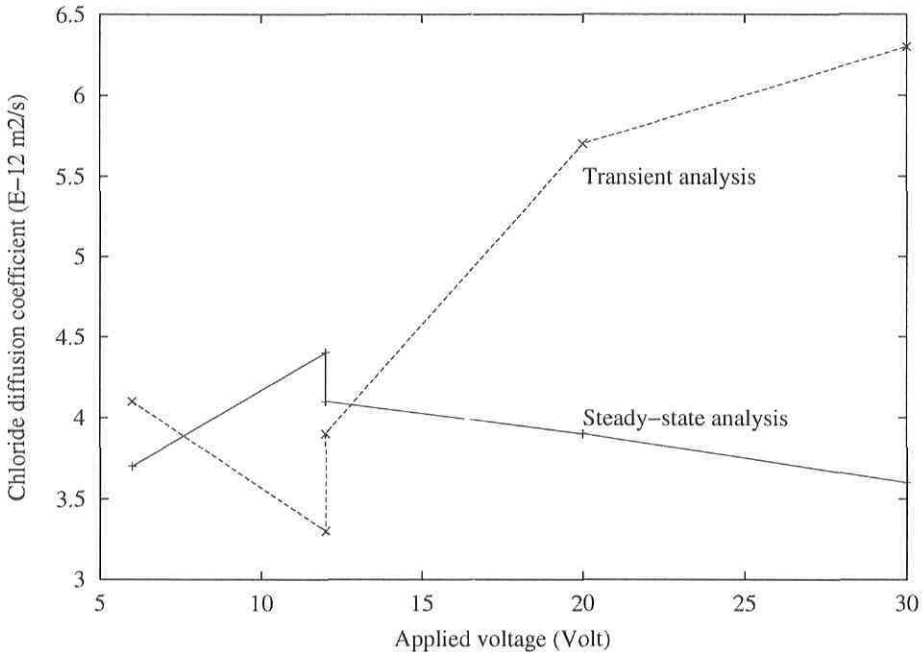

Figure 4.2: Influence of voltage determination on diffusion coefficients: comparison of two analysis methods (data from reference [124]).

4.2.4.3 Discussion on the validity of the constant field hypothesis

Over the years, numerous authors have investigated the use of equations (4.17) and (4.18) to calculate diffusion coefficients on the basis of migration test data. Many authors have found the diffusion coefficients derived from both equations to be sensitive to the boundary conditions. For instance, in a very comprehensive analysis of steady-state chloride migration experiments, Hauck [82] observed quite significant variations of D_i according to the concentration of the test solution in the upstream compartment. Similar results were later reported by Zhang and Gjorv [212].

In another series of migration experiments performed on samples of a 0.5 water/cement ratio concrete, McGrath and Hooton [124] investigated the influence of voltage on both the steady-state and non steady-state regimes. Their results are summarized in Figure 4.2. As can be seen, the applied potential was found to have a strong influence of the values of D_i. This is particularly the case for the diffusion coefficients calculated using equation (4.18), i.e. those obtained for the non steady-state migration experiments for which D_i values were found to vary by a factor of two.

The apparent sensitivity of diffusion coefficient values calls into question the validity of equations (4.17) and (4.18). As previously mentioned, D_i should be an *instrinsic property* of the material (and of the ionic species considered). Accordingly, its value should be independent of the boundary conditions used during the test (at least for migration experiments performed under isothermal conditions).

The significant variations of D_i with the concentration of the test solution and the voltage applied to the system can be, at least partially, explained by the fact that equations (4.17) and (4.18) were both developed on the basis of the constant field assumption. Although the validity of this hypothesis has been discussed by various authors in the past [10, 182, 9, 205], the question has apparently never been settled.

In order to validate the constant field assumption, a sample problem is studied. It consists in calculating the penetration of chloride ions within a sample during a migration test with three different transport models:

- Extended Nernst-Planck equation coupled with Poisson's equation (equations 4.14 and 4.15)
- Nernst-Planck equation coupled with Poisson's equation (equation 4.14 without the chemical activity term and equation 4.15)
- Constant field assumption without chemical activity effects (equation 4.19)

In all cases, it was assumed that a 35 mm thick concrete sample was subjected to a electrical potential of 14 V. The data needed to perform the calculations are given in Table 4.2. All calculations were done over a 20 h period.

The electrical potential distributions obtained from the resolution of the three different sets of equations after 20 h of test are shown in Figure 4.4. The figure reveals only slight differences between the potential profile predicted by the constant field assumption (i.e. equation (4.18)) and that predicted by the two versions of the extended Nernst-Planck equations (i.e. equations (4.14) with and without the chemical activity term). However, the slight differences in potential profiles lead to significant differences in chloride concentration profiles, as shown in Figure 4.3. As can be seen, the constant field assumption has not only a significant influence on the total depth of chloride penetration but it also markedly influences the distribution of ions across the

Table 4.2: Data for the non steady-state chloride migration simulation.

Properties	Values	Properties	Values
Thickness	35 mm	Tortuosity	0.01
Diffusion coefficients	(10^{-11} m^2/s)	Porosity	0.11
OH^-	5.27		
Na^+	1.33	Bound. cond. ($x = 0$)	
K^+	1.96	OH^-	300.0 mmol/L
SO_4^{2-}	1.06	Na^+	800.0 mmol/L
Ca^{2+}	0.79	K^+	0.0 mmol/L
Cl^-	2.03	SO_4^{2-}	0.0 mmol/L
		Ca^{2+}	0.0 mmol/L
Initial conditions		Cl^-	500.0 mmol/L
OH^-	400.0 mmol/L	Ψ	0.0 V
Na^+	100.0 mmol/L		
K^+	320.0 mmol/L	Bound. cond. ($x = L$)	
SO_4^{2-}	11.0 mmol/L	OH^-	300.0 mmol/L
Ca^{2+}	1.0 mmol/L	Na^+	300.0 mmol/L
Cl^-	0.0 mmol/L	K^+	0.0 mmol/L
Ψ	0.0 V	SO_4^{2-}	0.0 mmol/L
		Ca^{2+}	0.0 mmol/L
Temperature	25 °C	Cl^-	0.0 mmol/L
		Ψ	14.0 V

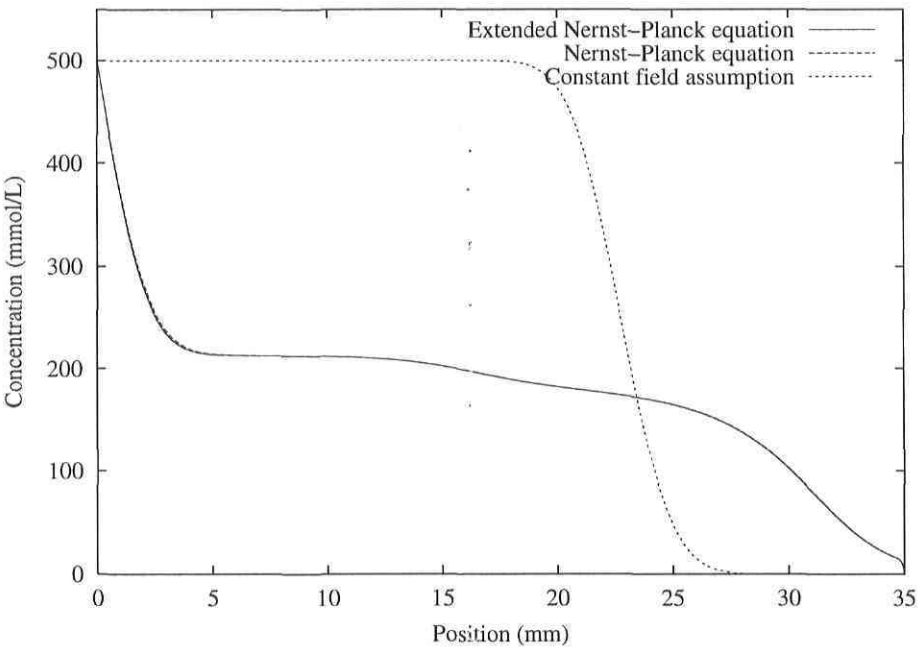

Figure 4.3: Sample problem – Comparison of the chloride profiles in the material after 20 h for the different models: extended Nernst-Planck (eq. 4.14), Nernst-Planck (eq. 4.14 without the activity term), constant field assumption (eq. 4.19).

entire sample. According to equation (4.19), chloride ions do penetrate the sample as a relatively sharp front, while the two profiles predicted by equations (4.14) and (4.15) are much more similar to those observed for a simple diffusion experiment. Results appearing in Figure 4.3 also indicate that chemical activity effects have little influence on the concentration profile during a non steady-state migration test.

Typical non steady-state migration test results previously reported by Tang and Nilsson [181] are given in Figure 4.5. These profiles are similar in shape to those usually found in the literature for non steady-state migration tests (see for instance reference [184]). The comparison of these two profiles to those appearing in Figure 4.3 illustrates the inherent difficulty of calculating diffusion coefficients using equation (4.19). As mentioned in the previous section, the value D_i is obtained by fitting the chloride profile calculated numerically to the one measured during the migration test. Given the marked difference between the shapes of the two curves, it is hard to see how the resolution of equation (4.18) can yield reliable diffusion coefficient values.

A comparison was also made between the steady-state flux calculated with the

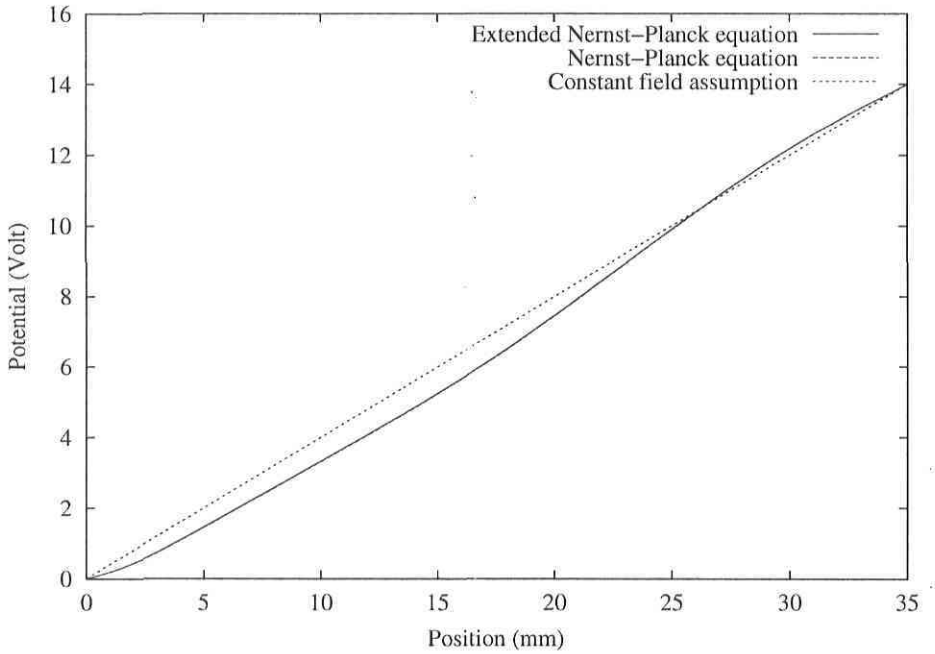

Figure 4.4: Sample problem – Comparison of the electrical potential in the material after 20 h for the different models: extended Nernst-Planck (eq. 4.14), Nernst-Planck (eq. 4.14 without the activity term), constant field assumption (eq. 4.19).

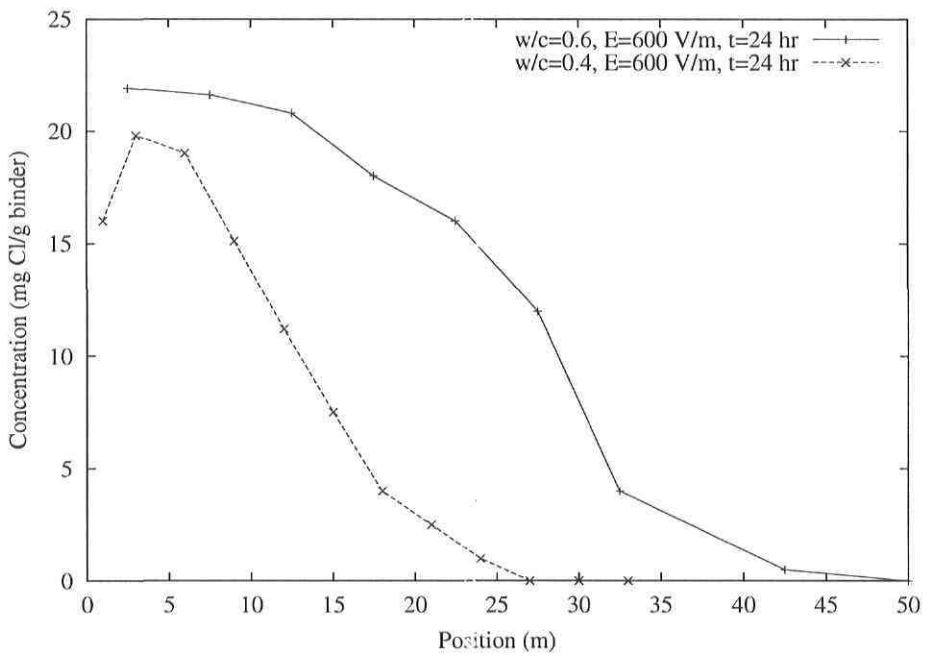

Figure 4.5: Chloride profile measured by Tang and Nilsson [181] on two different cement-based mixtures after a 24 h migration test.

Table 4.3: Steady-state flux calculation for three different ionic transport model.

Model	Flux ($mol/m^2/s$)
Extended Nernst-Planck	7.5×10^{-6}
Nernst-Planck	7.6×10^{-6}
$J_i = -\phi\frac{D_i z_i F}{RT}C_i\frac{\Delta\Psi_{ext}}{L}$	1.7×10^{-5}

extended Nernst-Planck model (equation 4.14), Nernst-Planck model (equation 4.14 without the chemical activity term), and the simplified steady state model (equation 4.17). Results are given in Table 4.3. On the one hand, the steady-state results show that the chemical activity gradient has only a minor influence on the transport of ions during the test. On the other hand, the simplified steady-state model overestimates the kinetics of transport of ions. The flux of chlorides calculated with the simplified model is 2.7 times higher than the one calculated with the extended Nernst-Planck model. These results are in good agreement with the observations made by various authors who found that diffusion coefficients calculated using a constant-field assumption are usually higher than those derived from the analysis of simple diffusion experiments [184, 67, 68].

4.2.5 An alternative approach to calculate diffusion coefficients using migration test results

The numerous advantages of using the Nernst-Planck/Poisson set of equations to analyze migration test results have been clearly illustrated in the previous section. Over the past years, a more systematic application of this approach has been developed and tested on both laboratory and field concrete samples. This method is briefly described in the following sections.

4.2.5.1 Description of the experimental procedure

The experimental method used to test the samples is essentially a non steady-state migration experiment and can be considered as a modified version of the ASTM C

1202 procedure. Two representative samples (100 mm in diameter) are usually tested per mixture. The thickness of the samples ranges from 25 mm for mortars to 50 mm for concrete mixtures. The samples are vacuum saturated in a 300 mmol/L NaOH solution prior to testing. The disks are then glued to plastic rims that fit between the upstream and the downstream cell (see Figure 4.1), leaving an exposed diameter of about 76 mm.

Both compartments of the migration cell are filled with a sodium hydroxide solution prepared at a pH of 13.5. As previously mentioned, the high pH of the test solutions contributes to minimize the risk of microstructural alterations during the experiment. The upstream compartment also contains another salt, like NaCl or Na_2SO_4. The transport of ions through the sample is accelerated by applying an electrical potential (usually 500 V/m) across the two surfaces of the sample. The current passing through the system and the chloride concentration of the downstream compartment are monitored during approximately 120 h. Electrical current measurements are easier to perform and less labor intensive than the determination of chloride profiles usually performed for non steady-state migration experiments. Current measurements are also inherently more precise due to modern instrumentation.

4.2.5.2 Description of the calculation method

The current values are analyzed with the coupled extended Nernst-Planck-Poisson set of equations, i.e. equations (4.14) and (4.15):

$$\frac{\partial C_i}{\partial t} - \frac{\partial}{\partial x}\left(D_i\frac{\partial C_i}{\partial x} + \frac{D_i z_i F}{RT}C_i\frac{\partial \Psi}{\partial x} + D_i C_i\frac{\partial \ln \gamma_i}{\partial x}\right) = 0 \quad \text{with} \quad D_i = \tau D_i^{\mu}$$

$$\tau\frac{d^2\Psi}{dx^2} + \frac{F}{\epsilon}\sum_{i=1}^{N} z_i C_i = 0$$

The boundary conditions correspond to the concentrations in both cells as well as the imposed potential difference across the sample. The short duration of the experiment, and the corresponding small total flux of species, allows for the assumption that concentrations in both the upstream and downstream reservoirs remain constant. As suggested earlier, the chemical reactions are neglected.

The initial conditions are determined by the pore solution chemistry and the porosity of the sample prior to the test. The total pore volume of the material can easily

be determined according to ASTM C 642. Information on the chemical make-up of the pore fluid can be obtained by performing a pore solution extraction experiment according to the procedure described by Barneyback and Diamond (see reference [16]). A special extraction cell specifically designed to accommodate concrete samples is used. Solution samples collected during the tests are analyzed by ion chromatography.

With these data, the equations are solved with different tortuosity values. The numerical current I_c^{num} is calculated at the measurement times according to [85]:

$$I_c^{\text{num}} = SF \sum_{i=1}^{N} z_i J_i \tag{4.20}$$

where S is the exposed surface area of the sample and J_i is the ionic flux given by equation (4.13):

$$J_i = -\phi D_i \frac{\partial C_i}{\partial x} - \phi \frac{D_i z_i F}{RT} C_i \frac{\partial \Psi}{\partial x} - \phi D_i C_i \frac{\partial \ln \gamma_i}{\partial x}$$

For each tortuosity value, the error between the model and the measurements is calculated as:

$$\text{error} = \sqrt{\sum_{k=1}^{M} (I_{c,k}^{\text{mes}} - I_{c,k}^{\text{num}})^2} \tag{4.21}$$

where M is the total number of measurements, and I_c^{mes} and I_c^{num} are the measured and predicted currents, respectively. The tortuosity value leading to the smallest error with the measurements yields the best estimate of the diffusion coefficient for each ionic species in the material considered. This analysis procedure is automated in a numerical code which yields the diffusion coefficients of OH^-, Na^+, K^+, SO_4^{2-}, Ca^{2+} and Cl^- that minimize the error with the measured currents.

4.2.5.3 Experimental validation of the method

For the purpose of this study, the method was tested on a series of mortar samples. The mortar mixture was prepared at a water/cement ratio of 0.5 with a CSA Type 10 cement and a standard (ASTM C109 Ottawa) sand. The volume proportion of the sand was 50 %. The specimens were cast in 100 mm diameter, 200 mm long cylindrical molds under vacuum to avoid air-void formation. The day after casting, the samples were demoulded and sealed in aluminum foil for 18 months. After the curing

Table 4.4: Pore solution extraction and porosity measurement. The extracted concentration showed are adjusted to respect the electroneutrality requirement.

Ions	Concentration (mmol/L)
OH^-	515.6
Na^+	176.6
K^+	354.8
SO_4^{2-}	9.0
Ca^{2+}	1.1
Porosity	0.184

period, the foil was removed and the cylinders were sawn into 25 mm thick disks. The samples to be tested were saturated in a 300 mmol/L NaOH solution for 24 h. An additional disk was saturated in the same conditions. It was then subjected to a pore pressing experiment in order to measure the ionic content of the pore solution. Finally, another sample was used to determine the porosity of the material. The porosity and pore solution measurements are given in Table 4.4. The measured concentrations were adjusted to respect the electroneutrality requirement. Otherwise, problems with the numerical model could occur.

The samples were then tested according to the non steady-state migration procedure described in the previous section. In order to validate the approach, the samples were subjected to different test conditions, which are summarized in Table 4.5. For each test condition, two disks were tested. The potentials cited in Table 4.5 are those applied to the whole migration cell (see Figure 4.1). During the experiment, a small drop of potential typically occurs in both compartments. So throughout the test, the potential difference across the sample V_s was measured regularly. The error estimation corresponds to the standard deviation over all the potential measurements made during a test. The small value of this error indicates stable conditions throughout the experiment. The value of V_s corresponds to the boundary condition of the potential at $x = L$ in the numerical code. The tests lasted 114 h for the first four samples and 121 h for the remaining ones. Six current measurements are made during the tests.

The numerical model is then used to analyze the measured currents. The tortuosity and chloride diffusion coefficient found for each disk tested are given in Table 4.5. Even

Table 4.5: Results of the migration test. V_s stands for the potential difference at the sample's boundaries. The uncertainty attributed to V_s corresponds to the standard deviation of the set of measurements performed during a test.

Conditions	Disks	V_s (V)	Tortuosity (1)	D_{Cl} (10^{-11} m^2/s)
500 mmol/L NaCl,	1	10.3 ± 0.2	0.0303	6.17
12 V	2	10.3 ± 0.2	0.0283	5.74
500 mmol/L NaCl,	1	5.1 ± 0.1	0.0245	4.97
6 V	2	5.2 ± 0.1	0.0273	5.55
100 mmol/L NaCl,	1	10.6 ± 0.1	0.0233	4.74
12 V	2	10.4 ± 0.2	0.0248	5.05
200 mmol/L Na_2SO_4	1	10.6 ± 0.1	0.0214	4.36
12 V	2	10.9 ± 0.1	0.0197	4.01
Average:			0.0250	5.07
Standard dev.:			0.0036	0.72

if the method gives the diffusion coefficient for all species present in the system, only the value for chloride is given. Equation (4.3), in combination with the diffusion coefficient in free water, must be used in order to have the diffusion coefficient values for the other species. The results listed in Table 4.5 have an average value of $(5.07 \pm 0.72) \times 10^{-11}$ m^2/s. The error value corresponds to the standard deviation. A typical current curve, showing the comparison between the measurements and the numerical results, is shown in Figure 4.6.

4.2.5.4 Discussion

The proposed method avoids the applied electrical potential dependency exhibited by other analysis procedures found in the literature. The constant field assumption, which neglects the internal coupling among the ions during a migration test, was identified as a possible cause for this behavior. The results for the 500 mmol/L NaCl in the upstream cell with 12 V and 6 V (see Table 4.5, the four first rows), show only a slight dependency upon the applied potential. The average value of the chloride diffusion

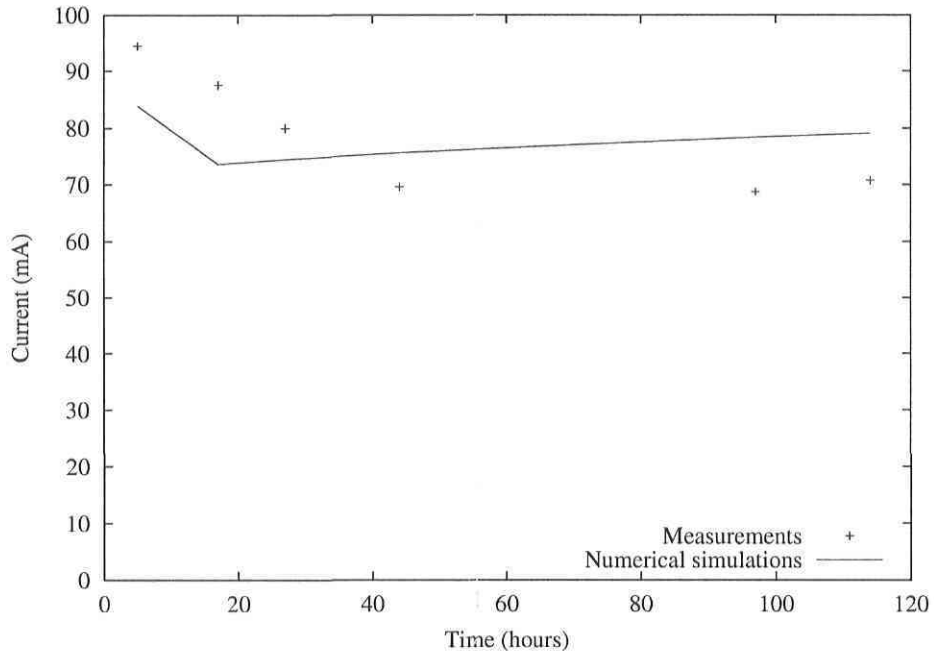

Figure 4.6: Comparison of the measured current with the numerical model for the case with 500 mmol/L NaCl in the upstream cell, 12 V applied, disk 1.

coefficient for the four disks is $(5.61 \pm 0.50) \times 10^{-11}$ m^2/s, the uncertainty (standard deviation) being smaller than the uncertainty for the whole set of experiments (± 0.72).

The migration tests performed with 100 mmol/L NaCl and 200 mmol/L Na_2SO_4 gave results that, although in the same range of values as the other results, are smaller. These results exhibit the effects of the concentration level and/or the migrating salt in the upstream cell on the diffusion coefficient. Since it was shown in Figure 4.3 that the chemical activity gradient has virtually no effect on the concentration profile, these variations related to the concentration could come from the neglected chemical reactions.

It is interesting to note that the current drop measured at the beginning of the test is also predicted by the model (see Figure 4.6). Upon closer examination, this behavior is to be expected. To transport chloride and sulfate ions out of the upstream reservoir, the electric field points from the downstream to the upstream reservoir. At the upstream interface, the chloride concentration in the sample is increasing, but the hydroxyl concentration is decreasing faster because the hydroxyl ions are more mobile. At the downstream interface, 0.3 mol/L sodium ions are replacing 0.18 mol/L sodium

and 0.35 mol/L potassium ions. Moreover, because the potassium ion has a greater mobility than sodium, the downstream interface is becoming depleted of cations. As a net result, the ionic strength at both ends of the sample decrease, decreasing the overall conductivity, leading to a reduction in the current. For one-dimensional transport, even a thin layer of low conductivity material can have a dramatic effect on the overall bulk conductivity.

4.2.6 Conclusion

This study demonstrated that the commonly used constant field hypothesis should not be used to model the migration experiment. Instead, a multiionic model considering the electrical coupling among the ions should be applied.

The proposed approach is based on a non-steady-state analysis of the migration test with the extended Nernst-Planck/Poisson set of equations. The chemical reactions are neglected from the analysis. Although the complete method requires a more sophisticated calculation than that typically employed, it also offers some advantages: It is based on current measurements that are less expensive and easier to perform than the chloride concentration evaluations that are frequently used with the migration test. The method gives the diffusion coefficient of each ionic species in the material, according to the theory of homogenisation used to develop the mathematical model. The tests have shown that it is not dependent on the external potential applied to the sample. Finally, it is slightly dependent on the concentration level in the upstream cell as well as on the type of electrolyte in this cell.

4.3 Theoretical analysis of the effect of weak sodium sulfate solutions on the durability of concrete

J. Marchand[12], E. Samson[12], Y. Maltais[12], J.J. Beaudoin[3]

[1]Centre de recherche interuniversitaire sur le béton,
Université Laval, Québec, Canada, G1K 7P4

[2]SIMCO Technologies inc.,
1400, boul. du Parc Technologique, Québec, Canada, G1P 4R7

[3]Materials Laboratory - Institute for Research in Construction,
National Research Council, Ottawa, Canada, K1A 0R6

Abstract

A theoretical analysis of the detrimental influence of weak sodium sulfate solutions (Na_2SO_4) on the durability of concrete is presented. It was conducted using a numerical model that takes into account the coupled transport of ions and liquid and the chemical equilibrium of solid phases within the (partially) saturated system. Numerous simulations were performed to investigate the influence of various parameters such as water/cement ratio (0.45, 0.65 and 0.75), type of cement (CSA Type 10 and Type 50), sulfate concentration (0 to 30 mmol/L of SO_4) and the gradient in relative humidity across the material. All input data related to the properties of concrete were obtained by testing well-cured laboratory mixtures. Numerical results indicate that exposure to weak sulfate solutions can result in a significant reorganization of the microstructure of concrete. The penetration of sulfate ions into the material is not only at the origin of the precipitation of sulfate bearing phases (such as ettringite and eventually gypsum) but also results in calcium hydroxide dissolution and C-S-H decalcification. Data also clearly emphasize the fact that water/cement ratio remains the key parameter that controls the durability of concrete to sulfate attack.

4.3.1 Introduction

Concrete subjected to sulfate attack can undergo a progressive and profound reorganization of its internal microstructure [176, 185]. These alterations have direct consequences on the engineering properties of the material. For instance, concrete undergoing sulfate attack is often found to suffer from swelling, spalling and cracking [83, 132, 176, 170]. There is also overwhelming evidence to show that the degradation also contributes to a significant reduction of the mechanical properties of concrete [27, 170]. Many structures affected by sulfate degradation often need to be repaired or, in the most severe cases, partially reconstructed.

Table 4.6: Recommendations for protecting concrete exposed to sulfate contaminated environments (from references [4, 5, 31, 191])

Exposure	Water soluble sulfate (SO_4) in soil, percent	Sulfate (SO_4) in water, ppm	Cement	Water-cement ratio, maximum
Mild	0.00 - 0.10	0-150	—	—
Moderate	0.10 - 0.20	150 - 1500	Type II, IP (MS), IS (MS),	0.50
Severe	0.20 - 2.00	1500 - 10000	Type V	0.45
Very severe	Over 2.00	Over 10000	Type V + pozzolan or slag	0.45

Given the deleterious effects of sulfate attack, building codes have traditionally specified precautionary measures to protect concrete against this type of degradation. Typical measures contained in North American building codes [4, 5, 191, 31] are summarized in table 4.6. As can be seen, the choice of cement (ASTM Type I, Type II, Type V or the equivalent) and the selection of water/cement ratio vary according to the severity of the exposure conditions.

It should be emphasized that recommendations concerning concrete exposed to negligible sulfate concentrations (i.e. soils containing less than 0.10% of water soluble sulfate or solutions for which the SO_4 concentration is less than 150 ppm) are relatively vague. Although building codes usually emphasize the importance of limiting the permeability of concrete to prevent the penetration of moisture and ions [4], none of them contains any specific limit concerning the maximum water/cement ratio that should be selected for the production of concrete elements to be exposed to negligible levels of sulfate (see table 4.6). This is unfortunate since, as emphasized by many authors, potentially destructive conditions may exist even though analyses indicate the ground water or soil to have a low sulfate content [50, 75, 78]. According to DePuy [50], this

[4] For instance, the Canadian Standard [31] limits the water/cement ratio of concrete exposed to salts without any freezing and thawing to 0.55. Similarly, in its Concrete Craftsman Series, the American Concrete Institute (ACI) [6] recommends to limit water/cement ratio to 0.7 for concrete to be used for the construction of slabs on grade.

is apparently often the case when concrete is exposed to wetting and drying cycles.

The present study was conducted to provide additional information on the potentially deleterious effects of weak sulfate solutions on the behavior of concrete. A numerical model, called STADIUM[5], was used to investigate the mechanisms of degradation. This model takes into account the coupled transport of ions and liquid and the chemical equilibrium of solid phases within the (partially) saturated system. Previous studies have indicated that numerical results yielded by the model for hydrated cement systems subjected to sulfate attack and calcium leaching compare favorably to those measured experimentally [112].

4.3.2 Description of the numerical model

4.3.2.1 Description of the various transport processes

STADIUM has been developed to predict the transport of ions in unsaturated porous media. As will be discussed in the following section, the model also accounts for the effect of dissolution/precipitation reactions on the transport mechanisms.

The description of the various transport mechanisms relies on the homogenization technique. This approach first requires writing all the basic equations at the pore scale. These equations are then averaged over a Representative Elementary Volume (REV) in order to describe the transport mechanisms at the macroscopic scale. More information on the transport equations at the pore scale and the averaging technique can be found in references [18, 156].

In the model, ions are considered to be either free to move in the liquid phase or bound to the solid phase. The transport of ions in the liquid phase at pore scale is described by the extended Nernst-Planck equation to which an advection term is added [85]. After integrating this equation over the REV, the transport equation becomes:

$$\frac{\partial\left((\theta_s C_{is})\right)}{\partial t} + \frac{\partial(\theta C_i)}{\partial t} - \frac{\partial}{\partial x}\left(\theta D_i \frac{\partial C_i}{\partial x} + \theta \frac{D_i z_i F}{RT} C_i \frac{\partial \Psi}{\partial x} + \theta D_i C_i \frac{\partial \ln \gamma_i}{\partial x} - C_i V_x\right) = 0 \tag{4.22}$$

In equation (4.22), θ_s is the solid content of the material, C_i is the concentration of

[5]STADIUM stands for Software for Transport And Degradation In (Un)saturated Materials.

the species i in the aqueous phase, C_{is} is the concentration of the solid phase, θ is the volumetric water content, D_i is the diffusion coefficient, z_i is the valence number of the species, F is the Faraday constant, R is the ideal gas constant, T is the temperature of the liquid, Ψ is the electrical potential, γ_i is the chemical activity coefficient and V_x is the velocity of the fluid.

Equation (4.22) has to be written for each ionic species present in the system. The behavior of hydrated cement materials (in chloride and magnesium free environments) can be reliably described by considering six different ionic species: OH^-, Na^+, K^+, SO_4^{2-}, Ca^{2+} and $Al(OH)_4^-$.

To calculate the chemical activity coefficients, several approaches are available. However, classical models such as those proposed by Debye-Hückel or Davies are unable to reliably describe the thermodynamic behavior of highly concentrated electrolytes such as the hydrated cement paste pore solution [133]. A modification of the Davies equation was found to yield good results [155]:

$$\ln \gamma_i = -\frac{Az_i^2\sqrt{I}}{1 + a_i B\sqrt{I}} + \frac{(0.2 - 4.17 \times 10^{-5}\, I)Az_i^2 I}{\sqrt{1000}} \tag{4.23}$$

where I is the ionic strength of the solution:

$$I = \frac{1}{2}\sum_{i=1}^{N} z_i^2 c_i \tag{4.24}$$

and A and B are temperature-dependent parameters. The parameter a_i in equation (4.23) depends on the ionic species. Its value (in meters) is 3×10^{-10} for OH^-, 3×10^{-10} for Na^+, 3.3×10^{-10} for K^+, 1×10^{-10} for SO_4^{2-}, 2×10^{-10} for Cl^- and 1×10^{-13} for Ca^{2+}[155].

A last relation is required to complete the system of equations and calculate the electrical potential Ψ appearing in equation (4.22). This can be done using the Poisson equation, which relates the electrical potential to the concentration of each ionic species [157, 158]. The equation is given here in its averaged form:

$$\frac{\partial}{\partial x}\left(\theta\tau\frac{\partial \Psi}{\partial x}\right) + \vartheta\frac{F}{\epsilon}\sum_{i=1}^{N} z_i C_i = 0 \tag{4.25}$$

where N is the total number of ionic species, ϵ is the dielectric permittivity of the medium, in this case water, and τ is the tortuosity of the porous network. The physical meaning of the tortuosity coefficient is discussed in references [18, 156].

The velocity of the fluid, appearing in equation (4.22) as V_x, can be described by a diffusion equation when the driving force for the movement of water is linked to the capillary forces arising in the porous solid during drying/wetting cycles [135]:

$$V_x = -D_w \frac{\partial \theta}{\partial x} \tag{4.26}$$

where D_w is the non-linear water diffusion coefficient. This parameter varies according to the water content of the material [135].

To complete the model, the mass conservation on the liquid phase must be taken into account [135]:

$$\frac{\partial \theta}{\partial t} - \frac{\partial}{\partial x}\left(D_w \frac{\partial \theta}{\partial x}\right) = 0 \tag{4.27}$$

As can be seen, moisture transport is described in terms of a variation of the (liquid) water content of the material. It should be emphasized that the choice of using the material water content as the state variable for the description of this problem has an important implication on the treatment of the boundary conditions. Since the latter are usually expressed in terms of relative humidity, a conversion has to be made. This can be done using an adsorption/desorption isotherm [135].

The system of non-linear equations has to be solved numerically. Information on the numerical resolution of the problem using the finite element method can be found in references [157, 158].

4.3.2.2 Chemical equilibrium step

The first term on the left-hand side of equation (4.22) (in which C_{is} appears), accounts for the ionic exchange between the solution and the solid. It can be used to model the influence of precipitation/dissolution reactions on the transport process. However, in the algorithm used in STADIUM, this term is eliminated and the chemical reactions are considered in a separate chemical equilibrium module [73]. The chemical equilibrium of the various solid phases present in the material is verified at each node of the finite element mesh by considering the concentrations of all ionic species at this location. If the equilibrium condition is not respected, the concentrations and the solid phase content are corrected accordingly.

Table 4.7: Equilibrium constants for solid phases in hydrated cement systems

Name	Chemical composition	Expression for equilibrium	Value of equilibrium constant (-log Ksp)
Portlandite	$Ca(OH)_2$	$Ksp = \{Ca\}\{OH\}^2$	5.2
C-S-H	$1.65CaO.SiO_2.(2.45)H_2O$ †	$Ksp = \{Ca\}\{OH\}^2$ ‡	5.6 ‡
Ettringite	$3CaO.Al_2O_3.3CaSO_4.32H_2O$	$Ksp = \{Ca\}^6\{OH\}^4\{SO_4\}^3\{Al(OH)_4\}^2$	44.0
Hydrogarnet	$3CaO.Al_2O_3.6H_2O$	$Ksp = \{Ca\}^3\{OH\}^4\{Al(OH)_4\}^2$	23.0
Gypsum	$CaSO_4.2H_2O$	$Ksp = \{Ca\}\{SO_4\}$	4.6

$\{\ldots\}$ indicates chemical activity

† C-S-H is assumed to have a C/S ratio of 1.65

‡ The C-S-H decalcification is modeled as the portlandite dissolution with a lower solubility

For instance, the equilibrium constant of calcium hydroxide (or portlandite) is given by:

$$K_{sp} = \{Ca\}\{OH\}^2 \tag{4.28}$$

where the curly brackets $\{\ldots\}$ indicate chemical activity. As previously mentioned, equation (4.28) must be verified at each node within the system. If, due to the transport process, the solution is locally supersaturated or undersaturated, the concentration in ions are corrected to restore the chemical equilibrium. This procedure is applied at each node to each solid phase present in the system.

The behavior of hydrated cement systems exposed to relatively weak sodium sulfate (Na_2SO_4) solutions is described by considering five different solid phases, namely: portlandite, C-S-H, ettringite, hydrogarnet, and gypsum. These phases are listed in table 4.7, along with their equilibrium constant [141].

Obviously, the treatment of an ill-crystallized phase such as the C-S-H presents some difficulties. As can be seen in table 4.7, an apparent equilibrium constant is attributed to the C-S-H. The value of this constant was established on the basis of previous published reports on the thermodynamic stability of hydrated cement systems [3, 23]. The *dissolution* of C-S-H (the so-called decalcification process) is assumed to proceed by the release of calcium and hydroxide ions (in a proportion of one Ca^{2+} to two OH^- in order to maintain the electroneutrality of the solution) leaving behind a silica gel. This approach is in good agreement with the observation of Faucon [63] who could analyze the composition of decalcified C-S-H using nuclear magnetic resonance (NMR) spectroscopy and Mossbauer spectroscopy (such as NMR).

Chemical reactions can also modify the transport properties of the material by

affecting its pore structure. For instance, the precipitation of gypsum may contribute to locally reduce the porosity of the material, thus decreasing the section across which ions are able to diffuse. This may have an effect on the diffusion coefficient of the material. This effect is taken into account using the equation proposed by Garboczi and Bentz [66]:

$$\frac{D_i}{D_i^{\mu}} = 0.001 + 0.07\phi_{\text{cap}}^2 + 1.8 \times H(\phi_{\text{cap}} - 0.18)(\phi_{\text{cap}} - 0.18)^2 \tag{4.29}$$

where ϕ_{cap} is the capillary porosity of the paste, D_i^{μ} is the diffusion coefficient of the ionic species i in free solution (as opposed to its diffusion coefficient in the porous solid) and H is the Heaviside function such that $H(x) = 1$ for $x > 0$ and $H(x) = 0$ for $x \leq 0$. The initial capillary porosity of the material can be calculated using the following relationship [140]:

$$\phi_{\text{cap}}^{\text{init}} = \frac{(w/c) - 0.36\alpha}{(w/c) + 0.32} \tag{4.30}$$

where w/c is the water/cement ratio of the paste and α is the degree of hydration of cement ($0 \leq \alpha \leq 1$). The influence of chemical reactions on the capillary porosity of the material can be calculated as follows:

$$\phi_{\text{cap}} = \phi_{\text{cap}}^{\text{init}} + \sum_{s=1}^{M} (V_{\text{s}}^{\text{init}} - V_{\text{s}}) \tag{4.31}$$

where V_s is the volume of a given solid phase, per unit volume of cement paste, and M is the total number of solid phases. According to this approach, the correction factor G that multiplies the diffusion coefficients D_i of each ionic species is given by:

$$G = \frac{\left.\frac{D_i}{D_i^{\mu}}\right|_{\text{Modified paste}}}{\left.\frac{D_i}{D_i^{\mu}}\right|_{\text{Initial paste}}} \tag{4.32}$$

The application of equations (4.31) and (4.32) to description of the influence of the C-S-H decalcification process on the diffusion properties of hydrated cement systems presents some obvious problems. Within the framework of this investigation, the value of the correction factor G has been arbitrarily fixed at 10 for fully decalcified systems. Sensitivity analyses have indicated that the value of this factor (for the decalcified C-S-H) has little influence on the kinetics of degradation.

Table 4.8: Characteristics of the concrete mixtures

	W/C=0.45	W/C=0.65	W/C=0.75
Cement (kg/m^3)	380.0	280.0	250.0
Water (kg/m^3)	171.0	182.0	187.5
Sand (kg/m^3)	719.0	833.0	931.0
Coarse aggregate (kg/m^3)	1127.0	1065.0	972.7
Volumetric paste content (%)	29.2	27.1	26.7

4.3.3 Characteristics of the materials

In order to obtain the input data required to run the model, six different concrete mixtures were cast and tested. Test variables included type of cement (CSA Type 10 and CSA Type 50) and water/cement ratio (0.45, 0.65 and 0.75). The characteristics of the six concrete mixtures are given in table 4.8 and the chemical and mineralogical compositions of the two cements are summarized in table 4.9.

All mixtures were prepared with a natural siliceous sand and a crushed granitic stone. The maximum size of the coarse aggregates used to prepare the concrete mixture was 14 mm.

All mixtures were prepared in a counter-current pan mixer (capacity = 0.1 m^3). The aggregates (coarse and fine) and the cement were first introduced in the mixer, and mixed for one minute to homogenize the materials. Water was then added to the dry materials over a period of 30 seconds. Concrete was initially mixed for three minutes. After a pause of three minutes, concrete was mixed for another two minutes. The concrete was then periodically mixed for thirty seconds every five minutes over a 20-minute period in order to simulate continuous mixing.

The fresh concrete mixtures were cast in plastic moulds (diameter = 100 mm and height = 200 mm). The moulds were filled in three layers in accordance with the requirements of CSA A23.2-3C (the Canadian version of ASTM C192/C 192M-95). Samples were demolded approximately 24 hours after casting, and sealed in an aluminum foil for 91 days in order to avoid any exchange of moisture with the surrounding

Table 4.9: Chemical and mineralogical analyses of the cements

Oxides	Type 10	Type 50
SiO_2	20.4	22.5
Al_2O_3	4.3	3.0
Fe_2O_3	3.0	3.7
CaO	62.1	63.5
MgO	2.8	3.2
SO_3	3.2	2.0
Na_2O	n/d	0.2
K_2O	n/d	0.4
Na_2O eq.	0.8	0.4
Free CaO	1.0	0.8
Loss on ignition	2.0	1.1
Insoluble residue	0.6	0.2
Bogue analysis		
C_3S	55.4	56.3
C_2S	16.7	22.0
C_3A	6.3	1.7
C_4AF	9.1	11.3

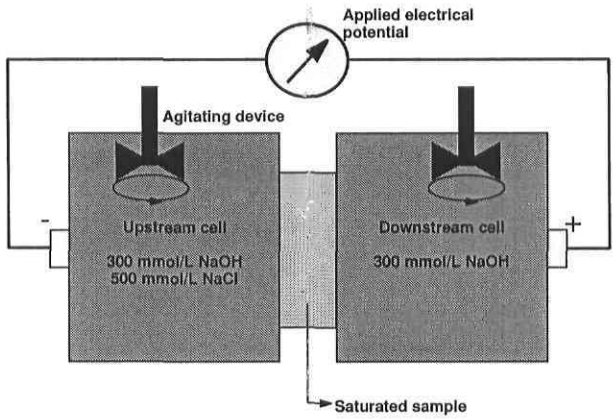

Figure 4.7: Experimental set-up for the migration test

environment.

At the end of the curing period, 25-mm thick disks were cut and tested for chloride migration. Migration tests were used to determine the diffusion coefficients of the ionic species in the various mixtures. Prior to testing, all samples were first immersed in a 300 mmol/L NaOH solution and vacuum saturated for about 48 hours. After this saturation period, samples were mounted on a migration cell consisting in two compartments (individual capacity of 3L) as shown in figure 4.7. The upstream compartment was filled with a solution of 300 mmol/L NaOH and 500 mmol/L NaCl, while a 300 mmol/L NaOH solution was placed in the downstream compartment. The high pH of the test solutions contributes to minimize the risk of microstructural alterations during the experiment. An electrical potential of about 12 Volt was then applied on the migration set-up in order to accelerate the transport of chlorides through the sample. A constant temperature of 23 °C was maintained during the entire duration of the test.

The current circulating through the system was regularly measured during the test, which lasted for about five days. A special version of STADIUM, called STADIUM-ACC, was used to analyze the migration test data and calculate the diffusion coefficients. Results are summarized in tables 4.10 and 4.11.

The pore solution of each mixture was also extracted and analyzed according to the procedure described by Longuet et al. [109] and Diamond [52]. Samples were placed in an extraction cell and crushed at a pressure of approximately 300 MPa. Typically, 2 to 5 ml of pore solution were extracted. The solution was delivered through

a drain ring and channel, and recovered with a syringe in order to limit exposure to the atmosphere. Chemical analyses of the pore solution were carried out shortly after the extraction test. The composition of the solution was then adjusted in order to respect the electroneutrality condition. Slight deviations from electroneutrality can arise due to the experimental error associated with the extraction procedure. The adjusted pore solution data are given in tables 4.10 and 4.11.

Another series of samples were used for porosity measurements, which were carried out according to the requirements of ASTM C 642. Results are also presented in tables 4.10 and 4.11.

The water diffusion properties of the six mixtures were estimated on the basis of Nuclear Magnetic Resonance Imaging (NMRI) measurements performed on companion mortar mixtures [84]. The diffusion coefficients of water used in the simulations are summarized in tables 4.10 and 4.11.

In order to run the model, one has to know the initial amount of each solid phase in the material. The initial amounts of calcium hydroxide and C-S-H were calculated assuming a complete hydration ($\alpha = 1$) of the C_2S and C_3S contained in the cement (see table 4.7), and using the following equations:

$$2(3CaO.SiO_2) + 6H_2O \rightarrow 3CaO.2SiO_2.3H_2O + 3(CaO.H_2O) \quad (4.33)$$

$$2(2CaO.SiO_2) + 4H_2O \rightarrow 3CaO.2SiO_2.3H_2O + CaO.H_2O \quad (4.34)$$

The initial amount of ettringite ($3CaO.Al_2O_3.3CaSO_4.32H_2O$) was calculated by considering that all the gypsum added to the unhydrated cement had reacted with the C_3A. The remaining C_3A, and 50% of the alumina contained in the C_4AF, was assumed to have reacted to form hydrogarnet ($3CaO.Al_2O_3.6H_2O$). The calculated quantities are given in tables 4.10 and 4.11.

4.3.4 Description of the numerical simulations

4.3.4.1 General information

The typical case of a concrete slab resting on a sulfate contaminated soil was considered in all the numerical simulations. In all cases, the thickness of the slab was fixed at 15

Table 4.10: Materials properties used to perform the numerical simulations - CSA Type 10 mixtures

Properties	W/C=0.45 Type 10 cement	W/C=0.65 Type 10 cement	W/C=0.75 Type 10 cement
Diffusion coefficients (m2/s)			
OH^-	10.8e-11	19.5e-11	29.4e-11
Na^+	2.7e-11	4.9e-11	7.4e-11
K^+	4.0e-11	7.2e-11	10.9e-11
SO_4^{2-}	2.2e-11	3.9e-11	5.9e-11
Ca^{2+}	1.6e-11	2.9e-11	4.4e-11
$Al(OH)_4^-$	1.1e-11	2.0e-11	3.0e-11
Water diffusivity (m2/s)	$3.42\times10^{-11}e^{40\theta}$	$3.34\times10^{-12}e^{75\theta}$	$3.33\times10^{-12}e^{77\theta}$
Initial pore solution (mmol/L)			
OH^-	427.97	269.42	268.94
Na^+	185.00	133.50	133.10
K^+	266.50	140.10	137.80
SO_4^{2-}	12.97	3.77	2.95
Ca^{2+}	1.25	1.70	2.00
$Al(OH)_4^-$	0.08	0.05	0.04
Porosity (%)	12.6	13.0	14.7
Tortuosity	0.020	0.037	0.056
Initial solid phases (g/kg)			
Portlandite	48.5	36.3	32.6
C-S-H	92.2	69.0	62.1
Ettringite	26.5	19.8	17.9
Hydrogarnet	11.7	8.7	7.9

Table 4.11: Materials properties used to perform the numerical simulations - CSA Type 50 mixtures

Properties	W/C=0.45 Type 50 cement	W/C=0.65 Type 50 cement	W/C=0.75 Type 50 cement
Diffusion coefficients (m2/s)			
OH^-	17.0e-11	25.8e-11	33.5e-11
Na^+	4.3e-11	6.5e-11	8.5e-11
K^+	6.3e-11	9.6e-11	12.4e-11
SO_4^{2-}	3.4e-11	5.2e-11	6.8e-11
Ca^{2+}	2.6e-11	3.9e-11	5.0e-11
$Al(OH)_4^-$	1.7e-11	2.7e-11	3.4e-11
Water diffusivity (m2/s)	$3.42\times10^{-11}e^{40\theta}$	$3.34\times10^{-12}e^{75\theta}$	$3.33\times10^{-12}e^{77\theta}$
Initial pore solution (mmol/L)			
OH^-	224.47	183.42	98.96
Na^+	107.10	71.40	55.50
K^+	116.50	108.90	34.30
SO_4^{2-}	1.88	1.17	0.30
Ca^{2+}	2.33	2.74	4.89
$Al(OH)_4^-$	0.03	0.03	0.02
Porosity (%)	12.2	13.6	15.3
Tortuosity	0.032	0.049	0.064
Initial solid phases (g/kg)			
Portlandite	51.0	38.1	34.3
C-S-H	101.7	76.1	68.5
Ettringite	16.6	12.4	11.2
Hydrogarnet	5.7	4.3	3.8

cm and the bottom part of the slab was considered to be directly in contact with the soil (containing $Na^+$and SO_4^{2-}ions). Furthermore, it was assumed that the top surface of the slab was free of any barrier and directly in contact with the external environment.

All simulations were performed assuming that the concrete slab was kept in isothermal conditions at 25 °C . Furthermore, the effects of carbonation were not taken into account in the numerical simulations.

4.3.4.2 Boundary conditions

In all the numerical simulations, the boundary conditions were kept constant during the entire service-life of the concrete. Two types of exposure conditions were taken into consideration. In the first case, the bottom surface of the (saturated) concrete slab was assumed to be in direct contact with a fully saturated soil (relative humidity equal to 100%). The air above the slab was also maintained at 100% relative humidity. In this initial case, ions were essentially transported by diffusion, the flux of water by capillary suction being nil.

In the second series of simulations, the bottom portion of the slab was assumed to be in contact with a partially saturated soil (relative humidity equal to 90%) and the air above the slab was kept at 75% relative humidity. In this second case, ions were transported by diffusion and advection (capillary suction) in the partially saturated concrete.

In all cases, the soil in contact with the concrete slab was considered to be contaminated with a sodium sulfate solution. Simulations were run for five different concentrations in SO_4 ranging from from 0 to 30 mmol/L (i.e. from 0 to 60 mmol/L of Na^+). The concentration of all other ions (except $Na^+$and SO_4^{2-}) was assumed to be equal to zero. In all simulations, the ionic flux near the upper part of the slab was considered to be zero.

4.3.4.3 Initial conditions

In all the simulations, the concrete was considered to be initially undamaged. The initial value of the potential Ψ was fixed at zero everywhere in the material. The potential

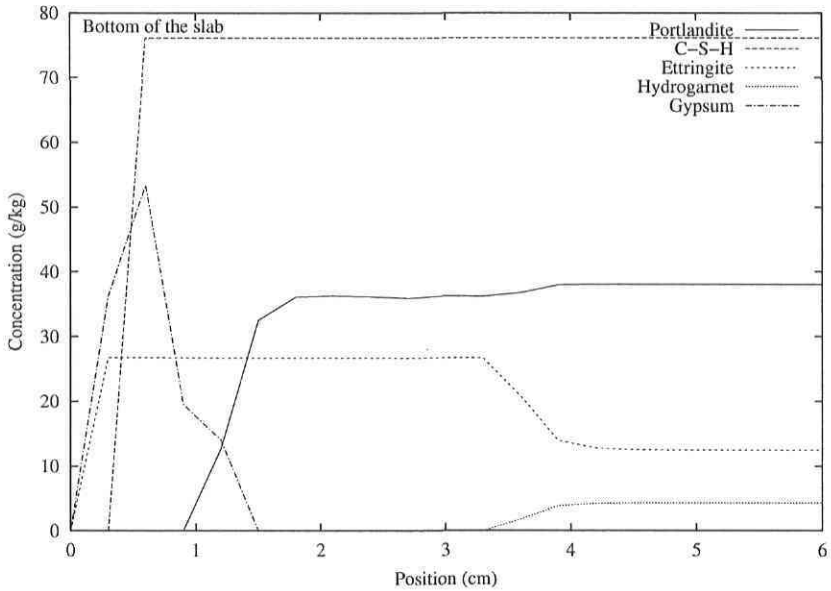

Figure 4.8: Distribution of the solid phases after 20 years for the 0.65 water/cement ratio concrete made with the CSA Type 50 cement and exposed to 10 mmol/L of sulfates - Saturated conditions

was also maintained at zero on the lower part of the slab during the simulations, in order to establish a reference point. The initial composition of the pore solution and the porosity of all mixtures are given in table 4.8.

4.3.5 Results of the numerical simulations

Numerical simulations indicate that the exposure of concrete to weak sodium sulfate solutions can result in an important reorganization of its internal microstructure. A typical example is shown in figure 4.8 where the distribution in calcium hydroxide (portlandite), C-S-H, ettringite, hydrogarnet and gypsum is given for a 0.65 water/cement ratio concrete made of a CSA Type 50 cement and that had been exposed in saturated conditions to 10 mmol of sulfate for 20 years. As indicated in the figure, the left-hand side of the graph corresponds to the surface of the slab in direct contact with the soil (bottom portion).

Figure 4.8 indicates that the reorganization of the internal microstructure of concrete is characterized by the presence of degradation *fronts* that penetrate from the

external (bottom) surface of the slab towards the center of the slab. These results are also in good agreement with most investigations that the microstructure of concrete subjected to external sulfate attack is usually characterized by a succession of layers (or zones) starting from the outer surface of the material [3, 185].

As shown in figure 4.8, the exposure to the sodium sulfate solution has resulted in the formation of additional ettringite. It is important to note that even if the external concentration in SO_4^{2-} was relatively weak, the model also predicts the formation of gypsum. This result is in good agreement with field observations [78, 126, 176].

The precipitation of new sulfate-bearing phases is also accompanied by the dissolution of calcium hydroxide and hydrogarnet and by the decalcification of C-S-H. These phenomena are usually observed for laboratory and field concrete mixtures exposed to sulfate solutions [28, 29, 176, 185]. During the degradation process, hydrogarnet is mainly consumed by a series of dissolution/precipitation reactions leading to the formation of ettringite. As can be seen in the figure, the initial amount of hydrogarnet limits the quantity of ettringite that can be formed during the degradation process. Once all the hydrogarnet is dissolved, the source of aluminum has vanished, which impedes the further precipitation of ettringite.

The dissolution of portlandite and the decalcification of C-S-H mainly occur due to the leaching of $Ca^{2+}$and OH^-ions that are diffusing out of the system (see the second dissolution front in figure 4.9). To supply the amount of calcium for the formation of ettringite, a slight portion of portlandite is also consumed ahead of the main dissolution front (see the first dissolution front in figure 4.9).

As previously mentioned, there is overwhelming evidence to show that the microstructural alterations resulting from sulfate attack contribute to significantly reduce the mechanical properties of concrete [27, 170]. SEM observations tend to indicate that this reduction is, at least in part, associated with the local development of microcracks induced by the formation of new sulfate-bearing phases. Over the past decades, numerous studies have also clearly emphasized the detrimental influence of portlandite dissolution on the mechanical properties of hydrated cement systems [118, 153, 187]. It should be noted that the decalcification of the C-S-H is, most probably, the most severe degradation that can happen to a concrete mixture. As previously mentioned,

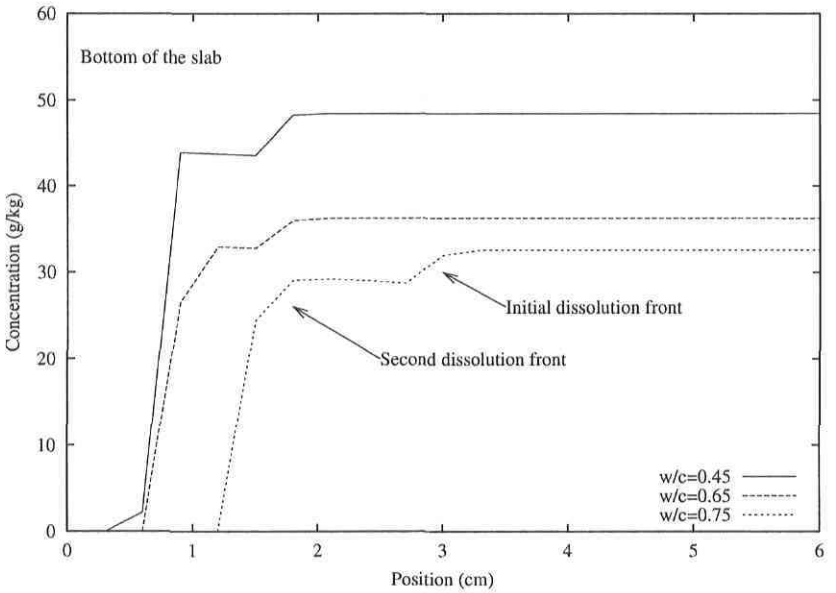

Figure 4.9: Calcium hydroxide profiles after 20 years for the concrete mixtures made with the CSA Type 10 cement and exposed to 10 mmol/L of sulfates - Saturated conditions

the gradual leaching of calcium from the C-S-H leaves a residual silica gel. This gel is extremely porous and permeable and has no binding capacity.

Numerical simulations also indicate that the kinetics of degradation is mainly controlled by the diffusion coefficient of the material (see figures 4.9 to 4.12). These results clearly emphasize the importance of limiting the water/cement ratio below a certain critical value. As can be seen, while the two mixtures prepared at a water/cement ratio of 0.45 do not exhibit any significant degradation after 20 years of exposure, the more porous mixtures are markedly affected by the exposure to the sulfate solution. It is noteworthy that the reduction of the water/cement ratio does not modify the mechanisms of deterioration but simply reduces the kinetics of attack. The profiles for the 0.45 type 10, and 0.65 type 10 concrete mixtures shown in the four figures are very similar, despite very different diffusion coefficients.

It is emphasized that the use of a sulfate-resisting cement is not a sufficient measure to protect concrete against degradation, even when the structure is exposed to weak concentrations of SO_4^{2-}. These results are in good agreement with the observations of many authors [78, 126, 176]. In the present study, the slightly detrimental influence

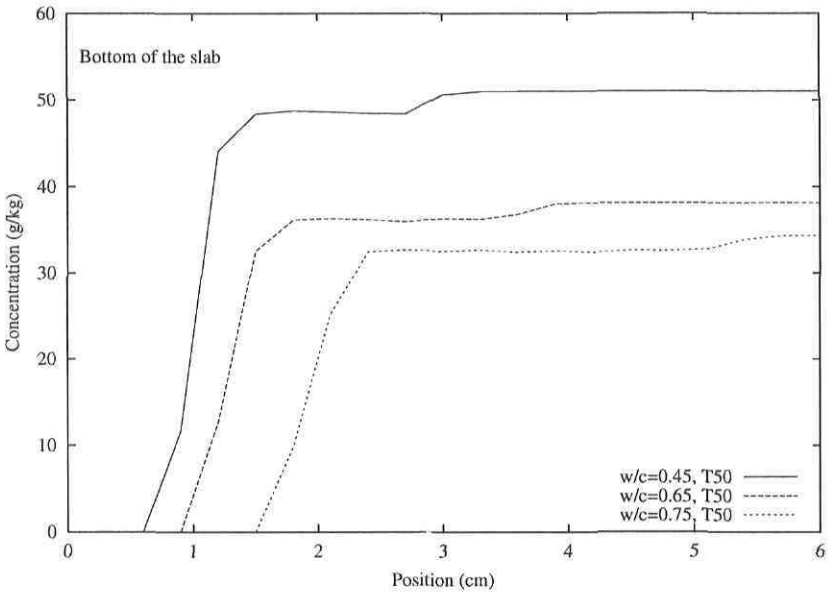

Figure 4.10: Calcium hydroxide profiles after 20 years for the concrete mixtures made with the CSA Type 50 cement and exposed to 10 mmol/L of sulfates - Saturated conditions

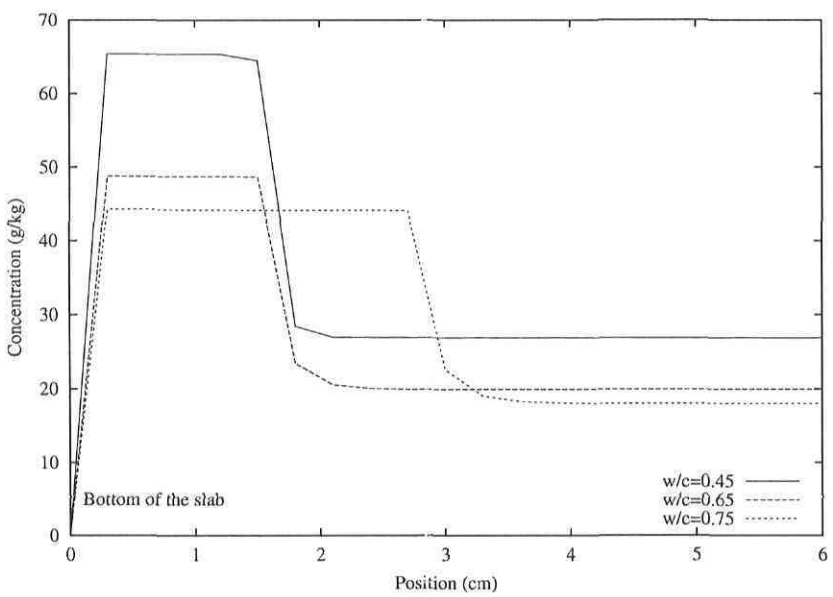

Figure 4.11: Ettringite profiles after 20 years for the concrete mixtures made with the CSA Type 10 cement and exposed to 10 mmol/L of sulfates - Saturated conditions

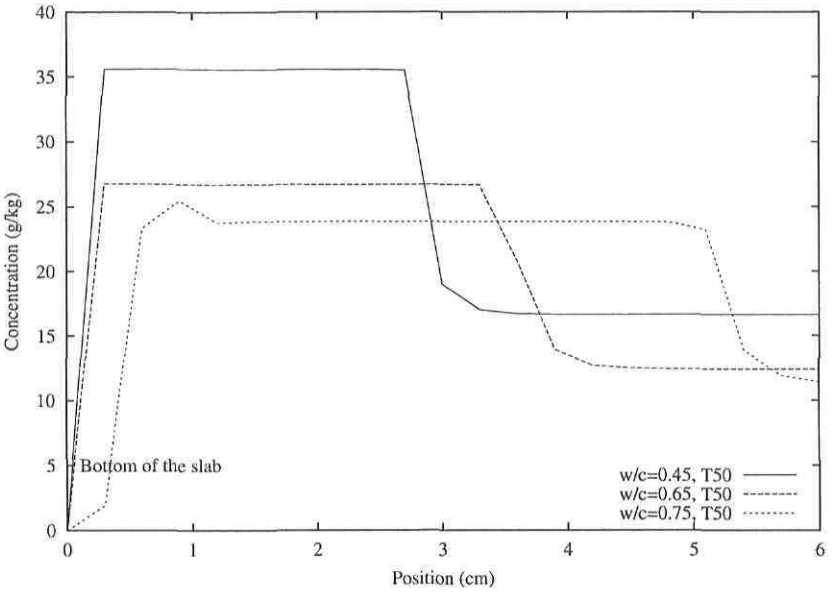

Figure 4.12: Ettringite profiles after 20 years for the concrete mixtures made with the CSA Type 50 cement and exposed to 10 mmol/L of sulfates - Saturated conditions

of the sulfate-resisting cement on the kinetics of degradation might be attributed to its effect on the diffusion coefficient of concrete. As can be seen in table 4.8, the use of the CSA Type 50 cement has contributed to increase the diffusion coefficient of all concrete mixtures whatever the water/cement ratio. This phenomenon is discussed in more detail in reference [112].

As shown in figure 4.13, an increase of the SO_4^{2-} concentration of the external solution (from 5 to 30 mmol/L) contributes only to a slight acceleration of the kinetics of penetration of the ettringite front. It is also interesting to note that the model predicts the formation of a weak peak of ettringite for the 0 mmol/L case, i.e. the case without any external sulfate. Its presence is due to the dissolution of ettringite near the bottom of the slab. As a result of diffusion and the electrical coupling, the $Al(OH)_4^-$ ions move deeper in the material after this dissolution and precipitate to form this peak.

The external SO_4^{2-} concentration has a more significant effect on the kinetics of portlandite dissolution (see figure 4.14). An increase in the SO_4^{2-} concentration tends to slightly accelerate the initial dissolution of calcium hydroxide. Subsequently, the formation of ettringite contributes to reduce the progression of the main portlandite

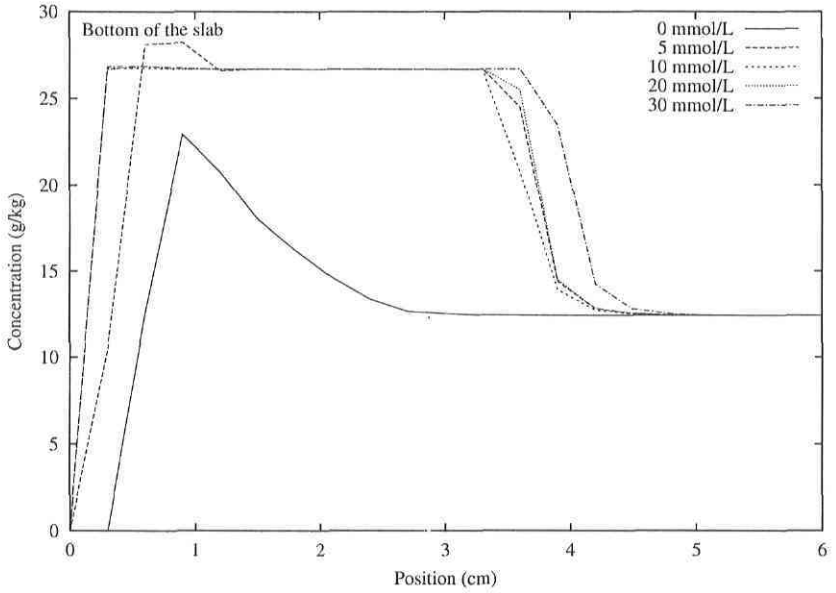

Figure 4.13: Ettringite profiles after 20 years for the 0.65 water/cement ratio concrete made with the CSA Type 50 cement and exposed to different sulfate concentrations - Saturated conditions

dissolution front. This phenomenon is linked to the fact that the precipitation of ettringite results in a local reduction of porosity of the material. However, these results should be considered with caution. The influence of microcracks (induced by the formation of ettringite and gypsum) is not taken into account by the model.

Finally, numerical results clearly indicate that the detrimental influence of weak sodium sulfate solutions is not predominantly due the suction of SO_4^{2-}ions by capillary forces. As can be seen in figures 4.15 and 4.16, the transport of water by capillary suction does not seem to have any significant effects on the behavior of concrete. These results are in good agreement with SEM observations and microprobe analyses recently made on a series of laboratory mixtures [112]. It should however be borne in mind that wetting and drying cycles may result in cracking and spalling especially for porous concrete mixtures [83, 132].

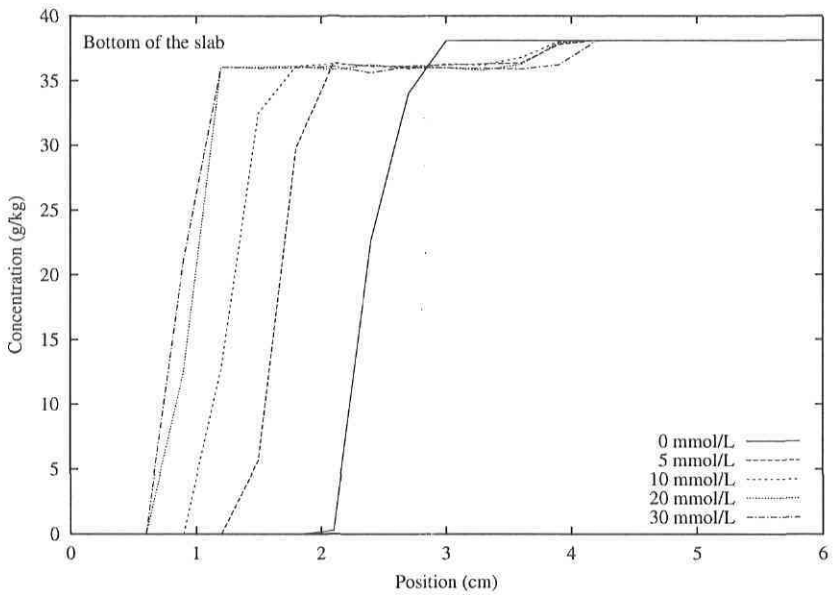

Figure 4.14: Calcium hydroxide profiles after 20 years for the 0.65 water/cement ratio concrete made with the CSA Type 50 cement and exposed to different sulfate concentrations - Saturated conditions

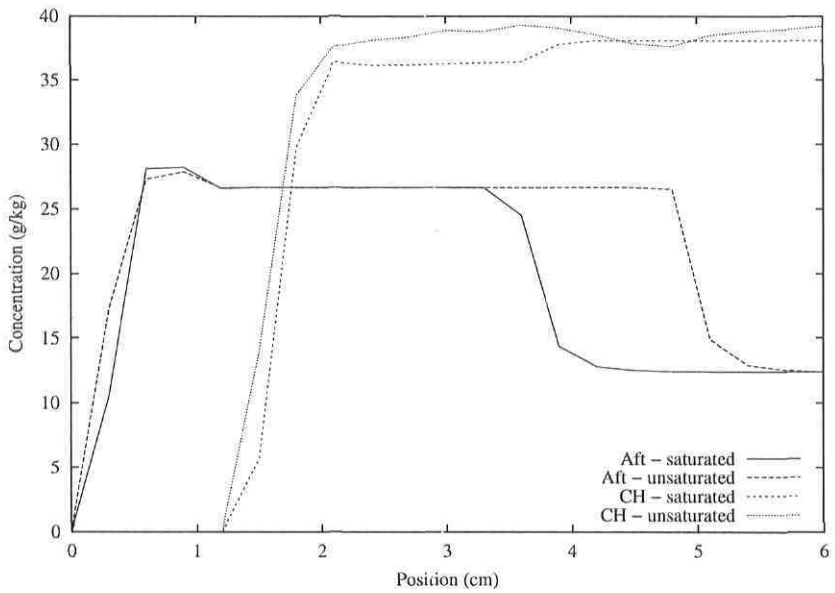

Figure 4.15: Ettringite profiles after 20 years for the 0.65 water/cement ratio concrete made with the CSA Type 50 cement and exposed to 5 mmol/L of sulfate - Unsaturated conditions

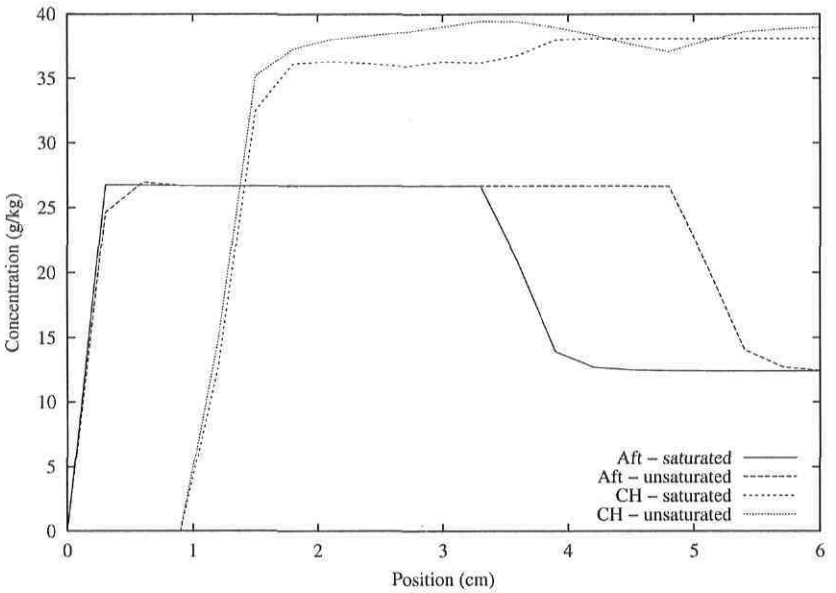

Figure 4.16: Calcium hydroxide profiles after 20 years for the 0.65 water/cement ratio concrete made with the CSA Type 50 cement and exposed to 5 mmol/L of sulfate - Unsaturated conditions

4.3.6 Concluding remarks

Numerical simulations indicate that the exposure to weak sodium sulfate solutions may yield to a significant reorganization of the internal microstructure of concrete. In addition to the formation of the new sulfate-bearing products, the penetration of external ions markedly accentuates the dissolution of calcium hydroxide and the decalcification of C-S-H.

The detrimental effects of weak sodium sulfate solutions do not appear to be linked to capillary suction effects.

Numerical simulations confirm that the quality of the concrete put in place is, by far, the main parameter that controls the deterioration process.

Conclusion

Les travaux effectués dans le cadre de cette thèse ont mené au développement d'un modèle de transport ionique dans les matériaux cimentaires non saturés. Il s'agit d'un modèle mutiionique dont la structure générale est de type SNIA (Sequential Non Iterative Approach). Cet algorithme permet de résoudre les problèmes de transport en milieu réactif en découplant le transport et la chimie, sans itérer entre ces deux phases de calcul.

Le modèle comporte certaines caractéristiques qui le distingue des modèles similaires que l'on retrouve dans le domaine de l'hydrogéologie ainsi que des rares modèles multiioniques à avoir été publiés dans le domaine du béton. Tout d'abord, le modèle considère le couplage électrique entre les différents ions présents en solution. Ce couplage est modélisé par l'équation de Nernst-Planck, qui introduit un potentiel électrique dans les équations de transport afin de maintenir l'électroneutralité de la solution dans le milieu poreux. Ce couplage entre les ions alourdit considérablement le modèle. Cependant, ce choix s'est trouvé justifié dans les simulations visant à reproduire les essais faits en laboratoire ; en négligeant ce terme, il n'est pas possible de reproduire correctement les profils de calcium et de sulfate mesurés sur des pâtes exposées à de l'eau pure ainsi qu'à différentes solutions de Na_2SO_4. Le couplage électrique s'avère donc un élément essentiel de la modélisation du transport ionique dans les matériaux cimentaires, en raison principalement de la solution fortement basique présente dans

leurs pores. Une partie du travail a été consacrée exclusivement à l'étude d'un algorithme permettant de résoudre le problème du couplage électrique pour des solutions fortement chargées. La conclusion en a été qu'une résolution itérative de type Picard ne permet pas d'atteindre cet objectif. La méthode choisie fait la résolution couplée des équations de transport et de l'équation de Poisson, qui relie le potentiel électrique aux différents profils de concentration.

Le modèle tient également compte de l'activité chimique dans le modèle de transport, ce qui correspond au modèle de Nernst-Planck étendu. Les tests numériques effectués sur ce terme ont montré que son influence sur la solution du modèle, aussi bien au niveau des profils de concentration qu'au niveau des phases solides, est faible. Cependant, comme le poids numérique de ce terme n'est pas important, il est conservé dans le modèle.

Toujours concernant l'activité chimique, des travaux ont été menés afin de déterminer une loi simple permettant de calculer ce paramètre pour des solutions très concentrées, ayant une force ionique se situant autour de 1 mol/L. Le résultat de ces travaux est la loi de Davies modifiée. Prenant pour point de départ la loi de Davies, le terme empirique de cette dernière à été remodelé afin de calculer l'activité chimique des différentes espèces ioniques présentes dans la solution interstitielle des matériaux cimentaires. Ce modèle est employé dans le modèle autant par la partie transport que pour les calculs d'équilibre chimique.

Une autre particularité du modèle se situe dans le traitement des réactions chimiques. Le modèle s'éloigne des isothermes d'interactions couramment utilisées dans le domaine du béton. Il propose plutôt l'utilisation d'un module d'équilibre chimique séparé des équations de transport. Il est ainsi possible, comme l'ont montré les simulations de dégradation de pâtes de ciment exposées à des solutions sulfatiques, de reproduire des phénomènes simultanés tels que la dissolution de la portlandite et la précipitation de gypse. Le code d'équilibre chimique greffé au modèle ne traite pour l'instant que les réactions chimiques de dissolution et de précipitation. Les autres réactions chimiques telles que la complexation et l'échange ionique ne sont pas considérées. En effet, l'utilisation d'une loi de comportement non linéaire pour modéliser le transport rend difficile de considérer l'ensemble des phénomènes chimiques se produisant dans une structure en béton. Cependant, en privilégiant les réactions de dissolution et

de précipitation, il a été possible de mettre en évidence les principaux mécanismes de l'attaque aux sulfates et de l'exposition à l'eau pure.

Un autre aspect important du travail de recherche a consisté à développer une nouvelle méthode d'analyse de l'essai de migration. La méthode proposée consiste à trouver les coefficients de diffusion qui permettent de reproduire les courants électriques mesurés tout au long de l'essai. Les méthodes généralement utilisées pour l'analyse de cet essai font l'hypothèse d'un découplage entre les ions dû au fort champ électrique externe. Selon cette hypothèse, le profil de chlore dans une éprouvette de béton soumise à un champ électrique aurait la forme d'un front similaire à la solution de l'équation de transport-advection: $\dot{u} - Du_{xx} + vu_x = 0$. Une analyse numérique effectuée avec le présent modèle a montré que cette hypothèse n'est pas valable; malgré le potentiel électrique appliqué à un disque de béton, le couplage électrique entre les ions ne peut être négligé. Cela permet d'expliquer la forme générale des profils mesurés sur des disques de béton soumis à cet essai, qui n'ont pas la forme d'un front. La méthode est indépendante des solutions utilisées pendant l'essai et de l'intensité du voltage: les coefficients de diffusion obtenus sont donc bien une caractéristique du matériau, et ne sont pas influencés par les conditions expérimentales. Les simulations ayant servi à valider le modèle ont tiré leurs coefficients de diffusion d'essais de migration analysés avec cette méthode.

La structure du modèle proposé permet facilement d'envisager plusieurs améliorations. Tout d'abord, en ayant un module séparé pour les réactions chimiques, il est possible d'ajouter rapidement la formation ou la dissolution de solides supplémentaires. On pense tout d'abord aux chloroaluminates (sels de Friedel) qui sont formés lorsque du chlore pénètre dans une structure en béton et réagit avec l'aluminium de la pâte de ciment. Ou alors la brucite, qui peut se former par réaction entre le magnésium et les ions OH^- présents dans le matériau; cette réaction est susceptible de se produire en présence d'eau de mer, fortement chargée en magnésium. Il est également possible d'envisager la modélisation d'autres types de réactions chimiques, telles que l'échange ionique et la formation de complexe. Dans ce cas, l'emploi d'un opérateur de transport non linéaire ne permettrait pas le genre de simplifications généralement employées dans les modèles multiioniques de transport de contaminants dans les sols.

Néanmoins, comme dans le cas des réactions de dissolution/précipitation, il serait possible d'éliminer les termes de réaction des équations de transport pour ensuite corriger les profils de concentration avec le code d'équilibre chimique.

Une autre amélioration à envisager du point de vue de la chimie est l'implantation d'un modèle de dissolution incongruente pour les C-S-H. Le modèle actuel simplifie la décalcification des C-S-H en les considérant comme de la portlandite avec une constante de dissolution plus faible. Il serait intéressant de voir si l'emploi d'un modèle tel que celui proposé par Berner [23] permettrait d'améliorer le comportement du modèle dans les cas où il y a dissolution de la pâte.

Certains aspects numériques pourraient faire l'objet de modifications. La plus évidente consisterait à transformer le modèle 1D pour résoudre des problèmes en deux ou trois dimensions. La version actuelle du modèle utilise la méthode de largeur de bande pour stocker les matrices globales calculées lors du calcul par éléments finis. Cette méthode convient très bien aux problèmes en une dimension. Afin de réduire les besoins en mémoire du modèle, il faudrait passer vers une méthode de stockage plus efficace, telle que la méthode par ligne de ciel, pour accommoder les problèmes 2D et 3D.

Ensuite, il serait intéressant de tester un algorithme SIA (Sequential Iterative Approach), dans lequel des itérations sont effectuées entre les phases transport et chimie du calcul. Cela permettrait de voir s'il est possible de réduire les temps de calcul en allongeant les pas de temps, en dépit des itérations supplémentaires que cela entraînerait dans le calcul de l'équilibre chimique. Liu et Narasimhan [108] ont mentionné que 99.9% du temps de calcul est consacré à la chimie dans leur modèle de transport de contaminant dans les sols. Cette proportion est sûrement beaucoup faible dans le cas de notre modèle, puisque les équations de transport non linéaires sont plus lourdes à résoudre que l'équation linéaire de transport/diffusion. Il serait ainsi possible de réduire le temps CPU pour les calculs en deux ou trois dimensions en trouvant un pas de temps optimal.

Il serait possible d'élargir le champ d'application du modèle en prenant en compte des phénomènes physiques supplémentaires. Ainsi, on pourrait considérer les effets de la température sur le transport ionique en ajoutant l'équation de conduction de

la chaleur au modèle. Cela impliquerait de connaître l'effet de la température sur la diffusion des ions. Il serait possible d'atteindre cet objectif en faisant une série d'essais de migration sur différents matériaux cimentaires à différentes températures. Le même type d'analyse devrait être fait pour quantifier l'effet de la température sur la diffusivité de l'eau. Les constantes d'équilibre chimique, quant à elles, sont reliées à la température via l'équation de Van't Hoff.

Le modèle serait également valorisé par l'ajout des équations nécessaires aux calculs de transport d'ions sous forme gazeuse. On pourrait ainsi évaluer la profondeur de la carbonatation sur des structures en béton en fonction du temps. Il faudrait pour cela, en plus des équations de transport dans la phase gazeuse, modifier le module chimique afin de considérer la dissolution de molécules dans l'air vers la solution de pores du béton.

Les méthodes numériques choisies dans le cadre de ce travail de recherche, soit la méthode des éléments finis pour résoudre les équations de transport et la séparation transport/chimie, ont permis de créer une plate-forme qui peut servir de point de départ pour des modèles de transport de plus en plus complets. Ce travail ouvre la porte à la création d'outils numériques qui pourront servir aussi bien à la recherche qu'à la consultation en génie civil.

Bibliographie

[1] Abate C., Scheetz B.E., *Aqueous phase equilibria in the system CaO-Al_2O_3-$CaCl_2$-H_2O: the signifiance and stability of Friedel's salt,* J. of the American Ceramic Society, vol.78,939-944, 1995.

[2] Adamson A.W., *Physical chemistry of surfaces,* John Wiley & Sons, 5ed., USA, 1990.

[3] Adenot F., *Caractérisation et modélisation des processus physiques et chimiques de dégradation du ciment,* Thèse de doctorat, Université d'Orléans, France, 1992.

[4] American Concrete Institute, *Guide to Durable Concrete*, ACI 201.2R-99, Farmington Hills, Michigan, U.S.A., 1999.

[5] American Concrete Institute, *Building Code Requirements for Structural Concrete*, ACI 318-99, Farmington Hills, Michigan, U.S.A., 1999.

[6] American Concrete Institute, *Slabs on Grade*, Concrete Craftsman Series, Farmington Hills, Michigan, U.S.A., 1995.

[7] Andersen A., *Investigation of chloride penetration into bridge columns exposed to deicing salts*, HETEK - The Danish Road Directorate, Report no. 82, 38 p., 1997.

[8] Andrade C., *Calculation of chloride diffusion coefficients in concrete from ionic migration measurements,* Cement and Concrete Research, vol.23, p.724-742, 1993.

[9] Andrade C., Cervigon C., Recuero A., Rio O., *A reply to the discussion by L. Tang and L.O. Nilsson of the paper-Calculation of chloride diffusivity in concrete from migration experiments in non-steady state conditions*, Cement and Concrete Research, vol.25, p.1138-1144, 1995.

[10] Andrade C., Sanjuan M.A., Recuero A., Rio, O., *Calculation of chloride diffusivity in concrete from migration experiments in non steady-state conditions*, Cement and Concrete Research, vol.24, p.1214-1228, 1994.

[11] Armatas G.S., Salmas C.E., Louloudi M., Androutsopoulos G.P., Pomonis P.J., *Relationships among pore size, connectivity, dimensionality of capillary condensation, and pore structure tortuosity of functionalized mesoporous silica*, Langmuir, vol.19, p.3128-3136, 2003.

[12] Bachmat Y., Bear J., *Macroscopic modelling of transport phenomena in porous media. 1: The continuum approach,* Transport in Porous Media, vol.1, p.213-240, 1986.

[13] Barbarulo, R., Marchand, J. and Snyder, K.A., *Dimensional analysis of ionic transport problems in hydrated cement systems Part 2. Application to various practical problems*, en préparation, 2003.

[14] Barbarulo R., Marchand J., Snyder K.A., Prené S., *Dimensional analysis of ionic transport problems in hydrated cement systems Part 1. Theoretical considerations,* Cement and Concrete Research, vol.30, p.1955-1960, 2000.

[15] Baroghel-Bouny V., Mainguy M., Lassabatère T., Coussy O., *Characterization and identification of equilibrium and transfer moisture properties for ordinary and high-performance cementitious materials,* Cement and Concrete Research, vol.29, p.1225-1238, 1999.

[16] Barneyback R.S., Diamond S., *Expression and analysis of pore fluid from hardened cement pastes and mortars*, Cement and Concrete Research, vol.11, p.279-285, 1981.

[17] Barry D.A., Miller C.T., Culligan-Hensley P.J., *Temporal discretisation errors in non-iterative split-operator approaches to solving chemical reaction/groundwater transport models,* Journal of Contaminant Hydrology, vol.22, p.1-17, 1996.

[18] Bear J., Bachmat Y., *Introduction to Modeling of Transport Phenomena in Porous Media,* Kluwer Academic Publishers (Pays-Bas), 1991.

[19] Bear J., Bachmat Y., *Macroscopic modelling of transport phenomena in porous media. 2: Applications to mass, momentum and energy transport,* Transport in Porous Media, vol.1, p.241-269, 1986.

[20] Ben-Yair M., *Studies on the stability of calcium chloroaluminate,* Israel Journal of Chemistry, vol.9, p.529-536, 1971.

[21] Bentz D.P., Garboczi E.J., *Modelling the leaching of calcium hydroxide from cement paste: effects on pore space percolation and diffusivity,* Materials and Structures, vol.25, p.523-533, 1992.

[22] Berezhkovskii A.M., Zitserman V.Y., Shvartsman S.Y., *Effective diffusivity in periodic porous materials*, Journal of Chemical Physics, vol.119, p.6991-6993, 2003.

[23] Berner U.R., *Modelling the incongruent dissolution of hydrated cement minerals*, Radiochimica Acta, vol.44/45, p.387-393, 1988.

[24] Bockris J.O'M., *The comprehensive treatise of electrochemistry*, Plenum Press, New York (USA), 1980.

[25] Bockris J.O'M., Conway B.E., Yeager E., *Comprehensive treatise of electrochemistry - volume 1; The double layer,* Plenum Press, USA, 1980.

[26] Bockris J.O'M., Reddy A.K.N., *Modern electrochemistry - an introduction to an interdisciplinary area,* Plenum Press, USA, 1970.

[27] Brown P.W., *An evaluation of the sulfate resistance of cements in a controlled environment*, Cement and Concrete Research, vol.11, p.719-727, 1981.

[28] Brown P.W., Doerr A., *Chemical changes in concrete due to the ingress of aggressive species*, Cement and Concrete Research, vol.30, p.411-418, 2000.

[29] Brown P.W., Badger S., *The distributions of bound sulfates and chlorides in concrete subjected to mixed NaCl, $MgSO_4$, Na_2SO_4 attack*, Cement and Concrete Research, vol.30, p.1535-1542, 2000.

[30] Byfors K., *Chloride binding in cement paste*, Nordic Concrete Research, vol.5, p.27-38, 1986.

[31] Canadian Standard Association, *A23.1-94, Concrete: Constituents and Construction Practices*, Rexdale, Ontario, Canada, 1994.

[32] Carpenter T.A., Davies E.S., Hall C., Hall L.D., Hoff W.D., Wilson M.A., *Capillary water migration in rock: process and material properties examined by NMR imaging,* Materials and Structures, vol.26, p.286-292, 1993.

[33] Castellote M., Andrade C., Alonso C., *Chloride-binding isotherms in concrete submitted to non-steady-state migration experiments,* Cement and Concrete Research, vol.29, p.1799-1806, 1998.

[34] Cederberg G.A., Street R.L., Leckie J.O., *A groundwater mass transport and equilibrium chemistry model for multicomponent systems,* Water Resources Research, vol.21, no.8, p.1095-1104, 1985.

[35] Chatterji S., *A discussion of the paper "Presence and possible implications of a membrane potential in concrete exposed to chloride solution" by Zhang and Buenfeld,* Cement and Concrete Research, vol.28, no.4, p.773-775, 1998.

[36] Chatterji, S., *Transportation of ions through cement based materials - Part 1: Fundamental equations and basic measurement techniques*, Cement and Concrete Research, vol.24, no.5, p.907-912, 1994.

[37] Clifton J.R., Predicting the remaining service life of concrete, Report NISTIR 4712, National Institute of Standard and Technology, 1991.

[38] Climent M.A., de Vera G., Hidalgo A., Andrade C., Alonso C., *Chloride ion activities in synthetic concrete pore solutions : Theoretical models and potentiometric measurements*, Materials Science of Concrete - The Sydney Diamond Symposium, American Ceramic Society, p.285-294, 1998.

[39] Cohen H., Cooley J.W., *The numerical solution of the time-dependant Nernst-Planck equations,* Biophysical Journal, vol.5, p.145-161, 1964.

[40] Conti F., Eisenman G., *The non-steady state membrane potential of ion exchangers with fixed sites,* Biophysical Journal, vol.5, p.247-256, 1964.

[41] Dormieux L., Barboux P., Coussy O., Dangla P., *A macroscopic model of the swelling phenomenon of a saturated clay,* European Journal of Mechanics - A/Solids, vol.14, no.6, p.981-1004, 1995.

[42] Crausse P., Bacon G., Bories S., *Etude fondamentale des transferts couplés chaleur-masse en milieu poreux,* Int. J. Heat Mass Transfer, vol.24, no.6, p.991-1004, 1981.

[43] CRC Handbook of Chemistry and Physics, 76th ed., CRC Press, Florida (USA), 1996.

[44] Daian J.-F., *Condensation and isothermal water transfer in cement mortar: 1.Pore size distribution, equilibrium water condensation and imbibition,* Transport in porous media, vol.3, p.563-589, 1988.

[45] Daly F.P., Brown C.W., Journal of Physical Chemistry, vol.76, p.3664-, 1972.

[46] Damidot D., Glasser F.P., *Thermodynamic investigation of the CaO-Al_2O_3-$CaSO_4$-$CaCl_2$-H_2O system and the influence of Na_2O,* 10th Congress on the Chemistry of Cement, Gothenburg, Sweden, 1997.

[47] Damidot D., Bimin-Yauri U.A., Glasser F.P., *Thermodynamic investigation of the CaO-Al_2O_3-$CaCl_2$-H_2O system at 25°C and the influence of Na_2O,* Il cemento, vol.4, p.243-254, 1994.

[48] Damidot D., Glasser F.P., *Thermodynamic investigation of the CaO-Al_2O_3-$CaSO_4$-H_2O system at 25°C and the influence of Na_2O,* Cement and Concrete Research, vol.23, no.1, p.221-238, 1993.

[49] Damidot D., Glasser F.P., *Thermodynamic investigation of the CaO-Al_2O_3-$CaSO_4$-K_2O-H_2O system at 25°C ,* Cement and Concrete Research, vol.23, no.5, p.1195-1204, 1993.

[50] DePuy G.W., *Chemical resistance of concrete,* in Significance of Tests and Properties of Concrete and Concrete-Making Materials, (P. Klieger and J. Lamond Eds.), STP 169C, ASTM, Philadelphia, p.263-281, 1994.

[51] De Vries D.A., *Simultaneous transfer of heat and moisture in porous media,* Trans. American Geophysical Union, vol. 39, no. 5, p. 909-916, 1958.

[52] Diamond S., *Effects of Two Danish Fly Ashes on Alkali Contents of Pore Solutions of Cement Fly Ash Pastes*, Cement and Concrete Research, vol.11, p.383-390, 1981.

[53] Dinulescu H.A., Eckert E.R.G., *Analysis of the one-dimensional moisture migration caused by temperature gradients in a porous media*, International Journal of Heat and Mass Transfer, vol. 23, p. 1069-1078, 1980.

[54] Dhatt G., Jacquemier M., Kadje C., *Modelling of drying refractory concrete*, Drying '86, vol. 1, Hemisphere Publishing Corporation, p. 94-104, 1986.

[55] Dolgonosov A.M., Khamisov R.K., Krachak A.N., Prudkovsky A.G., *Macroscopic model for multispecies ion exchange kinetics,* Reactive and Functional Polymers, vol.28, p.13-20, 1995.

[56] Dormieux L., Barboux P., Coussy O., Dangla P., *A macroscopic model of the swelling phenomenon of a saturated clay*, European Journal of Mechanics - A/Solids, vol.14, p.981-1004, 1995.

[57] Duchesne J., Reardon E.J., *Measurement and prediction of portlandite solubility in alkali solutions,* Cement and Concrete Research, vol.25, no.5, p.1043-1053, 1995.

[58] Dullien F.A.L., *Porous media - Fluid transport and pore structure,* Academic Press, 2eme ed. (USA), 1992.

[59] El-Belbol S.M., Buenfeld N.R., *Accelerated chloride ion diffusion tests*, Pore Structure and Permeability of Cementitious Materials, L.R. Roberts and J.P. Skalny eds., Materials Research Symposium Proceedings, vol.137, p.203-208, 1989.

[60] Emmanuel S., Berkowitz B., *Mixing-induced precipitation and porosity evolution in porous media*, Advances in Water Resources, vol.28, p.337-344, 2005.

[61] Engesgaard P., Kipp K.L., *A geochemical transport model for redox-controlled movement of mineral fronts in groundwater flow systems: a case of nitrate removal by oxidation of pyrite,* Water Resources Research, vol.28, p.2829-2843, 1992.

[62] Fagerlund, G. *Predicting the service-life of concrete exposed to frost action through a modeling of the water absorption process in the air pore system*, in The Modeling of Microstructure and its Potential for Studying Transport Properties and Durability, Edited by H. Jenning, J. Kropp and K, Scrivener, Nato ASI Series, Series E: Applied Science, vol. 304, Kluwers Academic Publishers, Dordrecht, The Netherlands, p. 503-539, 1996.

[63] Faucon, P., *Durability of concrete : Physico-chemistry of the degradation induced by pure water*, Thèse de doctorat, Université de Cergy-Pontoise, France, 1997.

[64] Feldman R.F., *Pore structure, permeability and diffusivity as related to durability*, Eighth International Congress on the Chemistry of Cement, vol.1, Theme 4, Rio de Janeiro, Brazil, 1986.

[65] Förster R., *A multicomponent transport model,* Geoderma, vol.38, p.261-278, 1986.

[66] Garboczi E.J., Bentz D.P., *Computer simulation of the diffusivity of cement-based materials,* Journal of Material Science, vol.27, p.2083-2092, 1992.

[67] Gautefall O., *Effect of condensed silica fume on the diffusivity of chlorides through hardened cement paste*, ACI Special Publication 91, p.991-997, 1986.

[68] Gautefall, O. and Havdahl, J., *Effect of condensed silica fume on the mechanisms of chloride diffusion into hardened cement paste*, ACI Special Publication 114, p.849-860, 1989.

[69] Glasstone S., *An introduction to electrochemistry,* Van Nostrand (USA), 1942.

[70] Goldman D.E., J. Gen. Physiol., vol.27, p.37-46, 1943.

[71] Gollop R.S., Taylor H.F.W., Microstructural and microanalytical studies of sulfate attack - 1: Ordinary portland cement paste, Cement and COncrete Research, vol.22, no.6, p.1027-1038, 1992.

[72] Gospodinov P.N., Kazandjiev R.F., Partalin T.A., Mironova M.K., *Diffusion of sulfate ions into cement stone regarding simultaneous chemical reactions and resulting effects,* Cement and Concrete Research, vol. 29, p.1591-1596, 1999.

[73] Grove D.B., Wood W.W., *Prediction and field verification of subsurface-water quality during artificial recharge, Lubbock, Texas,* Groundwater, vol.17, no.3, p.250-257, 1979.

[74] Hall C., *Barrier performance on concrete: a review of fluid transport theory,* Materials and Structures, vol.27, p.291-306, 1994.

[75] Hamilton J.J., Handegord G.O., *The performance of ordinary Portland cement concrete in crairies soils of high sulphate content*, in Performance of Concrete-Resistance of Concrete to Sulphate and Other Environmental Conditions: A Symposium in Honour of Thobergur Thorvaldson (E.G. Swenson Ed.), University of Toronto Press, p.135-158, 1968.

[76] Hansen E.J., Saouma V.E., *Numerical simulation of reinforced concrete deterioration - part 1: chloride diffusion,* ACI Materials Journal, vol.96, no.2, p.173-180, 1999.

[77] Hansen T.C., *Physical structure of hardened cement paste. A classical approach,* Matériaux et Constructions, vol.19, no.114, p.423-436, ????.

[78] Harboe E.M., *Longtime studies and field experiences with sulfate attack*, in Sulfate Resistance of Concrete (George Verbeck Symposium), ACI SP-77, p.1-20, 1982.

[79] Harden J.L., Viovy J.L., *Numerical studies of pulsed iontophoresis through model membranes,* Journal of Controlled Released, vol.38, p.129-139, 1996.

[80] Harned H.S., Owen B.B., *The physical chemistry of electrolytic solutions*, Reinhold Publishing Corp., 1943.

[81] Hassanizadeh M., Gray W.G., *General conservation equations for multi-phase systems: 1.Averaging procedure,* Advances in Water Resources, vol.2, p.131-144, 1979.

[82] Hauck K., *The effect of curing temperature and silica fume on chloride migration and pore structure of high-strength concrete*, Ph.D. Thesis, Department of Civil Engineering, University of Trondheim, Norway, 1993.

[83] Haynes H., O'Neill R., Mehta P. K., *Concrete deterioration from physical attack by salt*, Concrete International, vol.18, p.63-68, 1996.

[84] Hazrati K., *Etude des mécanismes de transport de l'eau par absorption capillaire dans des matériaux cimentaires usuels et de haute performance*, Thèse de doctorat, Université Laval, Canada, 1998.

[85] Helfferich F., *Ion exchange,* McGraw-Hill (USA), 1961.

[86] Henocq P., Ph.D. Thesis, Laval University (in progress), Canada, 2004.

[87] Herzer J., Kinzelbach W., *Coupling of transport and chemical processes in numerical transport models*, Geoderma , vol.44, p.115-127, 1989.

[88] Hong S.Y., Glasser F.P., Cement and Concrete Research, vol.29, no.12, p.1893-1904, 1999.

[89] Hwang Y., Helfferich F., *Generalized model for multispecies ion-exchange kinetics including fast reversible reactions,* Reactive Polymers, vol.5,p.237-253, 1987.

[90] Jackson J.D., *Classical electrodynamics*, Second Edition, John Wiley & Sons, New York, USA, 1975.

[91] James A.E., Stillman J.D., Williams D.J.A., *Finite element solution of the equations governing the flow of electrolyte in charged microporous membranes,* Int. J. for Num. Meth. in Fluids, vol.20, p.1162-1178, 1995.

[92] Jennings A.A., Kirkner D.J., Theis T.L., *Multicomponent equilibrium chemistry in groundwater quality models,* Water Resources Research, vol.18, no.4, p.1089-1096, 1982.

[93] Johannesson B.F., *Non-linear transient phenomena in porous media with special regard to concrete durability*, Advanced Cement Based Materials, vol. 6, p. 71-75, 1997.

[94] Kaluarachchi J.J., Morshed J., *Critical assessment of the operator-splitting technique in solving the advection-dispersion-reaction equation: 1. First-order reaction*, Advances in Water Resources, vol.18, no.2, p.89-100, 1995.

[95] Kato M., *Numerical analysis of the Nernst-Planck-Poisson system,* Journal of Thoretical Biology, vol.177, p.299-304, 1995.

[96] Kirkner D.J., Reeves H., *Multicomponent mass transport with homogeneous and heterogeneous chemical reactions: effect of the chemistry on the choice of numerical algorithm - 1. Theory,* Water Resources Research, vol.24, no.10, p.1719-1729, 1988.

[97] Kirkner D.J., Reeves H.W., Jennings A.A., *Finite element analysis of multicomponent contaminant transport including precipitation-dissolution reactions,* dans Finite El. in Wat. Res., ed. Laible J.L. & al., p.309-318, 1984.

[98] Kirkner D.J., Theis T.L., Jennings A.A., *Multicomponent solute transport with sorption and soluble complexation,* Advances in Water Resources, vol.7, p.120-125, 1984.

[99] Kotz J.C., Purcell K.F., *Chemistry and chemical reactivity,* Saunders College Publishing (USA), 1987.

[100] Kunzel, H.M., *Simultaneous heat and moisture transport in building components,* Ph.D. Thesis, IRB Verlag, Stuttgart, Germany, 102 p., 1995.

[101] D.L. Landau and I.M. Lifshitz, *Fluid Mechanics*, Pergamon Press, 1987.

[102] Lewis F.M., Voss C.I., Rubin J., *Solute transport with equilibrium aqueous complexation and either sorption or ion exchange: simulation methodology and applications,* Journal of Hydrology, vol.90, p.81-115, 1987.

[103] Li L.Y., Page C.L., *Modelling of electrochemical chloride extraction from concrete: influence of ionic activity coefficients,* Computational Materials Science, vol.9, p.303-308, 1998.

[104] Lichtner P.C., Oelkers E.H., Helgeson H.C., *Interdiffusion with multiple precipitation/dissolution reactions - Transcient model and the steady-state limit,* Geochimica et Cosmochimica Acta, vol. 50, p.1951-1966, 1986.

[105] Lichtner P.C., *Continuum model for simultaneous chemical reactions and mass transport in hydrothermal systems,* Geochimica et Cosmochimica Acta, vol. 49, p.779-800, 1985.

[106] Lichtner P.C. *Continuum formulation of multicomponent-multiphase reactive transport*, in Reactive Transport in Porous Media – Reviews in Mineralogy Vol.

34, P.C. Lichtner et al. eds., Mineralogical Society of America (Washington DC, USA), p.1-81, 1996.

[107] Liu Z., Beaudoin J.J., *The permeability of cement systems to chloride ingress and related test methods*, Cement Concrete and Aggregates, vol.22, p.16-23, 2000.

[108] Liu C.W., Narasimhan N., *Redox-conttrolled multiple-species reactive chemical transport, 1. Model development,* Water Resources Research, vol.25, no.5, p.869-882, 1989.

[109] Longuet P., Burglen L. Zelwer A., *La phase liquide du ciment hydraté*, Publication Technique CERILH, no.219, 1974.

[110] MacGillivray A.D.,, *Nernst-Planck equations and the electroneutrality and Donnan equilibrium assumptions,* Journal of Chemical Physics, vol.48, p.2903-2907, 1968.

[111] MacGillivray A.D., Hare D., *Applicability of Goldman's constant field assumption to biological systems,* Journal of Thoretical Biology, vol.25, p.113-126, 1969.

[112] Maltais Y., *Ion and fluid transport in hydrated cement systems*, Thèse de doctorat, Université Laval, Canada (en préparation).

[113] Marchand J., *Modeling the behavior of unsaturated cement systems exposed to aggressive chemical environments*, Materials and Structures, vol.34, p.195-200, 2001.

[114] Marchand, J., Gérard, B., *New development in the modeling of mass transport processes in cement-based composites*, ACI Special Publication SP-154, p.169-210, 1995.

[115] Marchand J., Gérard B., Delagrave A., *Ion transport mechanisms in cement-based materials,* Material Science of Concrete - V, ACS, p.307-400, 1995.

[116] Marchand J., Samson E., Maltais Y., *Modeling microstructural alterations of concrete subjected to external sulfate attack,* Materials Science of Concrete – Special Volume: Sulfate Attack Mechanisms, American Ceramic Society (USA), ed. J. Marchand & J.P. Skalny, p.211-257, 1999.

[117] Marchand J., Maltais Y., Samson E., Johansen V., Hazrati K, *Modeling ionic interaction mechanisms in cement-based materials – an overview,* Materials Science of Concrete – Special Volume: The Sydney Diamond Symposium, American Ceramic Society (USA), ed. M. Cohen, S. Mindess & J.P. Skalny, p.143-162, 1998.

[118] Marchand J., Beaudoin J.J., Pigeon M., *Influence of calcium hydroxide dissolution on the engineering properties of cement-based materials*, in Materials Science of Concrete Special Volume: Sulfate Attack Mechanisms (J.Marchand and J. Skalny, Eds.), The American Ceramic Society, p.283-294, 1999.

[119] Marchand, J., Samson, E., Maltais, Y., Lee, R.J. and Sahu, S., *Predicting the performance of concrete structures exposed to chemically aggressive environments – Field validation*, Materials and Structures, vol.35, p.623-631, 2002.

[120] Martín-Pérez B., *Service-life modelling of R.C. highway structures exposed to chlorides*, Thèse de doctorat, Université de Toronto, 1998.

[121] Martys N.S., *Diffusion in partially-saturated porous materials,* Materials and Structures, vol.32, p.555-562, 1999.

[122] Masi M., Colella D., Radaelli G., Bertolini L., *Simulation of chloride penetration in cement-based materials,* Cement and Concrete Research, vol.27, no.10, p.1591-1601, 1997.

[123] Mattson E.D., Bowman R.S., Lindgren E.R., *Electrokinetic ion transport through unsaturated soil: 1. Theory, model development and testing*, Journal of Contaminant Hydrology, vol. 54, p.99-120, 2002.

[124] McGrath P.F., Hooton R.D., *Influence of voltage on chloride diffusion coefficients from chloride migration tests*, Cement and Concrete Research, vol.26, p.1239-1244, 1996.

[125] Mehta, P.K. , *Durability of concrete exposed to marine environment*, ACI Special Publication SP-109, p.1-30, 1988.

[126] Mehta, P.K., *Sulfate attack on concrete: separating the myth from reality*, Concrete International, vol.22, p.57-61, 2000.

[127] Miller C.W., Benson L.V., *Simulation of solute transport in a chemically reactive heterogeneous system: model development and application,* Water Resources Research, vol.19, no.2, p.381-391, 1983.

[128] Mills and Lobo, *Self-Diffusion Coefficients*, Elsevier, USA, 1989.

[129] Munson B.R., Young D.F., Okiishi T.H., *Fundamentals of fluids mechanics*, John Wiley & Sons (Canada), 1990.

[130] Nagesh M., Bhattacharjee B., *Modeling of chloride diffusion in concrete and determination of diffusion coefficients,* ACI Materials Journal, vol.95, no.2, p.113-120, 1998.

[131] Nilsson, L.O., Poulsen, E., Sandberg, P., Sorensen, H.E., Klinghoffer, O., *Chloride penetration into concrete - State of the art*, Report no.53, The Road Directorate, Copenhagen, Denmark, 1996.

[132] Novak G.A., Colville A.A., *Effloresence mineral assemblages associated with cracked and degraded residential concrete foundation in southern California*, Cement and Concrete Research, vol.19, p.1-6, 1989.

[133] Pankow J.F., *Aquatic Chemistry Concepts,* Lewis Publishers, (USA), 1994.

[134] Patzay G., *A simplified numerical solution method for the Nernst-Planck multicomponent ion exchange kinetics model,* Reactive and Functional Polymers, vol.27, p.83-89, 1995.

[135] Pel L., *Moisture transport in porous building materials,* Thèse de doctorat, Eindhoven University of Technology, Pays-Bas, 1995.

[136] Pitzer K.S., *Thermodynamics of elecirolytes - Part 1: Theoretical basis and general equations*, Journal of Physical Chemistry, vol.77, p.268-277, 1973.

[137] Pitzer K.S., *Theory: Ion interaction approach*, in Activity Coefficients in Electrolyte Solutions, vol.1, Ed. by R.M. Pytkowicz, CRC Press Inc., p. 157-208, 1979.

[138] Planck M., *Ueber die potantialdifferenz zwischen zwei verdünnten lösungen binarer electrolyte*, Annals of Physics and Chemistry, vol.40, p.561-570, 1890 (in German).

[139] Planel N., Les effets couplés de la précipitation d'espèces secondaires sur le comportement mécanique et la dégradation chimique des bétons, Thèse de doctorat, Université de Marne-la-Vallée (France), 2002.

[140] Powers T.C., Brownyard T.L., *Studies of the Physical Properties of Hardened Portland Cement Paste*, Journal of the American Concrete Institute, vol.43 (neuf parties), 1946-47.

[141] Reardon E.J., *Problems and approaches to the prediction of the prediction of the chemical composition in cement/water systems,* Waste Management, vol.12, p.221-239, 1992.

[142] Reddy J.N., Gartling D.K., *The finite element method in heat transfer and fluid dynamics,* CRC Press (USA), 1994.

[143] Reeves H., Kirkner D.J., *Multicomponent mass transport with homogeneous and heterogeneous chemical reactions: effect of the chemistry on the choice of numerical algorithm - 2. Numerical results,* Water Resources Research, vol.24, no.10, p.1730-1739, 1988.

[144] Rendueles de la Vega M., Loureiro J.M., Rodrigues A.E., *Equivalence between Nernst-Planck and "corrected" Fick's law in modeling fixed-bed ion exchange,* Chemical Engineering Journal, vol.60, p.123-132, 1996.

[145] Revertégat E., Gégout P., Moine G., Effect of pH on the durability of cement pastes, Cement and Concrete Research, vol. 22, p. 259-272, 1992.

[146] Revil A., *Ionic diffusivity, electrical conductivity, membrane and thermoelectric potentials in colloids and granular porous media: A unified model,* Journal of Colloid and Interface Science, vol.212, p.503-522, 1999.

[147] Richards L.A., *Capillary conduction of liquids through porous mediums,* Physics, vol.1, p.318-333, 1931.

[148] Roy, D.M., *Mechanisms of cement paste degradation due to chemical and physical factors*, 8th International Conference on the Chemistry of Cements, Rio de Janeiro, Brazil, p.362-380, 1986.

[149] Rubin J., *Transport of reacting solutes in porous media: relation between mathematical nature of problem formulation and chemical nature of reactions,* Water Resources Research, vol.19, no.5, p.1231-1252, 1983.

[150] Rubin J., James R.V., *Dispersion-affected transport of reacting solutes in saturated porous media: Galerkin method applied to equilibrium-controlled exchange in unidirectional steady water flow,* Water Resources Research, vol.9, no.5, p.1332-1356, 1973.

[151] Saaltink M.W., Carrera J., Ayora C., *On the behavior of approaches to simulate reactive transport,* Journal of Contaminant Hydrology, vol.48, p.213-235, 2001.

[152] Saetta A., Scotta R., Vitaliani R., *Analysis of chloride diffusion into partially saturated concrete,* ACI Materials Journal, vol.90, no.5, p.441-451, 1993.

[153] Saito H., Deguchi A., *Leaching Tests on Different Mortars Using Accelerated Electrochemical Method*, Cement and Concrete Research, vol.30, p.1815-1825, 2000.

[154] Salmas C.E., Androutsopoulos G.P., *A novel pore structure tortuosity concept based on nitrogen sorption hysteresis data*, Ind. Eng. Chem. Res., vol.40, p.721-730, 2001.

[155] Samson E., Lemaire G., Marchand J., Beaudoin J.J., *Modeling chemical activity effects in strong ionic solutions,* Computational Materials Science, vol.15, no.3, p.285-294, 1999.

[156] Samson E., Marchand J., Beaudoin J.J., *Describing ion diffusion mechanisms in cement-based materials using the homogeneization technique,* Cement and Concrete Research, vol.29, no.8, p.1341-1345, 1999.

[157] Samson E., Marchand J., Robert J.-L., Bournazel J.-P., *Modelling ion diffusion mechanisms in porous media,* Int. J. for Num. Methods in Engineering, vol.46, p.2043-2060, 1999.

[158] Samson E., Marchand J., *Numerical solution of the extended Nernst-Planck model,* Journal of Colloid and Interface Science, vol.215, p.1-8, 1999.

[159] Samson E., Marchand J., Beaudoin J.J., *Modeling the influence of chemical reactions on the mechanisms of ionic transport in porous materials: an overview,* Cement and Concrete Research, vol.30, p.1895-1902, 2000.

[160] Samson E., Marchand J., *Influence of surface charge on ionic diffusion phenomena at the pore scale*, in preparation, 2001.

[161] Samson E., Marchand J., Snyder K.A., *Calculation of ionic diffusion coefficients on the basis of migration test results*, Materials and Structures, vol.36, p.156-165, 2003.

[162] Samson E., Marchand J., Snyder K.A., Beaudoin J.J., *Modeling ion and fluid transport in unsaturated cement systems for isothermal conditions*, Cement and Concrete Research, vol.35, p.141-153, 2005.

[163] Saripalli K.P., Serne R.J., Meyer P.D., McGrail B.P., *Prediction of diffusion coefficients in porous media using tortuosity factors based in interfacial areas*, Groundwater, vol.40, p.346-352, 2002.

[164] Scheidegger A.E., *The physics of flow through porous media*, 3rd ed., University of Toronto Press, Canada, 1974.

[165] Schlögl R., *Elektrodiffusion in freier Lösung und geladenen Membranen*, Zeitschrift fur Physikalische Chemie, vol.1, 1954 (in German).

[166] Schulz H.D., Reardon E.J., *A combined mixing cell/analytical model to describe two-dimensional reactive solute transport for unidirectional groundwater flow,* Water Resources Research, vol.19, no.2, p.493-502, 1983.

[167] Selih J., Sousa A.C.M., Bremner T.W., *Moisture transport in initially fully saturated concrete during drying,* Transport in porous media, vol.24, p.81-106, 1996.

[168] Silberbush M., Sorek S., Yakirevich A., *K+ uptake by root systems grown in soil under salinity: 1.A mathematical model,* Transport in porous media, vol.11, p.101-116, 1993.

[169] Simunek J., Suarez D.L., *Two-dimensional transport model for variably saturated porous media with major ion chemistry,* Water Resources Research, vol.30, no.4, p.1115-1133, 1994.

[170] Skalny J., Marchand J., Odler I., *Sulfate attack on concrete*, E & FN SPON, London, U.K., 2001.

[171] Snyder K.A., *The relationship between the formation factor and the diffusion coefficient of porous materials saturated with concentrated electrolytes: theoretical and experimental considerations*, submitted to Concrete Science and Engineering, 2001.

[172] Snyder K.A., Marchand J., *Effect of speciation on the apparent diffusion coefficient in nonreactive porous systems,* Cement and Concrete Research, vol.31, p.1837-1845, 2001.

[173] Snyder, K.A., Clifton, J.R., *4SIGHT: A computer program for modeling degradation of underground low level concrete vaults*, NISTIR 5612, National Institute of Standards and Technology, USA, 1995.

[174] Snyder K.A., Ferraris C., Martys N.S., Garboczi E.J., *Using impedance spectroscopy to assess the viability of the rapid chloride test for determining concrete conductivity*, Journal of Research of the National Institute of Standards and Technology, vol.105, p.497-509, 2000.

[175] Sposito G., *The surface chemistry of soils*, Oxford University Press, USA, 1984.

[176] St-John D.A., Poole. A.W., Sims I., *Concrete Petrography - A Handbook of Investigative Techniques*, Arnold Publisher, London, U.K., 474 p., 1998.

[177] Streicher P.E., Alexander M.G., *A chloride conduction test for concrete*, Cement and Concrete Research, vol.25, p.1284-1294, 1995.

[178] Swaddiwudhipong S., Wong S.F., Wee T.H., Lee S.L., *Chloride ingress in partially and fully saturated concretes,* Concrete Science and Engineering, vol.2, p.17-31, 2000.

[179] Tang L., *Concentration dependence of diffusion and migration of chloride ions - Parts 1 and 2*, Cement and Concrete Research, vol.29, no.9, p.1463-1474, 1999.

[180] Tang, L., *Electrically accelerated methods for determining chloride diffusivity in concrete*, Magazine of Concrete Research, vol.48, p.173-179, 1996.

[181] Tang, L. and Nilsson, L.O., *A new àppraoch to the determination of pore distribution by penetrating chlorides into concrete*, Cement and Concrete Research, vol.25, p.695-701, 1995.

[182] Tang L., Nilsson L.O. *A discussion of the paper: Calculation of chloride diffusivity in concrete from migration experiments in non-steady-state conditions*, Cement and Concrete Research, vol.25, p.1133-1137, 1995.

[183] Tang L., Nilsson L.O., *Chloride binding capacity and binding isotherms of OPC pastes and mortars,* Cement and Concrete Research, vol.23, p.247-253, 1993.

[184] Tang L., Nilsson L.O., *Rapid determination of the chloride diffusivity in concrete by applying an electrical field,* ACI Materials Journal, vol.89, no.1, p.49-53, 1992.

[185] Taylor H.F.W., *Cement Chemistry*, Second Edition, Thomas Telford Publishing, London, U.K., 1997.

[186] Teorell T., *Transport process and electrical phenomena in ionic membranes,* Prog. in Biophys. and Biophysical Chemistry, vol.3, p.305-369, 1953.

[187] Tremper B., *The effects of acid waters on concrete*, Journal of the American Concrete Institute, vol.28, No.9, p.1-32, 1931.

[188] Truc O., Ollivier J.P., Carcassès M., *A new way for determining the chloride diffusion coefficient in concrete from steady state migration test,* Cement and Concrete Research, vol.30, p.217-226, 2000.

[189] Truc O., Ollivier J.P., Nilsson L.O., *Numerical simulation of multi-species diffusion,* Materials and Structures, vol.33, p.566-573, 2000.

[190] Tumidajski P.J., *A rapid test for sulfate ingress into concrete*, Cement and Concrete Research, vol.25, p.924-928, 1995.

[191] Uniform Building Code, *Vol. 3 - Structural Engineering Design Provisions*, Chapter 19 - Concrete, International Conference of Building Officials, 1977.

[192] Valocchi A.J., Street R.L., Roberts P.V., *Transport of ion-exchanging solutes in groundwater: chromatographic theory and field simulation*, Water Resources Research, vol.17, no.5, p.1517-1527, 1981.

[193] Valocchi A.J., Malmstead M., *Accuracy of operator splitting for advection-dispersion-reaction problems*, Water Resources Research, vol.28, no.5, p.1471-1476, 1992.

[194] Verbeck G.J., Helmuth R.H., *Structures and physical properties of cement paste*, Proc. 5th Inter. Symposium on the Chemistry of Cement, vol.3 p.3-1 – 3-44, 1968.

[195] Vernet C., Stabilité chimique des hydrates - Mécanismes de défense du béton face aux agressions chimiques, *in* La durabilité des bétons, ed. Presse de l'Ecole Nationale des Ponts et Chaussées, p.129-170, 1992.

[196] Viallis H., Faucon P., Petit J.C., Nonat A., *Interaction between salts (NaCl, CsCl) and calcium silicate hydrates (C-S-H)*, Journal of Physical Chemistry, vol.103, p.5212-5219, 1999.

[197] Walsh M.P., Bryant S.L., Schechter R.S., Lake L.W., *Precipitation and dissolution of solids attending flow through porous media,* AIChE Journal, vol.30, no.2, p.317-328, 1984.

[198] Walter A.L., Frind E.O., Blowes D.W., Ptacek C.J., Molson J.W., *Modeling of multicomponent reactive transport in groundwater. 1. Model development and evaluation,* Water Resources Research, vol.30, no.11, p.3137-3148, 1994.

[199] Warren C.J., Reardon E.J., *The solubility of ettringite at 25°C* , Cement and Concrete Research, vol.24, no.8, p.1515-1524, 1994.

[200] Webb S.W., Pruess K. *The use of Fick's law for modeling trace gas diffusion in porous media*, Transport in Porous Media, vol.51, p.327-341, 2003.

[201] Whitaker S., *The transport equations for multi-phase systems,* Chemical Engineering Science, vol.28, p.139-147, 1973.

[202] Whitaker S., *Simultaneous heat, mass, and momentum transfer in porous media: a theory of drying,* Advances in Heat Transfer, vol.13, p.119-203, 1977.

[203] Xi Y., Bazant Z., Jenning H., *Moisture diffusion in cementitious materials - Adsorption isotherms,* Advanced Cement Based Materials, vol.1, p.248-257, 1994.

[204] Xi Y., Bazant Z., Molina L., Jennings H., *Moisture diffusion in cementitious materials - Moisture capacity and diffusivity,* Advanced Cement Based Materials, vol.1, p.258-266, 1994.

[205] Xu A., Chandra S., *A discussion of the paper: Calculation of chloride diffusion coefficients in concrete from ionic migration measurements*, Cement and Concrete Research, vol.24, p.375-379, 1994.

[206] Xu T., Samper J., Ayora C., Manzano M., Custodio E., *Modeling of non-isothermal multi-component reactive transport in field scale porous media flow systems,* Journal of Hydrology, vol.214, p.144-164, 1999.

[207] Yeh G.T., Tripathi V.S., *A critical evaluation of recent developments in hydrogeochemical transport models of reactive multichemical components,* Water Resources Research, vol.25, no.1, p.93-108, 1989.

[208] Yeh G.T., Tripathi V.S., *A model for simulating transport of reactive multispecies components: model development and demonstration,* Water Resources Research, vol.27, no.12, p.3075-3094, 1991.

[209] Zalc J.M., Reyes S.C., Iglesia E., *The effects of diffusion mechanism and void structure on transport rates and tortuosity factors in complex porous structures*, Chemical Engineering Science, vol.59, p.2947-2960, 2004.

[210] Zhang J.Z., Buenfeld N.R., *Presence and possible implications of a membrane potential in concrete exposed to chloride solution,* Cement and Concrete Research, vol.27, no.6, p.853-859, 1997.

[211] Zhang J.Z., Buenfeld N.R., *A reply to the discussion by Chatterji of the paper "Presence and possible implications of a membrane potential in concrete exposed to chloride solution",* Cement and Concrete Research, vol.28, no.4, p.777-778, 1998.

[212] Zhang T., Gjorv O.E., *An electrochemical method for accelerated testing of chloride diffusivity in concrete,* Cement and Concrete Research, vol.24, no.8, p.1534-1548, 1994.

[213] Zhang T., Gjorv O.E., *Diffusion behavior of chloride ions in concrete,* Cement and Concrete Research, vol.26, no.6, p.907-917, 1996.

[214] Zienkiewicz O.C., Taylor R.L., *The finite element method,* McGraw-Hill (USA), 4eme ed., 1989.

[215] Zysset A., Stauffer F., Dracos T., *Modeling of chemically reactive groundwater transport*, Water Resources Research, vol.30, no.7, p.2217-2228, 1994.

[216] Zyvoloski G.A., Robinson B.A., Dash Z., Trease L.L., *Models and methods summary for the FEHMN application,* FEHMN MMS, ECD-22, LA-UR-94-3787, Rev.1, 1995.